Middlesex University London

Middlesex University Research Repository

An open access repository of

Middlesex University research

http://eprints.mdx.ac.uk

Chitty, A. (1973) Low pressure pneumatic servomechanisms. PhD thesis, University of London. [Thesis]

This version is available at: https://eprints.mdx.ac.uk/9881/

Copyright:

Middlesex University Research Repository makes the University's research available electronically.

Copyright and moral rights to this work are retained by the author and/or other copyright owners unless otherwise stated. The work is supplied on the understanding that any use for commercial gain is strictly forbidden. A copy may be downloaded for personal, non-commercial, research or study without prior permission and without charge.

Works, including theses and research projects, may not be reproduced in any format or medium, or extensive quotations taken from them, or their content changed in any way, without first obtaining permission in writing from the copyright holder(s). They may not be sold or exploited commercially in any format or medium without the prior written permission of the copyright holder(s).

Full bibliographic details must be given when referring to, or quoting from full items including the author's name, the title of the work, publication details where relevant (place, publisher, date), pagination, and for theses or dissertations the awarding institution, the degree type awarded, and the date of the award.

If you believe that any material held in the repository infringes copyright law, please contact the Repository Team at Middlesex University via the following email address:

eprints@mdx.ac.uk

The item will be removed from the repository while any claim is being investigated.

See also repository copyright: re-use policy: http://eprints.mdx.ac.uk/policies.html#copy

Middlesex University London

Middlesex University Research Repository:

an open access repository of
Middlesex University research

http://eprints.mdx.ac.uk

Chitty, A, 1973.
Low pressure pneumatic servomechanisms.
Available from Middlesex University's Research Repository.

Copyright:

Middlesex University Research Repository makes the University's research available electronically.

Copyright and moral rights to this thesis/research project are retained by the author and/or other copyright owners. The work is supplied on the understanding that any use for commercial gain is strictly forbidden. A copy may be downloaded for personal, non-commercial, research or study without prior permission and without charge. Any use of the thesis/research project for private study or research must be properly acknowledged with reference to the work's full bibliographic details.

This thesis/research project may not be reproduced in any format or medium, or extensive quotations taken from it, or its content changed in any way, without first obtaining permission in writing from the copyright holder(s).

If you believe that any material held in the repository infringes copyright law, please contact the Repository Team at Middlesex University via the following email address:
eprints@mdx.ac.uk

The item will be removed from the repository while any claim is being investigated.

LOW PRESSURE PNEUMATIC SERVOMECHANISMS

A. CHITTY

UNIVERSITY OF LONDON
PH.D. THESIS
JANUARY 1973.

Copy No. 5.

ABSTRACT

Tests on a continuous action low pressure electro-pneumatic linear motion servomechanism are described. Data from individual tests on the components of this system, including the servo valve and the actuator, is used for analogue computer simulations. The simulations are shown to model the experimental system over a wide range of conditions. A simple linear equation is shown to model many aspects of the behaviour of the system. This equation is presented in a form which enables the importance of many system parameters to be easily assessed.

An all pneumatic linear-motion servo using discrete fluidic components is described. This system uses pulse-width modulated signals to control on/off valves. Tests on components of the system, including beam deflection proportional amplifiers, Schmitt triggers, valves and a fluidic displacement sensor and also on the complete servo are described.

Shortcomings in currently available components are shown to limit the performance of both systems, and modifications necessary to improve their closed loop behaviour are proposed.

CONTENTS

The total number of pages is 277 plus transparent overlays on pages 158, 159, 160, 161, 162, 163, 165 and 166.

NOTATION - SYMBOLS AND SUFFICES

Symbols

A	Piston area
ΔA	$A_2 - A_1$
A'	See table 3.1
a'	See table 3.1
a"	$\frac{V_m m_L}{nRT_{2a}A}$
B'	See table 3.1
b	Viscous friction coefficient
b'	See table 3.1
b"	$\frac{V_m b}{nRT_{2a}A}$
bar	A bar over a variable (e.g. $\bar{P}_2$) indicates a small perturbation from an operating point
C	Constant
C_1, C_2 ...etc.	"
C'	See table 3.1
c'	See table 3.1
c_1	Valve flow coefficient
c_2	Valve flow coefficient
D	Differential operator d/dt
D'	See table 3.1
d'	See table 3.1
e'	See table 3.1
F( )	Function
F_c	Coulomb friction force
F_F	Total friction force
F_L	Load force
f_n	$\omega_{n/2\pi}$
f'	See table 3.1
fn( )	Function
g'	See table 3.1
h'	See table 3.1
I	Valve signal current
I_D	Valve dither current amplitude
i	Total valve current
j'	See table 3.1
K	Constant
K_A	Amplifier gain
K_{ac}	Acceleration feedback coefficient
K_p	Potentiometer gain
K_{pr}	Pressure and transient pressure feedback coefficient
K_v	Velocity feedback coefficient
k'	See table 3.1
L	Laminar leakage coefficient
l'	See table 3.1
M	Instantaneous mass of gas in a chamber
m	Mass flow rate
m_L	Load mass (including load carriage mass)
M_{le}	Leakage mass flow rate
n	Polytropic exponent
P	Instantaneous pressure (absolute)
P_{at}	Atmospheric pressure (absolute)
P_e	Exhaust pressure (absolute)

Symbols continued

P_R	Reservoir pressure (absolute)
P_s	Supply pressure (absolute)
δP	Change in P
ΔP	$P_2 - P_1$
R	Gas constant
r	Pressure ratio
S	Spring stiffness
s	Laplace variable
T	Instantaneous temperature (absolute)
t	Time
V	Instantaneous volume
δV	Change in V
V_m	$\frac{1}{2}(V_1 + V_2)$
V_R	Reservoir volume (Appendix 6)
v	Specific volume

z_1 $\quad a'' \tau_m$

z_2 $\quad a'' + 2e' + g' + 2j'$

z_3 $\quad b'' \tau_m$

z_4 $\quad b'' + 2e' + g' + 2j' + \tau_m \left[2c' + 2f' + h' + 2k' + 2l'\right]$

z_5 $\quad 2c' + 2f' + h' + 2k' + 2l' + 2\tau_m d'$

z_6 $\quad 2d'$

γ	Ratio of specific heat capacities
γ_i	Command displacement (input)
γ_o	Output displacement
$\dot{\gamma}_{od}$	Drift velocity
ζ	Damping ratio
ζ_p	Damping ratio for the loaded actuator alone (Impulse Tests)
θ_v	Valve flow area
ρ	Density of air
τ	Time constant
τ_{dp}	Time period of damped oscillations for the loaded actuator (Impulse Tests)

$$\tau_m = \frac{V_m}{nRT_{2a}c_2}$$

τ_{np}	Time period of undamped oscillations for the loaded actuator (Impulse Tests)
τ_p	Pressure and transient pressure feedback time constant

Symbols continued

ω	Frequency
ω_d	Damped natural frequency
ω_n	Undamped natural frequency
ω_{np}	Undamped natural frequency for the loaded actuator alone (Impulse Tests)

Suffices

a	Average value
b	Inherent value for experimental apparatus
c	Closed loop
g	Gauge
o	Open loop (except γ_o for output displacement)
1	Referring to the right-hand chamber (figs. 2.1, 3.1 and 3.3)
2	Referring to the left-hand chamber (figs. 2.1, 3.1 and 3.3)

CHAPTER 1 INTRODUCTION

1.1 Background

1.1.1 Pneumatic Servomechanisms

Early work on the analysis of pneumatic servomechanisms was reported to the A.S.M.E. by J.L. Shearer in 1956 (1)*. This was described by the author as "merely a starting point in understanding pneumatic systems". The work described in the present thesis represents a further attempt to advance this understanding.

Shearer's paper was welcomed by Deavers (2) in the ensuing discussion on the grounds that there was a scarcity of reliable engineering information, making it difficult, for example, to carry out an effective computer simulation. Thus, it was said, pneumatic systems were often passed over in favour of hydraulic and electrical systems, even when a pneumatic system was the most logical choice. In 1957, Shearer (3) presented the results of frequency response tests on an experimental high pressure (800 lbf/in^2) continuous action servo and on analog computer models. This work by Shearer (1) & (3) had appeared in 1954 in a thesis (4). Levenstein's article (5) in 1955 simplified Shearer's equations and included sample numerical values for parameters in order to explain the operation of such a system to a wider audience. Auxiliary tanks for stabilization were used both by Shearer and Levenstein.

In 1959 Chelomey (6), using similar basic assumptions to those of Shearer, developed equations to describe a pneumatic system using mechanical feedback for control-surface positioning. Expressions for the quiescent pressures in the cylinder chambers in the presence of steady loads were developed. Experimental evidence supporting the latter expressions was also presented.

*( ) References are listed in Appendix 1.

In the missile and aero-space industry, systems using high temperature, high pressure gas have been developed, particularly in advanced weapons, though relatively little is published on this subject. There is reason to believe that considerable unpublished work has been done on gas-powered servos for military purposes both in this country and the United States (and probably the U.S.S.R. and other countries).

Eynon[7] (1960) compared gas-powered and hydraulic servo-systems for short life guided-weapon applications in which size and weight were of the utmost importance. Compressed air and hot-gas servos required high open loop gains to improve stiffness and consequently additional stabilizing arrangements had to be made. Hydraulic systems, on the other hand, required accumulators, tanks and pumps, which for low-powered servos comprised the major portion of the size and weight of the system. He concluded that the additional complexity of the former more than offset this and that gas-powered servos were viable for relatively low-powered purposes in missile and possibly other applications.

Sung and Taplin [8] (1963) discussed the growth of aerospace gas-powered control systems. The advantages of gas-powered systems were enumerated, including the absence of restrictive temperature limitations applying to hydraulic fluids and magnetic materials and the weight saving which results from the use of common power supplies for many systems within a vehicle and elimination of fluid return lines. Sources of power included hot gas generated from solid or liquid propellants, stored compressed gas and ram air. The limitations included the low stiffness of gas compared to hydraulic fluids, the high susceptibility to leakage and the lubrication problem. It was also pointed out that while energy storage in liquid

or solid form was attractive, very high temperature and often contaminated working gases result from chemically generated supplies. A number of applications were described illustrating that in certain cases gas-powered systems have clear advantages. Two applications involved nuclear engine control where the radiation resistance of the gas meant that no shielding was necessary for the control system. The major problems facing the designers of high performance systems were listed as the development of components, lubricants and transducers for severe temperature and radiation environments and the requirement for gas generators which could be controlled over a wide flow range. Sung and Taplin concluded that while gas-powered systems offered unique solutions to many aerospace control functions, substantial development effort would be required.

Vaughan [9] (1965) made a theoretical study of the effect of one important non-linear characteristic of hot gas systems, namely the limit to the gas flow rate due to the characteristics of the gas generator and valves. Using very simple mathematical models he showed that this flow saturation, in an otherwise linear system, imposes a large amplitude stability condition which results in poor small-signal performance. For comparison a switching criterion to give time optimal response was derived and it was suggested that the small signal behaviour of the continuous system could be made to approach this optimum, by the introduction of intentionally non-linear (amplitude-dependent) compensation.

Botting Eynon and Foster [8] (1970) discussed the design of hot-gas servos for weapons and described experimental work on a high pressure (1000 lbf/in^2) pneumatic system. They showed that using feedback compensation it was possible to employ high open loop gains and consequently to achieve acceptable static stiffness and accuracy.

They also made a theoretical study, using a digital computer, of the effects of a number of parameters including amplifier and valve saturation, friction and valve lap.

In a review paper on the subject of artificial limbs, published in February 1965, Hall and Lambert [11] observed that no closed-loop pneumatically powered prostheses were available although open-loop pneumatic systems, operating typically at 70 lbf/in^2, had been in use since 1955. Arm prostheses of this type were prescribed for a number of patients in this country. These are still in use in some cases, though they are no longer being fitted to new patients. At a Symposium on Powered Prostheses in October 1965 [12], speakers expressed the view that closed loop control of powered prostheses was desirable and Simpson described artificial arms using separate pneumatic position servomechanisms for four movements, which he had fitted to disabled children. Since 1965 a number of groups in the United Kingdom and Europe have been developing pneumatically-powered arm prostheses. The emphasis has been upon practical development and construction problems rather than on analysis, due to the urgency of the problem and the relative shortage of funds. Organizations concerned in this work together with representative publications include:-

The M.R.C. Powered Limbs Unit, West Hendon. London [13]

The Department of Medical Physics, University of Edinburgh [14]

The Lady Hoare Experimental Workshop and Training Unit, Chailey Heritage, Sussex [15]

The Department of Mechanical Engineering, University College London [16]

The SVEN Group, Sweden [17]

The University of Technology, Delft, Netherlands [18]

The Department of Engineering Science, University of Oxford, and

The Department of Mechanics, Technion-Israel Institute of Technology, Haifa, Israel [19]

Simpson has continued development of his arm-prosthesis and it is being used successfully by a number of patients in Scotland. It will shortly be available for more widespread use when it is scheduled by the Department of Health and Social Security for prescription throughout the United Kingdom. The "Hendon Arm" [13] is being evaluated by the Department of Health and Social Security in order that a decision can be made regarding further development and testing.

Brann [20] (1966) presented a linear analysis, based on Shearer's theory, for a proposed pneumatically-powered prosthetic control system and Brann and Kirkwood [21] described tests on a bench rig designed to evaluate this analysis. This proved to be impossible due to major non-linearities in the valve characteristic and in the load friction.

In the process industries, pneumatic control systems have been in use for many years. The reasons for which pneumatic systems are often preferred include cheapness and reliability, their ability to function at high and low temperatures and their acceptability in hazardous areas where electrical components are excluded. In most cases, where position control is required, it is achieved by controlling a diaphragm or cylinder pressure which is opposed by a spring force. However, when accurate positioning of a valve or power cylinder is required an additional "positioner" is fitted. This is a pneumatic servomechanism which measures and controls the actual valve or piston position. These are slow-acting devices and the processes for which they are used involve very long time constants.

In factories and workshops also, low pressure air has been used extensively as a power source, for many years. Applications include machine tools and vices, hand tools such as drills, torque

wrenches and polishers, transfer machines and other mechanical handling devices. The relatively recent development of "Low Cost Automation" includes the latter particularly, and is used to describe the application of simple automatic control techniques to machinery used for production. Pneumatic systems are particularly suitable and are widely used for this purpose due to their simplicity, ruggedness and cheapness. In general, such applications do not require high performance, so that the available components, including large electrically or pneumatically operated on/off valves with slow response and piston-type actuators with high friction forces, are quite satisfactory for most purposes. A range of commercially available valves described by Kay [22] are however much smaller and have much improved dynamic characteristics.

Recent work on low pressure servomechanisms includes a thesis, published in 1967 by Cutland [23], in which he compared the results from an experimental (80 lbf/in^2) continuous action electro-pneumatic system with analog computer studies based on Shearer's analysis. This comparison was to some extent foiled by the highly non-linear and sometimes inconsistent behaviour of the test rig. Cutland pointed out that very little experimental data was available on the behaviour of pneumatic servomechanisms when powered by low pressure air, such as was almost universally available in factories and workshops.

Andersen's book [24] published in 1967 presented design information for pneumatic systems and concluded with an analog computer study of a proposed all-pneumatic position servomechanism.

Burrows' thesis [25], published in 1969, described work on on/off pneumatic servomechanisms with supply pressures of 100 lbf/in^2. A comprehensive analog computer study was made on an on/off system

which included auxiliary stabilizing tanks and velocity and acceleration feedback. This system could not however be realized in practice due to the unavailability of a spool valve of the type simulated. Although it was therefore impossible to verify these computer results with results from an actual system, Burrows was able to predict the effects of many system parameters upon behaviour. An experimental system was however constructed using a flapper/nozzle valve positioned by a relay-driven torque motor. A linearised analog computer simulation of this system was conducted. In this case the simulation was performed in "real time" so that the relay from the experimental system could be incorporated. The step responses of the system and the analog computer were compared. A 'theoretical' open-loop harmonic response was also calculated by combining the linearized theory with experimental results for the relay alone. This 'theoretical' response was then compared with the harmonic response of the actual servo. Correlation was not altogether satisfactory and this was attributed to a possible discrepancy between the static behaviour of the valve, which had been measured, and the dynamic behaviour, which had not. Burrows pointed out the considerable difficulties involved in measuring the latter under the prevailing unsteady flow conditions. Burrows included a comprehensive review of literature, which is recommended, particularly on the subjects of valve design and on/off systems.

1.1.2 Fluidic Control

Following their initial development in the late 1950s, fluidic elements have been widely applied in positioning systems. Very few of these applications have involved accurate measurement of position but have been concerned rather with the presence or absence of an object at one or a small number of locations. This is the type of logic function for which fluidic devices are most obviously suited. Some

work, however, has been described which is relevant to the use of fluidic elements for the control of pneumatic servomechanisms.

A fluidic system for the measurement of linear motion in machine tool applications was developed at the National Engineering Laboratory and described in 1969 [26]. The system is the pneumatic equivalent of the established optical measuring technique which incorporates a grating, photocells and electronic logic. A series of air jets are directed at pneumatic gratings, which each consist of a series of regularly spaced shallow grooves. A large number of fluidic elements are used to perform the logic which determines the relative position of the air jet sensing head and the fixed gratings. The output from this system is thus digital though it is absolute and does not involve counting. Resolution is dependent upon groove dimensions and jet positions and better than 0.001 inch was achieved. A commercial version of this system has recently been produced with a maximum operating range of 36 inches.

Kent and Lenaerts [27] (1970) developed a fluidic stability augmentation system for use in aircraft. The aim of this system was to modify the pilot's commands so as to ease his task while flying an aircraft with poor stability characteristics. This was achieved by the use of a fluidic shaping circuit operating on the pilot's input. The signal thus generated was added to the pilot's input signal to produce a command signal for the elevator control system. As this system used feedforward compensation, it did not require the gyro which forms part of better known stability augmentation systems. On the other hand, "hands-off" flight was not possible with the new system, since the pilot was inside the control loop in this case. An integral part of the system described by Kent and Lenaerts was a fluidically controlled servo-actuator which converted the fluidic output from the shaping circuit into a mechanical movement for addition

to the original pilot's movement. The components of this servo-actuator included a fluidic operational amplifier, two fluidically signalled servo-valves, a low-cost industrial type linear actuator and a fluidic position sensor with analogue output, designed specifically for the purpose. Exhaustive tests were not conducted but it was concluded that the servo-actuator was the least satisfactory part of the whole system. The major reasons given for this were high friction in the actuator and feedback transducer and the non-linear input/output characteristic of the latter. The use of an operational amplifier, linear variable restrictors and two servo-valves made the servo-actuator very costly. It was suggested that the use of a recently developed rotary actuator and an alternative sensor (working on the back-pressure principle and described in refs. 28 and 29) would improve the performance while cost reductions might be achieved by the development of alternative amplifier and linear restrictor designs.

Lloyd [30] presented a paper to the 1970 Cranfield Fluidics Conference describing a proportional amplifier. It was intended that this amplifier should give an analogue differential pressure output proportional to the input differential pressure, through the use of simple bistable elements and pulse width modulation techniques. Good linearity was achieved from an integrated circuit prototype though a very large ripple signal appeared at the output. The belief was expressed that this ripple would be considerably reduced by further development, yielding an amplifier which would overcome the disadvantages of conventional beam deflection proportional amplifiers without the sophistication and expense of multi-stage operational amplifiers.

At the same conference, Taft and Nawaz [31] proposed a form of fluidic compensator or controller for use in analogue systems but

using digital techniques. The controller consisted of two stages. The output from the first stage was a pulse-width modulated form of the analogue input signal. In the second stage, one or more pulses were added to or subtracted from the incoming P.W.M. signal, each time the level of that signal changed. Depending on the design of the second stage, a variety of signal shaping modes were possible, providing alternatives to the conventional proportional, integral and derivative control strategies. A number of such modes were analysed and frequency response loci drawn. The output from such a controller would be in the form of a series of pulses which could be used directly to control an analogue system if the natural frequency of that system was well below the controller carrier frequency. The simplest type of compensator analysed was also built and tested and a frequency response locus was presented. This showed that the behaviour of the experimental system was close to the analytically predicted behaviour, when allowance was made for the finite time delay which arose due to the fluidic elements and connecting lines used.

Initial work on a servo for powering an artificial elbow joint was described by Johanssen et al in 1970 [17]. In that case an electronic amplifier generated a pulse width modulated signal which was used to drive small electrically signalled on/off pneumatic valves.

A fluidic pulse-width modulator and separate oscillator constructed at R.A.E. was described by Flood [32] in 1971. The system comprised a number of discrete digital and analogue beam-deflection amplifiers together with restrictors and capacitors. The output from the oscillator was nominally triangular, with a frequency of about 30 Hz, and the steps necessary to eliminate a high frequency component from this waveform were described. The

oscillator and command signals were each converted to push-pull pressure variations by separate proportional amplifiers. Summation was achieved simply by connecting these amplifier outputs together at the control ports of a bistable switch. The output from this switch constituted the P.W.M. signal and was fed via a buffer stage to the load which comprised a single fluidic element. A considerable amount of hysteresis in the bistable switch was shown to limit the operating range of the system to mark-space ratios between 0.15 and 0.90. Within this range a reasonably linear input/output characteristic was observed. Output waveforms for the complete system were given and reasons for variations in the mark-space ratio for a constant input signal were discussed. The most important of these was instability in the oscillator, which caused carrier frequency fluctuations. A simple restrictor/capacitor low-pass filter, for the conversion of the P.W.M. signal to analogue form, was tested. It proved impossible to attenuate the 30 Hz carrier yet maintain a good operating bandwidth by this method.

Surveying the range of fluidic displacement sensors in early 1972, Chitty and Lenaerts [33] showed that a large number of two-state devices for simple object detection were commercially available. These depended upon a small number of basic fluidic principles. Several of these detectors have been described separately, for example in references 34, 35 and 36. On the other hand, only a small number of sensors were available for measuring the actual position of an object and little information was published apart from manufacturers' data sheets.

In this Introduction, relevant previous work has been discussed only in general terms as it will be examined in detail at appropirate points in the remainder of the thesis.

1.2 This Project

1.2.1 General

Despite the ready availability of a power source in industrial locations, servomechanisms powered by compressed air have not been adopted. Recent workers in this field [23][37] have expressed the view that such systems offer a possible alternative to other systems. The response speed of a hydraulic system is considerably faster than can be expected from a low-pressure pneumatic system, but a hydraulic system requires an expensive power supply unit. Electric motors, on the other hand, are by far the most common source of mechanical power but an equivalent air motor or actuator is much less bulky. For example, a 10 horsepower air-driven hand tool can be manipulated by one man while an electric motor of comparable weight would deliver less than one horsepower [24a]. Thus for applications requiring precision and moderate response speeds and particularly where there is a plentiful supply of air, pneumatic systems can offer considerable advantages.

The term "Pneumatic Servomechanism" embraces a variety of systems (see footnote). While the power source and the function of the system are defined, a number of variations are possible for each of the system components. Essentially a pneumatic servomechanism must include a valve to control the flow of pressurised gas to an actuator which converts the energy of the gas to the required form. The behaviour of the system is monitored by one or more sensors

---

Servo-mechanism - "An automatic monitored kinetic control system which includes a power amplifier in the main forward path" - British Standard Glossary (1967) (38).

Although this term is often used to embrace a wider range of systems, the above definition is used in this thesis. The definition can be para-phrased using the basic definitions included in the same British Standard as "A closed loop system which does not include a human operator in the loop, the purpose of which is to control the displacement, velocity, or acceleration (or any higher derivative of position) of a device".

and the operation of the valve is governed by a controller acting upon information received from the sensors and upon a command signal from an input device.

(a) Valves

Valves which can be used for control of gas flow include: Poppet Valves, Ball Valves, Spool Valves, Flapper/nozzles, Jet-pipe Valves, Needle Valves, Plate Valves, Butterfly Valves, Gate Valves and Vortex Valves. The term servo-valve is used to describe precision-made valves having a proportional, or at least continuous, relationship between actuating signal and flow area. A valve is specified as three-way, four-way etc. according to the number of separate "chambers" to which it is connected. Leakage between the chambers is a function of the overlap or underlap of the valve or valves employed. The valve is fitted with a valve actuator which converts the input signal from the controller into a displacement. The incoming signal can be electrical, mechanical, pneumatic or even hydraulic. The valve may be single-stage or multi-stage according to the number of stages of amplifications involved between the input signal to the valve and the valve output.

(b) Actuators

Two basic forms of actuation are used, linear motion and rotary. Pressure can be applied to a sliding piston, a bellows or a diaphragm to produce direct linear motion or, through cranks, rotation. Alternatively, gas can be fed directly to a rotating machine. Working pressures may be applied to both sides of the piston of a linear actuator in which case it may have equal or unequal areas on the two faces. Alternatively, pressure may be applied to one side only while a spring is used for the return stroke. If large linear or rotary motions are required, rubbing surfaces will

almost certainly be involved and a compromise therefore must be reached between gas leakage and friction. Lubrication may be required for the actuator or the valve or both.

(c) Sensors and Controllers

Quantities to be measured will be the primary variable (position in a position servo, velocity in a velocity servo etc.) together with any others required for shaping purposes in the controller. Pressure, acceleration and velocity measurements are the most likely requirements for the latter. The selection of sensor(s) will depend upon the controller employed which in turn is a function of the form of the valve input signal. Simple linkage connections between the valve and actuator can be used to provide mechanical feedback. In the case of an electrically signalled valve there are few problems in finding suitable sensors and sophisticated shaping and compensation techniques can easily be incorporated in an electronic controller. In an all-pneumatic system, however, pneumatic or fluidic sensors and amplifiers will be required. The controller output signal may be continuous (e.g. proportional) or discontinuous (e.g. on/off or multi-zone) or quasi-continuous (e.g. high frequency modulated pulses).

(d) Input Devices

The command signal can vary from an electromyographic signal or a small displacement or force in the case of an artificial limb to a coded radio signal for a missile system. If the system is designed to be operated by a human being, in an aircraft or factory for example, a control stick or rotating knob will probably be preferred while in other applications a digital signal from a computer may be available as a command signal.

1.2.2 Low Pressure Servo Behaviour

While it is clear from the foregoing that a pneumatic servo can take many forms, it is also true that much fundamental theory is common to all such systems. The object of the first part of this investigation was to establish as much as possible of this common ground for servos working from a low pressure supply, by testing the validity of various proposed analyses and simplifications over a wide range of operating conditions.

The approach adopted was as follows:-

(a) A representative electro-pneumatic position servo was designed and constructed.

(b) Models for the experimental servo were proposed.

(c) The parameters of the individual system components were established experimentally.

(d) A series of tests was conducted on the complete experimental servo.

(e) Parameters obtained at stage (c) were fed into the models and computer simulation studies were made.

(f) Correlation between (d) and (e) was examined.

These procedures are described and discussed in Chapters 2 - 7.

As a result of this work, the limitations of available components became evident and these are further discussed in Chapter 10.

1.2.3 The Application of Fluidics to the Control of Pneumatic Servos

Following the work outlined above, on the electro-pneumatic position servo, some aspects of the application of fluidic devices to pneumatically-powered servos were investigated. Certain advantages could result from the use of fluidic devices, for example their capacity to operate under severe environmental conditions is well known (e.g. refs. 39, 40 and 41). Also, if all the electrical

components in a servo were replaced, the need for separate electrical power supplies and for electrical/fluidic interfaces would be avoided and servicing and maintenance would be simplified.

There are three important requirements for an all-pneumatic system.

(a) A pneumatically signalled valve is required.

(b) Sensors with pneumatic outputs are required for the controlled variable and for any others necessary for compensation.

(c) Computation and processing of the error signal must be carried out using pneumatic or fluidic elements.

A number of serious problems are posed by these requirements, some of which have been investigated in the literature discussed in section 1.1.2. In the second part of this project, a fluidic control system for a linear motion pneumatic servomechanism was developed and tested.

A servo-valve, whether pneumatically or electrically signalled, constitutes a considerable proportion of the cost of a pneumatic servo. An alternative to the use of an amplifier with analogue output signal together with a servo valve, is the use of on/off valves operated by pulse-width modulated signals. The latter arrangement, which could result in considerable cost saving in a finished system, was adopted for the experimental fluidic servo.

The P.W.M. amplifier, carrier frequency oscillator, valves and displacement sensor which make up the control system, are described in Chapter 8 and test results are presented and discussed in Chapter 9. The modifications necessary to achieve satisfactory closed loop performance, are discussed in Chapters 9 and 10.

CHAPTER 2 THE EXPERIMENTAL ELECTRO-PNEUMATIC POSITION SERVO

2.1 Constraints on the Design

As explained in section 1.2.2, experimental data from a low-pressure pneumatic servo was required so that comparisons could be made with theoretical predictions and results from computer models. The major considerations in designing a system were therefore:-

(a) It should be possible to establish parameters and characteristics for individual components of the system, leaving as few unknowns as possible.

(b) The complete system should be "representative" of as many aspects of pneumatic servos as possible, as discussed in section 1.2.1.

(c) The operating pressures should be of an order which could be supplied by typical low-pressure factory and workshop air-lines.

(d) Construction time should be minimized by using readily available components, particularly in areas where special expertise would be required, e.g. valve design and manufacture.

(e) Computer simulation should be simplified by the choice of the most suitable components.

The application of these constraints to the selection of components for the servo is included in the descriptions which follow.

The electro-pneumatic position servo which emerged is shown in schematic form in fig. 2.1 and consisted essentially of:-

(i) A three-way electrically signalled spool-type servo-valve.

(ii) A linear actuator with nominally equal areas on either side of the piston.

(iii) An electronic operational amplifier.

(iv) A carriage with adjustable inertial load.

(v) Electrical position, velocity and pressure sensors and associated signal processing equipment.

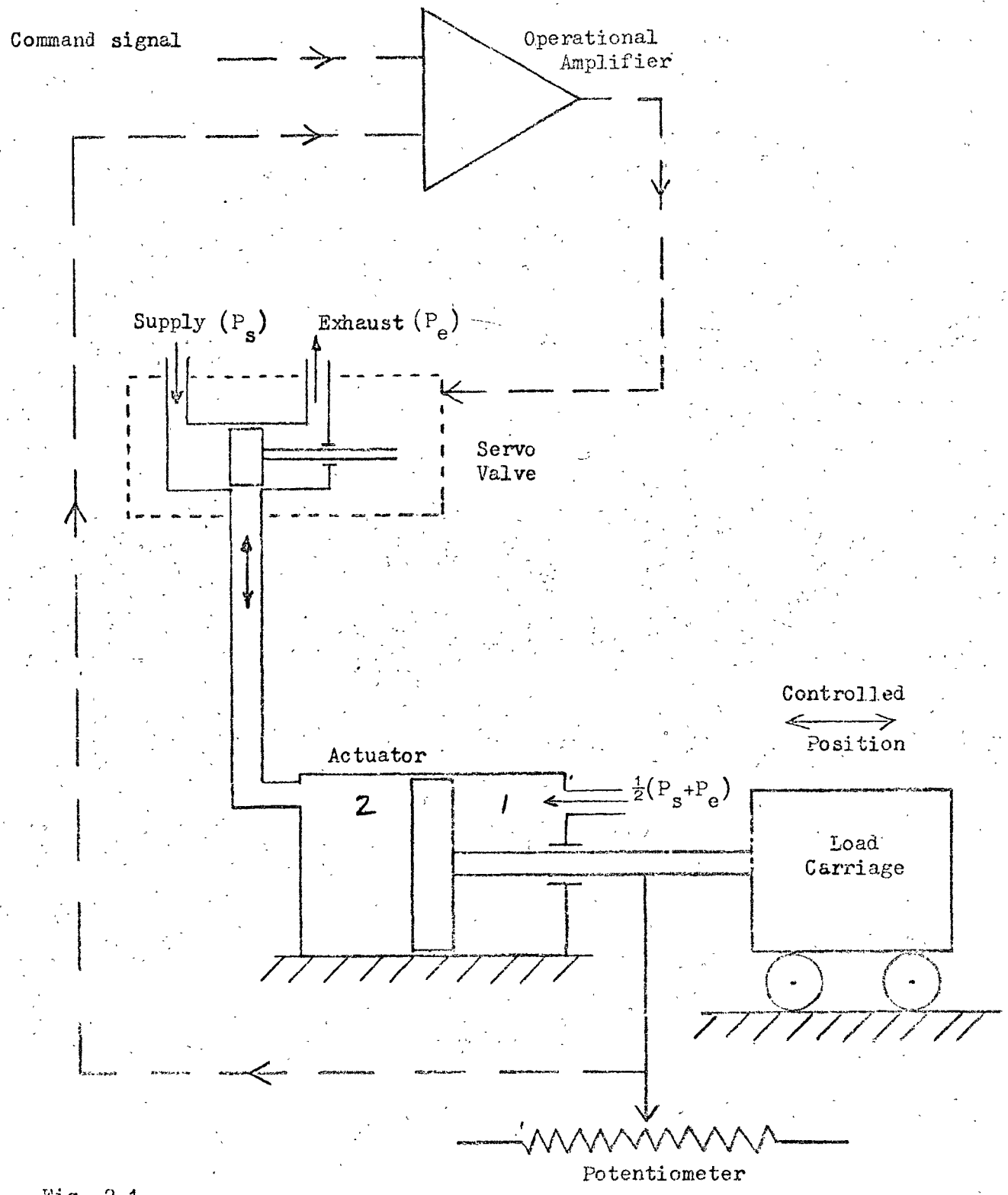

Fig. 2.1
Schematic Diagram of the Electro-Pneumatic Servomechanism

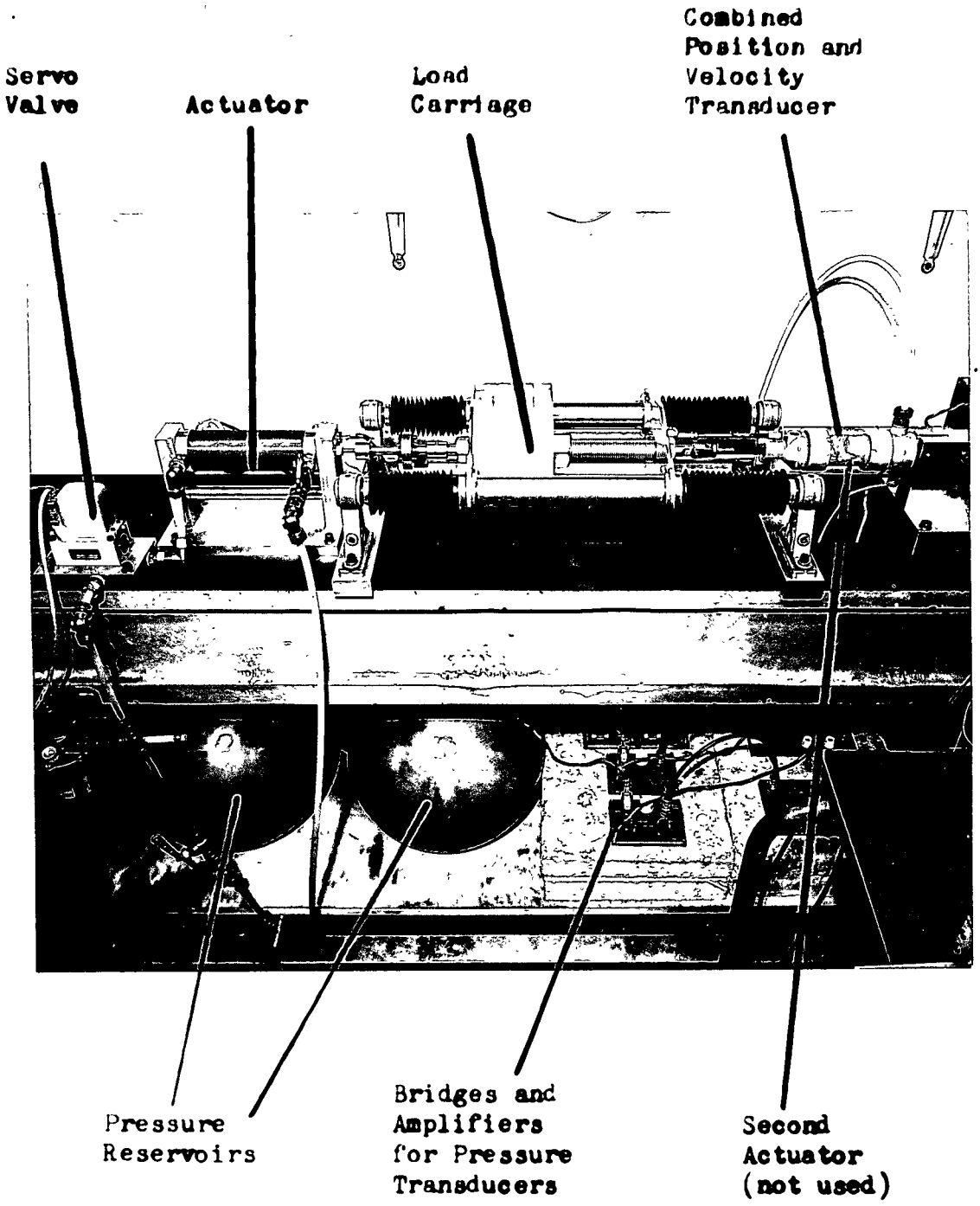

Fig. 2.2
The Electro-Pneumatic Servomechanism

Fig. 2.2 shows a photograph of the servo (the servo-amplifier is not shown).

2.2 Description of Components

2.2.1 The Servo Valve

The requirements listed in section 2.1 dictated that the valve should at least have continuous action, or better still be proportional, over a wide range of the input signal. To simplify adjustments of such things as gain, feedback and signal processing an electrically signalled valve would be preferred. In the event, only one type of servo-valve suitable for use with gas was found to be available. This was actually an electro-hydraulic valve, the Elliott type 610, manufactured for use in aircraft systems operating up to 3000 lbf/in^2. It was a single-stage proportional three-way spool valve driven by an electrically signalled torque motor. The manufacturers had only limited knowledge of its use with low pressure air, though they reported one (unnamed) customer in France who had used the valve with unlubricated air. Further data supplied by the manufacturers, and a sectioned drawing, are included in Appendix 4. For the present tests, the valve was lubricated occasionally with a mist lubricator and, as described in Chapter 4, dither was found to be necessary to overcome considerable hysteresis when the valve was used for air. A feature of the valve was its adjustable lap. Mounted integrally with the valve was an inductive transducer giving a measure of valve spool position. A schematic diagram of the valve is shown in fig. 2.3 and it can be seen in the photograph (fig. 2.4).

2.2.2 The Linear Actuator

A wide range of pneumatic actuators for use at pressures up to about 150 lbf/in^2 were available from commercial sources. In all cases, however, the friction forces at piston and rod seals were

very large, since manufacturers insisted on low leakage and durability as primary requirements. The use of such an actuator in a position servo would prevent any sort of precision being achieved. A further problem in the present case is highlighted by requirements (a) and (e) in section 2.1, in that the friction characteristics of such actuators are highly non-linear and dependent upon such parameters as age, temperature and lubrication, which are difficult to include in a theoretical analysis. A precision servo requires low and stable friction forces at the actuator and the load, a problem which is further discussed in Chapter 4 and Appendix 3. The solution which was therefore adopted was the use of an actuator which was designed for low friction while allowing a certain amount of inter-chamber and end leakage, which are relatively easily measured and accounted for.

The actuator can be seen in fig. 2.2. The cylinder body was machined from brass and fitted with aluminium end plates. The aluminium piston had shallow circumferential grooves machined into the surface, constituting a labyrinth seal. There was no additional sealing but the clearance between piston and cylinder walls was less than 0.001 in. The diameter of the piston was $1\frac{1}{2}$ in. and the stroke 3 in. The piston was nominally an "equal area" type and the difference in actual areas less than 3%. There was no seal around the piston rod as it emerged from the body. The bearing bush in the actuator at this point was nylon and the piston rod was plated steel. Air inlet channels were drilled through the end plates and a pressure transducer was mounted on each end plate.

The most efficient way to use a three-way servo valve is to use a differential area actuator, with the smaller area supplied at the same pressure as the valve. The smaller area would be half the

larger if symmetrical stall forces are required. In the present case the same effect was achieved by throttling the supply pressure to the right hand chamber (fig. 2.1) to approximately half the valve pressure.

2.2.3 Control and Feedback

The amplifier and feedback circuits are shown in fig. 2.5.

(a) Amplifier

The use of an operational amplifier in this "current drive" mode is described by Cutland [23a]. In this case the amplifier was a standard operational amplifier with an additional power output stage. The static gain of this arrangement was checked experimentally and the valve current was found to vary linearly with the input voltage. The amplifier gain and other constants are listed in Appendix 2.

(b) Feedback Potentiometer and Velocity Transducer

The feedback potentiometer was wire-wound with a resistance of 1000 ohms and having 300 turns/inch, manufactured by Penny & Giles Ltd. The stroke was 6 in. and the d.c. power supply, variable. The device also housed a moving magnet velocity transducer.

(c) Pressure Feedback

A strain gauge pressure transducer feeding a Mullard designed amplifier [42] produced a voltage signal proportional to pressure, over the range 0 - 100 lbf/in^2 g. A 15 μF capacitor could be inserted in the feedback path to the operational amplifier to give transient pressure feedback if required. The amount of pressure feedback was controlled by the variable resistor which had an arbitrary 0 - 10 scale. This particular arrangement had the side-effect that the time constant of the high-pass filter varied as the pressure feedback gain changed. Details of calibration are included in Appendix 2.

2.2.4 The Load Carriage

Fig.2.2 shows the arrangement by which the jack could be loaded with a mass of between about 8 lb. and 93 lb. The carriage ran on recirculating ball bearings and hardened steel rods, thus minimising friction.

2.2.5 Pneumatic Supply Arrangements

A compressor working at 150 lbf/in^{2}g supplied air through a 5 micron filter to two separate, identical circuits. These circuits each consisted of a pressure regulator and a reservoir of 1200 in^3 capacity. Thus independent supplies were available for the control valve (usually 100 lbf/in^{2}g) and for the right-hand jack chamber (usually 50 lbf/in^{2}g). The reservoirs can be seen in fig. 2.2.

2.2.6 Additional Instrumentation

A second strain gauge pressure transducer was used to monitor pressure variation in the right-hand chamber. For some tests, recordings were made using a Honeywell multi-channel ultra-violet recorder. A variety of galvonometers were used according to individual requirements, having flat frequency characteristics over the range 0 - 60 Hz or better.

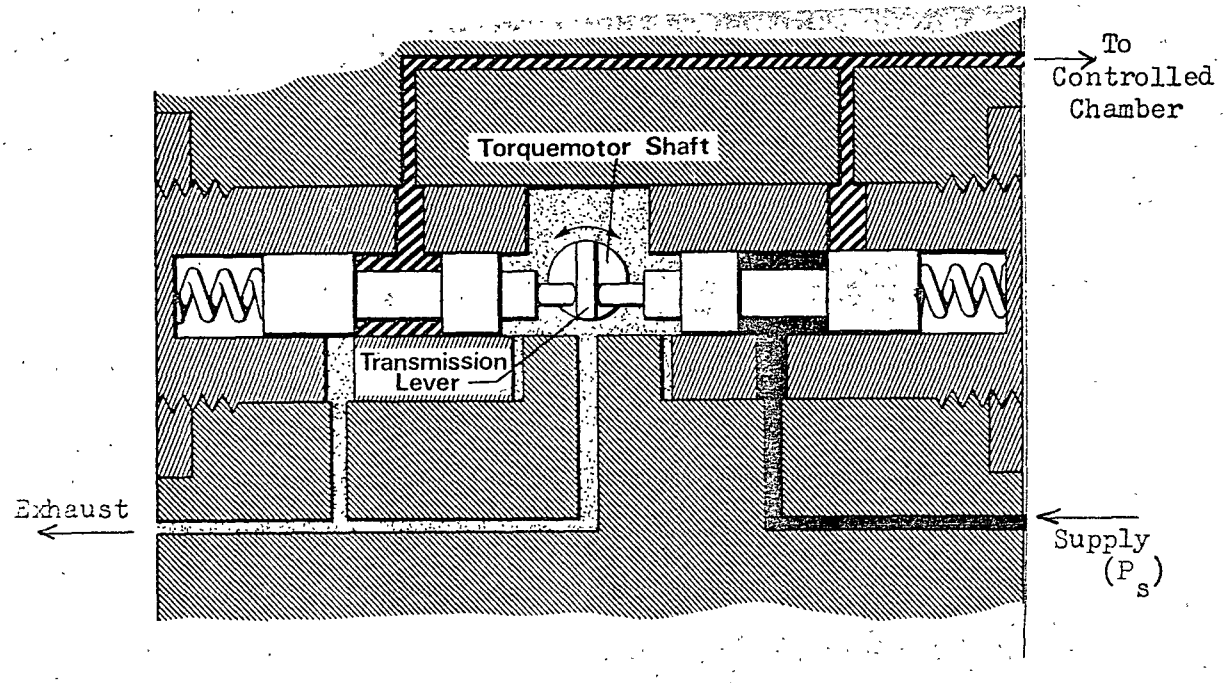

Fig. 2.3 Schematic Diagram of Servo-Valve

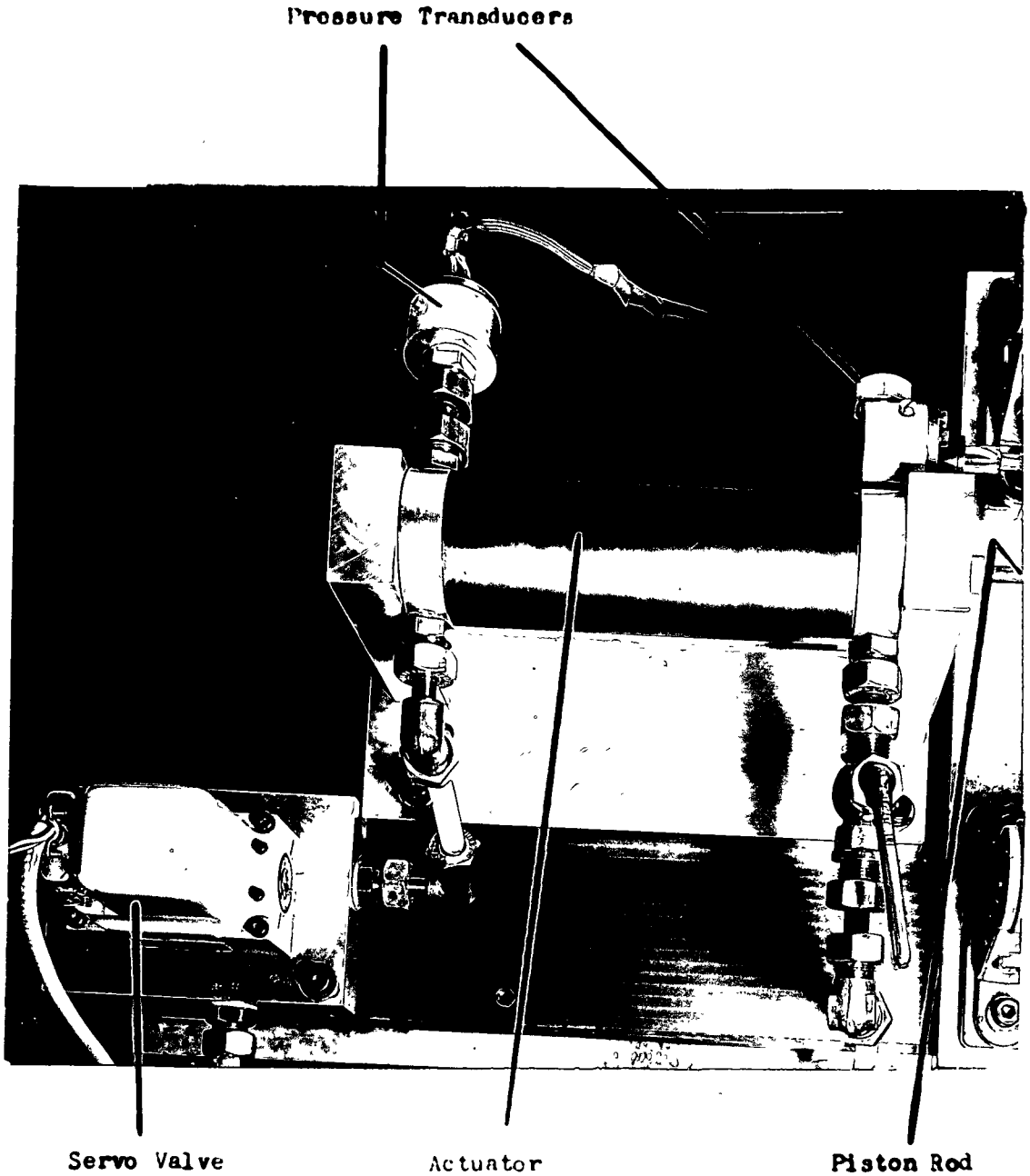

Fig. 2.4 **Arrangement of Valve, Actuator and Pressure Transducers**

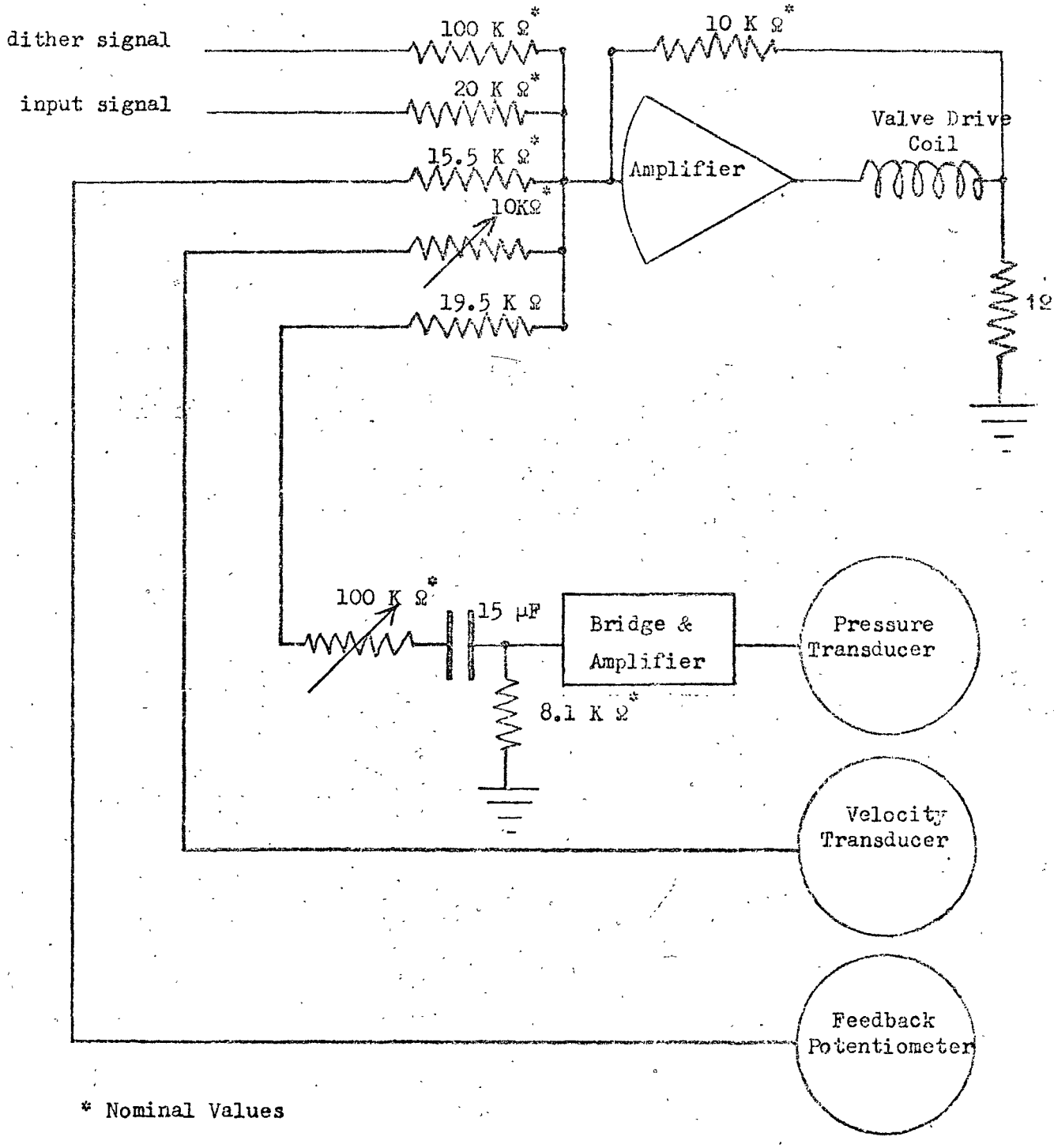

Fig. 2.5 Amplifier and Transducers

CHAPTER 3 PNEUMATIC POSITION SERVO ANALYSIS

3.1 Derivation of Equations of Motion for the Experimental Electro-pneumatic Servo

A theoretical treatment of the behaviour of a system using a four-way valve and equal-area actuator was first advanced by Shearer [4, 43] and has been used by subsequent authors, as indicated below. Of particular relevance to the present work is Brann's[20] extension of Shearer's analysis to describe a system consisting of a mechanically signalled three-way valve and a differential area actuator.

The analysis presented below modifies these treatments to cover the author's experimental system and also includes the more general assumptions of polytropic expansion and compression in the actuator chamber and imperfect piston sealing.

The symbols used are listed in pages 5-7 and many are also indicated in fig. 3.1.

3.1.1 Charging and Discharging of the Actuator Chamber

In general the mass of gas enclosed in the controlled chamber, chamber 2 (i.e. the left-hand chamber in fig. 3.1), is not constant, since gas enters or leaves the chamber through the valve and there may be leakage across the piston.

Assuming the air in chamber 2 to behave as an ideal gas, the equation of state [4a], providing that temperature and pressure are constant throughout the volume, is

$$M_2 = \frac{P_2 V_2}{R T_2} \qquad 3.1$$

where M_2 is the instantaneous mass of gas enclosed and includes the contents of the supply pipe and the pressure transducer.

At this point, either:

(a) a mass balance is performed for a control volume, a constant

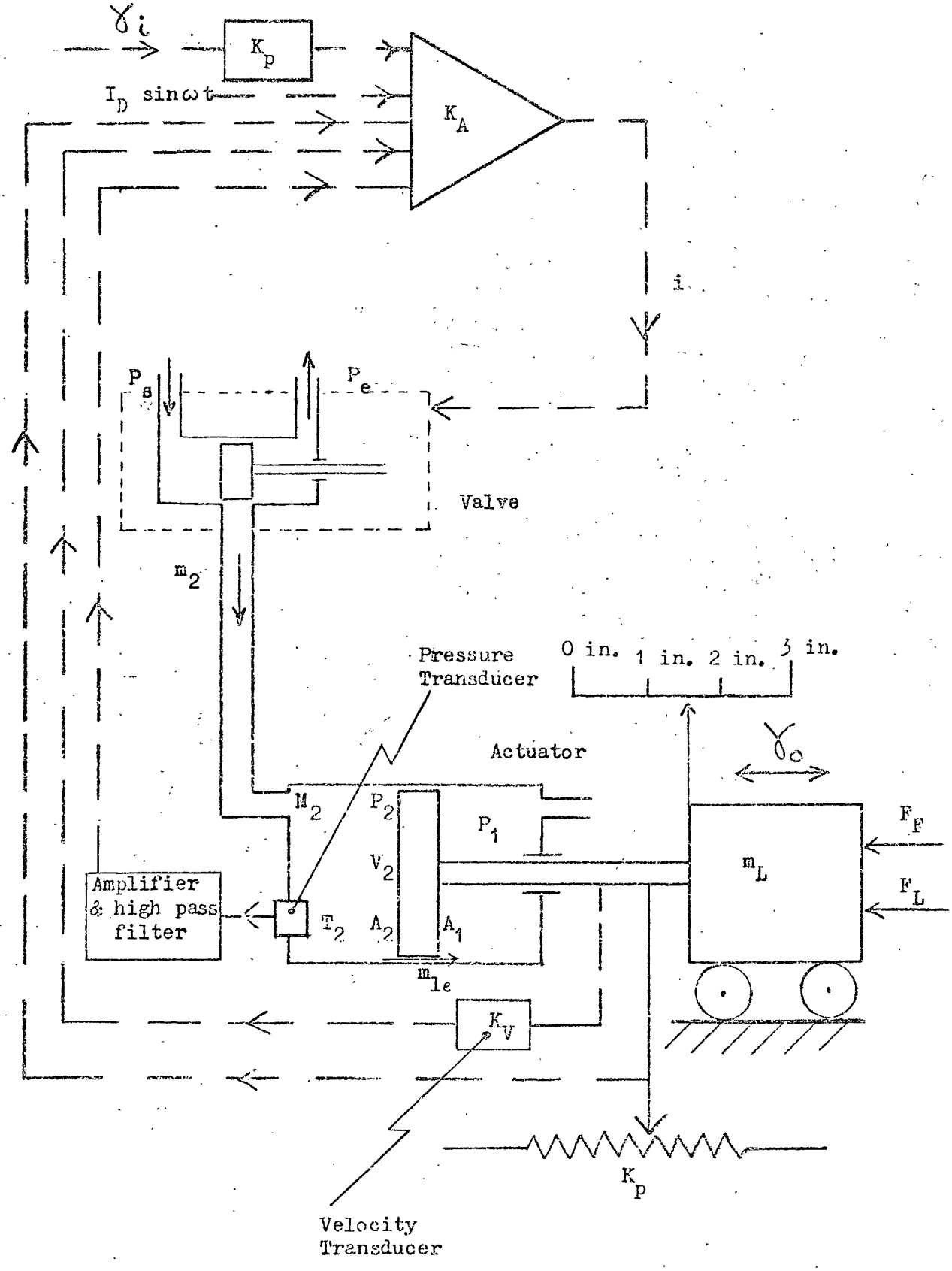

Fig. 3.1 Experimental Servo Showing Symbols

temperature process is assumed and a set of linear equations is derived for this (assumed) isothermal process[4] or,

(b) an energy balance is performed and the assumption made that the control volume is perfectly insulated, yielding linear equations for an adiabatic process [4, 6, 10, 20, 23, 25, 44] or,

(c) more generally:

If the pressure and specific volume are assumed to be related by a polytropic gas constant n [24b] where n is a number between 1 (constant temperature) and γ (constant entropy)

$$P_2 v_2^{\,n} = C \qquad 3.2$$

where $v_2 = \frac{V_2}{M_2}$ and C is constant.

Substituting eqn. 3.1 in eqn. 3.2

$$P_2^{\,1-n} R^n T_2^{\,n} = C \qquad 3.3$$

and differentiating eqn. 3.3 with respect to time (t)

$$n\, T_2^{\,n-1}\, P^{1-n} \frac{dT_2}{dt} + T_2^{\,n}(1-n)\, P_2^{\,-n} \frac{dP_2}{dt} = 0$$

i.e. $$\frac{1}{T_2}\frac{dT_2}{dt} = \left(\frac{n-1}{n}\right)\frac{1}{P_2}\frac{dP_2}{dt} \qquad 3.4$$

Now, differentiating eqn. 3.1 w.r.t. time (t) gives

$$\frac{1}{M_2}\frac{dM_2}{dt} = \frac{1}{P_2}\frac{dP_2}{dt} + \frac{1}{V_2}\frac{dV_2}{dt} - \frac{1}{T_2}\frac{dT_2}{dt} \qquad 3.5$$

Substituting eqn. 3.4 in eqn. 3.5 to eliminate T_2

$$\frac{1}{M_2}\frac{dM_2}{dt} = \frac{1}{V_2}\frac{dV_2}{dt} + \frac{1}{n}\frac{1}{P_2}\frac{dP_2}{dt} \qquad 3.6$$

Now if gas enters chamber 2 from the valve and leaks out past the piston

$$\frac{dM_2}{dt} = m_2 - m_{le} \qquad 3.7$$

also $$\frac{dV_2}{dt} = A_2 \frac{d\gamma_o}{dt} \qquad 3.8$$

and $$\rho_2 = \frac{M_2}{V_2} = \frac{P_2}{RT_2} \qquad 3.9$$

So that from eqns. 3.6, 3.7, 3.8 and 3.9

$$m_2 - m_{1e} = \rho_2 \left(A_2 \frac{d\gamma_o}{dt} + \frac{V_2}{nP_2} \frac{dP_2}{dt}\right) \qquad 3.10$$

For the case of laminar piston leakage

$$m_{1e} = L (P_2 - P_1) \qquad 3.11$$

and eqn. 3.10 becomes

$$m_2 = \rho_2 \left[A_2 \frac{d\gamma_o}{dt} + \frac{V_2}{nP_2} \frac{dP_2}{dt} + L(P_2 - P_1)\right] \qquad 3.12$$

3.1.2 Actuator Load

If the load on the system consists of mass (m_L) a variable load force (F_L) and variable friction forces totalling F_F, the equation of motion for the load is

$$A_2P_2 - A_1P_1 = m_L \frac{d\gamma_o}{dt^2} + F_L + F_F \qquad 3.13$$

For the case when the load consists only of mass and viscous friction, and if $A_2 = A_1 = A$

$$A(P_2 - P_1) = m_L \frac{d^2\gamma_o}{dt^2} + bd\frac{\gamma_o}{dt} \qquad 3.15$$

3.1.3 Control Valve

For the three-way valve shown in fig. 3.1 the rate of gas flow is a function both of the valve input current and of the pressure difference across the valve metering orifice.

i.e.
$$\left.\begin{aligned} m_2 &= fn\left[I, (P_2 - P_e)\right] \quad \text{for } I < 0 \\ m_2 &= fn\left[I, (P_s - P_2)\right] \quad \text{for } I > 0 \\ m_2 &= 0 \quad \text{for } I = 0 \end{aligned}\right\} \qquad 3.16$$

(The nature of this functional relationship is discussed in section 4.3.6.)

It will be assumed that the dynamic response of the valve is fast compared to that of the remainder of the system.

3.1.4 Amplifier and Feedback

For a proportional amplifier working in the current drive mode, with simple position feedback

$$I = K_A K_p (\gamma_i - \gamma_o) \qquad 3.17$$

If velocity and pressure feedback are added

$$I = K_A K_p (\gamma_i - \gamma_o) - K_{pr} P_2 - K_v \frac{d\gamma_o}{dt} \qquad 3.18$$

If a high-pass filter is incorporated in the pressure feedback path, to improve steady state performance in the presence of load forces, and using $D \equiv \frac{d}{dt}$,

$$I = K_A K_p (\gamma_i - \gamma_o) - K_{pr} \left(\frac{\tau_p D}{1 + \tau_p D} \right) P_2 - K_v D \gamma_o \qquad 3.19$$

and if a dither signal is also included

$$i = I + I_D \sin \omega t$$

$$= K_A K_p (\gamma_i - \gamma_o) - K_{pr} \left(\frac{\tau_p D}{1 + \tau_p D} \right) P_2 - K_v D \gamma_o + I_D \sin \omega t \qquad 3.20$$

3.1.5 Complete System Equations

The equations which describe the most general system are 3.10, 3.13, 3.16 and 3.20. However, as a result of the tests on individual system components described in Chapter 4, it is shown that the simplifying assumptions of eqns. 3.11 and 3.15 are justified for the particular system under investigation.

Thus the equations of motion for the experimental system are 3.12, 3.15, 3.16 and 3.20, and further simplification is possible.

If P_1 is constant and eqn. 3.15 is differentiated

$$\frac{dP_2}{dt} = \frac{m_L}{A}\frac{d^3\gamma_o}{dt^3} + \frac{b}{A}\frac{d^2\gamma_o}{dt^2} \qquad 3.21$$

Substituting eqns. 3.15 and 3.21 in eqn. 3.12

$$m_2 = \rho_2\left[\frac{Ad\gamma_o}{dt} + \frac{V_2 m_L}{nP_2A}\frac{d^3\gamma_o}{dt^3} + \frac{V_2 b}{nP_2A}\frac{d^2\gamma_o}{dt^2} + \frac{Lm_L}{A}\frac{d^2\gamma_o}{dt^2} + \frac{Lb}{A}\frac{d\gamma_o}{dt}\right] \qquad 3.22$$

This equation can be further simplified if variables ρ_2, V_2 and P_2 are replaced by average values ρ_{2a}, V_{2a} and P_{2a}. (It is valid to ignore changes in air temperature in this way, although rate of change of temperature is significant [4b].)

$$m_2 = \rho_{2a}\left[\frac{V_{2a}m_L}{nP_{2a}A}\frac{d^3\gamma_o}{dt^3} + \left(\frac{V_{2a}b}{nP_{2a}A} + \frac{Lm_L}{A}\right)\frac{d^2\gamma_o}{dt^2} + \left(A + \frac{Lb}{A}\right)\frac{d\gamma_o}{dt}\right] \qquad 3.23$$

Eqns. 3.15, 3.16, 3.20 and 3.23 are used for the Full Simulation, described in Chapter 6.

3.1.6 Equations for the Loaded Actuator Alone

If the supply pipe to chamber 2 is sealed

$$m_2 = 0 \qquad 3.24$$

Substituting eqn. 3.20 in eqn. 3.19 and integrating, with zero initial conditions

$$\rho_{2a}\left[\frac{V_{2a}m_L}{nP_{2a}A}\frac{d^2\gamma_o}{dt^2} + \left(\frac{V_{2a}b}{nP_{2a}A} + \frac{Lm_L}{A}\right)\frac{d\gamma_o}{dt} + \left(A + \frac{Lb}{A}\right)\gamma_o\right] = 0 \qquad 3.25$$

This second order equation can be written in the standard form

$$\frac{d^2\gamma_o}{dt^2} + 2\zeta_p\omega_{np}\frac{d\gamma_o}{dt} + \omega_{np}^2\gamma_o = 0 \qquad 3.26$$

where $$\omega_{np}^2 = \frac{nP_{2a}}{V_{2a}m_L}(A^2 + Lb) \qquad 3.27$$

and $$\zeta_p = \frac{A}{\sqrt{A^2 + Lb}} \left[\frac{b}{2A\sqrt{nP_{2a}}} \sqrt{\frac{V_{2a}}{m_L}} + \frac{L\sqrt{nP_{2a}}}{2A} \sqrt{\frac{m_L}{V_{2a}}} \right] \quad 3.28$$

Now if $A^2 \gg Lb$

$$\omega_{np}^2 = \frac{nP_{2a}A^2}{V_{2a}m_L} \quad 3.29$$

and $$\zeta_p = \frac{b}{2A\sqrt{nP_{2a}}} \cdot \sqrt{\frac{V_{2a}}{m_L}} + \frac{L\sqrt{nP_{2a}}}{2A} \cdot \sqrt{\frac{m_L}{V_{2a}}} \quad 3.30$$

These equations describe the free vibration of the Loaded Actuator, investigated in Chapter 4.

Under steady state conditions, with no load force and a constant pressure maintained in chamber 1, the load will either remain stationary or drift from left to right. Providing that the nature of the friction is not a function of piston position, the piston will achieve a constant drift velocity ($\dot{\gamma}_{od}$).

At constant velocity, the forces acting on the piston (shown in fig. 3.2) can be equated

$$P_2A_2 - P_1A_1 - P_{at}(A_2 - A_1) = F_F$$

or $$P_{2g}A_2 - P_{1g}A_1 = F_F \quad 3.31$$

where g indicates gauge pressure.

The flow equation (eqn. 3.12) becomes

$$0 = \rho_2 \left[A_2 \frac{d\gamma_{od}}{dt} + L(P_2 - P_1) \right] \quad 3.32$$

or $$P_1 - P_2 = \frac{A_2 \frac{d\gamma_{od}}{dt}}{L} = \Delta P \quad 3.33$$

Substituting $(P_1 - P_2) = (P_{1g} - P_{2g}) = \Delta P$

and $A_2 - A_1 = \Delta A$,

eqn. 3.31 becomes

$$(P_{1g} - \Delta P)A_2 - P_{1g}(A_2 - \Delta A) = F_F$$

i.e. $$P_{1g}\Delta A - A_2\Delta P = F_F \quad 3.34$$

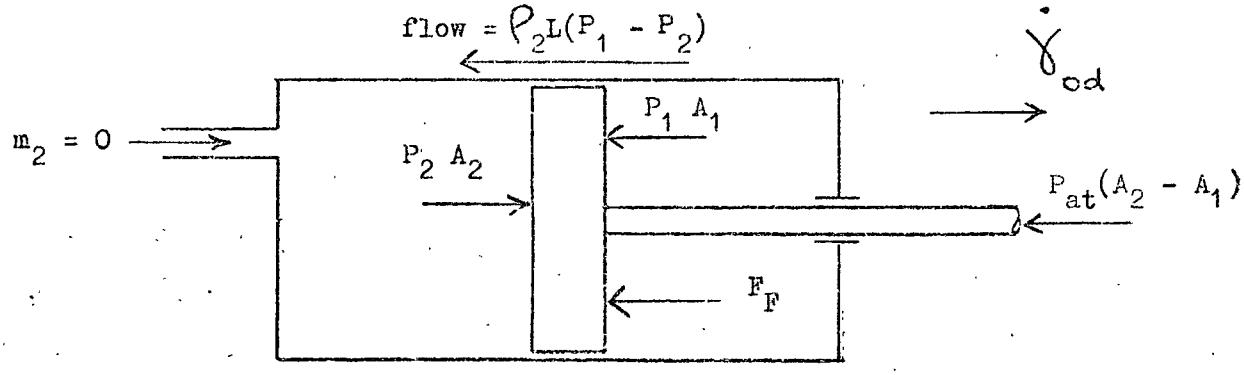

$P_1 > P_2$ hence leakage

$A_2 > A_1$

$P_2 A_2 > P_1 A_1$ hence force and drift

Fig. 3.2 Forces Causing Piston Drift

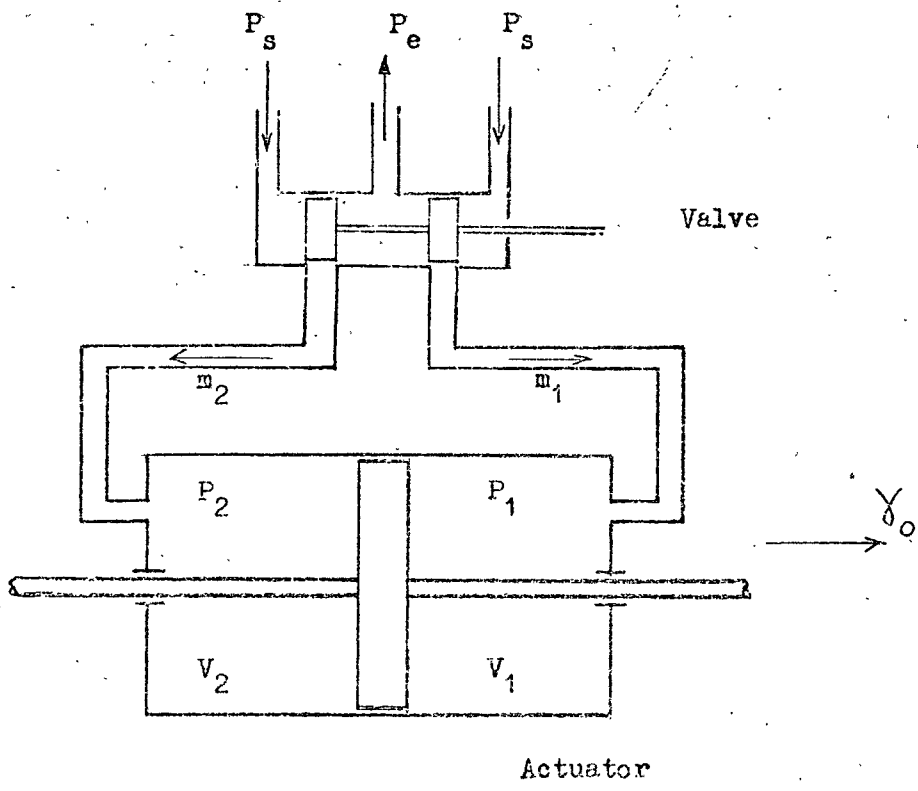

Fig. 3.3 Four way Valve and Balanced Actuator

Equations 3.33 and 3.34 are used to determine the total friction force, in section 4.1.6.

3.1.7 Linearized Valve Characteristics

A common approach used to deal with non-linear functions of one or more variables is to linearize the equations for small perturbations of the variables about fixed values. This approach has been used for linearization of pneumatic valve characteristics (4, 10, 20, 23, 25) and will be adopted here.

Eqns. 3.16 become

$$dm_2 = \frac{\partial m_2}{\partial i} dI + \frac{\partial m_2}{\partial P_2} dP_2$$

Using a "bar" to indicate small changes of variables from an operating point and using constant values c_1 and $-c_2$ for the gradients of the valve characteristics at that operating point,

$$\bar{m}_2 = c_1 \bar{i} - c_2 \bar{P}_2 \qquad 3.35$$

(The negative sign indicates that an increase in chamber pressure P_2 always results in a reduction of flow to the chamber.) Further discussion of the relevance of this form of linearization to this situation is included in Chapter 6.

3.1.8 Complete Linearized System Equations

A set of linear equations can now be manipulated to yield a transfer operator. The equations which will be used are:-

3.15	Load dynamics
3.18	Amplifier and feedback
3.23	Actuator
3.35	Valve

Substituting eqn. 3.18 in eqn. 3.35

$$\bar{m}_2 = K_A K_p c_1 (\bar{\gamma}_i - \bar{\gamma}_o) - K_{pr} c_1 \bar{P}_2 - K_V c_1 D \bar{\gamma}_o - c_2 \bar{P}_2 \qquad 3.36$$

For small perturbations, with P_1 constant, eqn. 3.15 becomes

$$A\bar{P}_2 = m_L D^2 \bar{\gamma}_o + bD\,\bar{\gamma}_o \qquad 3.37$$

Substituting eqn. 3.37 in eqn. 3.36

$$\bar{m}_2 = K_A K_p c_1 (\bar{\gamma}_i - \bar{\gamma}_o) - K_{pr} c_1 \frac{m_L}{A} D^2 \bar{\gamma}_o - K_{pr} c_1 \frac{bD\,\bar{\gamma}_o}{A}$$

$$- K_V c_1 D\,\bar{\gamma}_o - \frac{c_2}{A} m_L D^2 \bar{\gamma}_o - \frac{c_2 b}{A} D\,\bar{\gamma}_o \qquad 3.38$$

Rewriting in terms of constants d', j' etc. (defined in table 3.1)

$$\bar{m}_2 = d'(\bar{\gamma}_i - \bar{\gamma}_o) - j'D^2\bar{\gamma}_o - k'D\,\bar{\gamma}_o - l'D\,\bar{\gamma}_o - g'D^2\bar{\gamma}_o - h'D\,\bar{\gamma}_o \qquad 3.39$$

The coefficients in eqn. 3.23 can also be replaced by constants a' b' etc. and the 'bar' notation used

$$\bar{m}_2 = a'D^3\bar{\gamma}_o + (b' + e')D^2\bar{\gamma}_o + (c' + f')D\,\bar{\gamma}_o \qquad 3.40$$

Equations 3.39 and 3.40 yield a transfer operator

$$\frac{\bar{\gamma}_o}{\bar{\gamma}_i} = \frac{d'}{a'D^3 + (b' + e' + g' + j')D^2 + (c' + f' + h' + k' + l')D + d'} \qquad 3.41$$

This transfer operator is used for the Simple Simulation described in Chapter 6. In this form the transfer function is valuable, enabling the importance of individual system parameters upon closed loop behaviour to be examined.

[It is interesting to note the similarity between the behaviour of a pneumatic valve and that of an armature controlled d.c. motor. In the latter case, the output torque is controlled by the armature current but suffers considerable 'droop' as speed increases, in the same way as the valve flow 'droops' with pressure. If small perturbation linearization is applied to the motor, it can be shown that the viscous damping term in the transfer operator is increased by this 'droop' in the same way as the term g' is introduced into equation 3.41.]

Simplifying further

$$\frac{\bar{\gamma}_o}{\bar{\gamma}_i} = \frac{D'}{A'D^3 + B'D^2 + C'D + D'} \qquad 3.42$$

where the coefficients A', B', C' and D' are defined in table 3.1. Also the open loop transfer operator

$$\frac{\bar{\gamma}_o}{\bar{\gamma}_i - \bar{\gamma}_o} = \frac{D'}{A'D^3 + B'D^2 + C'D} \qquad 3.43$$

In subsequent sections, eqns. 3.42 and 3.43 are used in standard form

$$\frac{\bar{\gamma}_o}{\bar{\gamma}_i} = \frac{\omega^2_{nc}}{(1 + \tau_c D)(D^2 + 2\zeta_c \omega_{nc} D + \omega^2_{nc})} \qquad 3.44$$

$$\frac{\bar{\gamma}_o}{\bar{\gamma}_i - \bar{\gamma}_o} = \frac{\omega^2_{no}}{\tau_o D(D^2 + 2\zeta_o \omega_{no} D + \omega^2_{no})} \qquad 3.45$$

where
$$\left.\begin{aligned} \tau_o &= \frac{C'}{D'} \\ \omega^2_{no} &= \frac{C'}{A'} \\ \zeta_o &= \frac{B'}{2\sqrt{C'A'}} \end{aligned}\right\} \qquad 3.46$$

Eqns. 3.45 and 3.46 offer considerable insight into the effectiveness of the simple computer simulation, when the open-loop Bode diagrams for the servo and the computer are compared. This is discussed in sections 6.32 and 7.22.

3.1.9 Coulomb Friction and Load Forces

Whereas, in the foregoing analysis, friction was considered to be viscous only and no load forces were allowed, Coulomb friction and load forces can be included, so that eqn. 3.15 becomes

$$A(P_2 - P_1) = m_L \frac{d^2\gamma_o}{dt^2} + \frac{bd\gamma_o}{dt} + F_L + F_c\left(\operatorname{sgn} \frac{d\gamma_o}{dt}\right) \qquad 3.47$$

Now, however, a transfer operator as in eqn. 3.42 cannot be written.

$a' = \frac{V_{2a} m_L}{nRT_{2a} A}$	"mass"
$b' = \frac{V_{2a} b}{nRT_{2a} A}$	"viscous damping"
$c' = \frac{P_{2a} A}{RT_{2a}}$	"stiffness" (depends on pressure)
$d' = K_A K_p c_1$	"gain"
$e' = \frac{P_{2a} L m_L}{RT_{2a} A}$	"leakage" (viscous)
$f' = \frac{P_{2a} L b}{RT_{2a} A}$	"leakage" (extra)
$g' = \frac{c_2 m_L}{A}$	"valve" (viscous)
$h' = \frac{c_2 b}{A}$	"valve" (extra)
$j' = \frac{c_1 K_{pr} m_L}{A}$	"pressure feedback" (viscous)
$k' = \frac{c_1 K_{pr} b}{A}$	"pressure feedback" (extra)
$l' = K_V c_1$	"velocity feedback"
$A' = a'$	
$B' = b' + e' + g' + j'$	
$C' = c' + f' + h' + k' + l'$	
$D' = d'$	

Table 3.1 Coefficients in eqns. 3.41 and 3.42

The corresponding equation is

$$(A'D^3 + B'D^2 + C'D + D')\,\bar{\gamma}_o = D'\,\bar{\gamma}_i - \left(\frac{c_2}{A} + K_{pr}\frac{c_1}{A}\right)\left\{F_L + F_c\left(\operatorname{sgn}\frac{d\gamma_o}{dt}\right)\right\} \qquad 3.48$$

This equation indicates that even in a system with zero valve lap and no piston leakage and in the absence of pressure feedback, a steady-load force causes a steady state position error (due to the term $\frac{c_2 F_L}{A}$ on the right hand side). This highlights one of the shortcomings of the small perturbation linearization of the valve characteristics, in that the static stiffness of such an "ideal" valve system is actually infinite (for load forces less than the stall force).

3.1.10 Transient Pressure Feedback

The transfer operators shown in eqns. 3.41 and 3.42 include the effect of simple pressure feedback and not transient pressure feedback, which however was originally included in eqn 3.19. If transient pressure feedback is included in the linearized equations, eqn. 3.36 becomes

$$\bar{m}_2 = K_A K_p c_1\left(\bar{\gamma}_i - \bar{\gamma}_o\right) - K_{pr}\left(\frac{\tau_p D}{1 + \tau_p D}\right)\bar{P}_2 - K_v c_1 D\,\bar{\gamma}_o - c_2\bar{P}_2 \qquad 3.49$$

and eqn. 3.39 becomes

$$\bar{m}_2 = d'\left(\bar{\gamma}_i - \bar{\gamma}_o\right) - j'\left(\frac{\tau_p D}{1 + \tau_p D}\right) D^2\,\bar{\gamma}_o - k'\left(\frac{\tau_p D}{1 + \tau_p D}\right) D\,\bar{\gamma}_o - l'D\,\bar{\gamma}_o - g'D^2\,\bar{\gamma}_o - h'D\,\bar{\gamma}_o \qquad 3.50$$

and the transfer operator (eqn. 3.41) is changed to fourth order

$$\frac{\bar{\gamma}_o}{\bar{\gamma}_i} = \frac{D'(1 + \tau_p D)}{\left\{A'\tau_p D^4 + \left[A' + B'\tau_p\right]D^3 + \left[(b' + e' + g') + C'\tau_p\right]D^2 + \left[(c' + f' + h' + l') + \tau_p D'\right]D + D'\right\}} \qquad 3.51$$

3.2 Derivation of Equations for a Four-way Valve/Balanced Actuator System

The linearizing approach which produced the transfer operator, eqn. 3.41, for a system comprising a three-way valve and differential actuator will now be extended to derive transfer operators for a four-way valve/balanced actuator system, operating at any point along its stroke. This will enable comparisons to be made between the two types of system and will indicate the extent to which the results included in this thesis can be used to predict the behaviour of a four-way valve system.

Fig. 3.3 shows the valve and actuator of the system under consideration.

3.2.1 Piston Off-centre - Complete Equations

For the actuator

The equations corresponding to eqn. 3.12 are

$$\left.\begin{aligned} m_2 &= \rho_2\left[A_2\frac{d\gamma_o}{dt} + \frac{V_2}{nP_2}\frac{dP_2}{dt} + L(P_2 - P_1)\right] \text{ and} \\ m_1 &= \rho_1\left[-A_1\frac{d\gamma_o}{dt} + \frac{V_1}{nP_1}\frac{dP_1}{dt} + L(P_1 - P_2)\right] \end{aligned}\right\} \quad 3.52$$

Replacing variables ρ_1 V_1 etc. by fixed average values ρ_{1a}, V_{1a} etc. and assuming that $\rho_{1a} = \rho_{2a}$, $P_{2a} = P_{1a}$ and $A_1 = A_2 = A$

$$m_2 - m_1 = \rho_{2a}\left[2A\frac{d\gamma_o}{dt} + \frac{V_{2a}}{nP_{2a}}\frac{dP_2}{dt} - \frac{V_{1a}}{nP_{2a}}\frac{dP_1}{dt} + 2L(P_2 - P_1)\right] \quad 3.53$$

Now let $V_1 + V_2 = 2V_m$ and $V_{2a} = V_m(1 - x)$ and $V_{1a} = V_m(1 + x)$

Eqn. 3.53 becomes, for small perturbations

$$(\bar{m}_2 - \bar{m}_1) = \rho_{2a}\left[\frac{2Ad\bar{\gamma}_o}{dt} + \frac{V_m}{nP_{2a}}\cdot\frac{d}{dt}(\bar{P}_2 - \bar{P}_1) - \frac{xV_m}{nP_{2a}}\frac{d}{dt}(\bar{P}_2 + \bar{P}_1) + 2L(\bar{P}_2 - \bar{P}_1)\right] \quad 3.54$$

and $$(\bar{m}_1 + \bar{m}_2) = \rho_{2a}\left[\frac{V_m(1 - x)}{nP_{2a}}\cdot\frac{d\bar{P}_2}{dt} + \frac{V_m(1 + x)}{nP_{2a}}\frac{d\bar{P}_1}{dt}\right] \quad 3.55$$

For the actuator load

Eqn. 3.15 for small perturbations is

$$A(\bar{P}_2 - \bar{P}_1) = m_L \frac{d^2 \bar{\gamma}_o}{dt} + b\frac{d \bar{\gamma}_o}{dt} \qquad 3.56$$

For the valve

$$\left.\begin{aligned} \bar{m}_2 &= c_1 \bar{i} - c_2 \bar{P}_2 \\ \bar{m}_1 &= -c_1 \bar{i} - c_2 \bar{P}_1 \end{aligned}\right\} \qquad 3.57$$

So

$$\bar{m}_2 - \bar{m}_1 = 2c_1 \bar{i} - c_2 (\bar{P}_2 - \bar{P}_1) \qquad 3.58$$

and

$$\bar{m}_1 + \bar{m}_2 = -c_2 (\bar{P}_1 + \bar{P}_2) \qquad 3.59$$

For the amplifier

Eqn. 3.18 for small perturbations is

$$\bar{i} = K_A K_p (\bar{\gamma}_i - \bar{\gamma}_o) - K_{pr} (\bar{P}_2 - \bar{P}_1) - K_V \bar{\gamma}_o \qquad 3.60$$

From eqns. 3.59 and 3.55

$$-c_2(\bar{P}_1 + \bar{P}_2) = \frac{\rho_{2a}}{nP_{2a}} \left[V_m \frac{d}{dt} (\bar{P}_2 + \bar{P}_1) - xV_m \frac{d}{dt} (\bar{P}_2 - \bar{P}_1) \right] \qquad 3.61$$

And using $D \equiv \frac{d}{dt}$

$$(c_2 + \frac{\rho_{2a} \cdot V_m}{nP_{2a}} D)(\bar{P}_2 + \bar{P}_1) = \frac{\rho_{2a}}{nP_{2a}} xV_m D(\bar{P}_2 - \bar{P}_1) \qquad 3.62$$

$$(\bar{P}_2 + \bar{P}_1) = \frac{x\tau_m D}{1 + \tau_m D} (\bar{P}_2 - \bar{P}_1) \qquad 3.63$$

where $\tau_m = \frac{\rho_{2a} V_m}{nP_{2a} c_2} = \frac{V_m}{nRT_{2a} c_2}$

Eqns. 3.54, 3.56 and 3.63 give

$$(\bar{m}_2 - \bar{m}_1) = \frac{\rho_{2a}}{1 + \tau_m D} \left[\frac{V_m(1 - x^2)\tau_m m_L D^4}{nP_{2a}A} + \left\{ \frac{V_m m_L}{nP_{2a}A} + \frac{V_m(1 - x^2)\tau_m b}{nP_{2a}A} + \frac{2Lm_L \tau_m}{A} \right\} D^3 + \left\{ \frac{bV_m}{nP_{2a}A} + \frac{2Lm_L}{A} + 2A\tau_m + \frac{2Lb\tau_m}{A} \right\} D^2 + \left\{ 2A + \frac{2Lb}{A} \right\} D \right] \bar{\gamma}_o \qquad 3.64$$

And writing this equation in terms of the coefficients c' d' etc., used for the three-way valve/differential actuator system and introducing

$$a'' = \frac{V_m m_L}{nRT_{2a}A} \qquad \text{and} \qquad b'' = \frac{V_m b}{nRT_{2a}A}$$

(i.e. similar to a' and b' but with V_m replacing V_{2a})

$$\bar{m}_2 - \bar{m}_1 = \frac{1}{1 + \tau_m D}\left[a''(1 - x^2)\tau_m D^4 + \left\{a'' + b''(1 - x^2)\tau_m + 2e'\tau_m\right\} D^3 + \left\{2c'\tau_m + b'' + 2e' + 2f'\tau_m\right\} D^2 + \left\{2c' + 2f'\right\} D \right] \bar{\gamma}_o \qquad 3.65$$

Also, from eqns. 3.60 and 3.58

$$\bar{m}_2 - \bar{m}_1 = 2c_1 K_A K_p(\bar{\gamma}_i - \bar{\gamma}_o) - 2c_1 K_{pr}(\bar{P}_2 - \bar{P}_1) - 2c_1 K_V D\bar{\gamma}_o - c_2(\bar{P}_2 - \bar{P}_1) \qquad 3.66$$

$$\bar{m}_2 - \bar{m}_1 = 2d'(\bar{\gamma}_i - \bar{\gamma}_o) - (g' + 2j') D^2\bar{\gamma}_o - (h' + 2k' + 2l') D\bar{\gamma}_o \qquad 3.67$$

From eqns. 3.65 and 3.67

$$\frac{\bar{\gamma}_o}{\bar{\gamma}_i} = \frac{2d'(1 + \tau_m D)}{\left\{a''\tau_m(1 - x^2)D^4 + \left\{a'' + \tau_m\left[b''(1 - x^2) + 2e' + g' + 2j'\right]\right\}D^3 + \left\{b'' + 2e' + g' + 2j' + \tau_m\left[2c' + 2f' + h' + 2k' + 2l'\right]\right\}D^2 + \left\{2c' + 2f' + h' + 2k' + 2l' + 2\tau_m d'\right\}D + 2d'\right\}} \qquad 3.68$$

This transfer operator can be compared directly with eqn. 3.41 and it can be seen that the general transfer operator for the four-way valve system is of fourth order while a third order transfer operator describes the three-way valve system.

A fourth order transfer operator for this system was first proposed by Cutland[23b], and Burrows[45] later included stabilizing feedback while omitting all load friction. Eqn. 3.68 includes all these effects and in addition enables the importance of inter-chamber leakage to be assessed. Martin[46] successfully used a fourth order transfer operator to describe small perturbations of a hydraulic servo with

unsymmetrical oil volume conditions.

Eqn. 3.68 is greatly simplified if the piston is restricted to small movements about the mid-position and this will be considered in section 3.2.3.

3.2.2 Equations for the Loaded Actuator Alone (piston off-centre)

In section 3.1.6 eqn. 3.25 was derived to describe the behaviour of the loaded actuator with chamber 2 sealed and constant pressure on chamber 1 (fig. 3.1). If both supply pipes to the actuator are sealed, in the present case (fig. 3.3)

$$\bar{m}_1 = \bar{m}_2 = 0$$

and from eqn. 3.55

$$\bar{P}_2 + \bar{P}_1 = x(\bar{P}_2 - \bar{P}_1) \qquad 3.69$$

Substituting eqn. 3.69 in eqn. 3.54

$$0 = \rho_{2a}\left[2A\frac{d\bar{\gamma}_o}{dt} + \frac{V_m}{nP_{2a}}(1 - x^2)\frac{d}{dt}(\bar{P}_2 - \bar{P}_1) + 2L(\bar{P}_2 - \bar{P}_1)\right] \qquad 3.70$$

giving

$$\left[a''(1 - x^2)D^2 + \left\{b''(1 - x^2) + 2e'\right\}D + \left\{2c' + 2f'\right\}\right]\bar{\gamma}_o = 0 \qquad 3.71$$

which can be compared with eqn. 3.25, which for small perturbations is

$$\left[a' D^2 + (b' + e') D + (c' + f')\right]\bar{\gamma}_o = 0 \qquad 3.72$$

These equations describe the behaviour of the actuators following any disturbance from their equilibrium positions.

3.2.3 Piston in Mid Position - Complete Equations

In this special case $V_{1a} = V_{2a} = V_m$ and $x = 0$, and eqn. 3.65 becomes

$$\bar{m}_2 - \bar{m}_1 = \left[a'D^3 + (b' + 2e') D^2 + (2c' + 2f') D\right]\bar{\gamma}_o \qquad 3.73$$

and the closed loop transfer operator, eqn. 3.68, becomes

$$\frac{\bar{\gamma}_o}{\bar{\gamma}_i} = \frac{2d'}{a'D^3 + (b' + 2e' + g' + 2j')D^2 + (2c' + 2f' + h' + 2k' + 2l')D + 2d}$$

3.74

This is again third order and direct comparison with the transfer operator for the experimental system (eqn. 3.41) is possible.

3.2.4 Loaded Actuator Alone, (Piston in Mid-Position)

In this case eqn. 3.71 becomes

$$\left[a'D^2 + (b' + 2e')D + (2c' + 2f')\right] \bar{\gamma}_o = 0 \qquad 3.75$$

.....

The transfer operators derived in sections 3.1.6, 3.1.8 and 3.2.1 to 3.2.4 are shown in block diagram form in figs. 3.4 and 3.5 to assist the comparisons which follow.

3.3 Discussion of Proposed Equations

3.3.1 Prediction of Behaviour of the Experimental System

The linear equations developed in section 3.1 can be used to study the effect of various parameters upon the dynamic behaviour of the three-way valve/differential actuator system. At this point, observations are based solely upon the theoretically derived equations. In Chapters 5 and 7 the experimental results are discussed and co-related with these observations.

Applying the Routh-Hurwitz Criterion to eqn. 3.42

$$B' C' > A' D' \qquad 3.76$$

for closed loop stability, i.e.

$$(b' + e' + g' + j')(c' + f' + h' + k' + l') > a'd' \qquad 3.77$$

(a) Load mass variation

The terms a', e', g' and j' all increase linearly with load mass (m_L). It is therefore evident that mass increase is destabilizing. This effect will be minimized if the terms e', g' and j' dominate the first bracket of eqn. 3.77, i.e. particularly in the presence of large amounts of pressure feedback and piston leakage.

(a) Three-way valve/differential actuator system

Loaded actuator alone (eqn. 3.23 linearized to the form of eqn. 3.72)

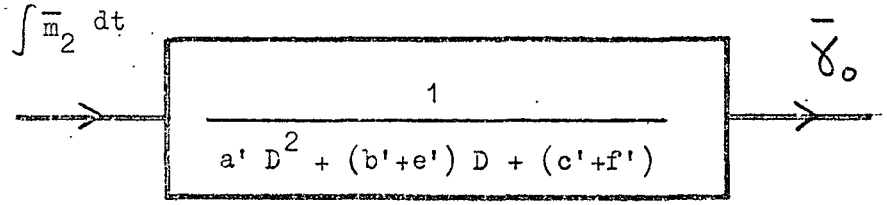

Open loop (valve and actuator)

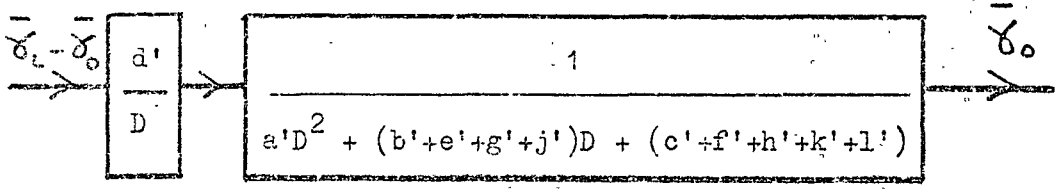

Closed loop (eqn. 3.41)

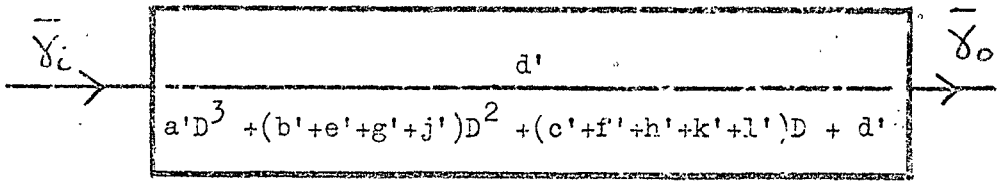

(b) Four-way valve/balanced actuator system. Piston in mid-stroke

Loaded actuator alone (eqn. 3.73)

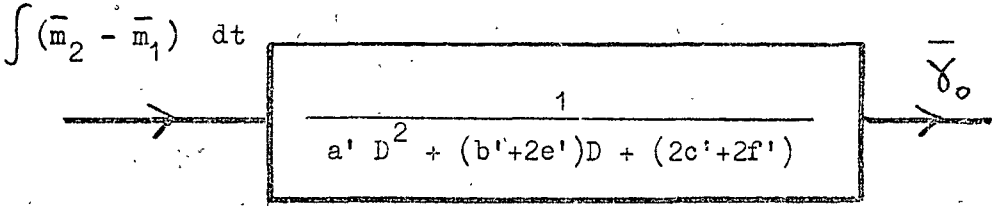

Open loop

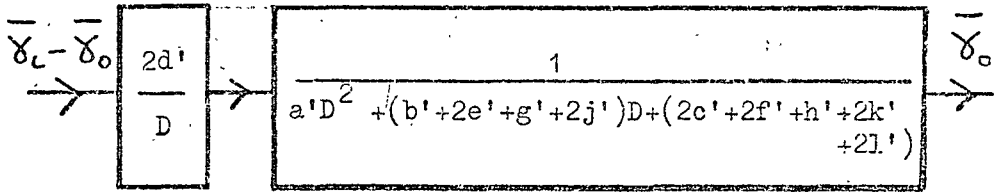

Closed loop (eqn. 3.74)

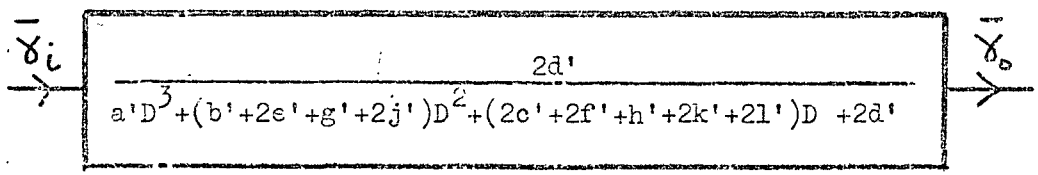

Fig. 3.4 Block Diagrams for systems (a) with differential actuator and (b) with balanced actuator at mid-stroke

(a) Four-way valve/balanced actuator system. Piston in mid-stroke

Loaded actuator alone (eqn. 3.73)

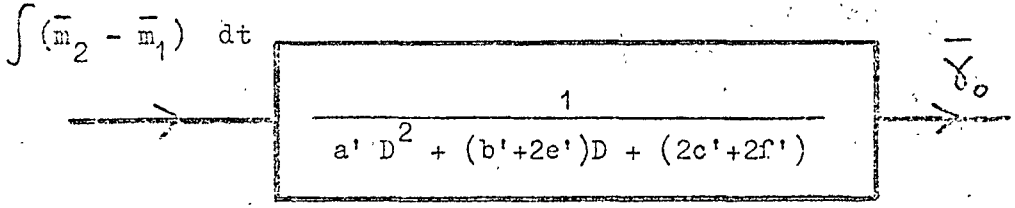

Open loop

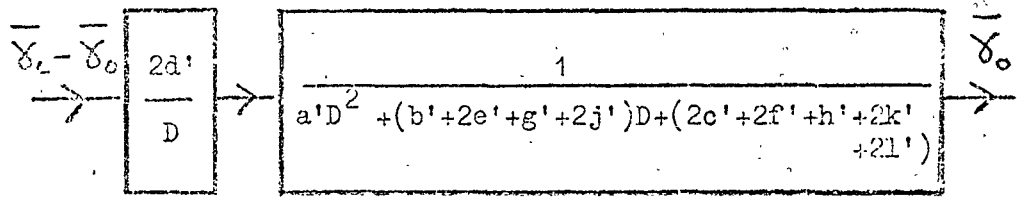

Closed loop (eqn. 3.74)

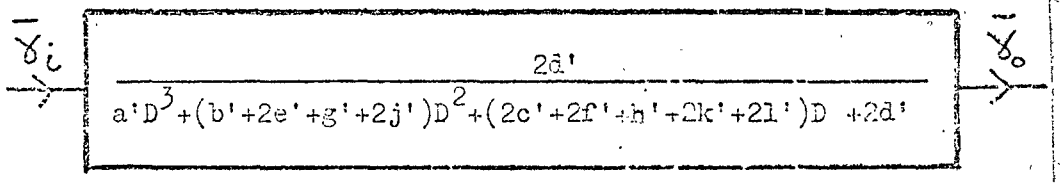

Fig. 3.5 Block Diagrams for systems using a balanced actuator (a) at mid-stroke and (b) off-centre

(b) Four-way valve/balanced actuator system. Piston off-centre

Loaded actuator alone (eqn. 3.71)

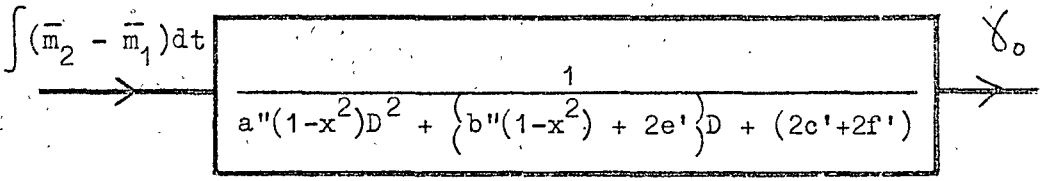

Open loop

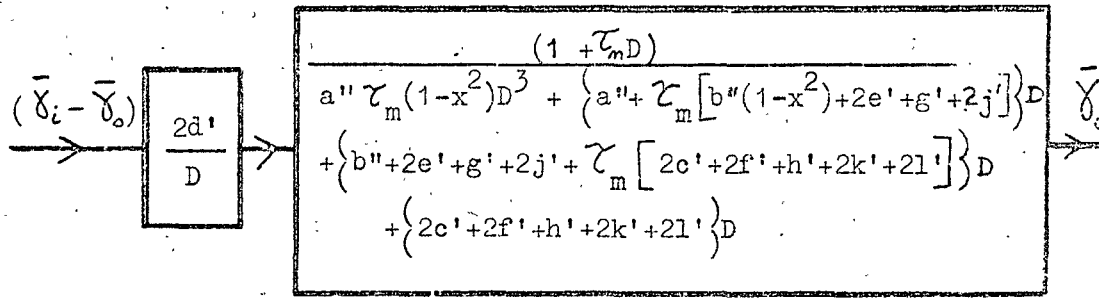

Closed loop (eqn. 3.68)

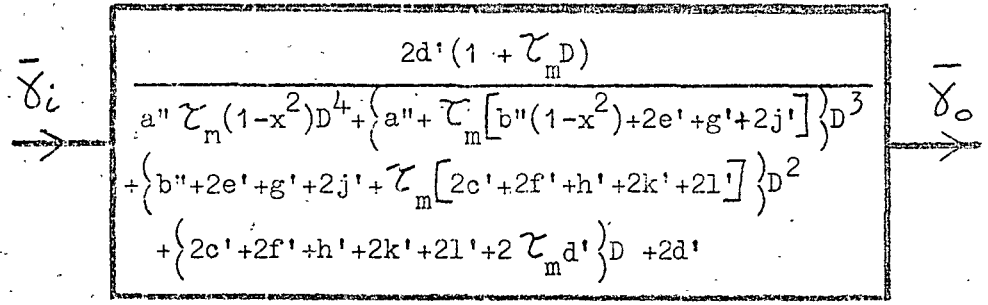

(b) Piston position variation

The volume of the controlled chamber (V_2) appears in terms a' and b' in eqn. 3.77. Thus oscillations of the piston about positions for which V_2 is large (i.e. piston well to the right in fig. 2.1) will be less stable than for smaller volumes. This effect will be most noticeable in the presence of large amounts of pressure feedback and leakage (when b' is least significant in the term B' in eqn. 3.76).

(c) Piston leakage

The effect of increased piston leakage is to increase the terms e' and f' and is therefore stabilizing under all circumstances.

(d) Stabilizing feedback

If the velocity feedback term l' in eqn. 3.77 is increased, for an unstable system, the effect will be to stabilize that system. The same can be said for pressure feedback, which increases the terms j' and k'.

It is also clear that the effect of pressure feedback is dependent upon the load mass, since

$$j' = \frac{c_1 K_{pr} m_L}{A}$$

Therefore for a system with fixed pressure feedback and variable load mass, the term j' will increase with the mass. This has the desirable effect that transient response will tend to be the same for all loads, as a' and j' in eqn. 3.77 counteract each other (this is another way of expressing the point made in (a) above).

The use of the Routh-Hurwitz Criterion gives only a coarse stability check and does not reveal, for example, whether a particular parameter change introduces a long lag into the closed loop transient response, as a side effect of improving the stability. Root loci are used to illustrate this point in section 3.4.4.

(e) Open loop gain

Increases in the gain parameters K_A and K_p increase the term D' which from eqn. 3.76 has a destabilizing effect.

(f) Steady load forces

The stability of the system in the presence of a steady load force can be predicted as follows. If the load force is in the direction shown in fig. 3.1 (from right to left), the pressure (P_2) in the controlled chamber rises. The coefficients in eqn. 3.77 are affected because

(i) P_{2a} is increased, and

(ii) new valve coefficients, c_1 and c_2, apply.

The effect of (i) is to increase c', e' and f' in eqn. 3.77 while all other coefficients remain constant, and therefore to improve stability.

The effect of (ii) is more difficult to predict from the linearised equations. If the quiescent pressure in chamber 2 is increased, the slope (c_1) of the valve characteristic (e.g. figs. 4.12 and 4.13) at this pressure is decreased for flow from the supply and increased for exhaust flow. This suggests unsymmetrical behaviour of the system. The response to left to right command signals will now be more sluggish while for right to left commands faster response can be expected. c_2 is also changed (e.g. increased for exhaust flow) though this probably has a relatively small effect on stability.

The converse arguments apply for load forces in the opposite direction to that considered above, i.e. those which result in reduced pressures in chamber 2. These predictions are summarized in table 3.2 and show clear effects for left to right command signals but effects tending to counter each other for command signals in the opposite direction.

Table 3.2 Effects of Steady Load Forces on Stability

(see section 3.3.1(f)).

		Left to right commands (flow from supply)	Right to left commands (flow to exhaust)
Steady load force from right to left in fig. 3.1	effect (i) i.e P_{2a} increase	stabilizes	stabilizes
	effect (ii) i.e. c_1 and c_2 change	more sluggish response	faster response
Steady load force from left to right in fig. 3.1	effect (i) i.e. P_{2a} decrease	destabilizes	destabilizes
	effect (ii) i.e. c_1 and c_2 change	faster response	more sluggish response

(g) Supply pressure

The quantities affected by a decrease in the valve supply pressure (P_s) and a corresponding decrease in the constant pressure in chamber 1 are P_{2a}, ρ_{2a}, c_1 and c_2 which are all reduced proportionately. As a result, all the terms in eqn. 3.77 except a' and b' are decreased and therefore the Routh-Hurwitz Criterion predicts a worsening of stability with supply pressure reduction.

(h) Loaded actuator alone

The inherent damping associated with the loaded actuator alone is indicated by

$$\zeta_p = \frac{b' + e'}{2\sqrt{(c' + f')\, a'}}$$

and it is evident that damping is reduced if

(i) load mass is increased or

(ii) the equilibrium position of the piston is moved to the left (fig. 3.1) (i.e. V_2 is decreased)

(iii) the constant pressure in chamber 1 is increased.

If this observation about piston position is compared to (b) above, it is interesting to note that a change of piston position which damps the open loop system tends to destabilize the closed loop system. On the other hand, mass increase reduces the damping of both the open and the closed loops.

3.3.2 Comparison of Differential Actuator and Balanced Actuator Systems

(a) Validity of results from the experimental system

As explained in Chapter 2, the availability of components dictated the use of a nominally equal-area actuator for the experimental system, so that in this case a constant pressure approximately equal to half supply pressure was necessary on one side of the piston. This is not, however, the best arrangement since it does not permit re-use of the air from the small area side of the piston in the way that a

differential-area actuator does. The following comments therefore relate to the latter system.

It has been argued [20] that the use of a three-way valve and a differential area actuator allows more economical use of the working fluid than does a four-way valve and balanced actuator. Lord [16] has pointed out that this is only so when the quiescent controlled pressure in the former system is permanently less than half the supply pressure, as is the case when there is a steady load force on the system. However, to realize this economy a reservoir at supply pressure is required. For general purpose use, where load forces in either direction are encountered, there is no difference in the efficiency of the two systems provided such a reservoir is available. If no reservoir is available the three-way valve system is actually less efficient, due to the time it spends operating with the quiescent controlled pressure greater than half the supply pressure.

An advantage which the use of a differential area actuator offers is the simplicity of the associated three-way valve, but against this is the reduced stall force available compared with a balanced actuator of the same dimensions. However, the foregoing linearized analysis suggests that all aspects of the behaviour of a four-way valve system are modelled by a three-way valve system, except one. The exception is that operation of the former system, away from piston mid-stroke cannot be simulated. Increasing the controlled volume (V_2) in the three-way valve system is equivalent to increasing the total volume ($2V_m$) in the four-way valve case, while maintaining the symmetry of the piston position.

(b) Four-way valve/balanced actuator in mid-position

Comparing the behaviour of the three-way valve system with

that of the four-way valve system about its mid position, the closed loop block diagrams, fig. 3.4(a) and (b) (lower pictures) show that the relative importance of certain terms is increased when a four-way valve is employed, i.e. whereas load damping and the valve 'damping' terms (b' g' and h') are unchanged, the leakage terms (e' and f'), the pressure feedback terms (j' and k') and the velocity feedback terms are doubled. Thus in a simple system with no stabilization or leakage, the characteristic equation

$$a'D^3 + (b' + g')D^2 + (c' + h')D + d' = 0$$

becomes

$$a'D^3 + (b' + g')D^2 + (2c' + h')D + 2d' = 0$$

and therefore Routh-Hurwitz Criterion shows that the four-way valve system is less stable. However, the use of any stabilization method (leakage, pressure feedback or velocity feedback) reverses this effect, i.e. the same amount of stabilization applied to the four-way valve system is more effective.

(c) Four-way valve system - piston off-centre

In order to study the effect of piston eccentricity, the coefficients in eqn. 3.68 can be simplified to

$$\frac{\bar{\gamma}_o}{\bar{\gamma}_i} = \frac{Z_6(1 + \tau_m D)}{Z_1(1 - x^2)D^4 + \left[Z_2 + Z_3(1 - x^2)\right]D^3 + Z_4 D^2 + Z_5 D + Z_6} \qquad 3.78$$

From the Routh-Hurwitz Criterion, for stability

$$Z_4 Z_5 \left[Z_2 + Z_3(1 - x^2)\right] - Z_5^2 Z_1(1 - x^2) - Z_6\left[Z_2 + Z_3(1 - x^2)\right]^2 > 0 \qquad 3.79$$

Remembering that x = 0 for piston mid-position and increases with eccentricity, it is clear that stability is improved as the piston moves away from its mid position. This is in agreement with Burrows[45]

prediction for a system without friction and leakage.

(d) Loaded actuator alone

In section 3.3.1 (e) it was noted, for the differential actuator, that a change of chamber volume which destabilizes the closed loop system, increases the damping of free vibrations of the loaded actuator alone. Exactly the same effect is observed for a balanced actuator, i.e. if the actuator supply pipes in fig. 3.3 are sealed, oscillations of the load following a disturbance from its rest position, are most damped about the piston mid-position.

3.4 Stability of Pneumatic Servomechanisms

In a well designed fluid-powered servo, friction is minimised in order to decrease the errors associated with the stiction and Coulomb components. Thus if fast response is desired and large loads are to be moved, there is likely to be insufficient damping and therefore instability. This problem is familiar to designers of hydraulic cylinder-driven systems and a number of methods have been adopted to counter it. Some of these methods are briefly discussed here and their relevance to pneumatic systems assessed.

3.4.1 Leakage

Leakage flow can be introduced deliberately into a fluid servo and since this results in energy dissipation, it can have a stabilizing effect. Leakage can occur either in the actuator or in the valve.

Leakage past the piston seals or through holes drilled in the piston or through by-pass passages between the two actuator chambers increases the open loop damping ratio. In this case flow occurs when there is a pressure difference across the piston, i.e. during transients and in the presence of a load force. (This was the case for the experimental servo described in Chapter 2 but for a differential area

actuator there is a pressure difference between chambers at all times and leakage is therefore always into the controlled chamber. The magnitude of this leakage is however still a function of the pressure difference across the piston and a similar damping effect results. If a differential area actuator is used there is continuous fluid loss, even at rest and in the absence of load forces.) The resultant energy wastage limits the usefulness of this method and Guillon [47] quotes 0.3 as the maximum additional open loop damping ratio which can be expected for a hydraulic system. In the hydraulic system described by Lambert and Davies [48] damping due to inherent piston leakage was about 25% of that due to viscous load friction.

Underlap in a four-way control valve introduces a similar damping effect for small perturbations about the null position. In this case, however, a permanent, null leakage flow is introduced direct from supply to exhaust, with consequent loss of efficiency. A similar effect would occur in an underlapped three-way valve and a valve leakage term could simply be added to the right hand side of eqn. 3.12. If laminar valve leakage is assumed, this is clearly seen to be analagous to laminar piston leakage.

While both piston leakage and valve leakage increase damping, a steady-state error results in each case, when a constant load force is applied. In the four-way valve/balanced actuator system, according to linearized theory [47], this error increases as the damping effect increases. The same is true for a three-way valve system. Of the two, piston leakage is to be preferred for either a hydraulic or pneumatic servo, due to its lower power wastage.

3.4.2 Feedback Compensation

Additional feedback loops are employed in hydraulic systems

to obtain controlled damping and the use of pressure, acceleration and velocity feedback has been studied by Bell and de Pennington [49].

The effect of negative pressure feedback is identical to that of laminar leakage. This is well illustrated by reference to the linearized equation for the author's experimental servo, eqn. 3.41, where it is seen that the leakage and negative pressure feedback terms are always added together. Pressure feedback can be achieved using mechanical arrangements of dashpots, springs and restrictors, or, if an electrically signalled valve is employed, using pressure transducer(s). The major disadvantage of pressure feedback is that it again results in reduced output stiffness.

In the complete absence of friction, pressure is proportional to piston acceleration (e.g. eqn. 3.21). Thus in a practical system acceleration feedback can be expected to have a somewhat similar damping effect to pressure feedback, with the important advantage that no position error is caused by applied load forces. Acceleration measurement is, however, less easily achieved.

The effect of velocity feedback is less clear. An electro-hydraulic system was studied by Bell and de Pennington [49]. In this system, the valve dynamics could not be neglected, and therefore an additional time constant was included in the transfer function. Thus the transfer function was fourth order and negative velocity feedback was shown to destabilize while the added damping from positive velocity feedback was only small. (The effect of negative velocity feedback in this case is confirmed in section 3.4.4(e).) On the other hand, Burrows [25] found negative velocity feedback to have a stabilizing effect, both in theory and practice, for his on/off pneumatic servo, for which a third order equation was used. A combination of negative velocity feedback and negative quasi-acceleration feedback (derived from the velocity signal) was used by

Botting et al [10] in their high pressure pneumatic servomechanism. The individual coefficients were not varied, so that the effect of the separate terms could not be judged in this case. Velocity feedback does not reduce output stiffness and velocity is fairly easily sensed electrically but negative velocity feedback increases the velocity error, which may be important.

Certain aircraft and industrial hydraulic systems, using the type of valve which was used in the experimental system described in Chapter 2, utilise feedback of valve position. Since valve position controls flow and since in the steady-state piston velocity is proportional to flow, this feedback has an effect akin to velocity feedback. Guillon [47] has shown that, according to linear analysis, this is not an effective way of introducing damping, but in practice it is said to have a useful stabilizing effect [50]. Valve current feedback is also used in a similar way, since for frequencies below the valve natural frequency, the current is proportional to the valve position.

3.4.3 Dynamic or Transient Methods

In order to eliminate the static errors introduced by the most effective stabilizing techniques described above, a high-pass filter is employed. (The filter corner-point is selected so that incoming transient oscillations are not significantly modified.) This is achieved, either using hydromechanical networks or using passive electrical components. Hydromechanical networks to achieve dynamic piston leakage or dynamic pressure feedback are described in reference 47. A neat method is employed in certain commercially available electro-hydraulic valves in which a restrained piston and restrictor are incorporated in the valve body to achieve dynamic pressure feedback [51, 52]. Such solutions are viable for a manufacturer producing large numbers of components, but for

experimental systems electrical networks are more suitable and equally effective.

Bell and de Pennington [49] found negative transient acceleration feedback very effective for stabilizing their hydraulic servo, i.e. a high-pass filter was used, even though in this case it was unnecessary for the purpose of increasing output stiffness. In their system, in which the effective valve corner frequency was either equal to or lower than that of the load, acceleration feedback was much less effective. Analysis showed that acceleration feedback would be the more useful technique for systems in which the valve response was reasonably fast compared with that of the remainder of the system. This is likely to apply for a low-pressure electro-pneumatic servo, though the use of a pneumatically signalled valve may make the inclusion of a high-pass filter in an acceleration feedback path desirable.

The addition of a tank, connected via a restrictor to each of the controlled chambers (just one if a differential actuator is employed) has been proposed for aircraft hydraulic systems [47]. This method, which has an equivalent effect to transient pressure feedback, has been shown to be effective for a high pressure pneumatic servo [4] and for low-pressure on/off servos [25, 53]. However, the additional bulk and weight of the tanks together with the resultant power wastage will often prohibit the use of this method.

Lord and Chitty [54] examined several methods used to stabilize pneumatic prosthetic systems and concluded that transient pressure feedback offered the best prospects in this case. A bellows/restrictor network for use with a mechanically signalled valve was proposed. This design was briefly tested and an unstable artificial arm was stabilized using the device.

From the foregoing it can be seen that the methods developed for stabilizing hydraulic systems can be (and in some cases have been)

applied to pneumatic systems. It is also clear that the use of a three-way valve/differential actuator system does not invalidate any of these techniques. It was therefore concluded that velocity and pressure feedback were most likely to be useful in stabilizing the author's experimental servo and accordingly velocity and pressure sensors were incorporated in the design.

3.4.4 Root Locus Study of Feedback Compensation

In order to study the effects of stabilizing feedback on the experimental servo, the linearized system is represented as in fig. 3.6(a). (The Laplace variable (s) replaces the differential operator D in order that the Root Locus Method can be used.) In this case the uncompensated closed loop servo forms the forward path, while additional stabilization is shown as a negative feedback loop. If, for example, negative pressure feedback is used, the appropriate block diagram is fig. 3.6(b). This representation is equivalent to that in the lower picture in fig. 3.4(a), but is to be preferred in this case, since it isolates the effects of stabilizing feedback. This is a slightly different approach to that adopted in reference[s] [48] and 49, where the stability of "minor" (stabilizing) loops was considered in isolation. The root locus method was also used in reference 55, to examine the effect of various parameter changes on the open loop poles of pneumatic servo-motors, when fitted with auxiliary stabilizing tanks.

The transient behaviour of the servo in the absence of stabilizing feedback is either:-

(a) overdamped, i.e. three real negative poles,

(b) stable, underdamped, i.e. one negative real pole and two complex poles with negative real parts, or

(c) unstable, i.e. one negative real pole and two complex poles with positive real parts.

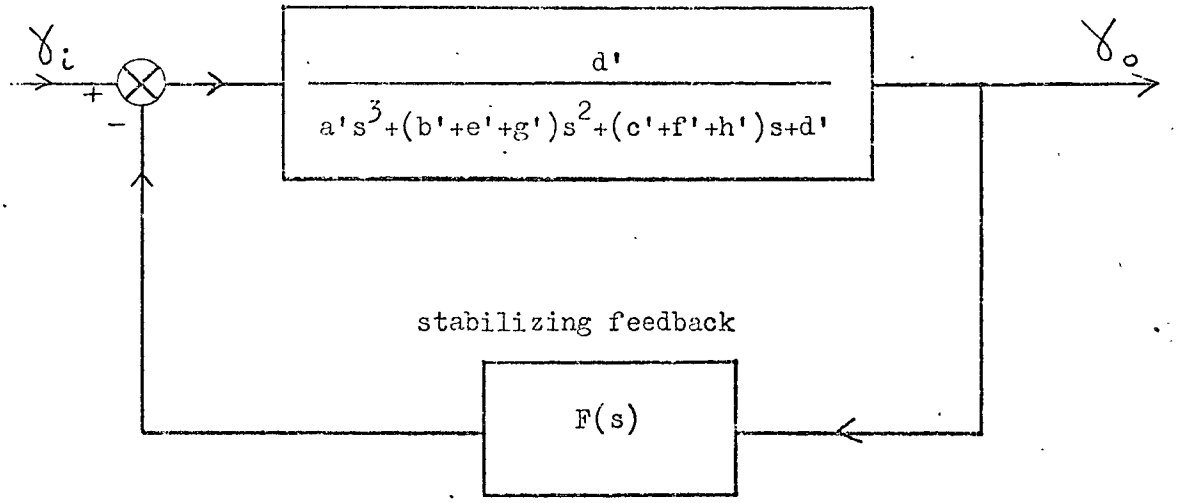

(a) General case

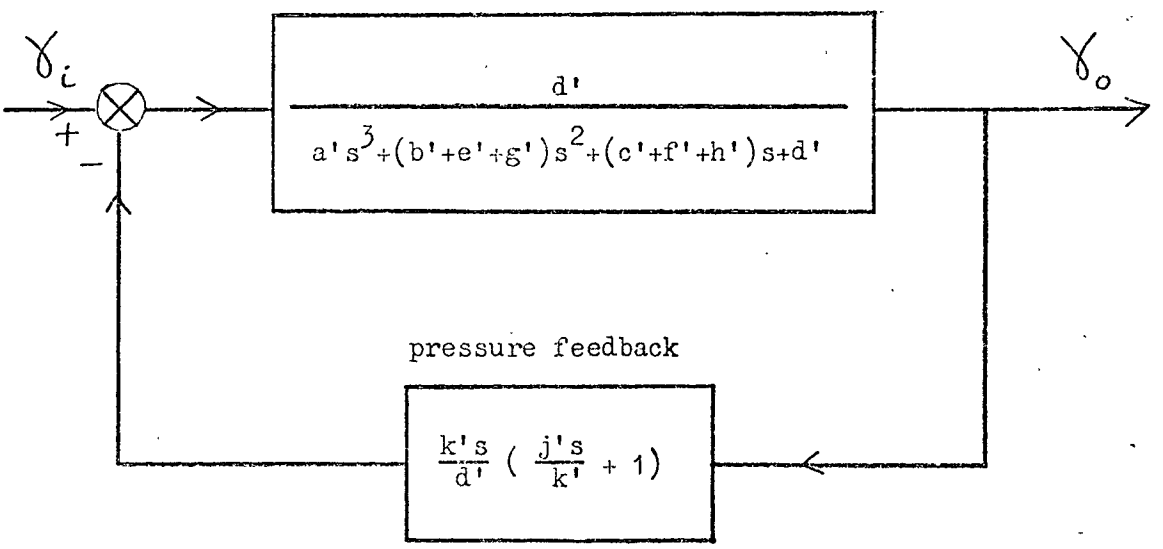

(b) Pressure feedback

Fig. 3.6 Block Diagrams used for Root Locus study of Stabilization

(Although at first sight it would seem unlikely that stabilizing feedback would be considered in case (a), it must be remembered that stabilization will be designed for the worst case and very large changes of parameters (i.e. load, piston position, etc.) are then possible, giving rise to widely different servo pole positions.)

The effect of various stabilization techniques will therefore be considered for each of these cases.

(a) Negative velocity feedback

The feedback transfer function in fig. 3.6(a) is simply $F(s) = K_v s$, and the alternative root locus diagrams are sketched in fig. 3.7. The Routh-Hurwitz Criterion can be used to confirm that the high gain asymptote is always to the left of the imaginary axis, even in case (c).

It is seen that negative velocity feedback stabilizes an already unstable servo (c) and never causes a stable servo, (a) and (b), to become unstable. On the other hand, the closed loop damping ratio of the complex poles decreases and the negative real pole approaches the origin as the velocity feedback is increased. This real pole may correspond to an excessively long time constant in the closed loop response.

(b) Negative acceleration feedback

In this case $F(s) = K_{ac} s^2$, and the root loci are sketched in fig. 3.8. Again the Routh-Hurwitz Criterion confirms that in (a) and (b) all poles remain in the left hand half of the s-plane for all values of K_{ac} and that in case (c) the system is stabilized at high values of K_{ac}. The negative real pole moves to the left and therefore becomes less significant as acceleration feedback increases. It is noticeable in cases (b) and (c) that, even with very high feedback gains, the transient response can never be overdamped, due to the double pole at the origin. Also in figs. 3.7(a) and 3.8(a)

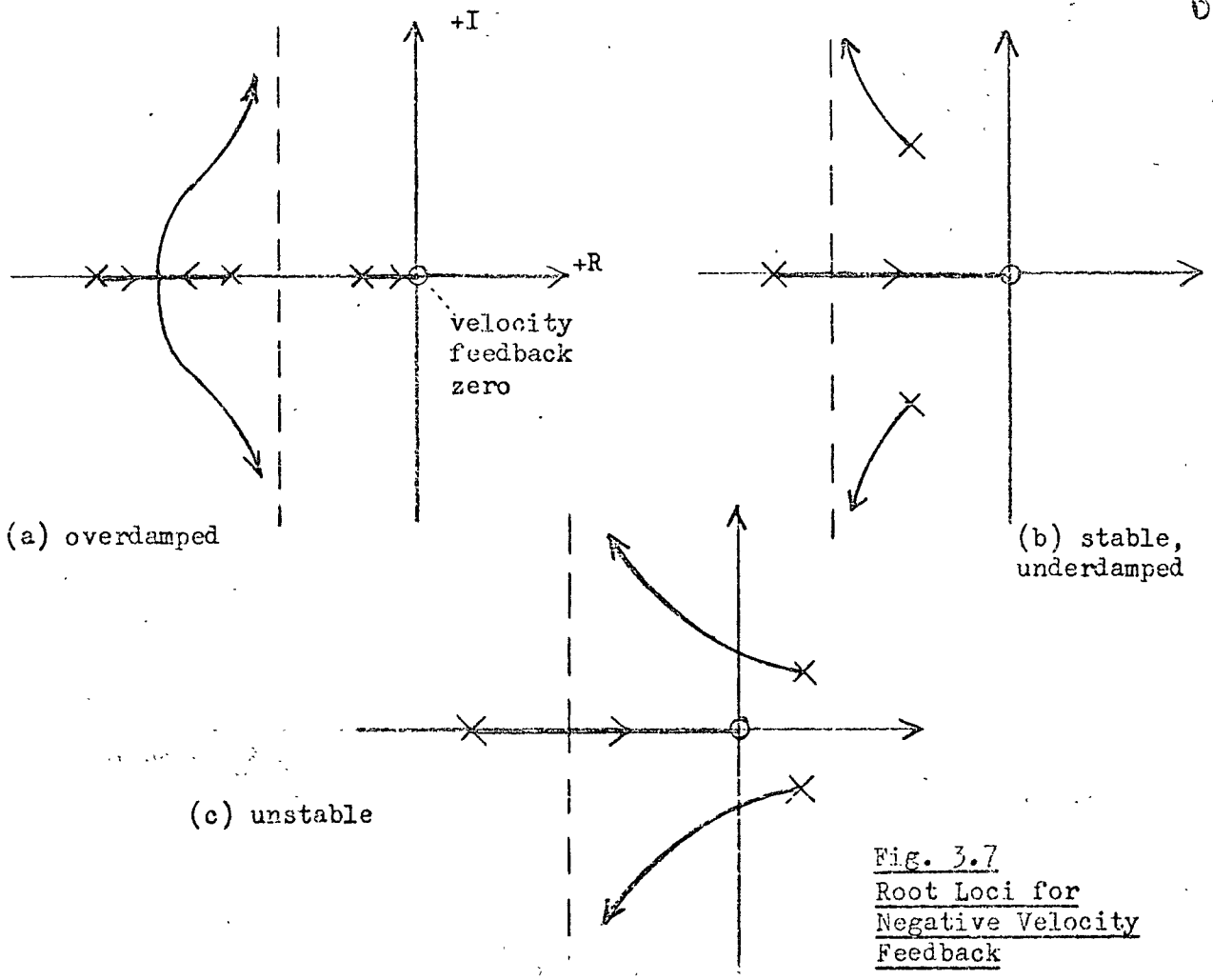

Fig. 3.7
Root Loci for
Negative Velocity
Feedback

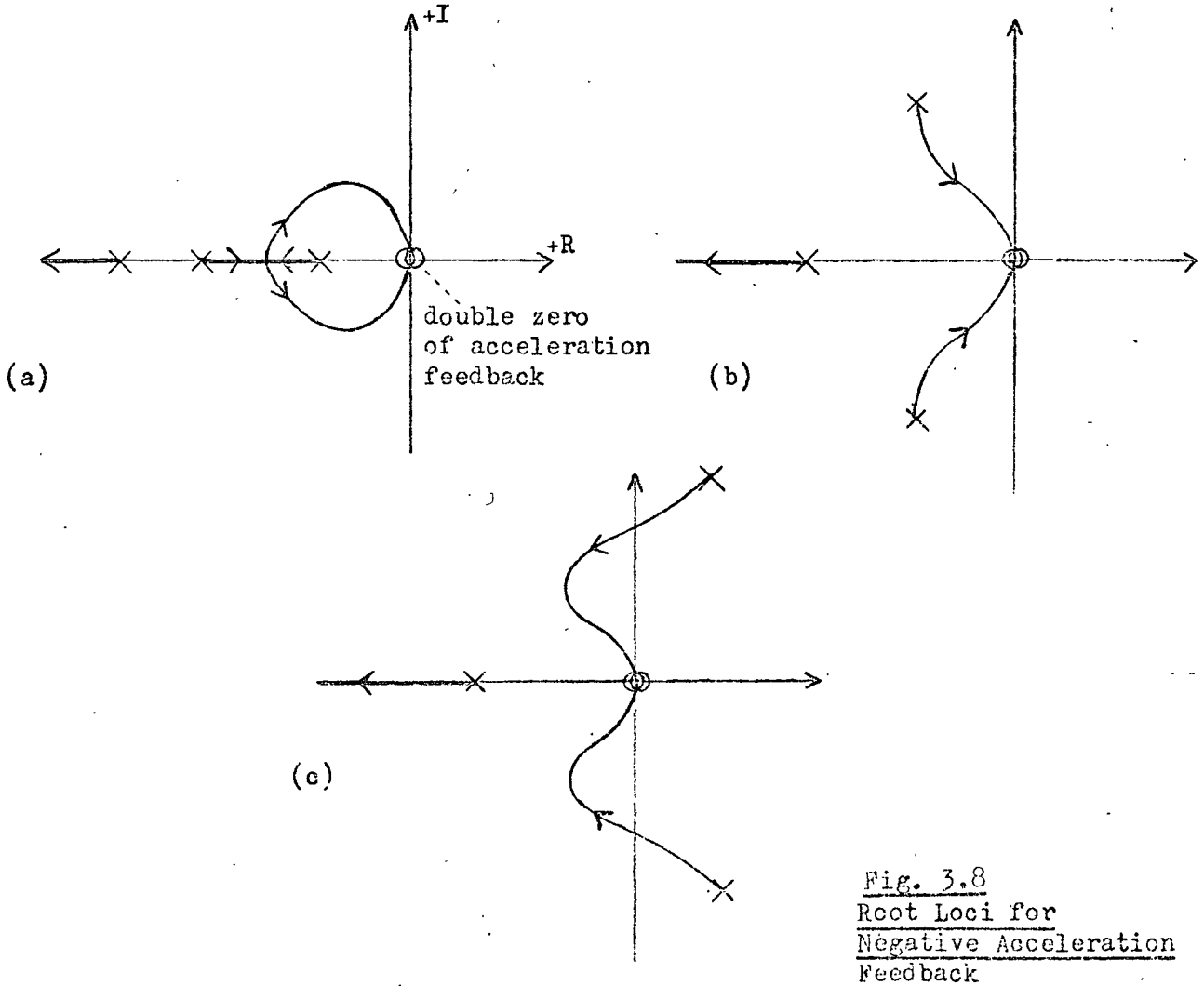

Fig. 3.8
Root Loci for
Negative Acceleration
Feedback

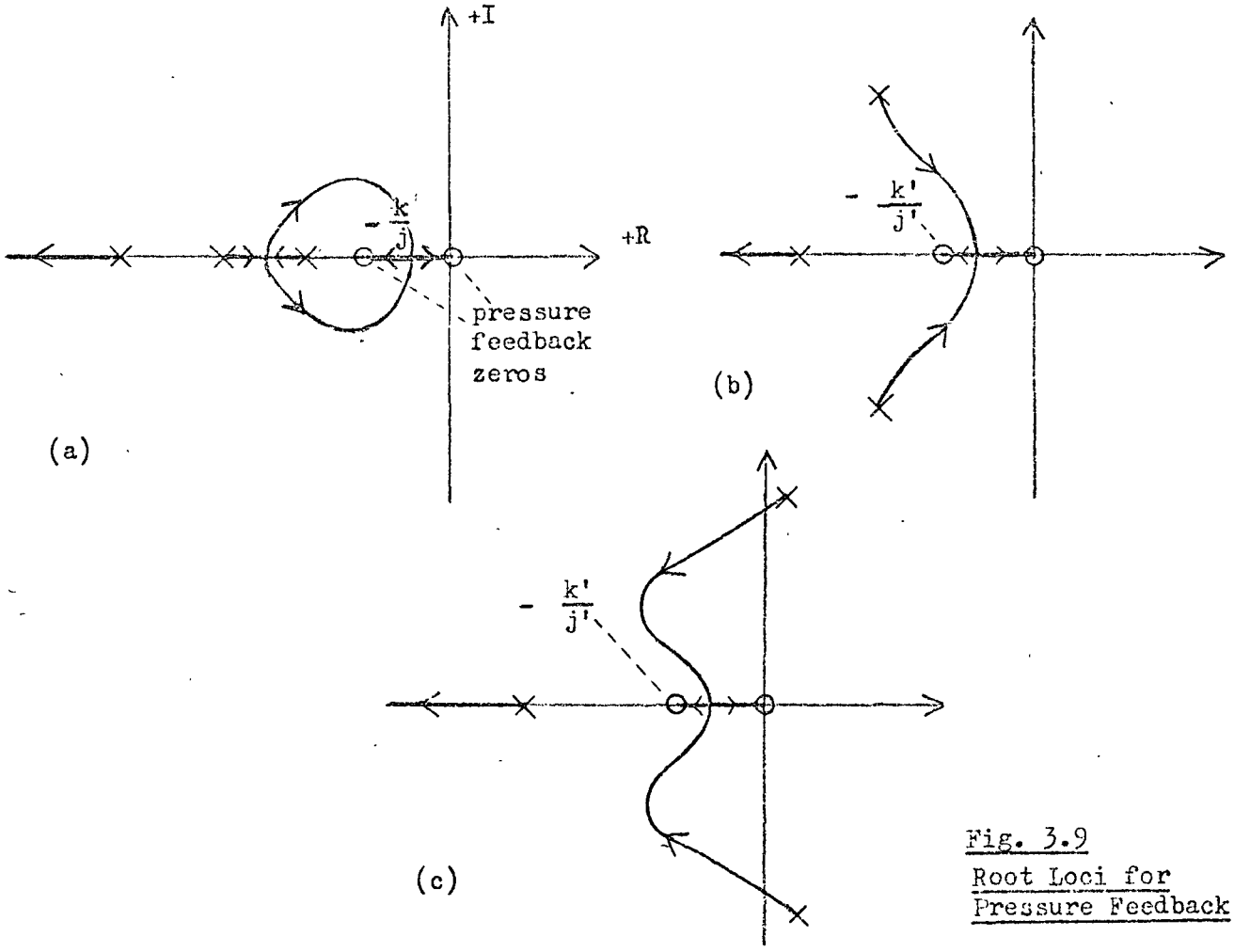

Fig. 3.9
Root Loci for
Pressure Feedback

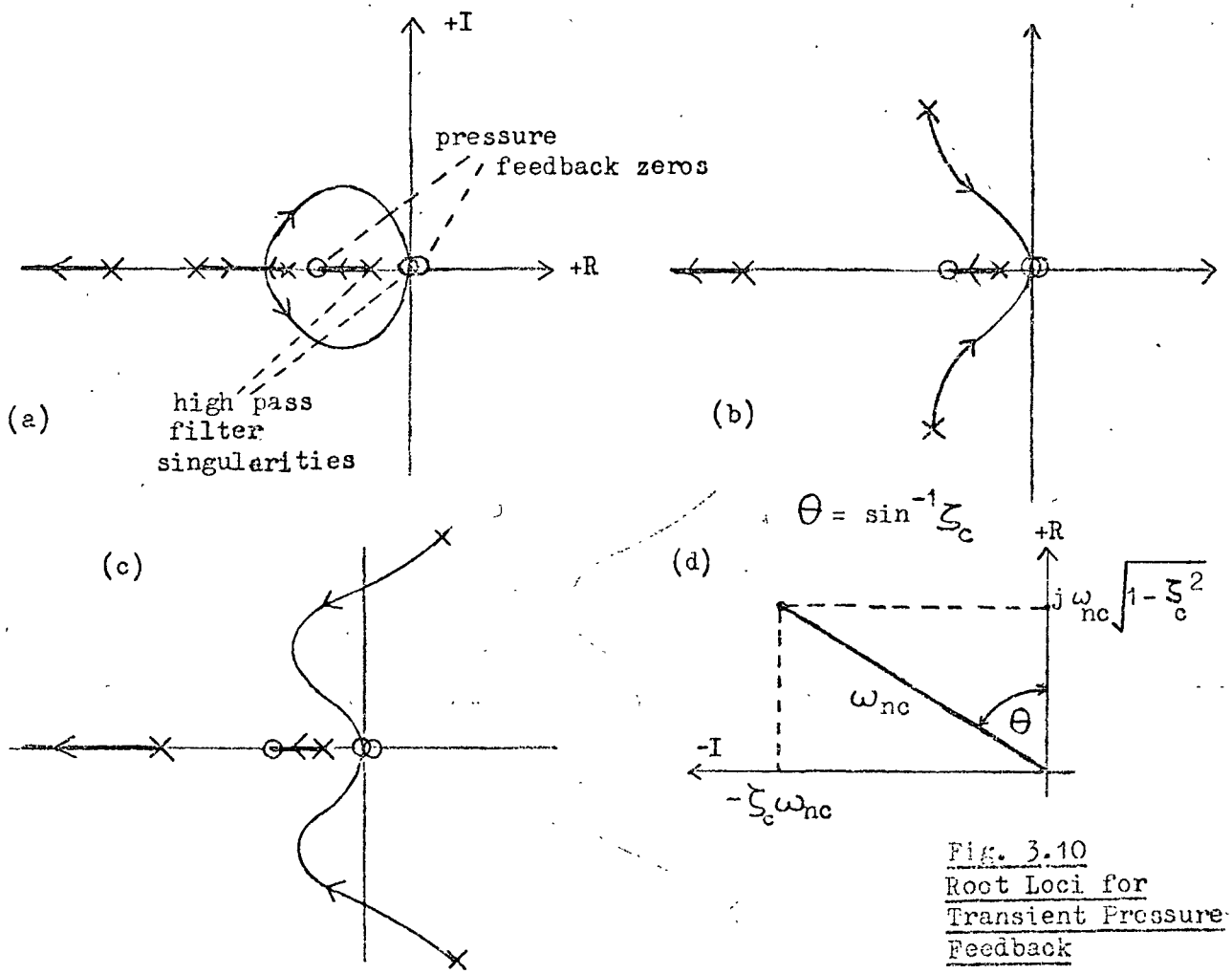

Fig. 3.10
Root Loci for
Transient Pressure
Feedback

it is seen that negative velocity or acceleration feedback can produce oscillatory behaviour even in a system for which the uncompensated response is overdamped. These oscillatory components probably constitute only a small part, which it may not even be possible to detect, of the closed loop response.

(c) Negative pressure feedback

Examination of fig. 3.6(b) shows the pressure feedback is equivalent to the simultaneous feedback of velocity (k') and acceleration (j'). (The coefficient of the velocity portion contains the viscous friction coefficient (b) and is sometimes equated to zero for the purposes of analysis in systems with little inherent damping (e.g. in reference 49).)

Here $F(s) = \frac{k'}{d'} (1 + \frac{j'}{k'} s) s$

The root loci for this case are shown in fig. 3.9.

Negative pressure feedback is seen to have a stabilizing influence and if the feedback gain is sufficiently high the response can be made heavily damped and even overdamped.

(d) Negative transient pressure feedback

Negative feedback of the first derivative of acceleration (known by environmental engineers as "jerk") is a destabilizing influence on the system of fig. 3.6(a). This is readily seen by reference to eqn. 3.77. While velocity feedback (k') and acceleration feedback (j') increase terms on the left hand side, jerk feedback increases the term a'. Using the same reasoning as for pressure feedback above, first derivative of pressure feedback is predominantly jerk feedback for systems with low inherent damping, and is therefore also destabilizing. This point is stressed as confusion exists over the parallel between transient pressure feedback and first derivative of pressure feedback. Reference 56 appears to advocate the latter while intending the former, and in reference 45 the substitution of

first derivative of pressure for transient pressure feedback, in order to simplify analysis, has the side-effect of reversing the stabilizing effect.

Transient pressure feedback is achieved by the use of a high-pass filter in series with pressure feedback, giving the transfer function

$$F(s) = \frac{\tau_p s}{1 + \tau_p s} \cdot \frac{k'}{d'} (1 + \frac{j'}{k'} s) s$$

If the time constant τ_p is very small, the filter acts as a differentiator giving the destabilizing effect of first derivative of pressure feedback discussed above. On the other hand, if τ_p is very large, the recovery after application of a steady load force (the reason for the insertion of the filter) takes an excessive time. Thus there is need for a compromise value of τ_p, such that the corner frequency of the filter ($\frac{1}{\tau_p}$) is less than the frequencies of pressure fluctuations to be encountered, or at least close enough to those frequencies to make the pressure feedback effective under dynamic conditions.

The root loci for such a system are shown in fig. 3.10. In addition to modifying the position of the existing poles, an additional negative real pole is introduced in this case.

The usefulness of these root loci for the prediction of system behaviour is discussed in Chapter 5, after experimental results have been presented.

(e) Negative velocity feedback for system with an additional time constant

In section 3.4.2, such feedback was said to have a destabilizing effect [49]. This is most easily illustrated with the root locus technique used above. If a fourth pole is added to fig. 3.7, the root loci shown in fig. 3.11 result and clearly velocity feedback in this case is destabilizing. (Case (b) from fig. 3.7 is used as an example but (a) and (c) show the same effect.)

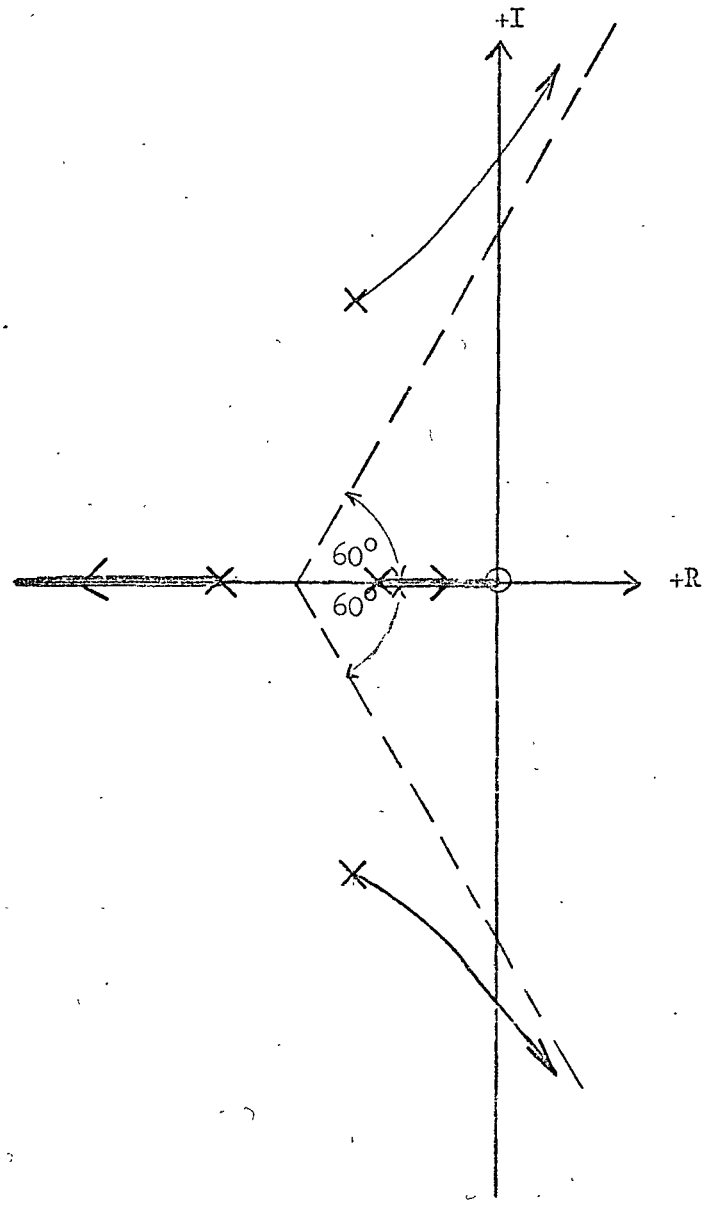

Fig. 3.11 Root Loci for System of Fig. 3.7(b) with an Additional Time Constant

CHAPTER 4 TESTS ON INDIVIDUAL COMPONENTS OF THE ELECTRO-PNEUMATIC SERVO

Extensive tests were conducted on the components of the experimental system, particularly the actuator.

The purpose of the tests described in this Chapter were to:

(a) investigate the validity of proposed equations

(b) obtain accurate data on the many parameters of the components, for use in the computer simulations (Chapter 6)

(c) enable judgements to be made on the relative importance of system features, to assist in the design of future systems.

4.1 The Loaded Actuator

An important part of the experimental work on the loaded actuator consisted of a series of "Impulse" Tests, conducted with the supply pipe to chamber 2 sealed (fig. 2.1). In these tests the load carriage was given a sharp thump (by hand) and the ensuing oscillations were observed and recorded. The test was repeated for a wide range of loads and piston positions. The results were used to explain the nature of the expansion and compression process in the actuator (section 4.1.4) and also as a contribution to understanding the effects of piston leakage and load friction (section 4.1.5).

Other tests to examine actuator friction were also conducted (sections 4.1.6 and Appendix 3). The nature of the inherent piston leakage and the effect of deliberately increased inter-chamber leakage were examined (sections 4.1.1 and 4.1.5). A study of the (nominally constant) pressure in chamber 1 is described in Appendix 6.

4.1.1 Inter-Chamber Leakage

(a) Inherent piston leakage

There was considerable leakage past the piston and this was measured using the arrangement shown in fig. A5.1. Full details of the tests conducted and results are given in Appendix 5. In these tests the static leakage flow was measured for various values of pressure difference and it was shown that a constant laminar leakage coefficient (L_b) could reasonably be used. The value calculated was

$$L_b = 1.3 \times 10^{-7} \ (ft^3/s)/(lbf/ft^2)$$

(Air volume measured at 64.7 lbf/in^2)

The relevance of this static figure to the dynamic case is discussed in section 4.3.4.

The leakage from chamber 1 past the piston rod bearing was always less than 10% of the corresponding piston leakage. (This leakage does not affect the analysis of the system in any way, since chamber 1 was held at constant pressure.)

(b) Additional leakage

Some tests were conducted in the presence of additional inter-chamber leakage. In this case a needle-type by-pass valve was used. The calibration of this valve is also described in Appendix 5, where it is shown that a reasonable, laminar approximation can be made for this additional flow. The maximum additional laminar leakage is about $6\frac{1}{2}$ times the inherent piston leakage.

4.1.2 Impulse Test Results

As explained in the introduction to section 4.1, a number of transient decays were recorded for different inertial loads and piston positions. In each case the load displacement and velocity

and the pressures in chambers 1 and 2 were recorded using an ultra-violet recorder. The natural frequency of the system was varied between 2.5 and 10 Hz during the course of these experiments. The maximum piston speed was about 60 ft/min.

In Chapter 3, linearization led to the development of a second order differential equation (eqn. 3.25) to describe these free vibrations. The results shown in table 4.1 were obtained, assuming these equations to apply, as follows:

(a) Measurement of undamped natural time period (τ_{np})

The damped natural time period was measured from each experimental record, and in all cases it was possible to check this time period for several successive oscillations. The several values obtained from a given record were found to agree, mostly within about 3% and in the worst cases within 5%. No tendency was observed for the time period either to increase or decrease as the oscillation decayed.

This value of τ_{dp} was then used to calculate τ_{np} from

$$\tau_{np} = \tau_{dp}\sqrt{1 - \zeta_p^2}$$

(b) Measurement of damping ratio (ζ_p)

The damping ratio was measured from the velocity and displacement records using a standard curve to obtain ζ_p from two successive peaks of the decaying curve. Again, this was repeated, for each record, for as many oscillations as possible.

The accuracy of the values for ζ_p obtained was considerably less than that for the time period measurement, discussed above. The values of ζ_p obtained from different parts of the same decay curve agreed within $\pm$ 10% of the average value in many cases (average value is shown in table of results). In some cases, however, the spread was as much as $\pm$ 20%. It was noticed that

again there was no tendency for the measured damping ratio to increase or decrease as an oscillation decayed.

A sample trace from the u-v recorder is shown in fig. 4.1. An oscillation is treated as a transient relaxation from an initial position I.

Additional information

(a) Maximum piston displacement, from initial position, during transient, for fig. 4.2 (i.e. displacement γ_{om} in fig. 4.1) ..... Between 0.15 in. and 0.4 in.

(b) Maximum piston displacement, from initial position, during transient, for fig. 4.3 ..... Between 0.2 in. and 0.4 in.

(c) Fluctuation of pressure (nominally constant) in chamber 1 (P_1) (see Appendix 6) ..... Less than ± 1¼% in P_1. Between 1% and 5% of the corresponding fluctuation in P_2.

(d) Fluctuation of pressure (P_2) in chamber 2 ..... Between ± 4 and ± 20 lbf/in^2

(e) Maximum change in V_2 during a transient ..... + 20%/-12%

(f) Values of ζ_p marked * in table 4.1 are not plotted in fig. 4.3. In these cases the damping ratio could not be accurately obtained, due to the small amplitude of the experimental traces. Therefore an approximate ζ_p is tabulated. This was only used in the calculation of τ_{np} from τ_{nd} (where an approximate value for ζ_p was acceptable).

(g) There was a slow drift of the piston throughout each test, due to the slight difference in areas of the two sides of the piston

Fig. 4.1 Impulse Test - Sample Trace

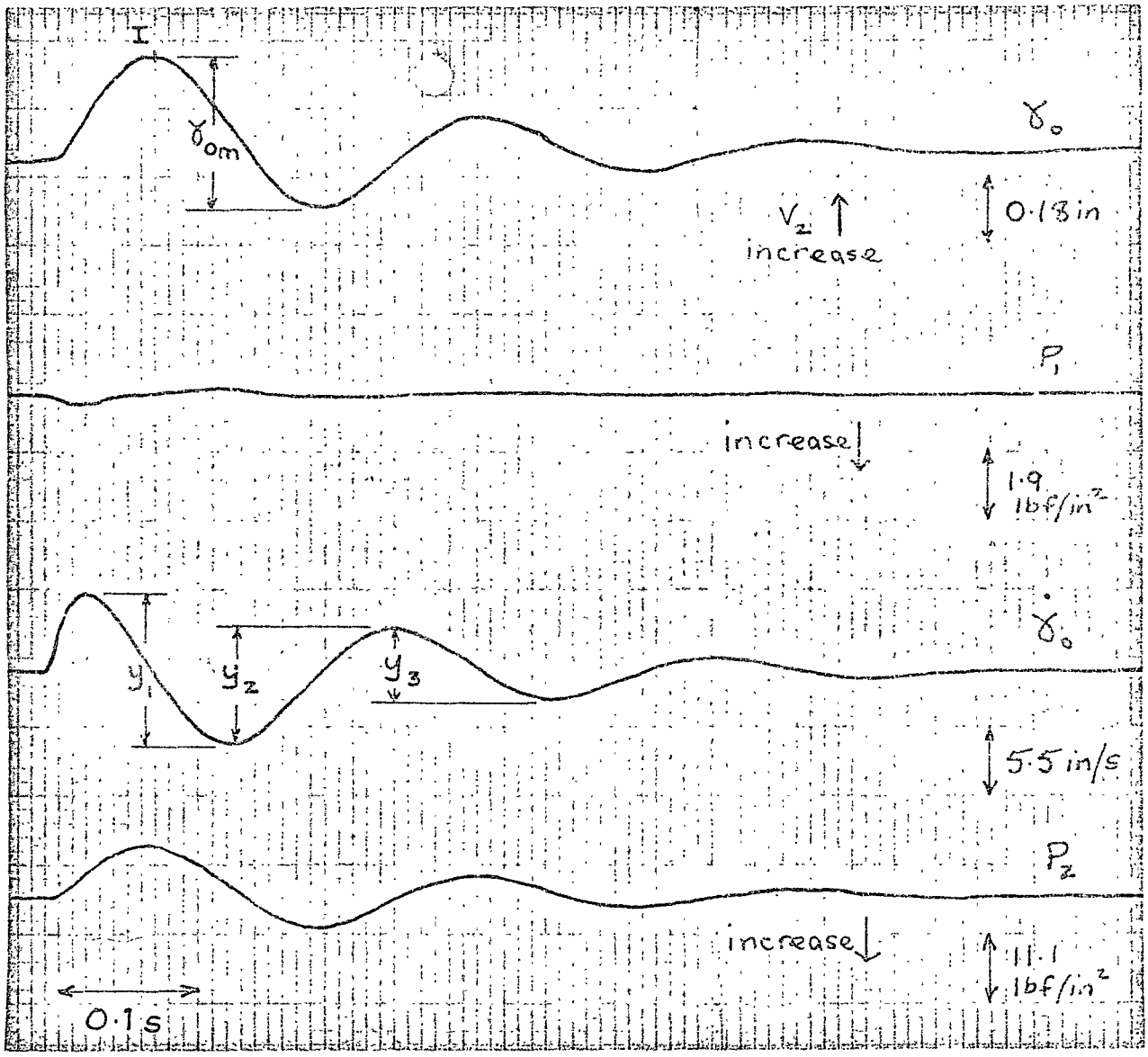

m_L = 28.7 lb

V_{2a} = 2.8×10^{-3} ft^3

(<3%). An average figure (V_{2a}) for the chamber volume is tabulated in Table 4.1. The magnitude of this drift in volume, as a fraction of average volume, obviously depends on the position of the piston at which an individual test takes place. For very low values of V_{2a} this drift constituted not more than 5% of V_{2a}, while for very high values of V_{2a} it was less than 1%.

(h) In an independent test in which a spring balance was used to pull the unloaded carriage by hand at a low, approximately constant, velocity, the spring balance reading fluctuated between 1 and 3 lbf.

4.1.3 Gas Expansion and Compression in the Controlled Chamber

A number of publications in this and other fields have included references to the nature of the gas compression and expansion processes during transients. Shearer [4c] developed equations to describe the cylinder dynamics for a similar, though high pressure (800 lbf/in^{2}g.) system for the two extreme cases of isothermal and adiabatic changes. Shearer subsequently used the adiabatic case, as a basis for an analogue computer study of a system with a closed loop natural frequency of about 4 or 5 Hz, saying that the heat transfer rate is negligible in most fast-acting systems, but it may be appreciable in slower acting systems. Skinner andWagner [57] showed experimentally that for the process of charging and discharging constant volume tanks with air, the polytropic exponent (n) approached 1.0 (isothermal) for a very slow charging rate and increased as the charging rate increased.

Chelomey [6] referred to "experimental investigations" which have shown that the operation of such pneumatic systems is described by "polytropy which is close to the adiabat" (translation). No reference was quoted and the experimental results were not given. Many subsequent workers, including Vaughan [9], Brann [20],

Cutland [23], Burrows [25], Raven [44] and Botting et al [10] have followed Shearer's suggestion, and have assumed an adiabatic charging process, and therefore used n = 1.4. Levenstein [5] developed highly simplified equations, assuming constant temperature conditions (n = 1.0).

In a comprehensive design study which included analogue computer simulation, Andersen [24] also assumed isothermal conditions to apply to a double acting piston actuator. The closed loop transient frequency, in this case, was about 15 Hz.

Hirtreiter [59] in a review paper on the subject of air springs, in which the air is confined within a rubber and fabric container, stated that a polytropic spring rate is most common at natural vibration frequencies of 60 cycles per minute or less. He implied that for higher frequencies a "dynamic or adiabatic" rate applies.

Towill and Carne [60] developed a design procedure for obtaining a pneumatic cylinder stiffness for any piston position provided that a polytropic index (between 1.0 and 1.4) is assumed.

In another, related field, reciprocating air compressor cylinders are either water cooled or finned and air cooled, in order to increase the heat transfer during compression and reduce the polytropic index. With good cooling the value of n is usually between 1.2 and 1.3 [61] whereas the compression work is a minimum when n = 1.0. For a medium size, air-cooled, single cylinder, reciprocating compressor, of the general type which forms the majority of compressors manufactured in this country, typical figures are: Speed 1500 rev/min, mean piston speed between 600 and 1000 ft/min, Stroke 4 inch, polytropic index of expansion 1.25 to 1.29, polytropic index of compression 1.36 to 1.39 [62]. The low index for expansion indicates the relatively good heat transfer

Table 4.1 Impulse Test Results

Impulse Test Number	Volume of Chamber 2 $V_{2a}(ft^3)$* x 10^{-3} (measured)	Load Mass m_L(lb) (measured)	Damping ratio of oscillation ζ_p (measured from trace)	Time period of damped oscillation τ_{dp}(s) (measured from trace)	(Natural undamped time period)^2 $\tau^2_{np}(s^2)$ x 10^{-2} (calculated from ζ_p and τ_{dp})
I1	0.66	18.7	0.125	0.10	0.98
I2	1.70	18.7	0.120	0.15	2.20
I3	0.64	38.7	0.14*	0.14	2.04
I4	0.74	38.7	0.100	0.15	2.23
I5	0.65	38.7	0.103	0.14	1.94
I6	3.00	38.7	0.125	0.29	8.30
I7	2.98	48.7	0.140	0.32	10.00
I8	0.59	48.7	0.11*	0.15	2.22
I9	0.69	68.7	0.125*	0.19	3.50
I10	1.49	68.7	0.14*	0.27	7.15
I11	2.99	68.7	0.147	0.38	14.20
I12	0.54	33.7	0.11*	0.12	1.42
I13	1.61	33.7	0.110	0.19	3.58
I14	2.96	33.7	0.140	0.26	6.65
I15	1.26	33.7	0.095	0.175	3.03
I16	2.61	33.7	0.133	0.25	6.12
I17	0.93	48.7	0.10*	0.18	3.22
I18	2.19	48.7	0.100	0.27	7.20
I19	2.59	48.7	0.120	0.295	8.60
I20	2.94	58.7	0.110	0.34	11.40
I21	1.79	58.7	0.085	0.27	7.25
I22	1.04	58.7	0.085	0.21	4.38
I23	1.01	68.7	0.089	0.225	5.04
I24	2.39	68.7	0.085	0.34	11.50
I25	2.02	68.7	0.103	0.31	9.53
I26	2.06	18.7	0.154	0.165	2.66
I27	1.85	8.7	0.18*	0.11	1.18

* See note (g) in section 4.1.2

* See note (f) in section 4.1.2

which occurs as the very small volume of air trapped in the clearance space, is rapidly expanded, prior to the induction of fresh air. While these observations on air compressors are not directly relevant to the present study, they must be considered since in both cases expansion and compression processes occur, which can be represented by the expression

$$Pv^n = \text{constant.}$$

The main purpose of the Impulse tests described in section 4.1.2 was to establish the appropriate value of n for the particular circumstances of the present experimental system.

4.1.4 Evaluation of the Polytropic Exponent

A value for n, the polytropic exponent, can be obtained from the Impulse Test results as follows:

Eqn. 3.29 can be rewritten

$$\gamma_{np}^2 = \frac{(2\pi)^2}{nP_{2a}A^2} \cdot (V_{2a}m_L)$$

i.e. a graph of γ_{np}^2 vs$(V_{2a}m_L)$ will be a straight line with

slope $\frac{4\pi^2}{nP_{2a}A^2}$.

This graph is shown in fig. 4.2.

A straight line has been drawn through these points, yielding a value for n, as follows:

Measured gradient = $21.8\ \text{lbf}^{-1}\ \text{ft}^{-2}$

Gradient = $\frac{4\pi^2}{nP_{2a}A^2} = \frac{28.0}{n}\ \text{lbf}^{-1}\ \text{ft}^{-2}$

$\therefore\ n = \frac{28.0}{21.8}$

i.e. $n = 1.28$

In addition, for reference, the straight lines corresponding to an adiabatic (n = 1.4) and an isothermal (n = 1.0) process are

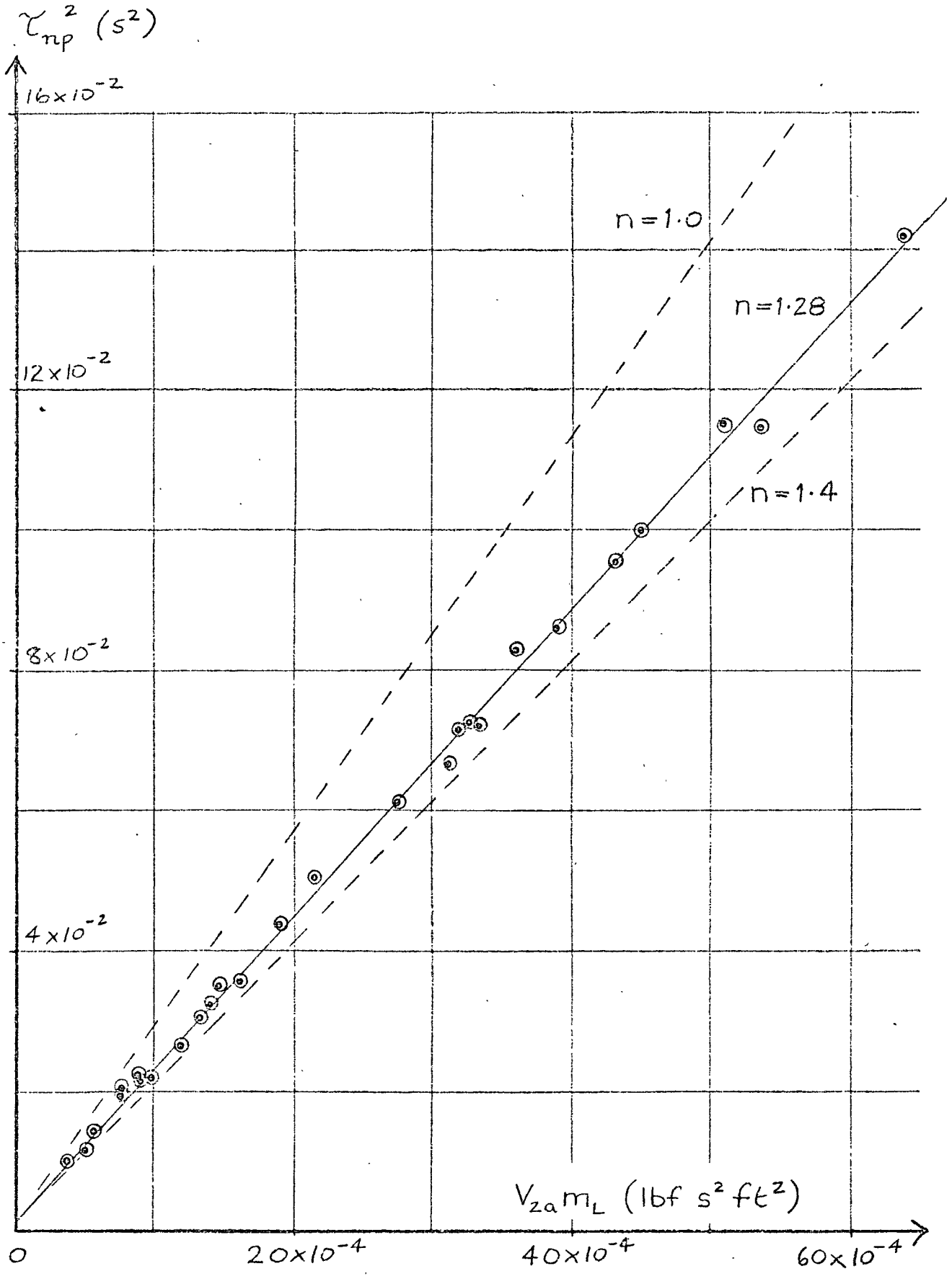

Fig. 4.2
Impulse Tests

Showing the variation of Undamped Natural Time Period with Chamber Volume and Load Mass

shown in fig. 4.2.

This figure and its derivation are further discussed in section 4.3.2.

4.1.5 Actuator and Load Friction - Impulse Tests

As explained earlier, a low-friction actuator and low friction load bearings were used for the experimental system, but of course a small friction force remained. It is quite easy to gather data relating to friction, for a practical pneumatic system, on the other hand it is very difficult to express this data in a suitable form for the purpose, say, of a computer simulation. This is because the friction is not only non-linear but also a function of more than one variable. The results of a number of tests on the experimental system are presented below and in Appendix 3, and their significance is discussed in section 4.3.3.

(a) Eqn. 3.30, which rests on the assumption that the damping for the Impulse Tests was due solely to viscous friction and leakage, can be written in the form

$$\zeta_p = C_1\sqrt{\frac{V_{2a}}{m_L}} + C_2\sqrt{\frac{m_L}{V_{2a}}} \qquad \text{where } C_1 = \frac{b}{2A\sqrt{nP_{2a}}}, \quad C_2 = \frac{L\sqrt{nP_{2a}}}{2A}$$

If ζ_p is plotted against $\sqrt{\frac{V_{2a}}{m_L}}$, the resultant curve is the sum of two components:-

I) a straight line due to viscous friction, and

II) part of a rectangular hyperbola due to piston leakage.

The experimental results are plotted in this form in fig. 4.3. The inherent piston leakage coefficient L_b applies here and is known from section 4.1.1:

$$L_b = 1.3 \times 10^{-7} \ (ft^3/s)/(lbf/ft^2)$$

and so C_2 was calculated and part II of the above-mentioned curve

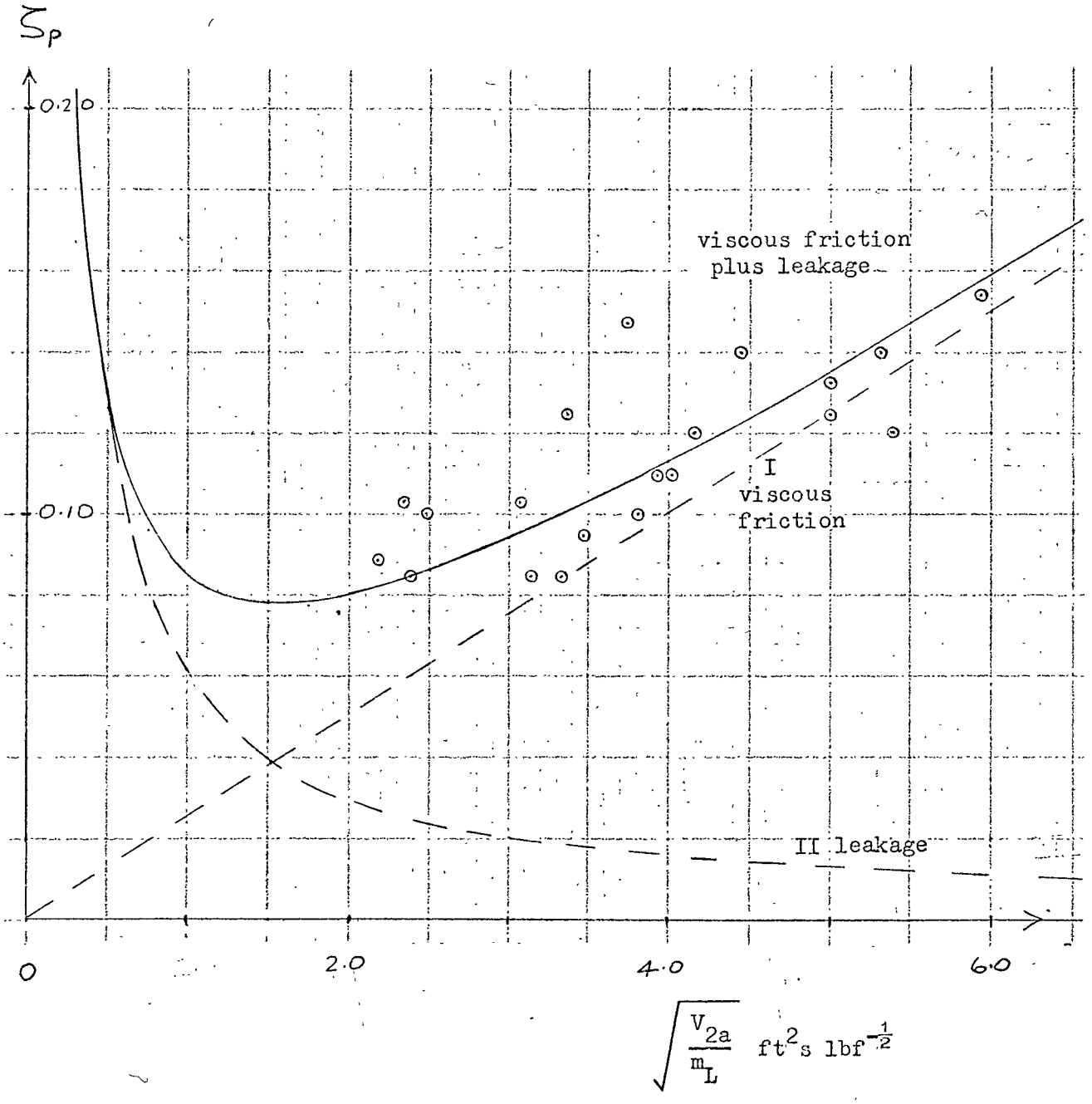

Fig. 4.3 Impulse Tests

Showing the variation of damping ratio with Chamber Volume and Load Mass

drawn in fig. 4.3.

By trial and error a suitable value of C_1 was selected to give the best "fit" with experimental points in fig. 4.3. Using this value of C_1, a value for the load viscous friction coefficient (b) could be calculated.

Gradient of line I in fig. 4.3 is

$$C_1 = 2.5 \text{ ft}^{-2} \text{ lbf}^{\frac{1}{2}}\text{s}.$$

And from eqn. 3.30

$$C_1 = \frac{b}{2A\sqrt{nP_{2a}}} = \frac{b}{2.67} \text{ ft}^{-2} \text{ lbf}^{\frac{1}{2}}\text{s}.$$

Giving, $$b = 6.7 \text{ lbf/(ft/s)}$$

(b) The Impulse Tests were repeated with a piston by-pass needle valve* in position, for various amounts of leakage. Thus the effect of varying the leakage coefficient (L), on the behaviour of the system was demonstrated. The results are shown in table 4.2. For these tests, constant values of V_{2a} and m_L were maintained. Assuming that the friction is wholly viscous, eqn. 3.30 becomes

$$\zeta_p = C_3 b + C_4 L \qquad 4.1$$

where $C_3 = \frac{1}{2A}\sqrt{\frac{V_{2a}}{nP_{2a}m_L}}$ and $C_4 = \frac{1}{2A}\sqrt{\frac{nP_{2a}m_L}{V_{2a}}}$ } constants for this series of dynamic leakage tests

Now if impulse tests are carried out for various values of L, then ζ_p and γ_{dp} can be determined from the individual transient decay records as before.

These results can be considered as follows:-

(a) If ζ_p is plotted against L, a straight line will result, with slope C_4 and intercept $C_3 b$.

(b) The undamped natural frequency (ω_{np}) is a function of the piston leakage (eqn. 3.27). If this dependence is

* For calibration see Appendix 5

Test Number	Bypass valve setting (rotations)	Net leakage Coefficient (from Appendix 5)	Measured time period τ_{dp}	ζ_p (measured)
I28	7	$L_b = 1.3 \times 10^{-7}$ $(ft^3/s)/(lbf/ft^2)$	constant throughout	0.13
I29	5	2.1 L_b	i.e. all	0.155
I30	6.4	L_b	results	0.125
I31	5.84	1.25 L_b	between 0.27s	0.14
I32	5.6	1.45 L_b	and 0.28s with	0.135
I33	5.3	1.7 L_b	no discernible	0.145
I34	4.4	3.2 L_b	pattern	0.16
I35	4	4.4 L_b		0.165
I36	3	7.6 L_b		0.225
I37	3.4	5.9 L_b		0.20

Table 4.2 Impulse Tests with Additional Leakage - Results

($V_{2a} = 2.25 \times 10^{-3}$ ft^3 see Note 1 below, $m_L = 48.7$ lb)

Notes on table 4.2 and fig. 4.4

(1) The volume of the left-hand chamber increased slightly during each Impulse Test, due to the drift caused by inter-chamber leakage. This effect was also observed during the main Impulse Tests. The average value (V_{2a}) was used for all calculations. The drift in volume varied from $<$ ± 1% for no additional leakage to ± 4% for maximum leakage.

(2) Accurate interpretation of the trace from test I37 was difficult due to the rapid transient decay. An estimate of the likely range of possible error in this result is shown in fig. 4.4. Despite this wide tolerance it has been included, for reference. The range of error associated with a more typical result, test I35 ($L = 4.4\ L_a$) has also been shown, for comparison.

(3) The maximum pressure difference across the piston during these tests never exceeded the "linear leakage" range illustrated in fig. A5.6 and in all cases was between 4 and 10 lbf/in^2.

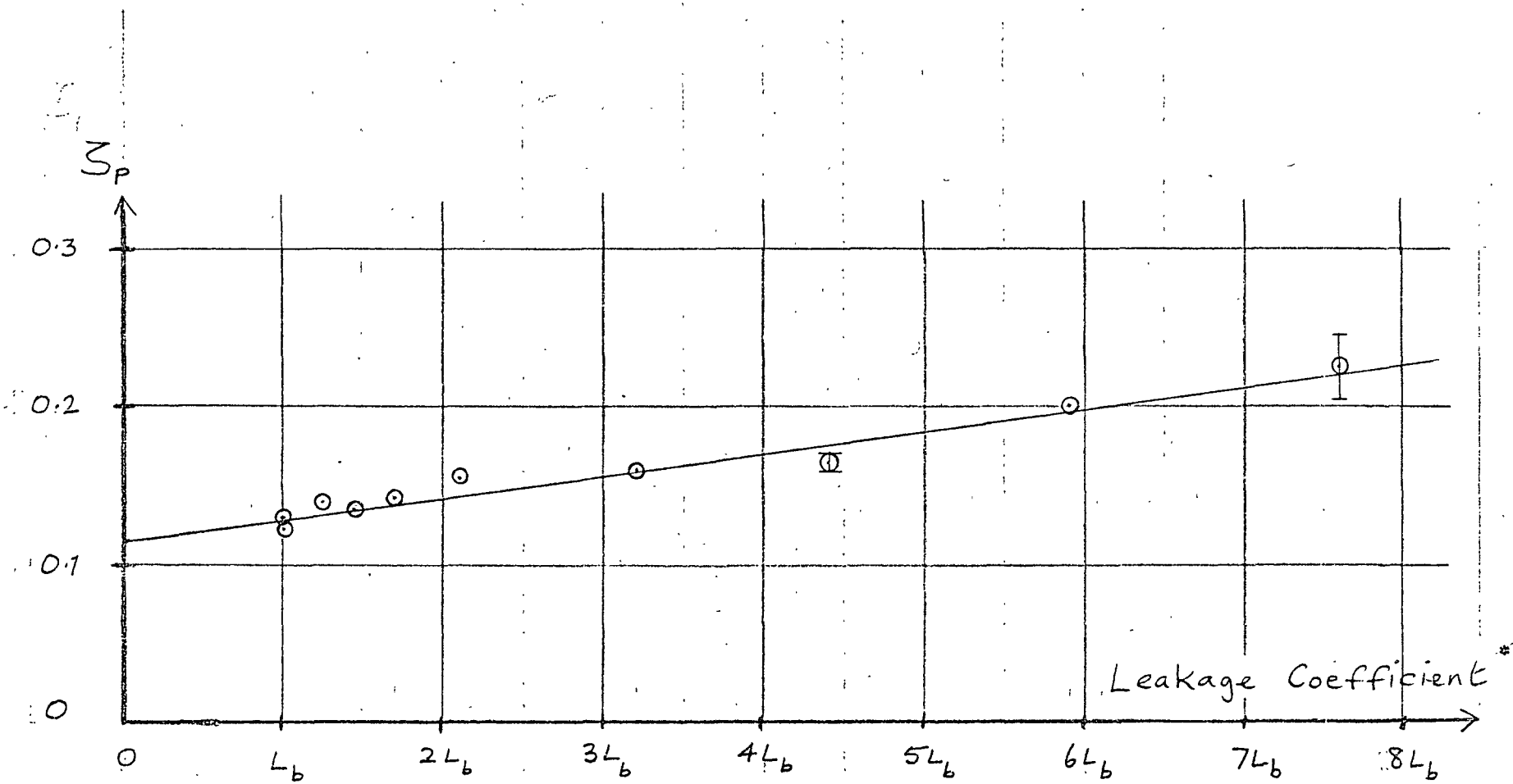

(* based on static calibration)

Fig. 4.4

Impulse Tests

Showing the Effect of Additional Leakage on the Damping Ratio

slight, i.e. $A^2 \gg Lb$, ω_{np} will be constant throughout these tests.

The measured values of the damping ratio (ζ_p) are plotted against leakage coefficient (L) in fig. 4.4. According to eqn. 4.1 these points fall on a straight line and such a line has been drawn. The slope of this line can be predicted from eqn 4.1 as

$$C_4 = \frac{1}{2 \times 1.23 \times 10^{-2}} \cdot \sqrt{\frac{1.28 \times 9300 \times 1.51}{2.25 \times 10^{-3}}}$$

$$= \underline{1.14 \times 10^{-5} \text{ lbf s ft}^{-5}}$$

and the slope of the line measured from fig. 4.4 is

$$C_4 = \underline{1.12 \times 10^{-5} \text{ lbf s ft}^{-5}}$$

Also, from the intercept on the vertical axis, $\zeta_p = 0.115$, a value for b can be calculated, in this case $\underline{b = 8.0 \text{ lbf/(ft/s)}}$

4.1.6 Drift Test

In this case, the system of fig. 3.1 was observed in the absence of any disturbances and after the decay of any transients. Under these conditions, a slow, constant velocity drift of the piston, from left to right, occurred. This drift velocity was measured, using the displacement transducer and ultra-violet recorder:-

(i) with inherent piston leakage only,

(ii) with a calibrated by-pass valve, connecting chambers 1 and 2 (see Appendix 5).

The analysis in section 3.1.6 shows how the results of these drift tests can be used to evaluate the friction force at the actuator and load. The load mass was 48.7 lb in each case and the results are shown in table 4.3.

Specimen calculation for test D1

Assuming, $b = 6.7$ lbf/(ft/s) (determined in section 4.1.5),

and $P_{1g} = 50 \text{ lbf/in}^2 \equiv 7200 \text{ lbf/ft}^3$.

Table 4.3

Test Number	Measured Drift Velocity (ft/s)	By-pass valve setting (rotations)	Net leakage Coefficient (from Appendix 5)	F_F (lbf) (derived)
D1	6.15×10^{-4}	-	$L_b = 1.3 \times 10^{-7}$ $(ft^3/s/(lbf/ft^2)$	1.79
D2	6.8×10^{-3}	4	$4.4\ L_b$	0.70
D3	12.2×10^{-3}	3	$7.6\ L_b$	0.64

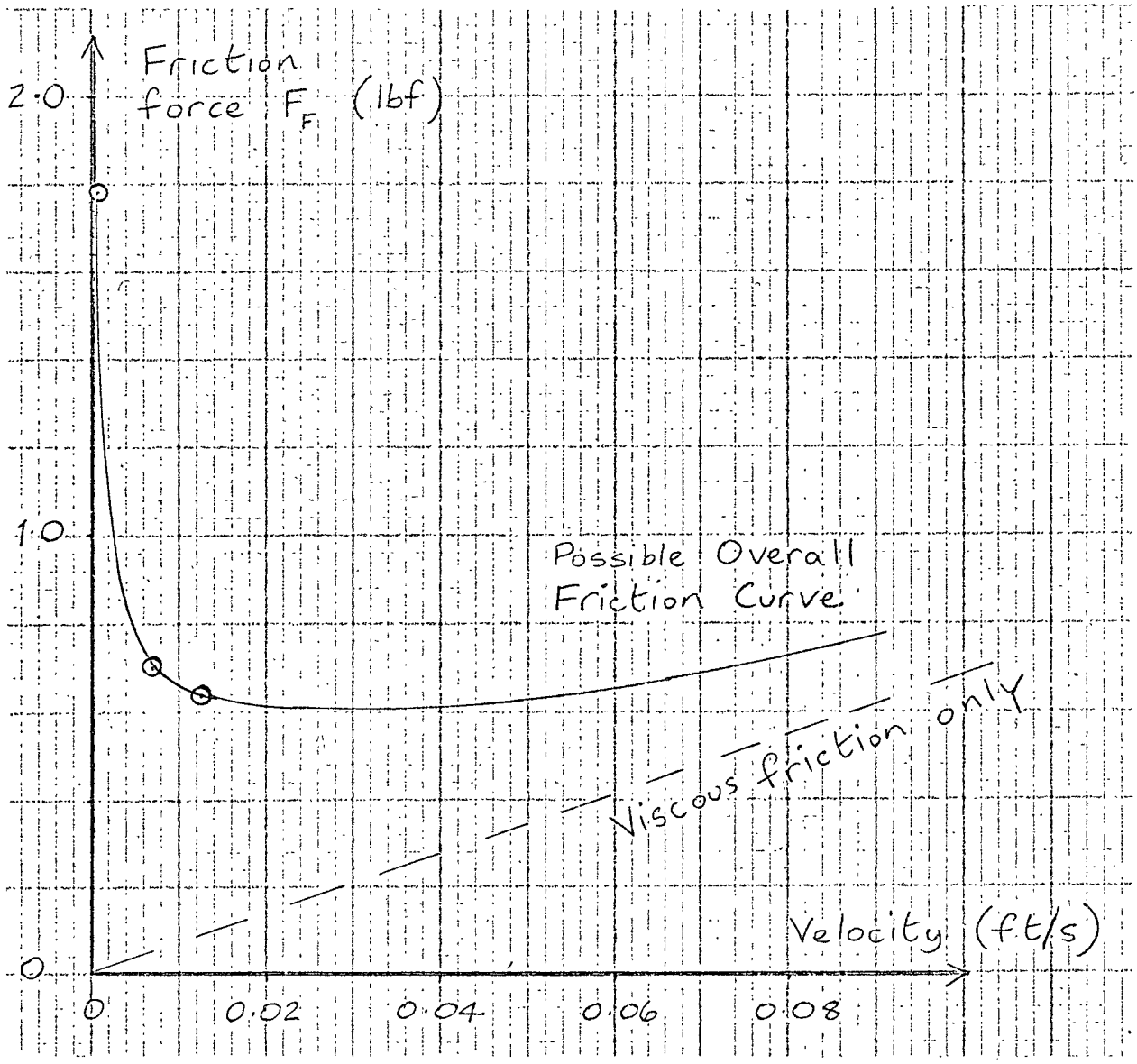

Fig. 4.5 Drift Tests. Variation of friction force with velocity

eqn. 3.33 becomes

$$\Delta P = \frac{1.23 \times 10^{-2} \times 6.15 \times 10^{-4}}{1.3 \times 10^{-7}}$$

$$= 58.1 \text{ lbf/ft}^2$$

and substituting this in eqn. 3.34

$$(7200 \times \frac{0.05}{144}) - (1.23 \times 10^{-2} \times 58.1) = F_F$$

$$2.5 - 0.715 = F_F$$

i.e. $\underline{F_F = 1.79 \text{ lbf}}$

Interpretation of results

Only three results were obtained but these are plotted in fig. 4.5 as some indication is given of the nature of friction at these low velocities.

Measurement of friction forces at very low velocities is very difficult and this Drift test, using controlled leakage, offers a possible solution. The idea has since been pursued by Rashid (63) and is further discussed in Appendix 3.

The curve through the three results obtained is extrapolated in fig. 4.5 to show a possible interpretation, using the value for viscous friction coefficient established in section 4.1.5.

These results are fully discussed later in section 4.3.3 but it is apparent from fig. 4.5 that the Coulomb friction force is below $\frac{1}{2}$ lbf.

4.1.7 Analogue Computer Tests

A brief analogue computer study was conducted to examine the effect which Coulomb friction would have on the traces obtained in the Impulse Tests. It was noted in section 4.1.3 that the decay curves showed a characteristic viscous damped shape (i.e. approximately constant ratio of any two successive peaks) and the limited results

from section 4.1.6 suggest that Coulomb friction was less than 1 lbf. Therefore, the present test was conducted with a small Coulomb friction force in order to estimate the maximum amount of Coulomb friction which could pass unnoticed in the Impulse Test results.

The computer was connected to solve the second order differential equation for a mass-spring system

$$m_L \frac{d^2 \gamma_o}{dt^2} + \frac{bd\,\gamma_o}{dt} + F_c(\text{sgn}\,\frac{d\,\gamma_o}{dt}) + S\,\gamma_o = 0$$

Three separate decay curves were recorded, for relaxation from an initial displacement for,

(i) viscous friction only, ($F_c = 0$)

(ii) Coulomb friction only, ($b = 0$)

(iii) viscous and Coulomb friction, with magnitudes as used in (i) and (ii).

For <u>case (i)</u>, the circuit shown in fig. 4.6 was arranged with approximately the potentiometer setting shown in that figure. The actual values of ζ and ω_d were measured from the resulting trace (fig. 4.7) using the same technique as had been used on the traces from the loaded actuator.

For <u>case (ii)</u>, potentiometers were set to give a small amount of Coulomb friction and zero viscous friction. Again, actual values were established by making measurements from the resulting decay curve (fig. 4.8).

For <u>case (iii)</u>, the values for b and F_c established in case (i) and (ii) above were used together and from the transient decay curve (fig. 4.9) the magnitudes of peak amplitude measured.

<u>Results</u>

Initial displacement	= 0.2 in.	Initially specified, to correspond approximately with actual experimental results.
b	= 6.7 lbf/(ft/s)	

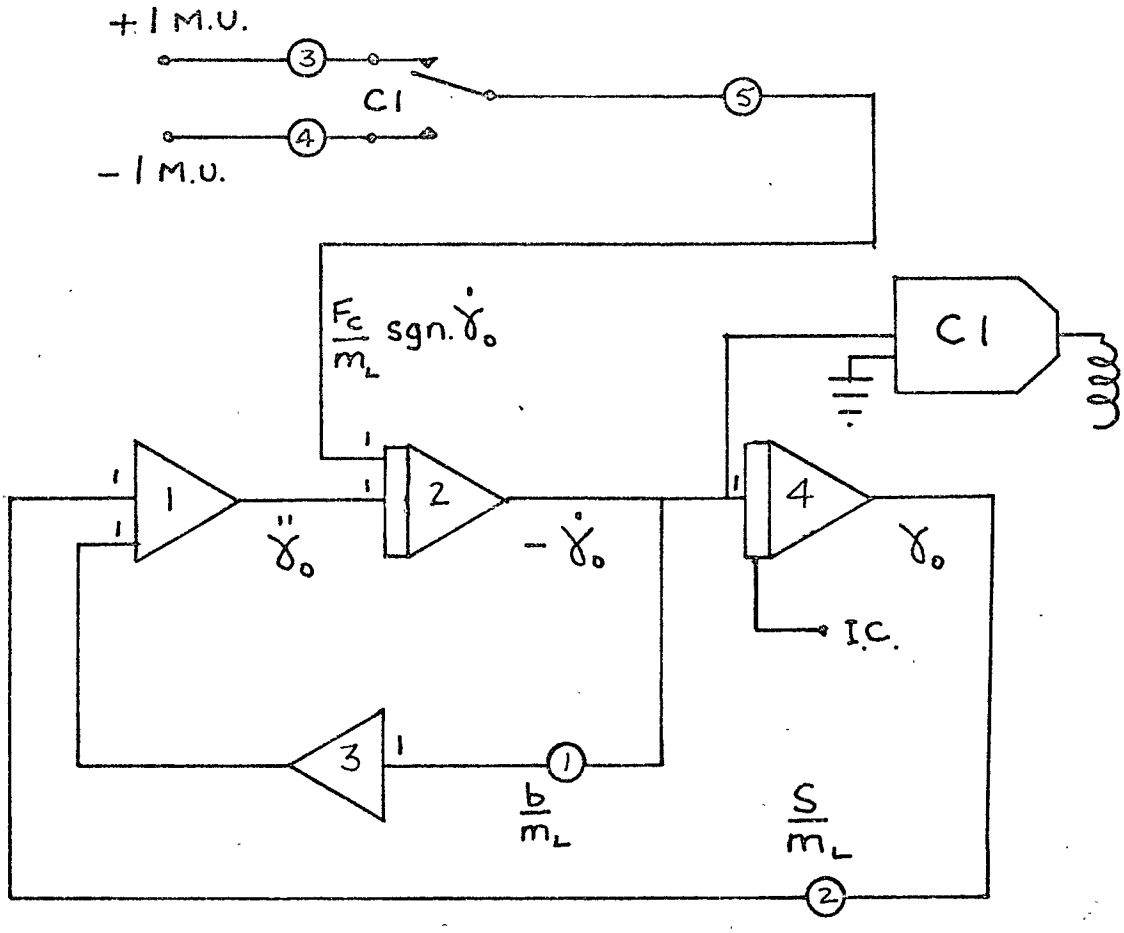

Approximate Potentiometer Settings

Potentiometer	Case (i)	Case (ii)	Case (iii)
1	0.05	0	0.05
2	0.3	0.3	0.3
3	0	0.2	0.2
4	0	0.2	0.2
5	0	0.1	0.1

Fig. 4.6 Actuator Friction - Analogue Computer Circuit

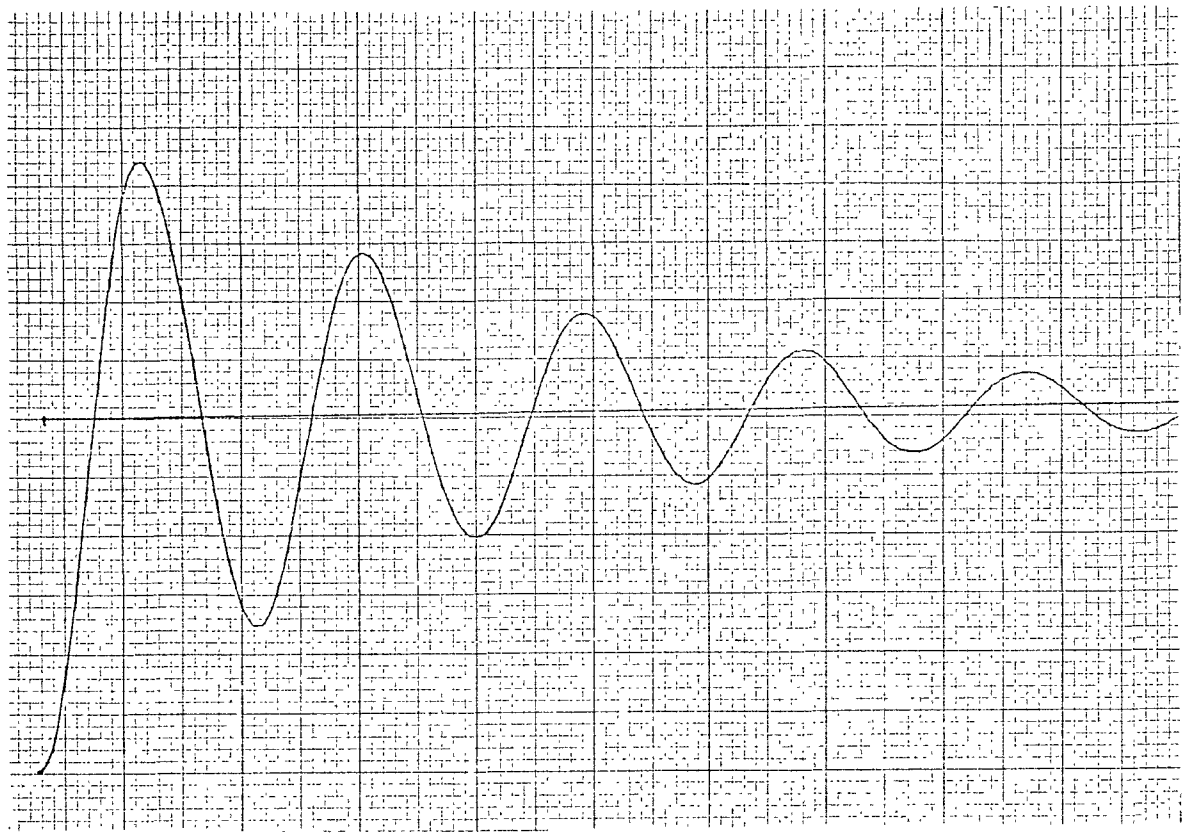

Fig. 4.7 Analogue Computer Tests
Case (i) Viscous friction only

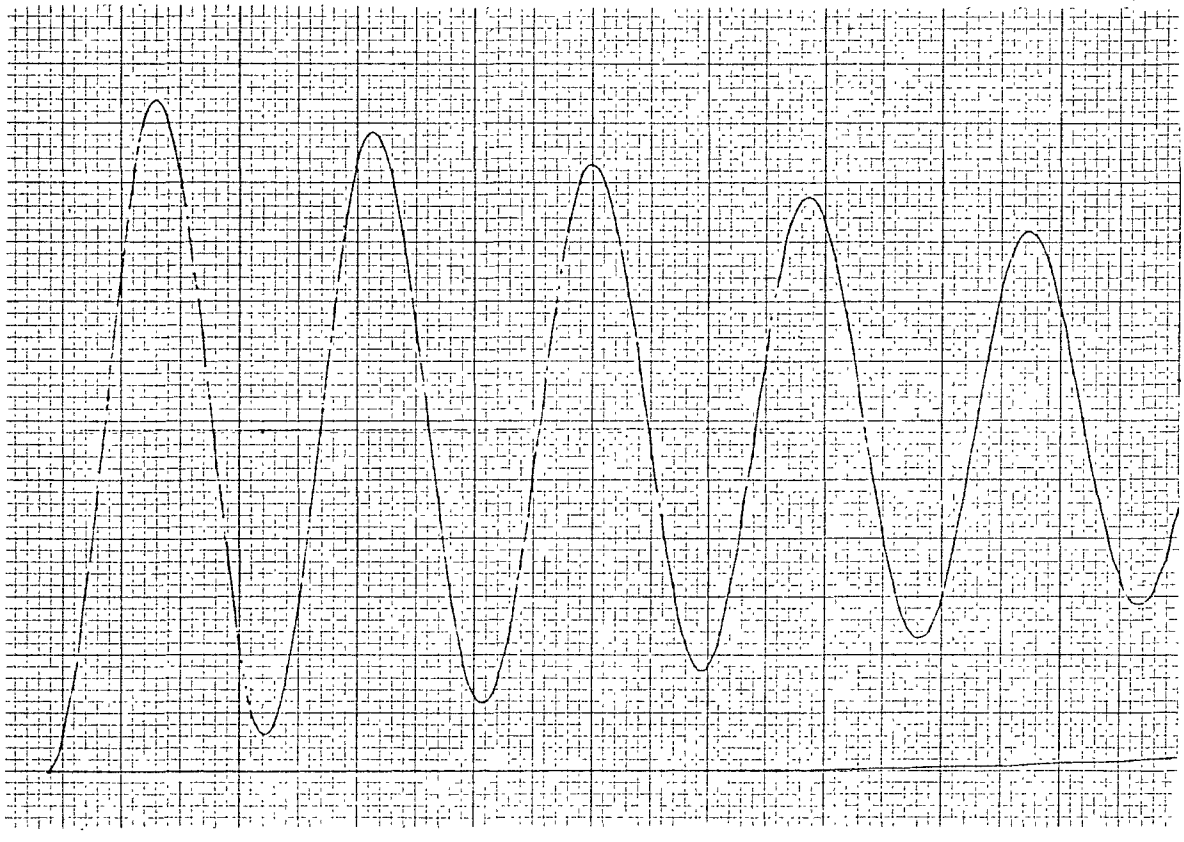

Fig. 4.8 Analogue Computer Tests
Case (ii) Coulomb friction only

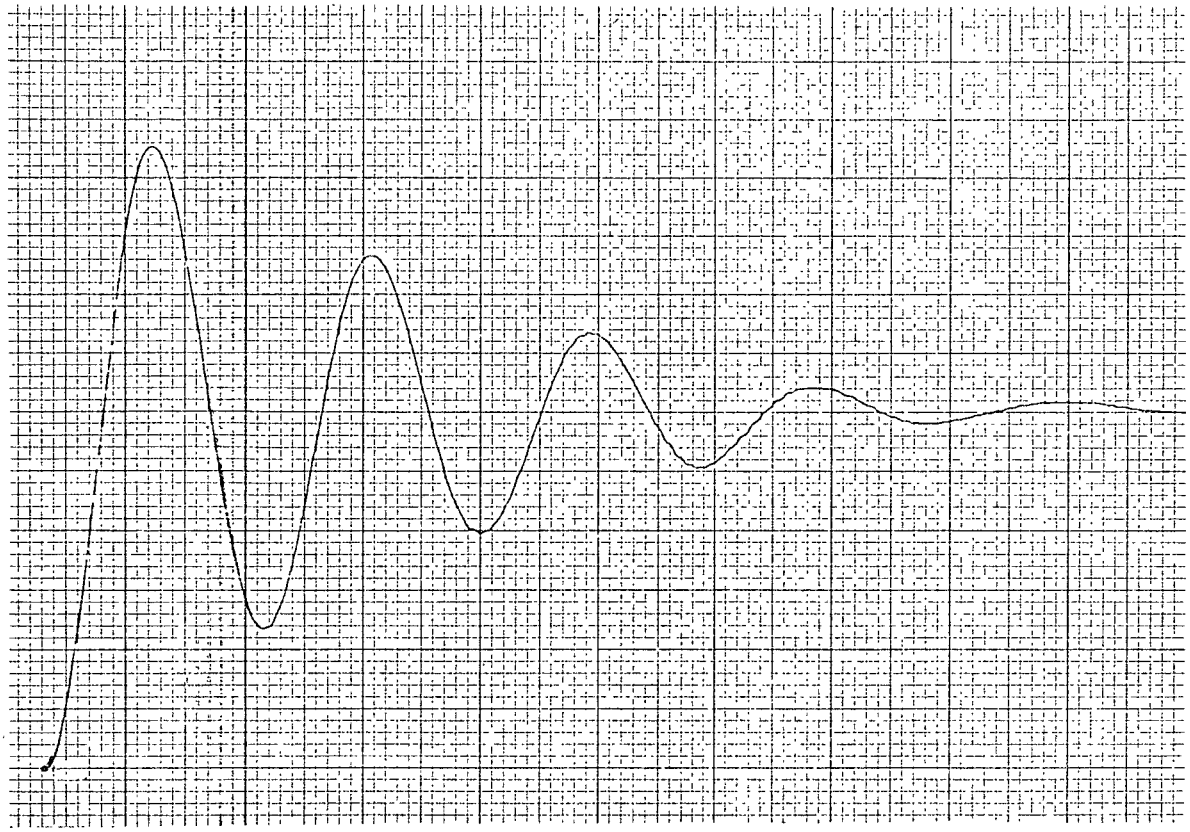

Peak to peak amplitude measured from fig.4.7	Amplitude Ratio	Peak to peak amplitude measured from fig.4.8	Amplitude Ratio	Peak to peak amplitude measured from fig.4.9	Amplitude Ratio
5.20		5.70		5.30	
	1.65		1.12		1.69
3.96		5.40		4.10	
	1.63		1.12		1.75
3.15		5.10		3.14	
	1.66		1.13		1.85
2.43		4.80		2.35	
	1.67		1.13		2.04
1.90		4.55		1.70	
	1.68		1.14		2.54
1.45		4.27		1.15	
	1.67		1.15		3.84
1.13		4.00		0.67	
			1.16		
0.87		3.72		0.30	
		3.44			

Fig. 4.9 Analogue Computer Tests
Case (iii) Viscous and Coulomb

Peak amplitudes and the ratios of successive peaks are noted for the 3 decay curves, below fig. 4.9.

Case (i)

By measurement from fig.4.7 and using a standard curve,

$\zeta = 0.08$ and $\omega_d \simeq \omega_n = 52$ rad/s

so that $\frac{S}{m_L} = 52^2$ and $\frac{6.7}{2\sqrt{Sm_L}} = 0.08$

Hence $m_L = 0.805$ lbf s^2/ft and $S = 2180$ lbf/ft.

Case (ii)

By measurement from fig. 4.8 the amplitude decrease in

4 cycles = 0.07 in.

i.e. $4 \times \frac{4F_c}{S} = \frac{0.07}{12}$

and if $S = 2180$ lbf/ft from (i) above,

then $F_c = 0.8$ lbf

As expected, for the viscous plus Coulomb friction case, (fig. 4.9.) the ratio of successive peaks increased as the oscillations decayed.

Another effect of Coulomb friction is the existence of a "dead zone" within which the load may finally settle. This was calculated, as an example, for test I2. For a Coulomb friction force of 1 lbf the dead zone would be 0.011 in., which would be represented by 0.6 mm. on the u-v record used for these tests.

The significance of this and of the analogue computer results are discussed in section 4.3.3.

4.2 The Servo Valve

4.2.1 Valve Calibration

When supplied, the valve had been adjusted by the manufacturers using high pressure oil, to have slight overlap when no dither signal was applied. This meant that when a dither signal

was applied there was overlap, (i.e. simultaneous flow from the supply port to the control port and from the latter to the exhaust port) with no d.c. actuating signal present. The lap was therefore adjusted by trial and error to give approximately zero overlap in the presence of a sinusoidal dither signal of ± 110 mA (peak) at 200 Hz (see section 4.2.2 for details of the selection of this dither signal). With this new setting of valve lap, full static calibration curves were obtained.

(a) Exhaust flow

Using the arrangement of fig. 4.10 the points shown in fig. 4.12 were obtained. In this case the valve supply pressure and the dither signal were maintained constant while the d.c. valve actuating signal was varied. This was repeated for various control port pressures. These curves are replotted in fig. 4.14.

(b) Supply flow

In this case the arrangement of fig. 4.11 was used. For these tests the valve dither and d.c. signal were kept constant while the control port pressure was varied. This was repeated for various values of the d.c. input. These results are shown in figs. 4.13 and 4.14.

These calibration curves applied for all the closed loop tests described in Chapter 5 and were simulated in the analogue computer tests (Chapter 6).

(c) Valve lap

One effect of valve dither was to make the exhaust noisy. A 200 Hz whine could be heard for any exhaust flow below the maximum. A slight exhaust noise could be heard when the d.c. valve current was between -20mA and 0mA. This exhaust flow was not measured but this indicates that, although the valve had nominally zero lap with no flow in either direction at I = -20mA, there was in fact underlap

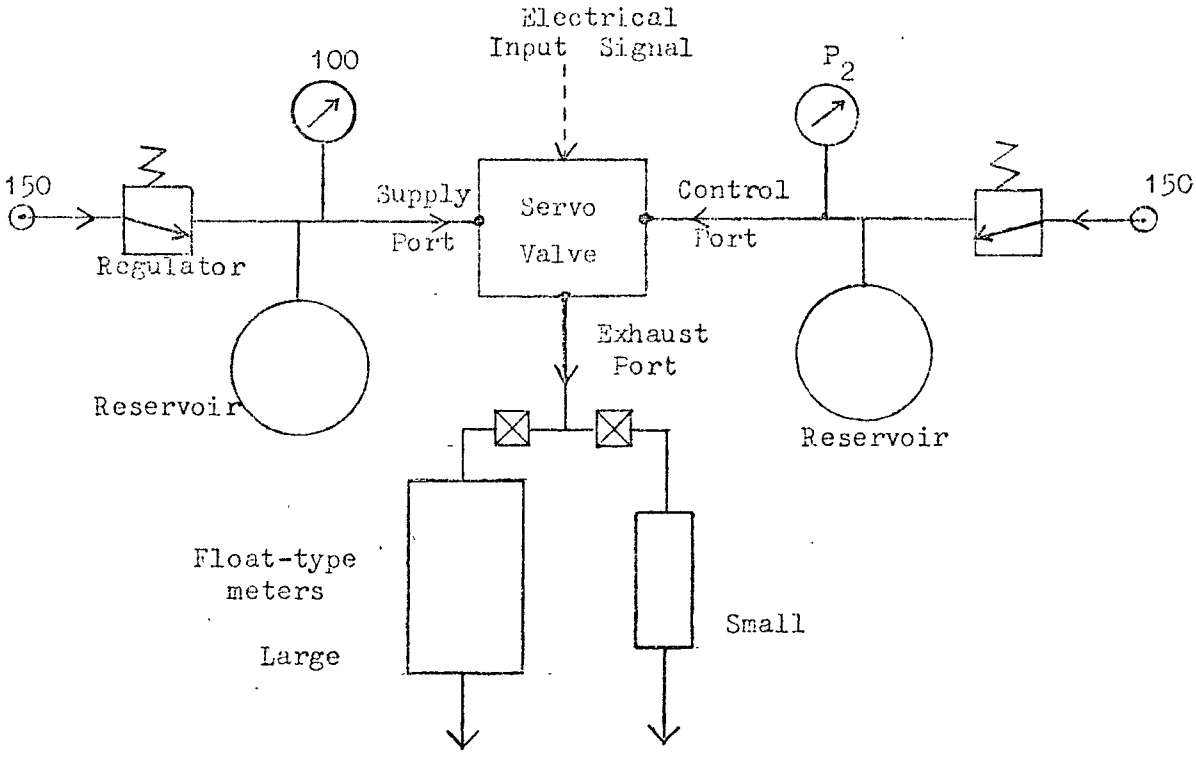

Fig. 4.10 Servo Valve Calibration Circuit - Exhaust flow

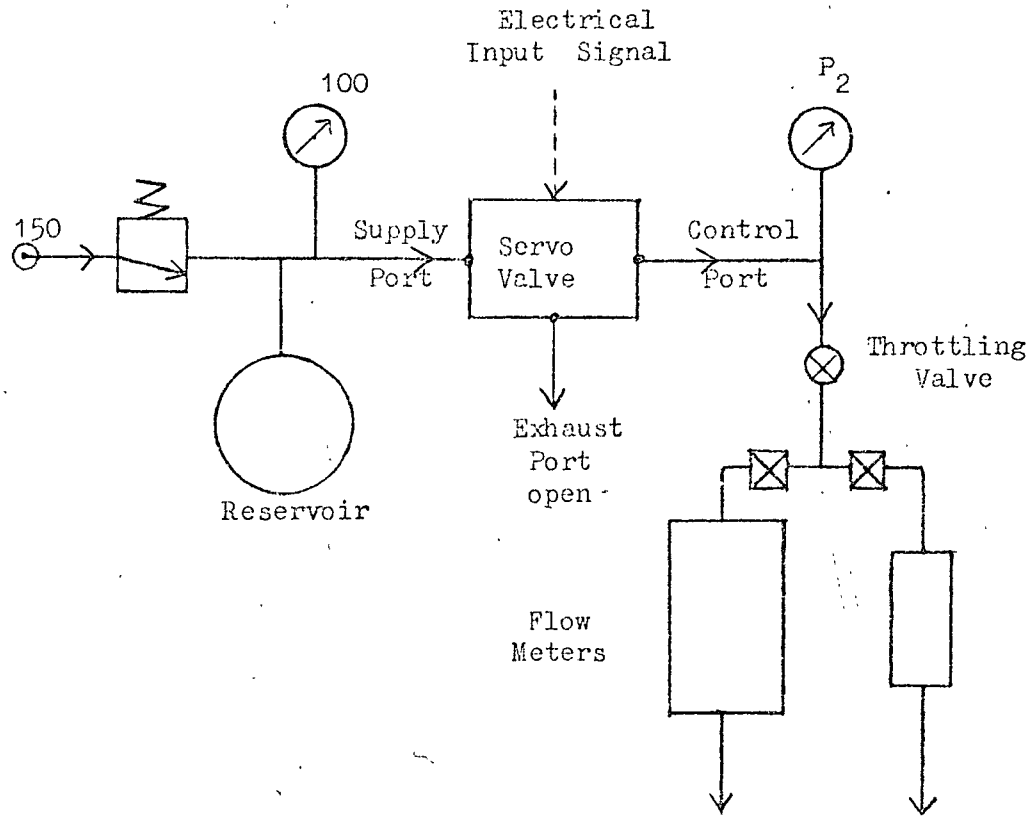

Fig. 4.11 Servo Valve Calibration Circuit - Supply flow

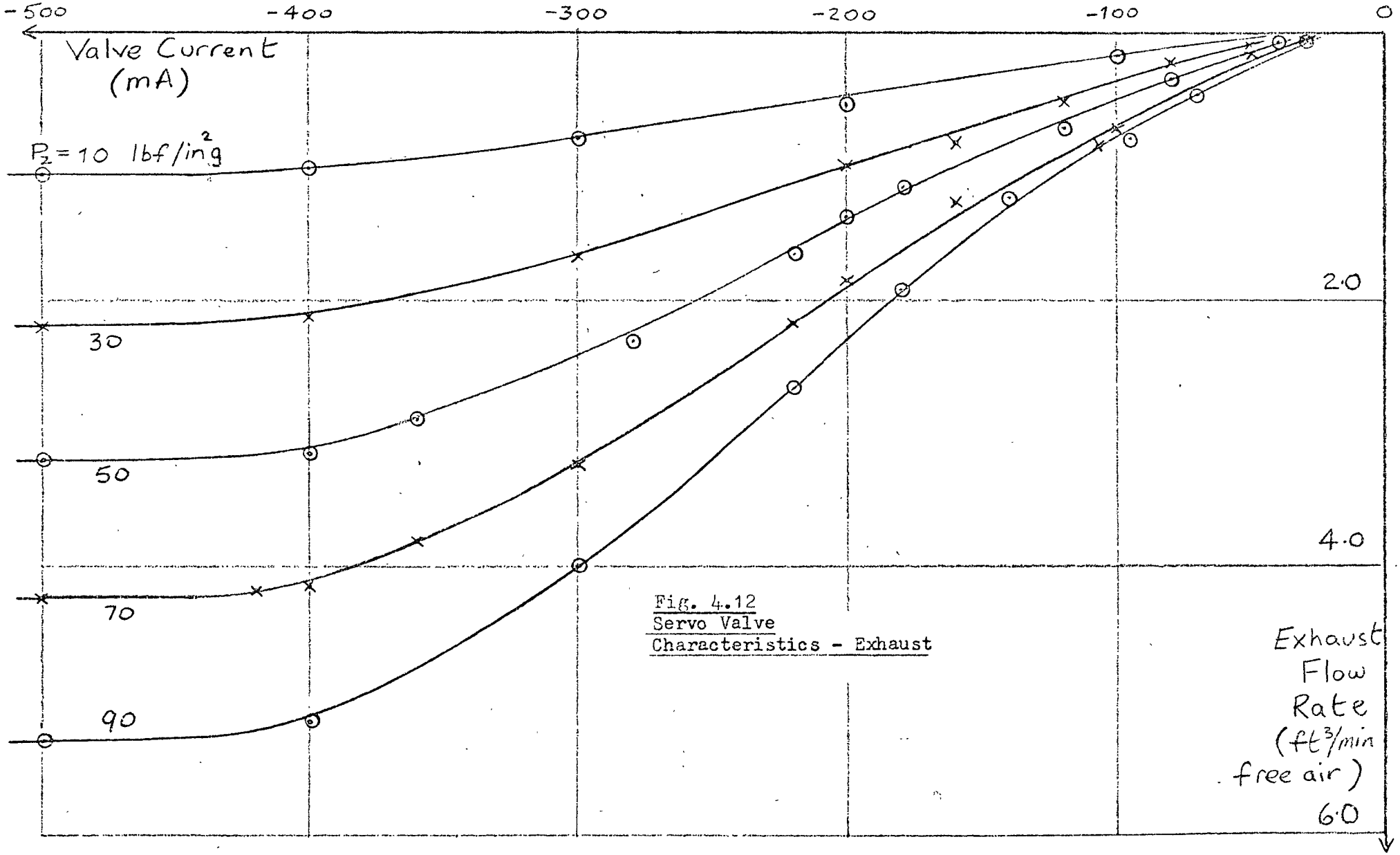

Fig. 4.12
Servo Valve
Characteristics - Exhaust

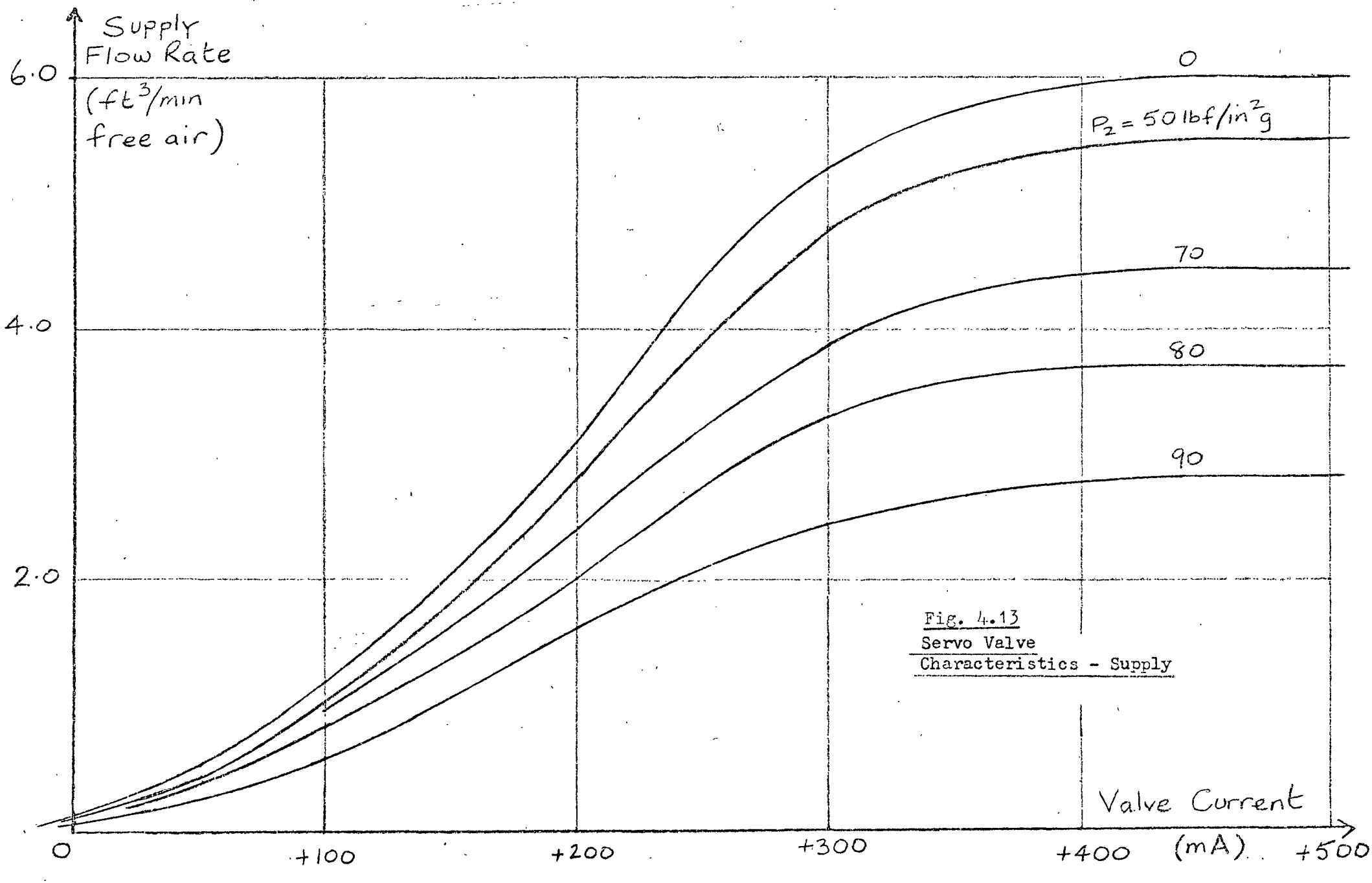

Fig. 4.13
Servo Valve
Characteristics - Supply

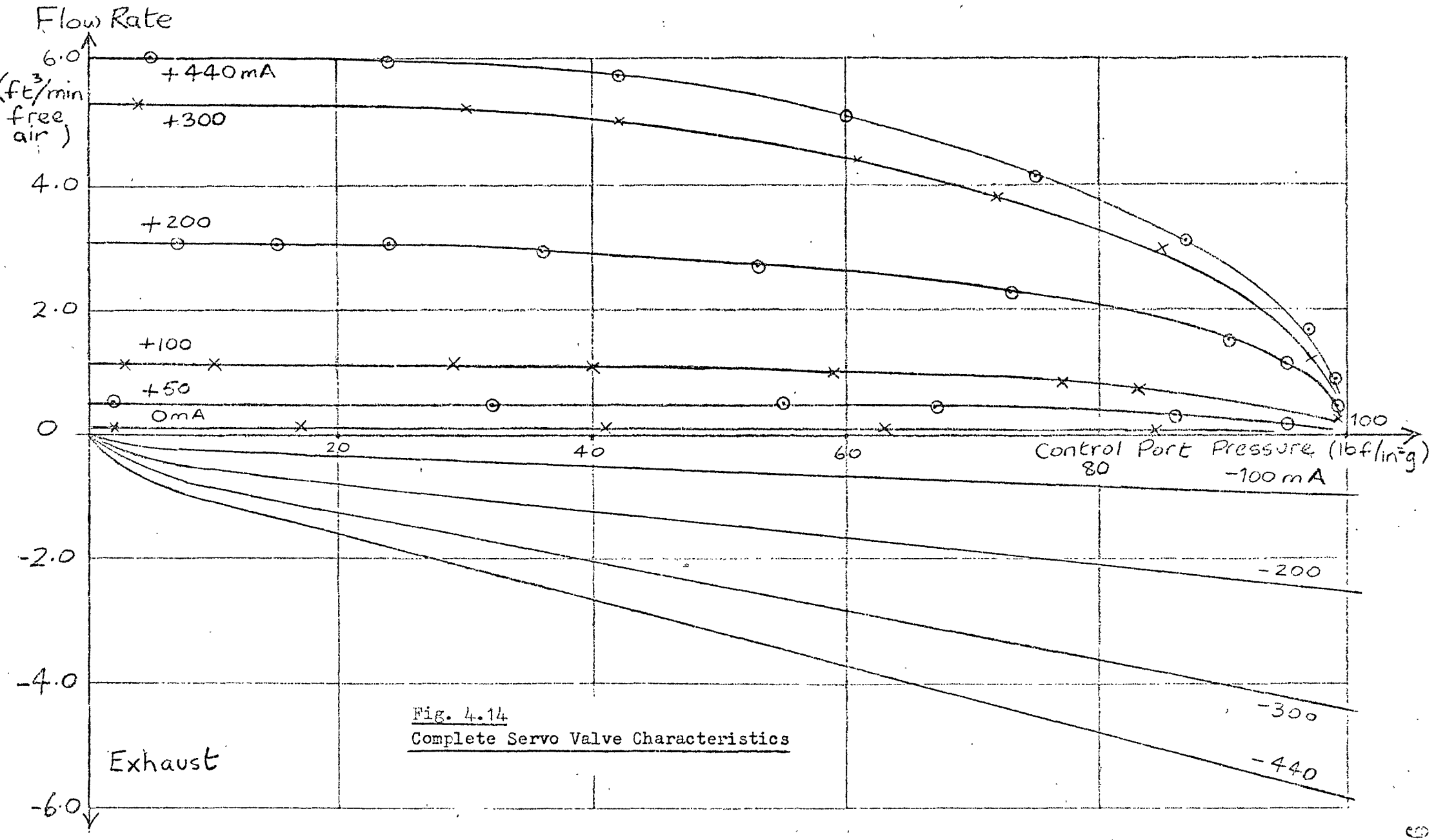

Fig. 4.14
Complete Servo Valve Characteristics

of about ± 20mA about this point.

4.2.2 Dither Optimization

In the absence of dither on the servo valve input signal, hysteresis of as much as 20% of maximum current was observed. This was considerably more than the figure quoted by the manufacturer, for use with hydraulic fluid, but was not unexpected in view of the reduced spool lubrication. Dither is commonly used to reduce hysteresis in this and other hydraulic valves. A dither frequency of 200 Hz was selected since this is well above the natural frequency of the jack/load combination, well within the frequency range of the operational amplifier and quite close to the natural frequency of the valve itself. The maximum flow was not affected by dither since in all cases, with a sufficiently large d.c. input signal level, the valve opening was saturated. In the presence of dither, "buzzing" at 200 Hz could be heard, as the valve spool hammered against the end stops, for valve positions approaching fully open in either direction.

A dither signal in excess of 70mA (peak) was found to be required to reduce the hysteresis to acceptable proportions and 110mA (peak) was selected for normal servo operation. In this case the maximum hysteresis was about 3% of full flow.

4.2.3 Valve Dynamic Response

The manufacturer's data showed that the valve response had a slight resonance at about 250 Hz. Observation of the a.c. output signal from the integrally mounted valve position transducer confirmed this to be correct. In addition, the accuracy of valve current measurement as an indication of valve position was checked. In this case the valve current response was flat to about 700 Hz (at which frequency the valve position transducer output and the valve movement were negligible). It can therefore be concluded that the spool amplitude is reasonably represented by the valve current signal for

frequencies up to about 200 Hz though there is some phase shift (e.g. about 90^{o} at resonance).

4.3 Discussion of Chapter 4

4.3.1 Impulse Tests

The linearized second order equation (eqn. 3.25) proposed in Chapter 3 has been shown to describe the behaviour of the loaded actuator for a wide range of parameters. The justification for this statement is that for the large number of experimental transient response recordings examined, the characteristic behaviour of a damped second order system was observed. For each separate response:-

(a) The damped natural frequency was constant throughout the decaying oscillation, and

(b) The damping ratio, as measured from the ratio of successive oscillation amplitudes, was approximately constant throughout the decaying transient.

The maximum values of pressure and displacement fluctuations during the tests were limited by the force which could comfortably be administered manually to the load. The controlled pressure (P_2) and the chamber volume (V_2) varied by up to 40% and 20% respectively of their mean values. These quantities are represented by constants P_{2a} and V_{2a} in the theoretical equations, a linearization which is justified for these and probably larger variations, since the fluctuation of the actual values about these mean values constitutes an averaging effect over one complete oscillation.

The Impulse Test establishes important parameters for a loaded actuator and is easily conducted for a low-pressure pneumatic system.

4.3.2 The Expansion and Compression Processes

It can be seen that in fig. 4.2 a reasonable straight line can be drawn through the experimental points. This line does not pass through the origin, implying a small error in the measurement of the volume of chamber 2. These points span a very wide range of piston position and inertia load values and therefore a wide range of natural frequencies and piston speeds.

The polytropic index 'n' will vary with the speed of the process. Points close to the origin, representing high natural frequencies can be expected to approach the n = 1.4, adiabatic, case. At low speeds, however, n will approach 1.0, isothermal. There is no evidence of this trend over the frequency range of these tests, i.e. $2\frac{1}{2}$ to 10 Hz.

During a decaying, constant frequency, vibration, the actual piston velocity falls. The maximum piston velocity in these tests was about 60 ft/min. The points in fig. 4.2, resulting from tests in which the transient amplitude was comparatively large, were examined. These points represent relatively high piston speeds. There was no tendency for these points to be closer to the n = 1.4 curve than other points at about the same frequency.

A value for n has been determined (n = 1.28) which describes the behaviour of the actuator over a wide range of frequencies and piston speeds.

In section 4.1.3 values for polytropic indices are quoted for reciprocating compressors. These relate to totally different conditions from the present case. In particular in that case, the piston speeds are very much greater, cylinder heat exchange is deliberately encouraged and a "steady state" cycling rather than a transient oscillation occurs. In view, particularly, of the relative

piston speeds, a lower value for n might be expected for the present system than for such compressors.

4.3.3 Actuator and Load Friction

One of the most severe problems in obtaining satisfactory models of hydraulic and pneumatic control systems is the absence of a good theoretical representation of the friction forces at the actuator and load. In specific cases a number of solutions have been found varying from the substitution of "equivalent" viscous damping for the Coulomb component [48] to the simulation of stiction plus Coulomb plus viscous friction by digital [10] or analogue computer [64].

The difficulty arises from the dependence of friction, usually in a non-linear fashion, upon such varied factors as position, velocity, load magnitude, time, temperature and quality of lubrication. The most difficult problem encountered by Cutland [23] was to account for friction in his low-pressure pneumatic servo-mechanism and Parnaby, who has made an extensive study of non-linear effects in control systems, has observed that scatter in readings is typical of experimental work on systems with friction [65].

Not only is friction difficult to analyse and to observe experimentally but it also presents problems in practical systems as it results in inaccuracy, power wastage and sometimes instability. In systems where a little gas leakage can be tolerated it may be desirable to reduce friction in the actuator in the same way as was done in the one used for these tests. Surprisingly little work has been done on the design of low friction linear actuators. As far as commercial organizations are concerned, this is mainly because of the very low demand for such devices [66a]. As mentioned in Appendix 3, the author is currently constructing a series of experimental pneumatic actuators, using composite P.T.F.E. and rubber seals, of the

type used fairly commonly in hydraulic actuators. The design of low-friction load bearings presents further problems, but in some cases gas bearings present a possible solution, again the cost being a certain amount of gas leakage.

No analytical expression is proposed to represent the experimental results obtained in sections 4.1.5 to 4.1.7 and Appendix 3. However, it can be said that friction forces were small compared to the available driving force and certainly compared with the friction forces for any currently available actuators involving sliding rubber or plastic. A number of points can be made from the experimental results:-

(a) Inspection of the Impulse Test traces showed that the damping was predominantly viscous. This observation is based upon the fact that the envelope of the decaying oscillations was always closely exponential. On the other hand, in the case of pure Coulomb damping this envelope is a straight line. Referring to fig. 4.1, for pure viscous damping $\frac{y_1}{y_2} = \frac{y_2}{y_3}$ while for pure Coulomb damping $\frac{y_1}{y_2} < \frac{y_2}{y_3}$

i.e. the presence of any appreciable Coulomb friction in addition to viscous friction and leakage will make the ratio of successive later peaks greater than earlier ones, i.e. $\frac{y_2}{y_3} > \frac{y_1}{y_2}$ etc. No such trend was observed in the 20 decay curves used for fig. 4.3 or the 10 in table 4.2. The results of the analogue computer study of section 4.1.7 demonstrate that the effect of a Coulomb friction force greater than 0.8 lbf, as in fig. 4.9 , would certainly have been observed in the test traces. However, anything much less than this would probably not have been detected, bearing in mind the relatively small size of the u-v traces used. In section 4.1.7 a specimen calculation was made of the dead zone which would result from a small amount of Coulomb friction being present during the Impulse Tests. This value

(0.6 mm on the u-v record) is too small to be of any use in estimating the actual Coulomb friction force. The figure for the viscous friction coefficient (b = 6.7 lbf/(ft/s)) was derived from a scattered set of points, but taken in conjunction with other results is a useful guide.

(b) The Drift Tests described in section 4.1.6 and in Appendix 3 give a valuable indication of the friction characteristic at low velocities. As expected from the simple design of the actuator, the static friction force was low, less than 2 lbf for the actuator alone and about 2 lbf for the actuator plus load carriage. Similarly, low Coulomb friction forces are evident. Referring to the Drift Test curves (figs. A3.1 & 4.5), if the Coulomb force is taken as the intercept of the straight line (high velocity) portion and the vertical axis, figures of less than $\frac{1}{4}$ lbf and less than $\frac{1}{2}$ lbf are obtained for the two cases. The usefulness of the "Drift Test" is further discussed in Appendix 3.

(c) The simple picture of the actuator friction presented by figs. A3.1 and A3.2 is complicated by the results of the saturation velocity tests shown in fig. A3.3. In this case the friction at relatively high velocities was shown to increase with load mass. On the other hand, there is no trend in fig. 4.3 for the experimental points corresponding to high load masses to fall above the remainder, as would be expected if this assumption were true.

(d) The assumptions implicit in drawing the straight line in fig. 4.4 were laminar leakage and viscous friction. The former is discussed in section 4.3.4 and the latter provided an independent figure for b for comparison with that obtained from the Impulse Tests. In this case a figure of b = 8.0 lbf/(ft/s) emerged. Again, it must be said that the points are somewhat scattered, but this result together with point (c) above suggests that a reasonable approximation for the

friction at higher velocities might be to assume a linear dependence on velocity but with the coefficient increasing with load mass.

(e) Although a number of independent tests have contributed data on friction in the experimental system, the picture is still incomplete. Further work on the nature of friction in actuators would clearly be of value.

4.3.4 Inter Chamber Leakage

Static Leakage Tests have been described in section 4.1.1 and Appendix 5. The further Impulse Tests described in section 4.1.5, in which additional leakage was introduced through a by-pass valve, yield information on the relevance of the static figures to the dynamic situation. The theoretical prediction of the slope of the straight line in fig. 4.4 assumes that the horizontal axis is calibrated in terms of actual leakage, measured under dynamic conditions. In fact, the calibration is in terms of leakage measured under static conditions. The very close agreement between predicted and measured slope (within 2%) shows that the static leakage coefficient can be used under dynamic conditions.

From the same test results (table 4.2) it can be seen that piston leakage variation had no measurable effect on the frequency of free vibrations (ω_{dp}) of the actuator/load combination. In that case the inter-chamber leakage was increased to over seven times the inherent leakage and since $\omega_{dp} = \omega_{np}\sqrt{1 - \zeta_p^2}$ and ζ_p varied only slightly, it can be concluded that ω_{np} was also constant. This is further confirmation that piston leakage can be neglected in equation 3.27. (A simple calculation, using the value for b obtained from fig. 4.3, shows that $A^2 > 150\ L_b$.)

Leakage has been shown to have a small but sometimes important damping effect on the free vibration of the loaded actuator. This is illustrated in fig. 4.3 where the contribution of piston leakage to

system damping is shown. For the range of load mass (m_L) and chamber volume (V_2) used in these tests, leakage contributed between 7% and 30% of the total damping. Leakage becomes important for very large inertial loads and small volumes.

4.3.5 Pressure in Chamber 1

In normal closed loop operation the pressure in chamber 1 (P_1) is maintained nominally constant and equal to half the pressure of the valve air supply. In these tests, chamber 1 was connected to a reservoir, which was supplied from a pressure regulator at 50 lbf/in^{2}g. In practice, if there is any movement of the piston, fluctuation in pressure in chamber 1 must result. The magnitude of this fluctuation, for a given piston displacement, will depend upon the nature of the connection between actuator and reservoir and the size of the reservoir.

For the particular arrangement used for these tests, fluctuations in P_1 were always small in magnitude. (Details appear in Appendix 6.)

The importance of these already small pressure fluctuations will be reduced if they are 90° out of phase with the displacement (and therefore with the pressure in chamber 2). From the information available, it appears that such a 90° phase difference occurred at the frequencies used in these tests. This behaviour can be explained using the simple transfer operator developed in Appendix 6.

4.3.6 The Servo Valve

Gas flow through an orifice is either choked, when the pressure ratio across the orifice is low, or unchoked for higher pressure ratios. If isentropic conditions are assumed, the well known flow/pressure ratio curve shown in fig. 4.15 (upper line) results. This shows the variation of the flow through the orifice, resulting from downstream pressure changes, while the upstream pressure

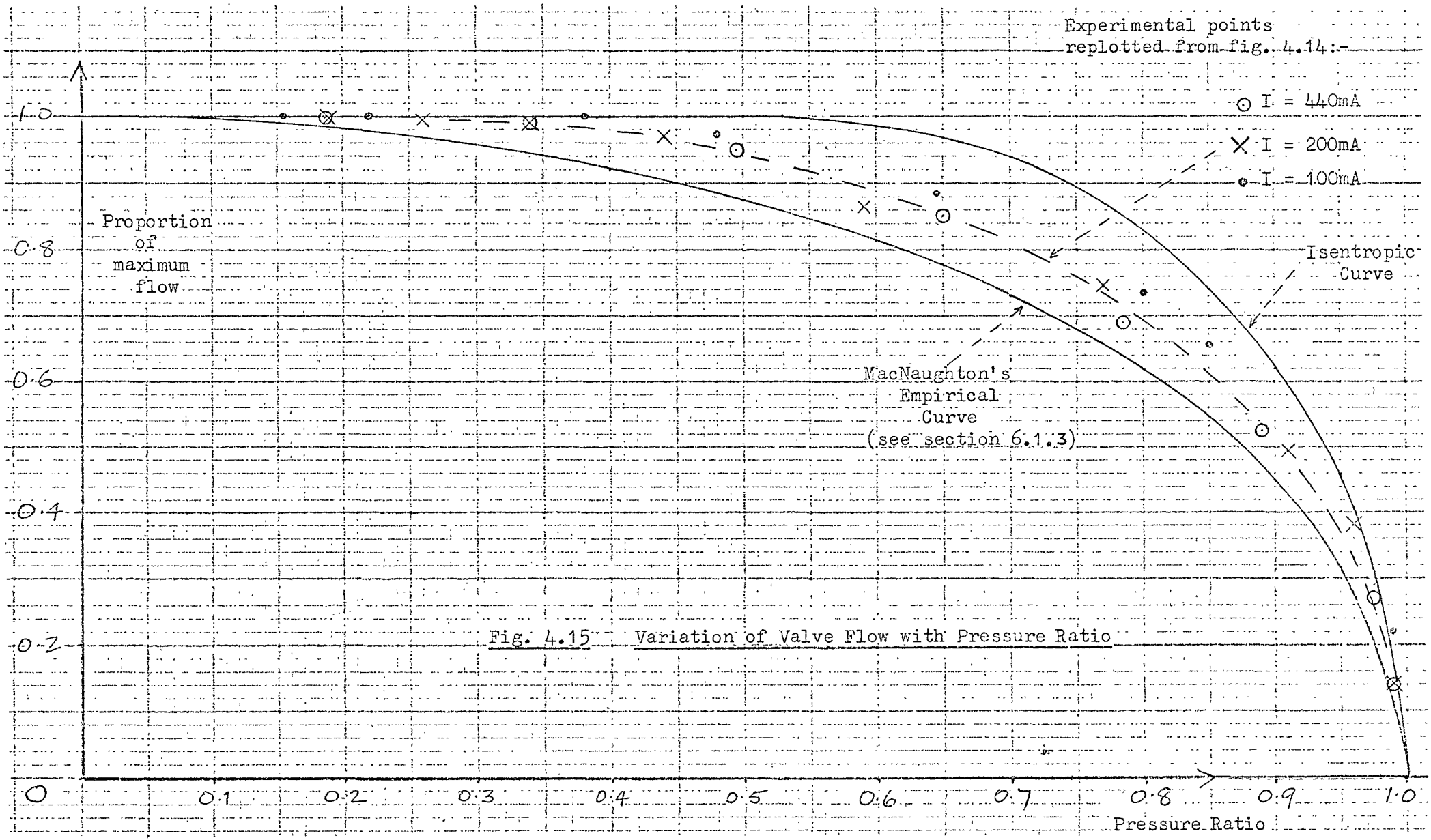

Fig. 4.15 Variation of Valve Flow with Pressure Ratio

is held constant. In this case the flow regime is seen to change at the critical pressure ratio, which for air is 0.528. This isentropic curve is known to be a good representation of the flow through such orifices as smoothly contoured nozzles.

Also shown in fig. 4.15 are some experimental points for the servo valve, replotted from fig. 4.14. These points do not fall very close to the isentropic curve. The departure of experimental results from the isentropic curve is probably explained by reference to the sectioned drawing of the valve (fig. A4.1). This shows that the flow path was actually quite tortuous, involving four right angle turns, the sharp metering orifice and other discontinuities. Valve dither further disturbed the flow, though once the valve was fully open, in either direction (e.g. I = 440mA), the dither signal was ineffective.

In fig. 4.15 the points for I = 440mA and I = 220mA lie close to a common curve suggesting that valve spool dither, which only operated in the latter case, did not seriously affect the nature of the flow. The I = 100mA points lie above the others but great importance is not attached to this as it is possible that the flow measurements were slightly inaccurate in this case. (A float type meter was used, towards the bottom of its range.)

The ports of the servo valve were annular orifices and the relationship between spool movement and flow area was linear. When dither was introduced this relationship ceased to be linear, the effects being to reduce the gain of the valve at low input signal levels, and to make the saturation of the flow gradual rather than sudden. These effects, seen in figs. 4.12 and 4.13, could be counteracted if required, by reshaping the valve ports, for a specific amount of dither. The nature of the non-linearity is further discussed in Chapter 6, where an analytical expression is derived for the purpose of simulating the valve characteristics.

CHAPTER 5 TESTS ON THE ELECTRO-PNEUMATIC SERVO

In Chapter 2 the construction of an experimental electro-pneumatic servo is described and tests on the individual components of the servo are described in Chapter 4. A large number of tests were conducted on the closed-loop system and these are described below. Except where it is stated to the contrary, the servo-valve air supply pressure was 100 lbf/in^{2}g and the constant pressure in chamber 1 was 50 lbf/in^{2}g. Other constants for the system appear in Appendix 2.

Command signals for the system were obtained from a low frequency signal generator, fed to one input of the operational amplifier shown in fig. 2.5.

5.1 Step Response Tests

A series of 34 tests was conducted for widely differing values of the following parameters:

Load Mass

Step Size

Step Direction

Final Load Position

Loop Gain

Transient Pressure Feedback Coefficient

The data for these tests appears in table 5.1. During the tests the command signal, (γ_i), the actual load displacement, (γ_o), the pressure in chamber 2, (P_2), and the valve current (i) were recorded using an ultra violet recorder, and specimen traces are shown in figs. 5.1 and 5.2.

Almost all of these tests were used for simulation studies (see Chapter 6) as indicated in table 5.2. In these cases the

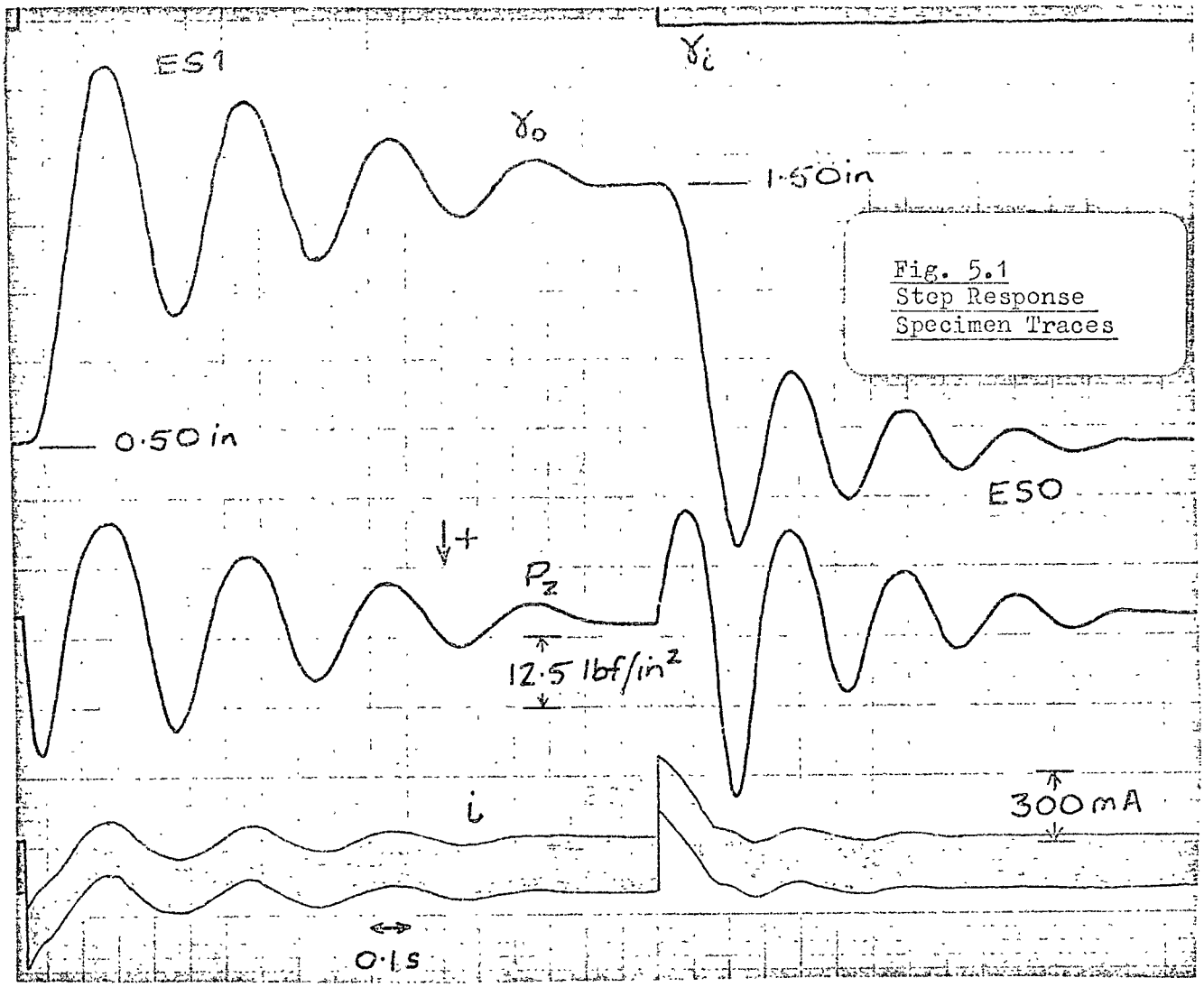

Fig. 5.1
Step Response
Specimen Traces

(a)

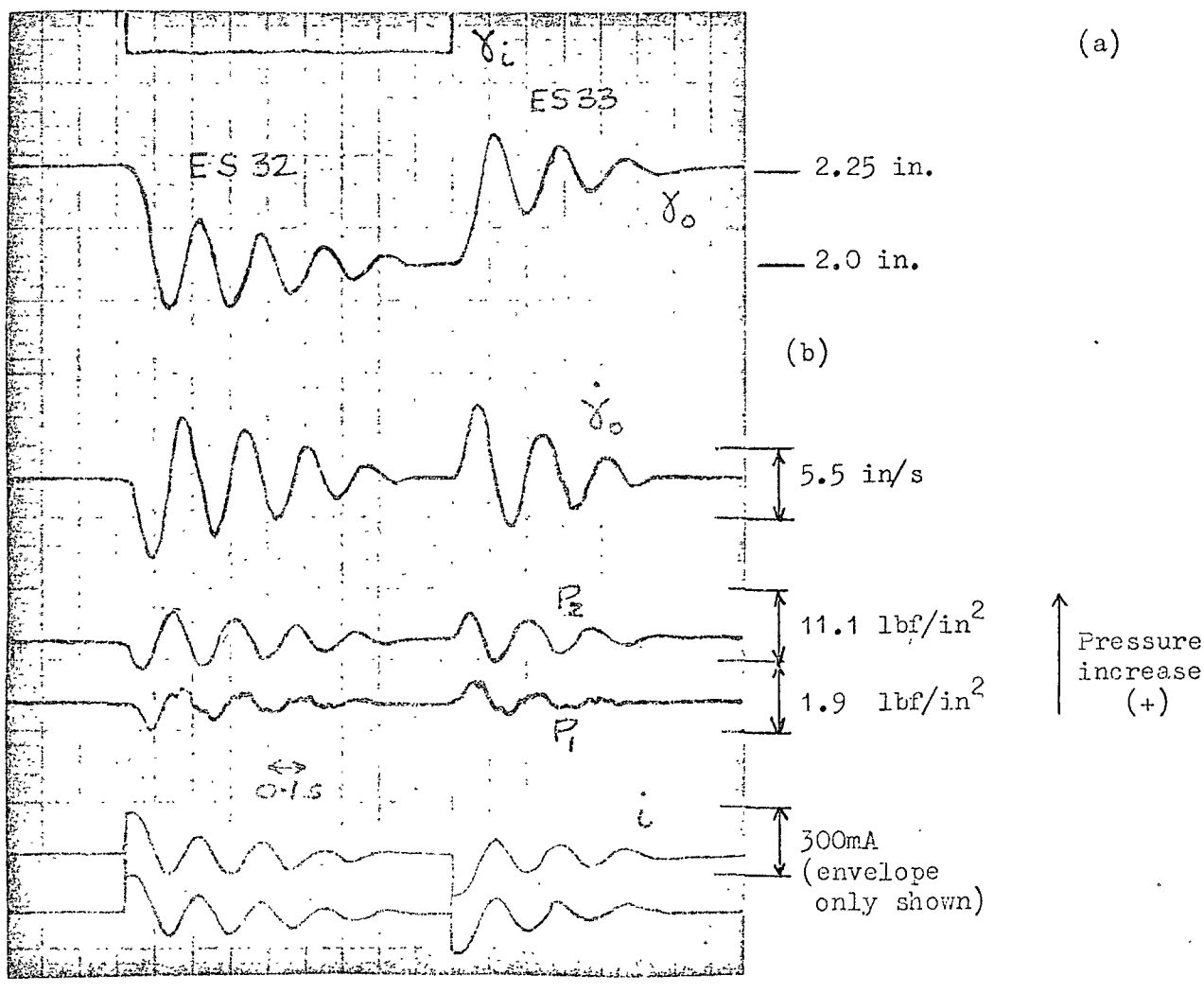

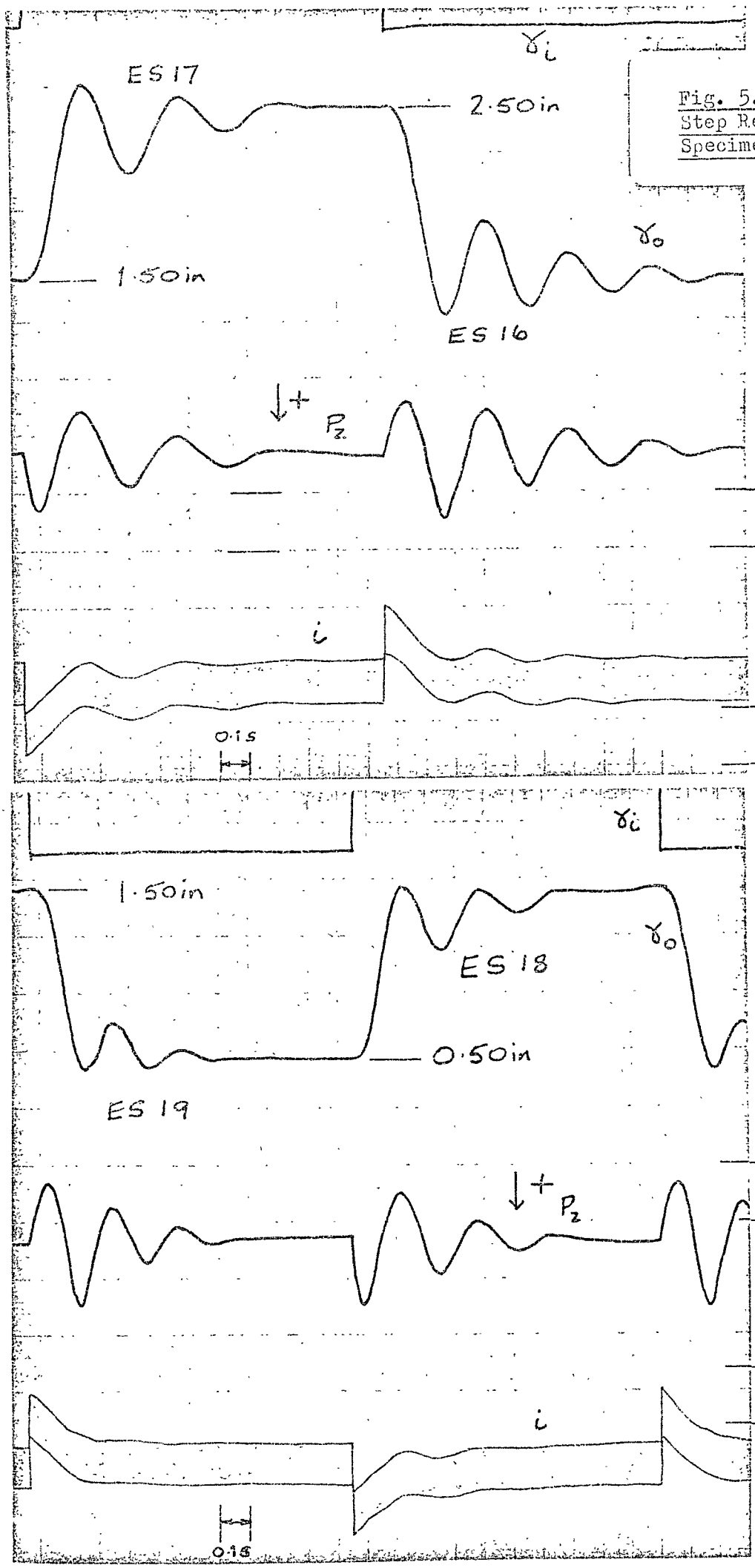

Fig. 5.2
Step Response
Specimen Traces

Table 5.1 Experimental Servo Step Response Data

Step Test No.	Load Mass (lb)	Load Carriage Position (Scale shown in fig. 3.1)		Feedback Potentiometer Gain (K_p V ft^{-1})	Transient Pressure Feedback	
		Initial (in)	Final (in)		Coefficient (K_{pr} mA ft^2 lbf^{-1} x 10^{-2})	Time Constant (τ_p s)
ES0	93.7	1.50	0.50	7.30	3.47	1.69
ES1	93.7	0.50	1.50	7.30	3.47	1.69
ES2	93.7	2.50	1.50	7.30	3.47	1.69
ES3	93.7	1.50	2.50	7.30	3.47	1.69
ES4	93.7	0.50	1.50	7.30	18.75	0.293
ES5	93.7	2.50	1.50	7.30	18.75	0.293
ES6	93.7	2.50	1.50	12.2	7.30	0.750
ES7	93.7	0.50	1.50	12.2	7.30	0.750
ES8	93.7	2.50	1.50	12.2	18.75	0.293
ES9	93.7	0.50	1.50	12.2	18.75	0.293
ES10	93.7	2.90	0.90	5.70	3.47	1.69
ES11	93.7	2.90	0.90	5.70	18.75	0.293
ES12	93.7	0.10	2.10	5.70	3.47	1.69
ES13	93.7	0.10	2.10	5.70	18.75	0.293
ES14	48.7	2.90	0.90	5.70	3.47	1.69
ES15	48.7	2.90	0.90	5.70	18.75	0.293
ES16	48.7	2.50	1.50	5.70	3.47	1.69
ES17	48.7	1.50	2.50	5.70	3.47	1.69
ES18	48.7	0.50	1.50	5.70	3.47	1.69
ES19	48.7	1.50	0.50	5.70	3.47	1.69
ES20	48.7	2.50	1.50	5.70	18.75	0.293
ES21	48.7	0.50	1.50	5.70	18.75	0.293
ES22	48.7	2.00	1.50	5.70	0	-
ES23	48.7	1.00	1.50	5.70	0	-
ES24	8.7	2.00	1.50	6.00	10.6	0.550
ES25	8.7	1.00	1.50	6.00	10.6	0.550
ES26	8.7	1.25	1.00	8.20	0	-
ES27	8.7	1.00	1.25	8.20	0	-
ES28	8.7	1.25	1.00	2.85	0	-
ES29	8.7	1.00	1.25	2.85	0	-
ES30	8.7	2.25	2.00	8.20	0	-
ES31	8.7	2.00	2.25	8.20	0	-
ES32	13.7	2.25	2.00	8.20	0	-
ES33	13.7	2.00	2.25	8.20	0	-

Table 5.2 Servo and Computer Step Response Tests and Records

Step Test No.	Full Simulation Test No.	Simple Simulation Test No.	Test Record Location
ES0	-	-	Fig. 5.1
ES1	FS1	SS1	Fig. 7.1
ES2	FS2	SS2	Fig. 7.1
ES3	-	-	(Unstable. No record made)
ES4	FS4	SS4	Fig. 7.2
ES5	FS5	SS5	Fig. 7.2
ES6	FS6	SS6	Fig. 7.3
ES7	FS7	SS7	Fig. 7.3
ES8	FS8	SS8	Fig. 7.4
ES9	FS9	SS9	Fig. 7.4
ES10	FS10	SS10	Fig. 7.5
ES11	FS11	SS11	Fig. 7.5
ES12	FS12	SS12	Fig. 7.6
ES13	FS13	SS13	Fig. 7.6
ES14	FS14	-	Fig. 7.7
ES15	FS15	-	Fig. 7.7
ES16	FS16	SS16	Figs. 7.8/5.2
ES17	-	-	Fig. 5.2
ES18	FS18	SS18	Figs. 7.8/5.2
ES19	-	-	Fig. 5.2
ES20	FS20	SS20	Fig. 7.9
ES21	FS21	SS21	Fig. 7.9
ES22	FS22	-	Fig. 7.10
ES23	FS23	-	Fig. 7.10
ES24	FS24	-	Fig. 7.11
ES25	FS25	-	Fig. 7.11
ES26	FS26	-	Fig. 7.12
ES27	FS27	-	Fig. 7.12
ES28	FS28	-	Fig. 7.13
ES29	FS29	-	Fig. 7.13
ES30	FS30	-	Fig. 7.14
ES31	FS31	-	Fig. 7.14
ES32	-	-	Fig. 5.1
ES33	-	-	Fig. 5.1

displacement and pressure traces are presented in Chapter 7 to facilitate comparison with computer results. The location of these and other test records is shown in table 5.2. An arbitrary 3 inch scale is used in table 5.1 to indicate the position of the load carriage along its stroke. This scale is shown in fig. 3.1.

In all the step response test recordings, the phase difference between the displacement (γ_o) and pressure (P_2) traces was almost exactly 180°. This supports earlier evidence of very low friction forces. This can clearly be seen in the specimen traces, figs. 5.1 and 5.2.

Large variation in system parameters occurred during the step response tests. The maximum pressure recorded gave almost 80% of stall force, i.e. the absolute pressure (P_2) in the controlled chamber approached 90% of supply pressure (e.g. test ES10). The valve drive current exceeded the saturation value during many of the tests (nos. ES6-15) and the lower traces in figs. 5.1 and 5.2 show the drive current and the dither signal.

Observations on the pressure in chamber 1 are included in Appendix 6.

5.2 Harmonic Response

5.2.1 Closed Loop Harmonic Response Tests

The behaviour of the servo in response to sinusoidal command signals of constant amplitude was observed for a number of different values of:

Load Mass

Command Amplitude

Loop Gain

Transient Pressure Feedback Coefficient

The Lissajou figure method, using a variable phase oscillator

Table 5.3 Closed Loop Harmonic Response Test Data

Test No.	Load Mass (m_L lb.)	Command Signal Amplitude (in.)	Feedback Potentiometer Gain (K_p V ft^{-1})	Transient Pressure Feedback Coefficient (K_{pr} mA ft^2 lbf^{-1}) x 10^{-2}	Corresponding Step Response Tests
EH1	93.7	± 0.50	7.30	18.7	ES4 and ES5
EH2	93.7	± 0.25	7.30	18.7	ES4 and ES5
EH3	48.7	± 1.00	5.70	18.7	ES20 and ES21
EH4	48.7	± 0.50	5.70	18.7	ES20 and ES21
EH5	48.7	± 0.50	5.70	3.47	ES16 and ES18
EH6	8.7	± 1.00	6.00	10.6	ES24 and ES25
EH7	8.7	± 0.25	6.00	10.6	ES24 and ES25

and oscilloscope, was used to measure phase shift. Details of the tests appear in table 5.3. All oscillations were centred on the piston mid-stroke position.

The load carriage displacement was closely sinusoidal at frequencies above about 1.0 to 1.5 Hz. Below these frequencies, the waveform peaks flattened somewhat. There was also a tendency at low frequencies for the left to right movement to follow a sinusoidal pattern while the right to left displacement approached a ramp form. At low frequencies, therefore, the phase had to be measured, by judging the best null Lissajou pattern by eye.

Bode plots of the experimental results appear in Chapter 7 while fig. 5.3 shows two sample recordings of the command signal (γ_i), the load displacement (γ_o), the controlled pressure (P_2) and the valve current (i).

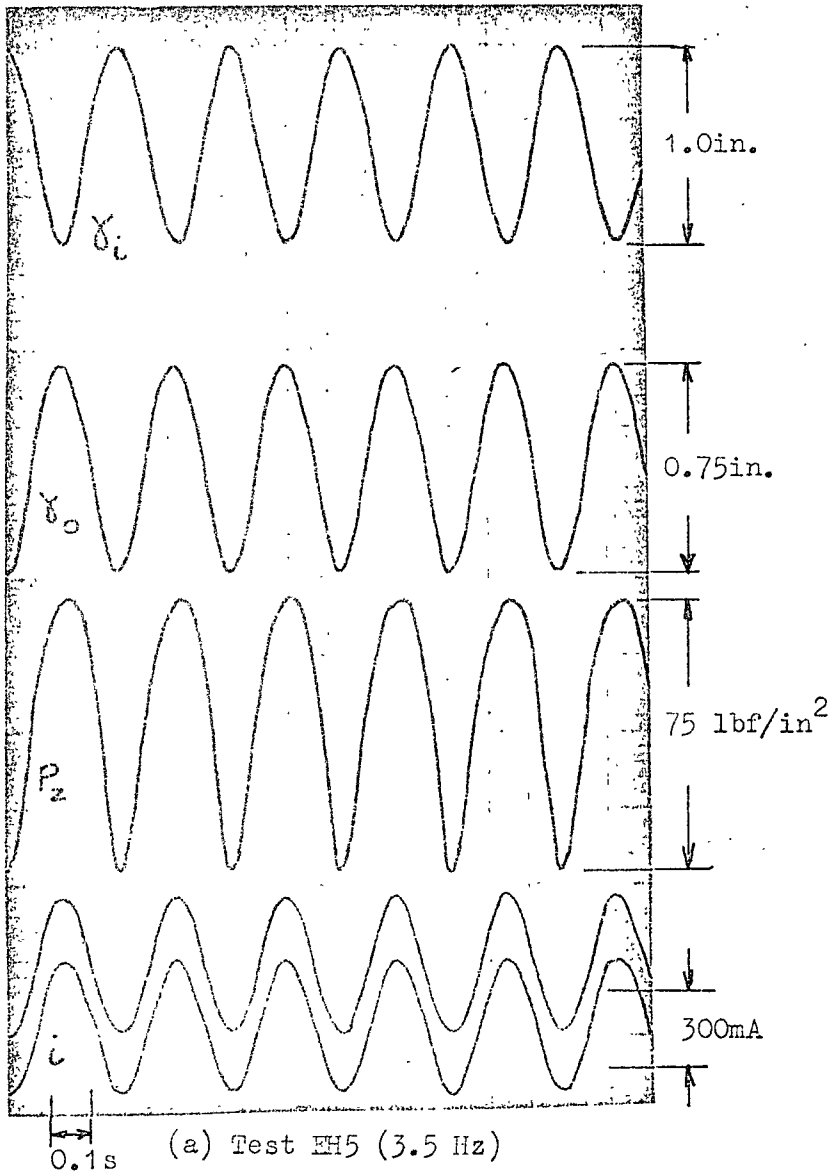

(a) Test EH5 (3.5 Hz)

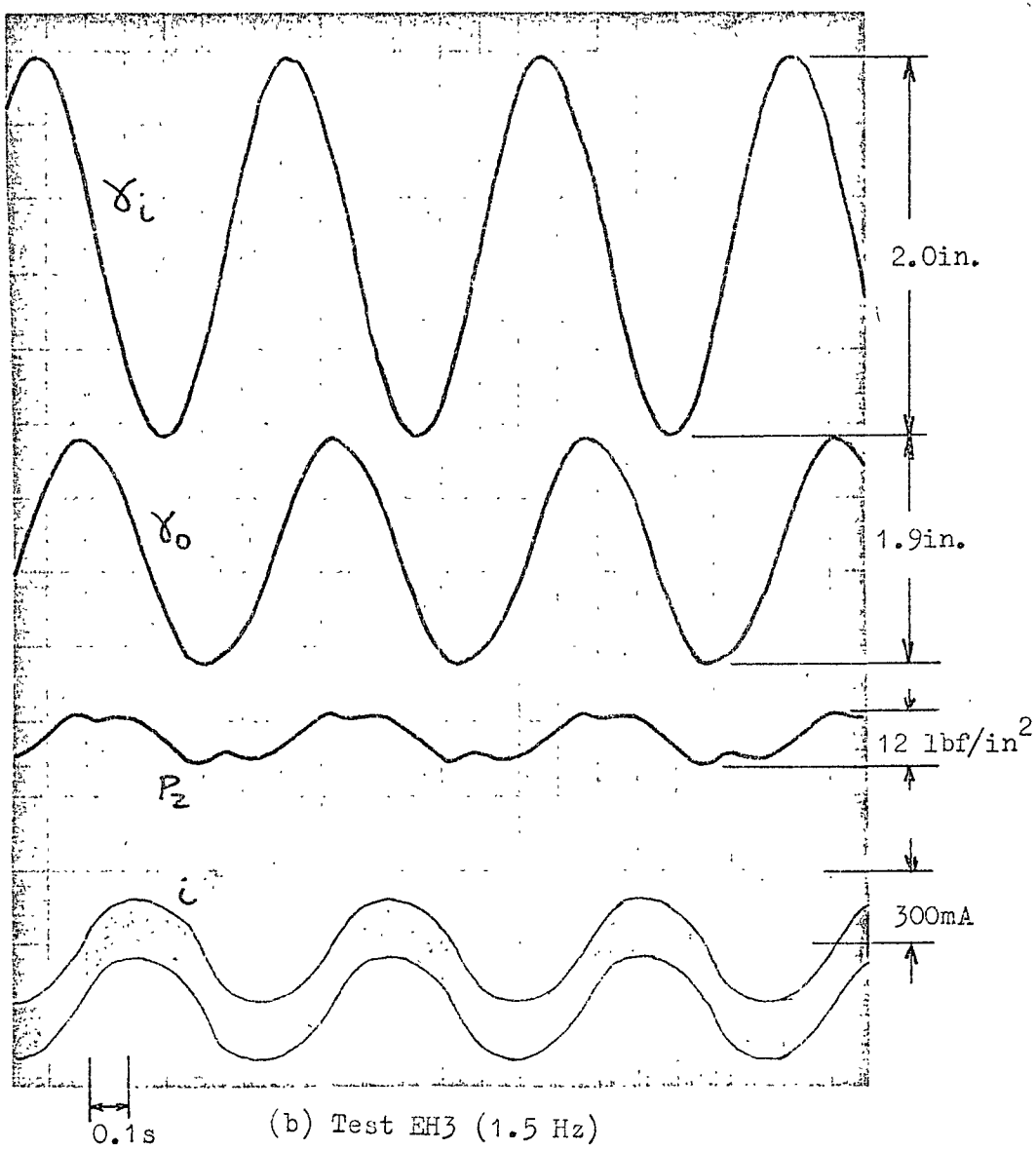

(b) Test EH3 (1.5 Hz)

Fig. 5.3 Harmonic Response - Specimen Traces

5.2.2 Open Loop Harmonic Response

Due to the integrating action of the valve and actuator, open loop harmonic response testing was impossible (due to the slow drift which is common for such systems in these circumstances). The closed loop results were therefore replotted onto a Nichol's Chart in order to obtain some indication of open loop behaviour. No great significance should be attached to a single open-loop Bode diagram, obtained in this way, for a system with amplitude dependent non-linearities. This is because the input amplitude to the open-loop is not constant during a closed loop test, as it would be during a true open-loop test. However, in this case the Bode plots were used for comparison with those obtained in a similar way from computer simulations and to assess the merit of such simulations under varying circumstances. The resulting open-loop Bode diagrams are shown in figs. 7.22 to 7.28 in Chapter 7.

5.3 Additional Tests

The results of a number of additional tests are included here. For these tests the component values for the high pass filter, when it was used, were not as shown in fig. 2.5. The appropriate time constant (τ_p) for the network is stated for the individual tests below.

5.3.1 Velocity Feedback

Negative velocity feedback using the moving-magnet velocity transducer, described in Chapter 2, was briefly investigated.

It was possible to stabilize the otherwise unstable servo in this way but at the cost of introducing a long time constant into the closed loop step response. Fig. 5.4 shows the system in a stable mode (a) and compares velocity (b) and transient pressure (c) feedback. When the velocity and transient pressure feedback used in (b) and (c)

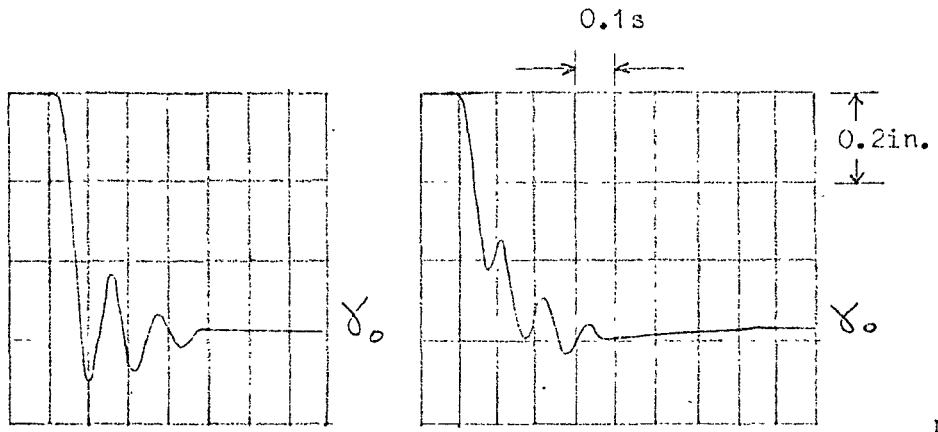

(a) No stabilizing feedback

(b) Negative velocity feedback

Fig. 5.4
Velocity Feedback

m_L = 8.7 lb
K_A = 590mA/V
K_p = 8.2 V/ft
τ_p = 0.06s

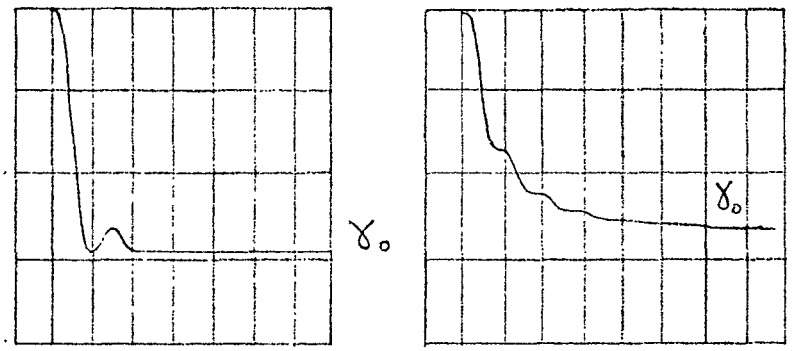

(c) Negative transient pressure feedback

(d) Simultaneous velocity and transient pressure feedback as in (b) and (c) (slightly smaller step size)

Right to left movement (fig. 2.1)

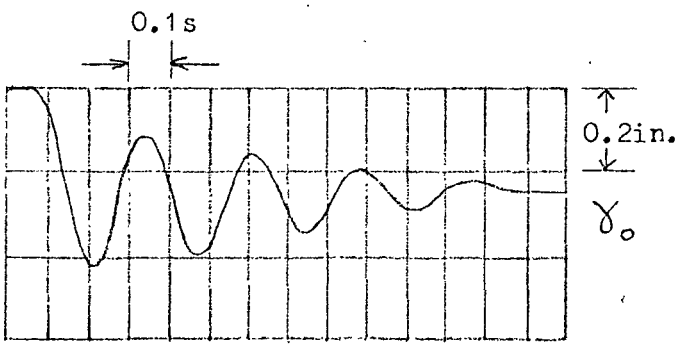

Right to left (fig.2.1)

(a) Transient pressure feedback

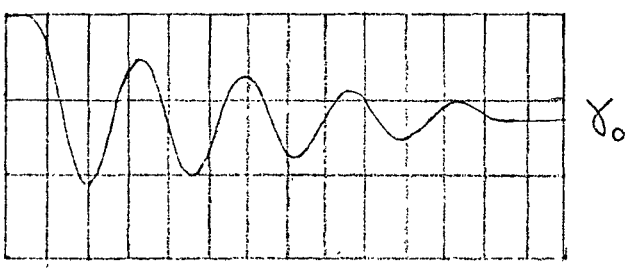

(b) Simple pressure feedback

Fig. 5.5
Pressure Feedback

m_L = 53.7 lb
K_A = 590mA/V
K_p = 8.2 V/ft
τ_p = 0.113s
K_{pr} = 5.55mAft^2/lbf
Final load position = 1in. (fig.3.1)

were applied simultaneously, the step response shown in (d) resulted.

5.3.2 Pressure Feedback

Fig. 5.5 compares the step response of the servo for (a) transient pressure and (b) simple pressure feedback, i.e. the only change between (a) and (b) is the removal of the high pass filter. In this case the frequency of transient oscillations was about 4 Hz and therefore well above the corner point of the high pass filter network (1.4 Hz). The removal of the filter is seen to have very little effect on the transient response.

5.3.3 Output Stiffness

While the use of a correctly designed high pass filter has little or no effect on response to a step command signal, its effects on the behaviour of the closed loop servo, in the presence of load forces, is demonstrated in fig. 5.6. In this case a horizontal force was suddenly applied to the load carriage, by leaning heavily upon it. The load displacement and the left hand chamber pressure (P_2) were recorded with:-

(a) no pressure feedback

(b) transient pressure feedback

(c) simple pressure feedback (exactly as in (b) but with the high pass filter capacitor shorted).

The pressure traces in fig. 5.6 show that a constant applied force was not quite achieved, but approximate values for the forces and load deflections were calculated from the traces and figures for the output stiffness found. These figures, shown on fig. 5.6, show the serious loss of output stiffness which occurred, in the absence of the high pass filter.

5.3.4 Transient Response in the Presence of Steady Load Forces

The constant pressure (P_1) in chamber 1 was set at values other than the normal pressure (50.1bf/in^{2}g.) to simulate the effect

Fig. 5.6 Output Stiffness

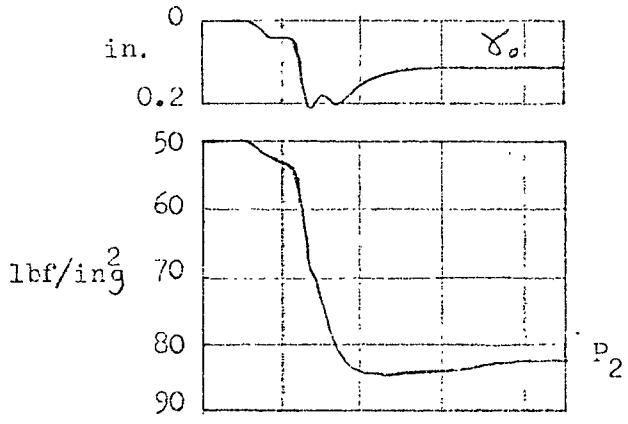

(a) No pressure feedback

Steady state deflection ≙ 0.12in.

Pressure ≙ 33 lbf/in^2

Applied force ≙ 33 x 1.77in.^{2}

≙ 58 lbf

Stiffness = $\frac{58}{0.12}$

= 485 lbf/in

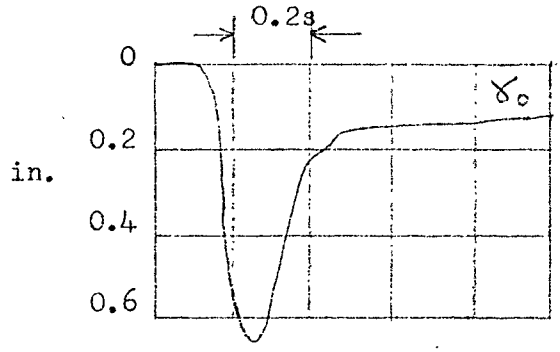

(displacement, right to left, fig. 3.1)

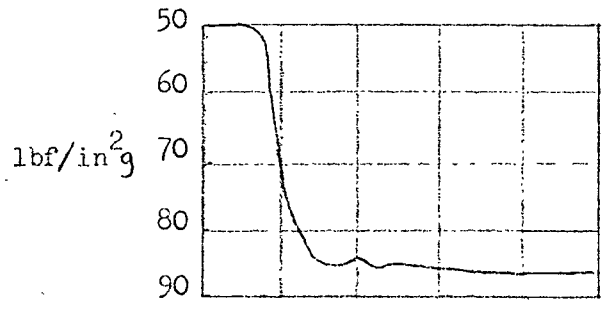

(b) Transient pressure feedback

Stiffness ≙ $\frac{65}{0.14}$

≙ 465 lbf/in

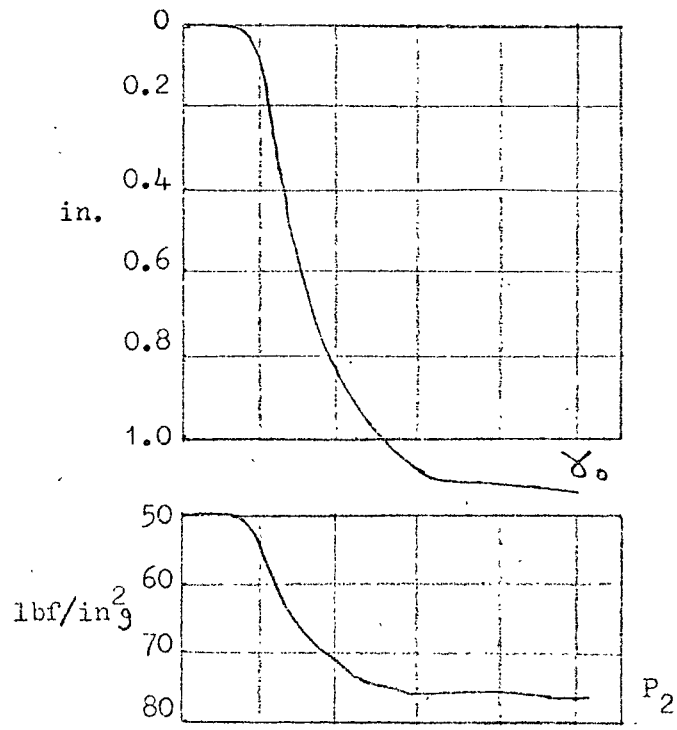

(c) Simple pressure feedback

Stiffness ≙ $\frac{49}{1.11}$

≙ 44 lbf/in

Parameters for (a) (b) and (c)

m_L = 8.7 lb

K_A = 590mA/V

K_p = 8.2 V/ft

τ_p = 0.06s

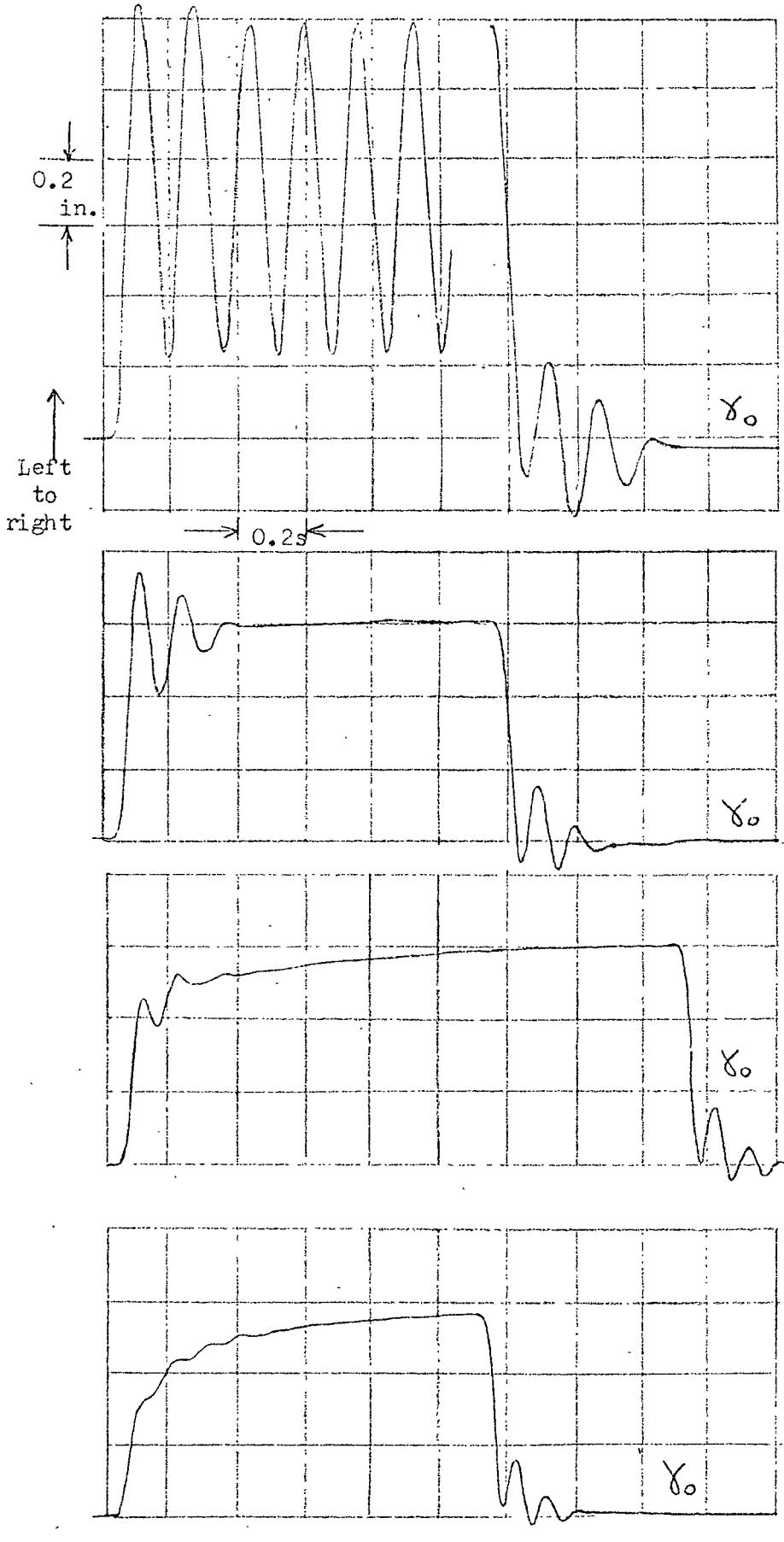

(a) P_1 = 20 lbf/in^{2}g
$F_L \triangleq$ -52 lbf
(pushing load carriage to the right in fig. 3.1)

(b) P_1 = 50 lbf/in^{2}g
F_L = 0

(c) P_1 = 80 lbf/in^{2}g
$F_L \triangleq$ +52 lbf
(pushing load carriage to the left)

(d) P_1 = 94 lbf/in^2
$F_L \triangleq$ 76 lbf
(pushing load carriage to the left)

Fig. 5.7 Transient Response in the Presence of Steady Load Forces

m_L = 8.7 lb, K_A = 8.2 V/ft

K_p = 590mA/V, K_{pr} = 0

of a steady load. The step responses for pressures of 20, 50, 80 and 94 lbf/in^{2}g were recorded and are shown in fig. 5.7. Adjusting P_1 had the same effect as applying a steady force, except that in the former case there was no piston leakage when the piston was at rest, as there would have been in the presence of a differential pressure across the piston. This small leakage would result in a steady state position error but would have negligible effect on transient behaviour. Trace (a) in fig. 5.7 illustrates the destabilizing effect of a steady load force, whose direction is such as to reduce the quiescent pressure in the controlled chamber. It is noticeable that steps in one direction (left to right in fig. 3.1) are very much affected by load forces, while in the other direction load forces have very little effect.

5.3.5 Supply Pressure

For these tests, the supply pressure (P_s) was reduced and the pressure (P_1) in chamber 1 was always $\frac{1}{2}(P_s + P_e)$.

The servo was operated initially at 100 and 50 lbf/in^{2}g. (P_s and P_1 respectively) with parameters adjusted so that the step response was just stable. The operating pressures were then reduced successively to 80 and 40 lbf/in^{2}g., 50 and 25 lbf/in^{2}g. and 30 and 15 lbf/in^{2}g. In each of these three cases the servo was unstable.

5.4 Discussion of Chapter 5

The effects of variations in a number of parameters on the behaviour of the closed loop system are discussed individually below.

5.4.1 Equilibrium Position (Tests ES0/2, ES1/3, ES16/19, ES18/17, ES26/30, ES29/31)

In the above pairs of step response tests, only the final

equilibrium position differed. The most obvious difference in each of these cases is the increase in the frequency of the transient oscillations which occurred as the controlled chamber volume (V_2) was decreased. It is possible to predict that the open-loop undamped natural frequency (ω_{no}) changes in this way, from the linearised equation (eqn. 3.46), where, if all other parameters are constant, $\omega_{no} \propto (V_{2a})^{-\frac{1}{2}}$

The ratio of the oscillation frequencies for each of the above six pairs of results was measured and found to vary in just this way (within 6%). Thus it is possible to predict the variation in closed-loop frequency, due to piston position change, from a calculation of the open-loop natural frequencies.

In section 3.3.1 it was predicted that stability would deteriorate with volume increase, particularly in the presence of pressure feedback. This effect is noticeable in the first four of the above-named pairs of traces but in the last two, where no pressure feedback was employed, no change in damping is discernible.

5.4.2 Load Mass (Tests ES10/14, ES11/15, ES30/32, ES31/33)

In these cases, only the load mass differed between each test in a pair. Here the transient frequency decreased with load increase. In eqn. 3.46, if all parameters are constant except load mass, $\omega_{no} \propto (m_L)^{-\frac{1}{2}}$.

In this case the ratio of measured oscillation frequencies for each pair of tests agreed with this open loop relationship within about 15%.

In the last two pairs of the above-listed tests the pressure feedback was zero and in these circumstances a worsening of stability with mass increase was forecast in section 3.3.1. This is evident as a decrease in the damping in those cases.

5.4.3 Transient Pressure Feedback (Tests ES1/4, ES2/5, ES6/8, ES7/9, ES10/11, ES12/13, ES14/15, ES16/20, ES18/21, EH5/6 and Eo5/6)

In the above cases, the second named test represents an increase in negative transient pressure feedback over the first. In all cases the effect is quite clearly to reduce oscillations and also to reduce the frequency of oscillations. The root loci of fig. 3.10(b) and reference to fig. 3.10(d) indicate that a reduction in transient frequency is predicted by the linear theory. The root loci are sketches only and the observed increase of damping in the experimental traces suggests that the complex branches are of the general shape drawn in fig. 3.10(b) (i.e. allowing an increase of the angle θ with gain).

The increased damping is also obvious on the closed-loop Bode diagrams and the improved stability is indicated by the gain margin increase from 6 dB to 16 dB in the open-loop Bode diagrams.

5.4.4 Open Loop Gain (Tests ES4/9, ES5/8, ES28/26, ES29/27)

In all cases gain increase is seen to reduce closed loop damping though in the case of tests ES28/26 and ES29/27 the predominant effect is to reduce the importance of the first order time constant (τ_c in eqn. 3.44) so that it no longer dominates the step response.

5.4.5 Step Direction (Tests ES1/2, ES4/5, ES6/7, ES8/9, ES16/18, ES20/21, ES22/23, ES24/25)

In the above tests only the direction of approach to the final equilibrium position varied. In all cases the damping for left to right steps (fig. 2.1) is slightly greater than that for right to left steps. There is also evidence of a longer first order lag (in addition to the oscillatory portion) for certain of the left to right responses (tests ES18, 21, 23). These observations run counter to what might be expected, since left to right motion was initiated by flow from the supply to the actuator, and the valve characteristic was steeper for

supply flow than for exhaust flow. On this basis more rapid, rather than more sluggish, response would be expected. The transient frequencies in the two directions were always within 5% of each other.

5.4.6 Command Signal Amplitude (Tests EH1/2, EH3/4, EH6/7 and EO1/2, EO3/4, EO6/7)

Inspection of the open-loop Bode plots shows that when the harmonic input amplitude is reduced, there is a reduction in gain (i.e. the modulus curve drops) while the phase angle remains almost constant. This effect is more noticeable for EO2 and EO7, for which the command amplitude is very small ($\pm$ 0.25 in.), than for EO4, where the amplitude is larger ($\pm$ 0.5 in.) An alternative way of expressing this point is that the servo has a larger gain margin, and is therefore more stable, for small amplitudes.

5.4.7 Velocity Feedback (Section 5.3.1)

The long time constant in the step response shown in fig. 5.4(b) can be explained on the basis of linear theory, by reference to fig. 3.7. In these root locus plots, while the damping of complex poles may be increased by velocity feedback, and indeed an unstable system is always stabilized, the real pole is seen to approach the origin. Thus a fairly large time constant forms part of the transient response and clearly the coefficient of this term was large in this case. By contrast the real poles in fig. 3.10 for transient pressure feedback do not constitute a significant part of the response, which is demonstrated in fig. 5.4(c).

A similar effect can also be seen in reference 37, figs. 2 and 3, showing step responses for a low pressure on/off pneumatic servo. The increasing dominance of a first order lag, as velocity feedback was progressively increased, was not discussed by the authors for whom the main point of interest in those figures was the validity of a computer simulation.

5.4.8 Steady Load Forces (Section 5.3.4)

Linear theory was used in section 3.3.1(f) to predict that the stabilizing and destabilizing effects of steady loads would be as observed for the left to right commands in fig. 5.7. It was also shown that mutually opposing effects ((i) and (ii) in table 3.2) operated for right to left commands, making prediction of behaviour difficult. The results in fig. 5.7(a) to (d) for right to left commands show that the destabilizing effect of the reduced quiescent pressure in chamber 2 (effect (i)) was approximately compensated by the decrease in the valve coefficient c_1 for exhaust flow (effect (ii)). This resulted in similar transient responses for all right to left steps.

Brann [20] examined the theoretical effects of load forces on stability for such a system but as he considered only effect (i) and did not allow for the changes in the valve coefficients, c_1 and c_2, he was unable to foresee the unsymmetrical behaviour described here. In hydraulic systems, where the bulk modulus is virtually independent of pressure, only effect (ii) is present. This means that, when a load force is applied, the response to steps in the same direction as the force become less damped and even unstable while if the force opposes the motion the response is more damped. This was observed by Davies [67] both in an analogue simulation and in an experimental hydraulic servo.

5.4.9 Supply Pressure

The destabilizing effect of supply pressure reduction noted in section 5.3.5 is explained according to the linear theory in section 3.3.1.

CHAPTER 6 SIMULATION OF THE ELECTRO-PNEUMATIC SERVO

In order to assess the relevance of the models proposed in Chapter 3, to the results of tests on the experimental servo described in Chapter 5, two series of analogue computer simulations were conducted. In the first case a medium-sized computer with a full set of non-linear units, the E.A.L. TR 20, was used for a "full" simulation, and in the second case a very small but accurate machine, the Vidac 169, was used for a simple simulation. These are described in sections 6.1 and 6.2 respectively. In each case a number of the closed loop step and harmonic response tests carried out on the experimental servo were also conducted on the computer.

6.1 Full Simulation

The non-linear equations 3.15, 3.16, 3.20 and 3.23 developed in section 3.1.5 were used as the basis of this model. The realisation of these equations is discussed below, and the complete computer circuit is shown in figs. 6.1 and 6.2.

6.1.1 Actuator and Load

No simple expression to describe actuator and load friction emerged from the study reported in Chapter 4. Friction forces were, however, small and the assumption of viscous friction gave reasonable agreement with experimental results. Viscous friction was therefore used for the computer simulation.

Eqns. 3.15 and 3.23 rewritten in terms of the quantities a', b' etc. introduced in section 3.1.8 become

$$P_2 - P_1 = \frac{m_L}{A} D^2 \gamma_o + \frac{b}{A} D \gamma_o \qquad 6.1$$

and

$$D^3 \gamma_o = \frac{m_2}{a'} - \left(\frac{b' + e'}{a'} \right) D^2 \gamma_o - \left(\frac{c' + f'}{a'} \right) D \gamma_o \qquad 6.2$$

This summation was performed by amplifier 3 in fig. 6.1.

The computation of m_2 is described below.

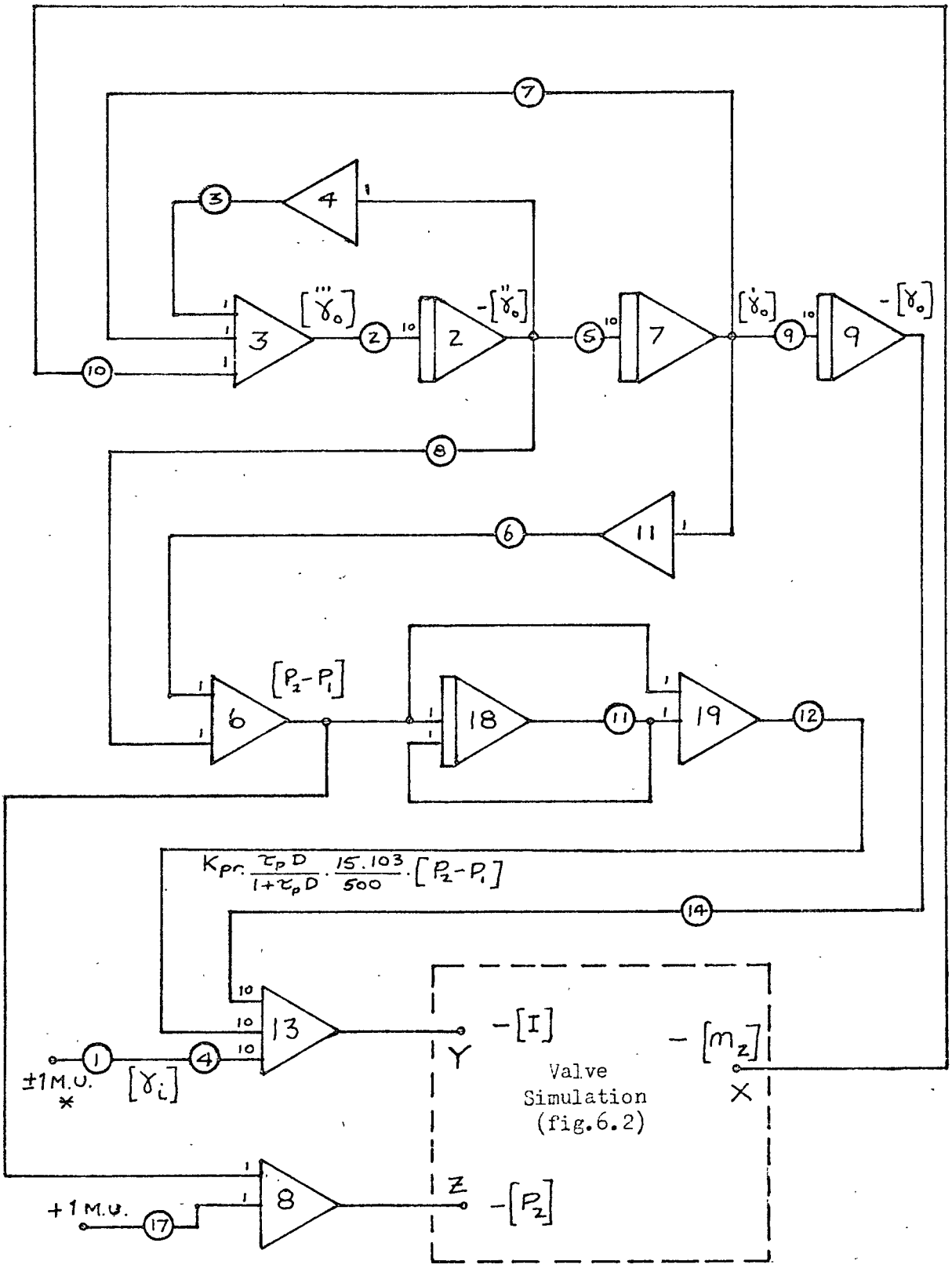

Fig. 6.1 Full Simulation Circuit Diagram

[ ] indicates a scaled variable in Machine Units (section 6.1.6)

See Appendix 7, Table A7.1, for potentiometer settings.

* for step response tests

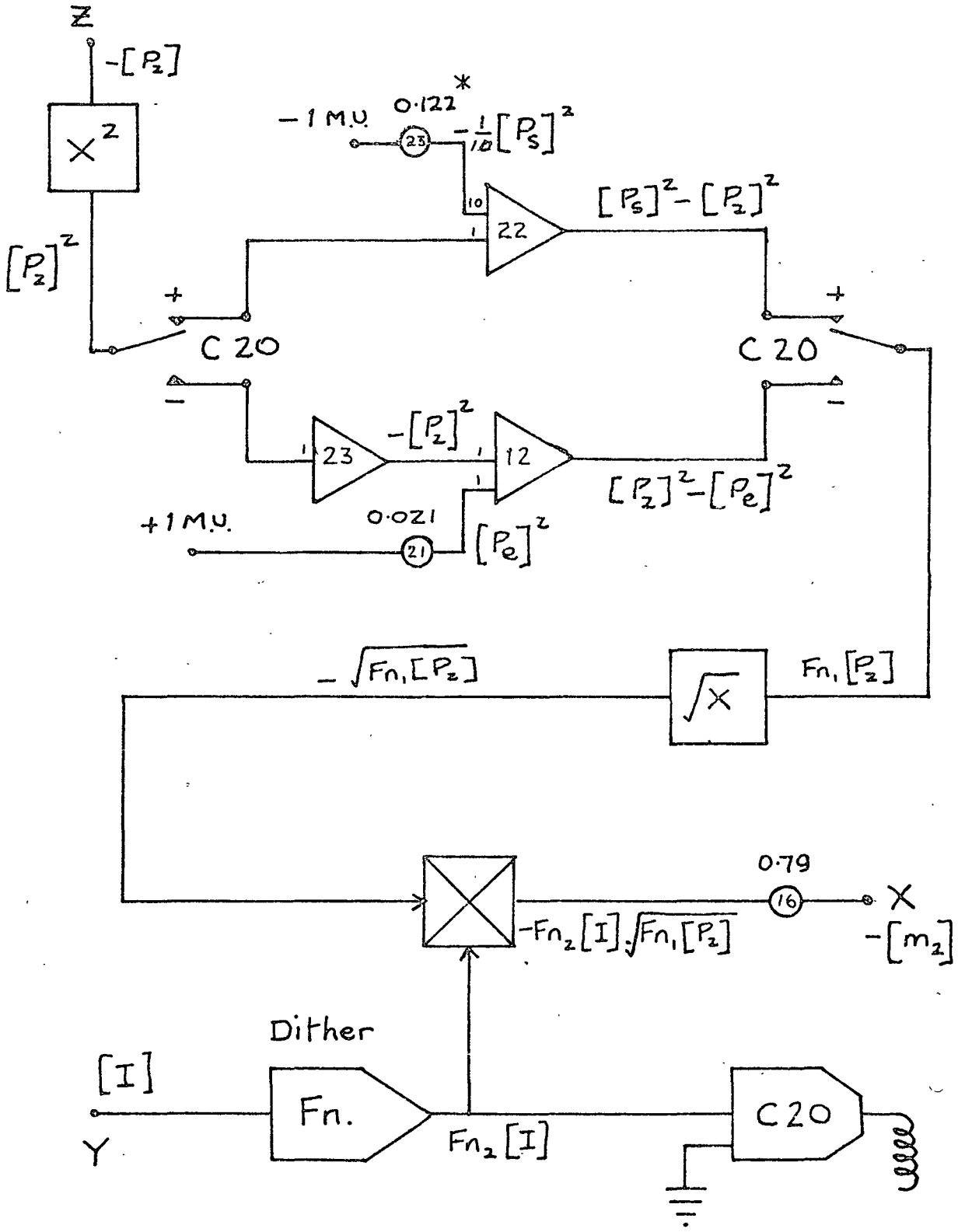

Fig. 6.2 Full Simulation - Complete Valve Simulation using MacNaughton's Expression and Including Dither

[ ] indicates a scaled variable in M.U.

* N.B. P_s = 115 lbf/in^{2}a and $[P_s]$ = 1.1 M.U.

The quantities a', b' etc. were constants for any particular computer run.

6.1.2 Valve Input

Eqn. 3.20 represents the derivation of the valve input current. For the present tests, no velocity feedback was used (i.e. $K_V = 0$) and the dither signal was accounted for separately, as part of the valve characteristic (see section 6.1.4 below). Thus eqn. 3.19 simplifies to

$$I = K_A K_p (\gamma_i - \gamma_o) - K_{pr} \left[\frac{\tau_p D}{1 + \tau_p D} \right] P_2 \qquad 6.3$$

This summation was performed by amplifier 13 in fig. 6.1 and amplifiers 6, 18 and 19 were used to simulate the high pass filter.

6.1.3 Valve Characteristics

In Chapter 4, section 4.3.6, the considerable divergence of the actual valve characteristics from the theoretical isentropic curves was discussed. In a paper on pneumatic servo valve design, MacNaughton [68] gave an empirical expression for modelling such characteristics. MacNaughton's expression gives a continuous curve (shown in fig. 4.15) with no discontinuity between choked and unchoked flow. MacNaughton reported satisfactory agreement between experimental results and this empirical expression for "small orifices", though no results were given. Cutland [23c] examined the leakage flow past an underlapped four-way spool valve and found that MacNaughton's equations were a better model than the isentropic flow equations. Cutland did not attempt to fit any analytical expressions to his valve flow/opening characteristics. Fig. 4.15 shows that in the present case MacNaughton's curve is rather closer to the experimental points than is the isentropic curve.

MacNaughton stated that at constant temperature, the flow through an orifice is proportional to the flow area, to the upstream pressure and to the function $\sqrt{1 - r^2}$, where r is the pressure ratio.

For a valve with flow area θ_v, the flow from the supply to

the control port is therefore

$$m_2 = C_6 P_s \theta_v \sqrt{1 - \left[\frac{P_2}{P_s}\right]^2}$$

and the exhaust flow is

$$m_2 = -C_6 P_2 \theta_v \sqrt{1 - \left[\frac{P_e}{P_2}\right]^2}$$

which can be written, for supply and exhaust respectively

$$m_2 = C_6 \theta_v \sqrt{P_s^2 - P_2^2} \qquad 6.4$$

and $$m_2 = C_6 \theta_v \sqrt{P_2^2 - P_e^2} \qquad 6.5$$

These equations were used to simulate the servo-valve characteristic using the circuit shown in fig. 6.2. (The function generator shown in fig. 6.2 was used to allow for the valve dither signal and is described in section 6.1.4.)

The empirical expression was originally developed in order to simplify orifice design calculations. It is also considerably easier to model on an analogue computer than is the theoretical isentropic expression, which requires the function

$$F(r) = r\sqrt{1 - r^{\frac{\gamma-1}{\gamma}}}$$

to be evaluated, in addition to the necessity for a discontinuity at r = 0.528.

The static valve characteristics* resulting from the use of this circuit are shown in figs. 6.3 and 6.4. (details of scaling appear in section 6.1.6). The method adopted was to adjust potentiometer 16 to give exact agreement, between the computer characteristic, and the known servo-valve static characteristic (fig. 4.14) at one point.

---

* The actual valve characteristic shows nominally zero flow at I = -20mA approximately, but for simplicity the computer characteristic was zeroed at I = 0mA. The effect of this was that, for example +180mA in the servo valve corresponded to +200mA in the computer. No allowance was made for the slight underlap observed in section 4.2.1.

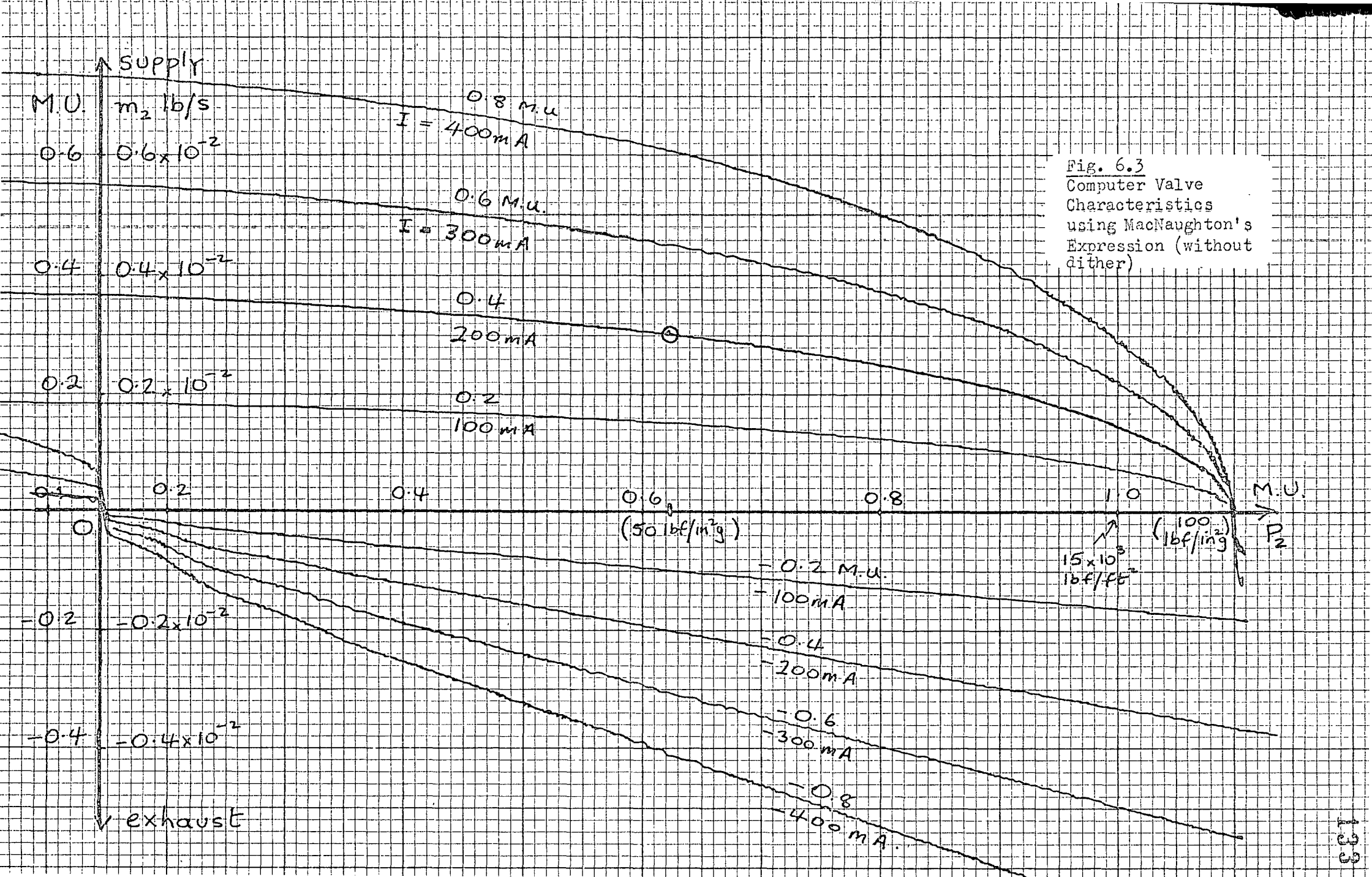

Fig. 6.3
Computer Valve Characteristics using MacNaughton's Expression (without dither)

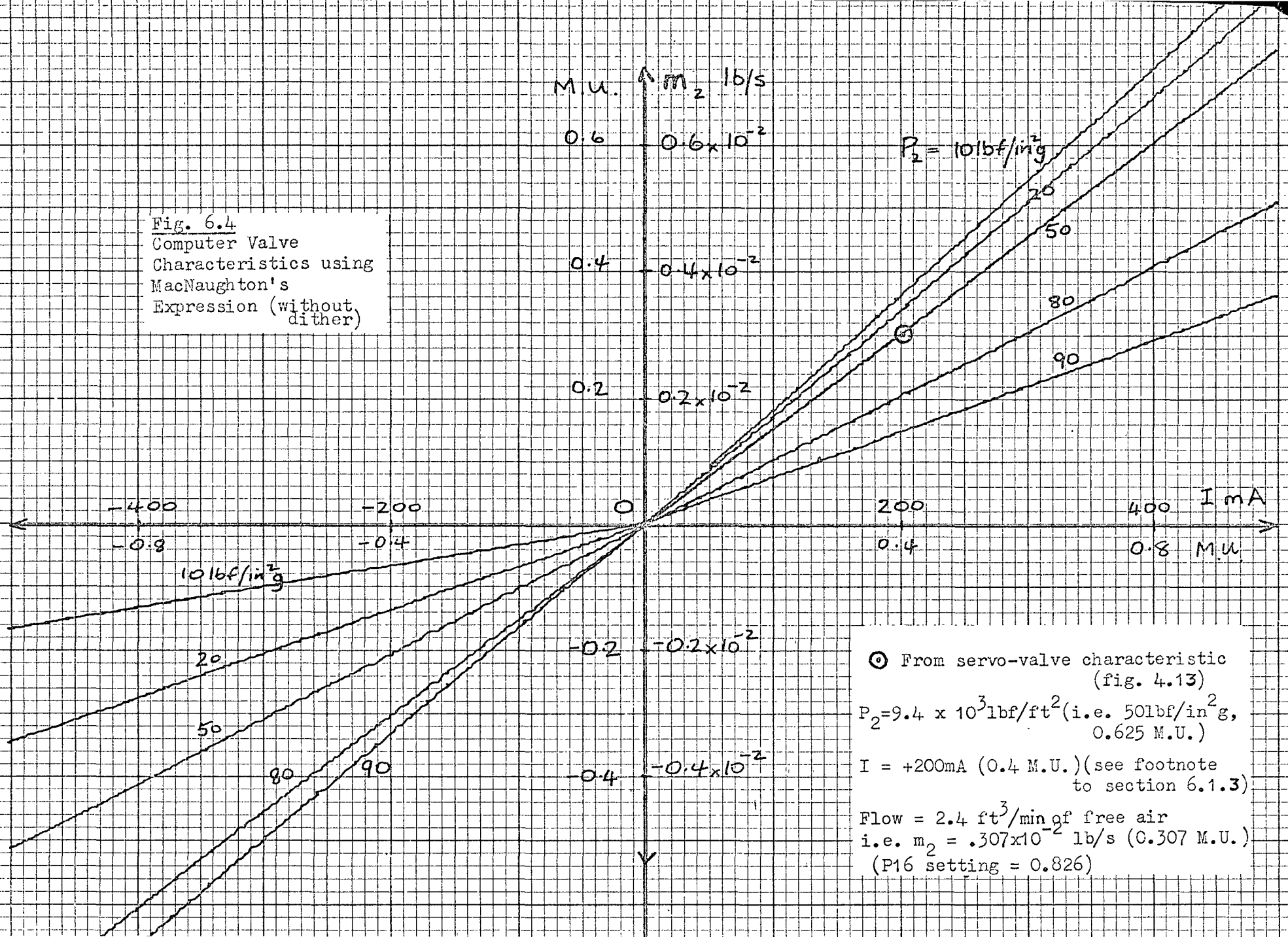

Fig. 6.4
Computer Valve Characteristics using MacNaughton's Expression (without dither)

⊙ From servo-valve characteristic (fig. 4.13)

$P_2 = 9.4 \times 10^3$ lbf/ft² (i.e. 50lbf/in²g, 0.625 M.U.)

I = +200mA (0.4 M.U.) (see footnote to section 6.1.3)

Flow = 2.4 ft³/min of free air
i.e. $\dot{m}_2 = .307\times10^{-2}$ lb/s (C.307 M.U.)
(P16 setting = 0.826)

This point is indicated in figs. 6.3 and 6.4.

6.1.4 Valve Dither

In section 4.2.2 the need was explained for a fairly large, high frequency (200 Hz) dither signal to be applied to the servo valve. Thus the valve input current was

$$i = I + I_D \sin \omega t$$

The valve laps were adjusted to give zero flow in either direction when a sinusoidal dither signal of 110mA amplitude was applied. The valve began to open to the supply for any signal current greater than the zero flow value (I = -20mA) and opened to exhaust for smaller currents. Thus the area for flow changed 200 times a second and the average flow area was not linearly related to the applied signal current. Also, from the experimental valve characteristics, the valve flow saturated at about +420mA and -460mA.

Fig. 6.5(a) shows this diagramatically with the zero flow point transposed from I = -20mA to I = 0mA for convenience. The area available for flow (shaded) during each cycle can be seen to increase from zero for zero signal current (I) to half the maximum for I = $\pm$220mA and to maximum for I = $\pm$440mA. Referring to fig. 6.5(b), the form of the characteristic relating the flow area per cycle and the signal current can be calculated.

To evaluate the area Z_1:-

$$Z_1 + Z_2 = \int_o^x y \, dx$$

$$Z_1 = \int_o^x y \, dx - x \cos x$$

$$= \int_o^x \cos x \, dx - x \cos x$$

$$= \sin x - x \cos x$$

The relationship required is that between y (= cos x) and Z_1 and values are tabulated in table 6.1. The last columns in that table show the scaling of these figures into computer machine units

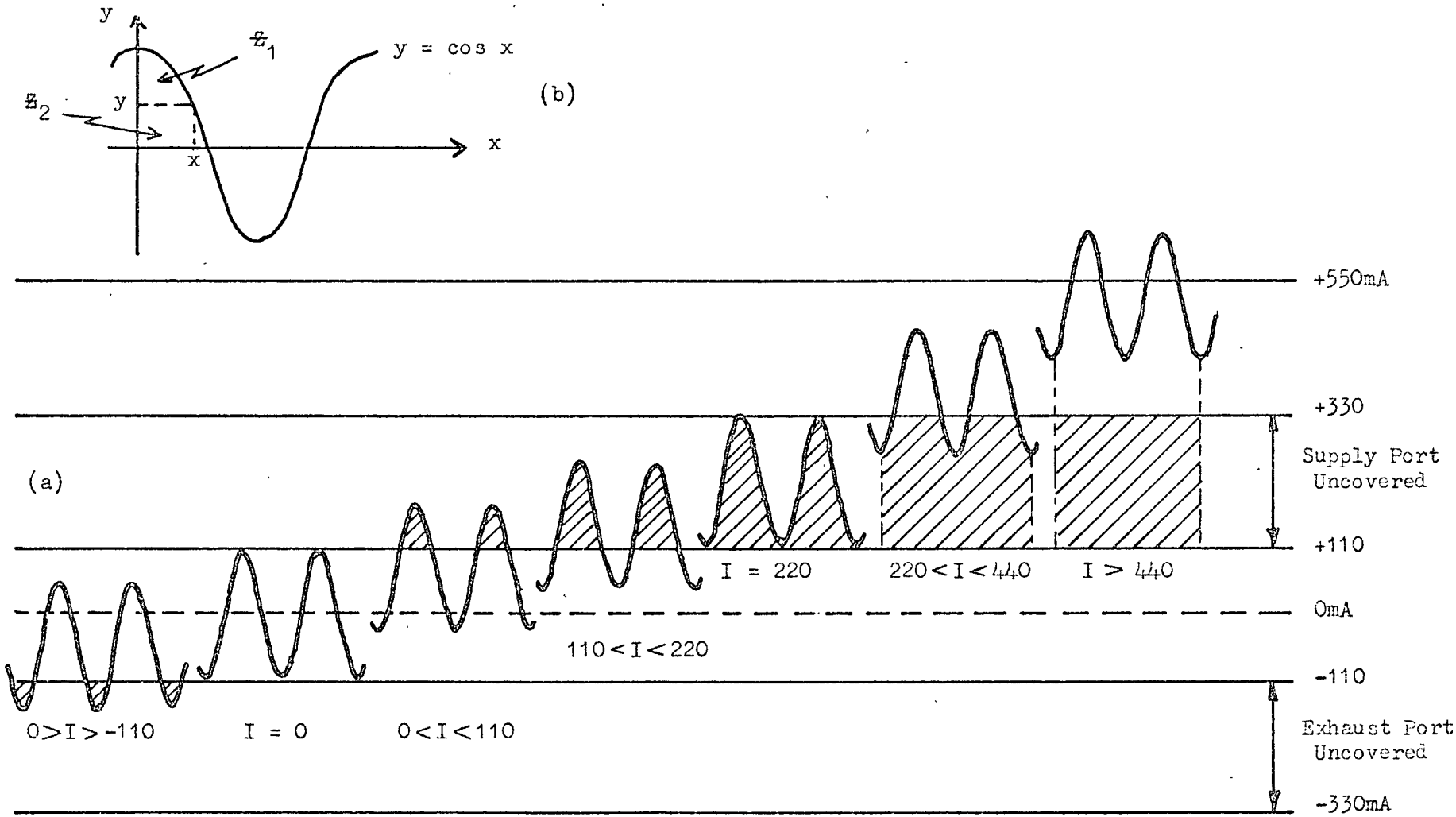

$i = I + I_D \sin \omega t$ and $I_D = 110$ (All currents in mA)

Fig. 6.5 Servo Valve Flow area in the presence of dither

Table 6.1 Valve Dither Characteristic

x degrees	x rad	y = cos x	z_1 = sin x − x cos x	(1 − cos x)	y scaled for computer (valve current) M.U.	z_1 scaled for computer (flow area) M.U.
0	0	1.00	0	0	0	0
40	0.70	0.77	0.10	0.23	0.05	0.02
60	1.05	0.50	0.34	0.50	0.11	0.05
90	1.57	0	1.00	1.00	0.22	0.16
110	1.92	-0.34	1.59	1.34	0.29	0.25
120	2.10	-0.50	1.92	1.50	0.33	0.31
140	2.40	-0.77	2.49	1.77	0.39	0.40
180	3.14	-1.00	3.14	2.00	0.44	0.50

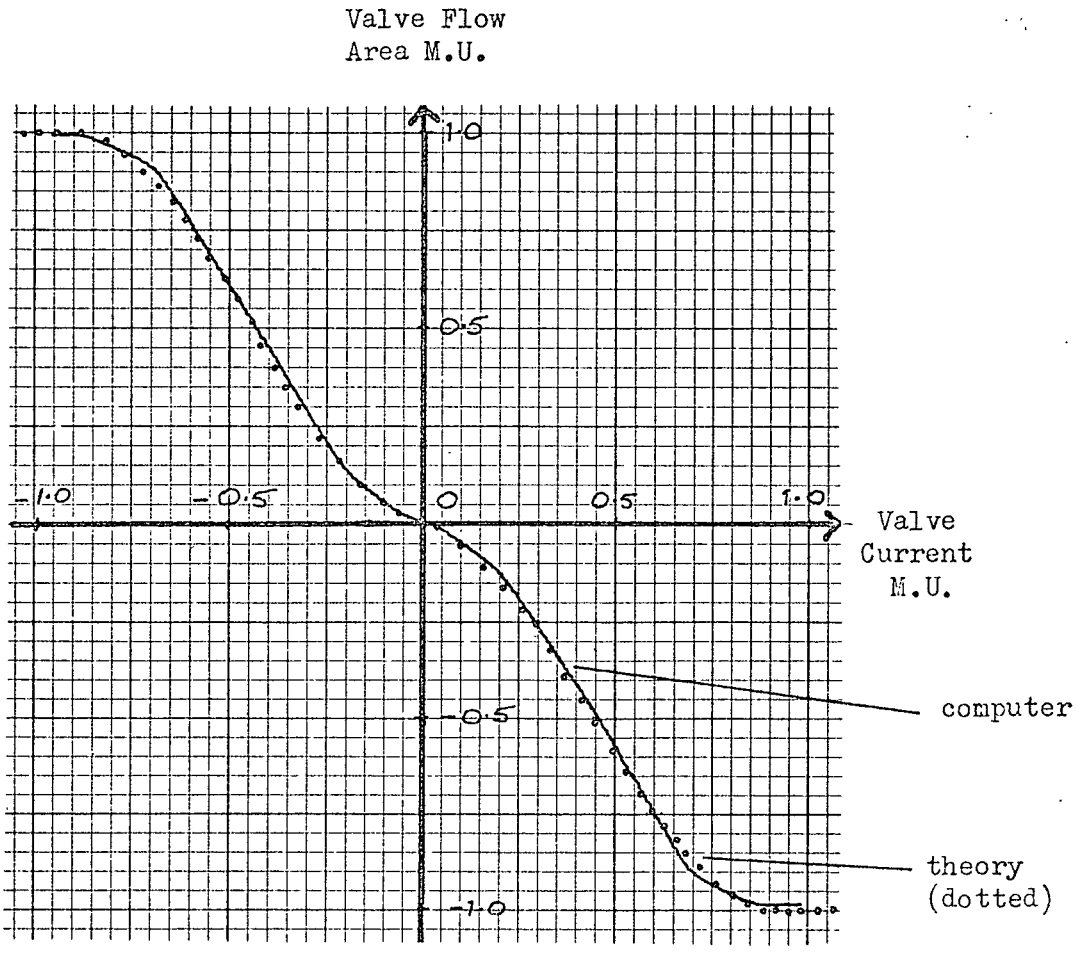

Fig. 6.6 Theoretical and Computer Dither Characteristics

for use with a variable diode function generator (V.D.F.G.). The scaling for valve current (1M.U. ≡ 500mA) is discussed in section 6.1.6 and for flow area an arbitrary 1M.U. maximum was selected.

Thus one quarter of the valve dither characteristic was defined and the remainder was plotted from the known symmetry of the curve. The V.D.F.G. in fig. 6.2 was adjusted by trial and error and the calculated and computer curves are shown in fig. 6.6.

6.1.5 Complete Valve Simulation

Fig. 6.2 shows the complete valve simulation circuit. Potentiometer 16 was adjusted to give agreement between experimental and computer characteristics at the one point, I = +200mA, P_2 = 50 lbf/in^{2}g. The computer characteristics are shown in figs. 6.7 and 6.8 with the experimental calibration curves from figs. 4.12, 4.13, and 4.14 superimposed, for comparison.

6.1.6 Scaled Equations

(a) Amplitude scaling

The amplitude scale factors used were:

γ_o and γ_i	0.25 ft	≡ 1 M.U. (10V)
$\frac{d\gamma_o}{dt}$	5 ft/s	≡ 1 M.U.
$\frac{d^2\gamma_o}{dt^2}$	150 ft/s^2	≡ 1 M.U.
$\frac{d^3\gamma_o}{dt^3}$	4000 ft/s^3	≡ 1 M.U.
P_1 and P_2	15 x 10^3 lbf/ft^2	≡ 1 M.U.
m_2	1.0 x 10^{-2} lb/s	≡ 1 M.U.
I	500mA	≡ 1 M.U.

Many parameter values are listed in Appendix 2.

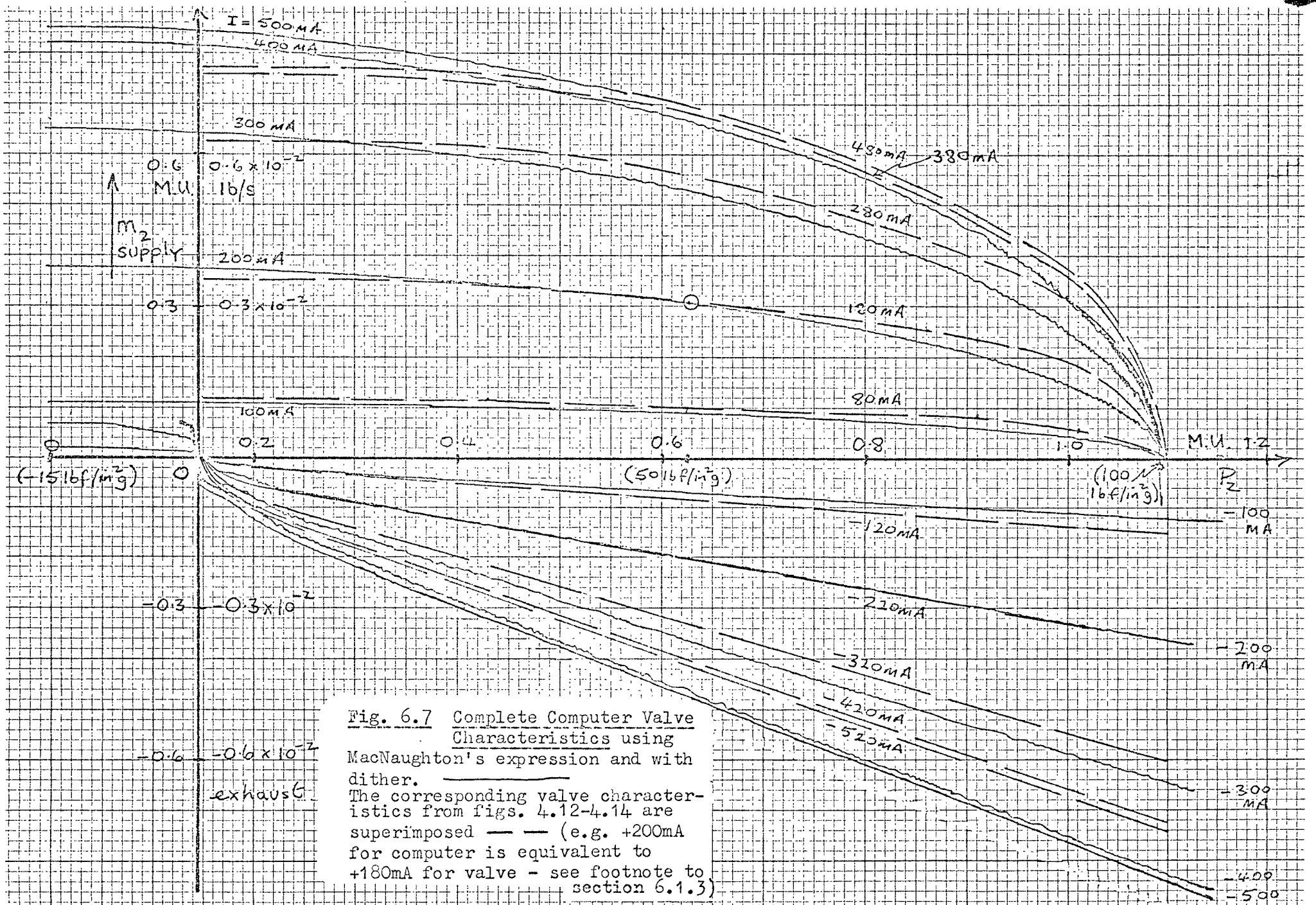

Fig. 6.7 Complete Computer Valve Characteristics using MacNaughton's expression and with dither.

The corresponding valve characteristics from figs. 4.12-4.14 are superimposed — — (e.g. +200mA for computer is equivalent to +180mA for valve - see footnote to section 6.1.3)

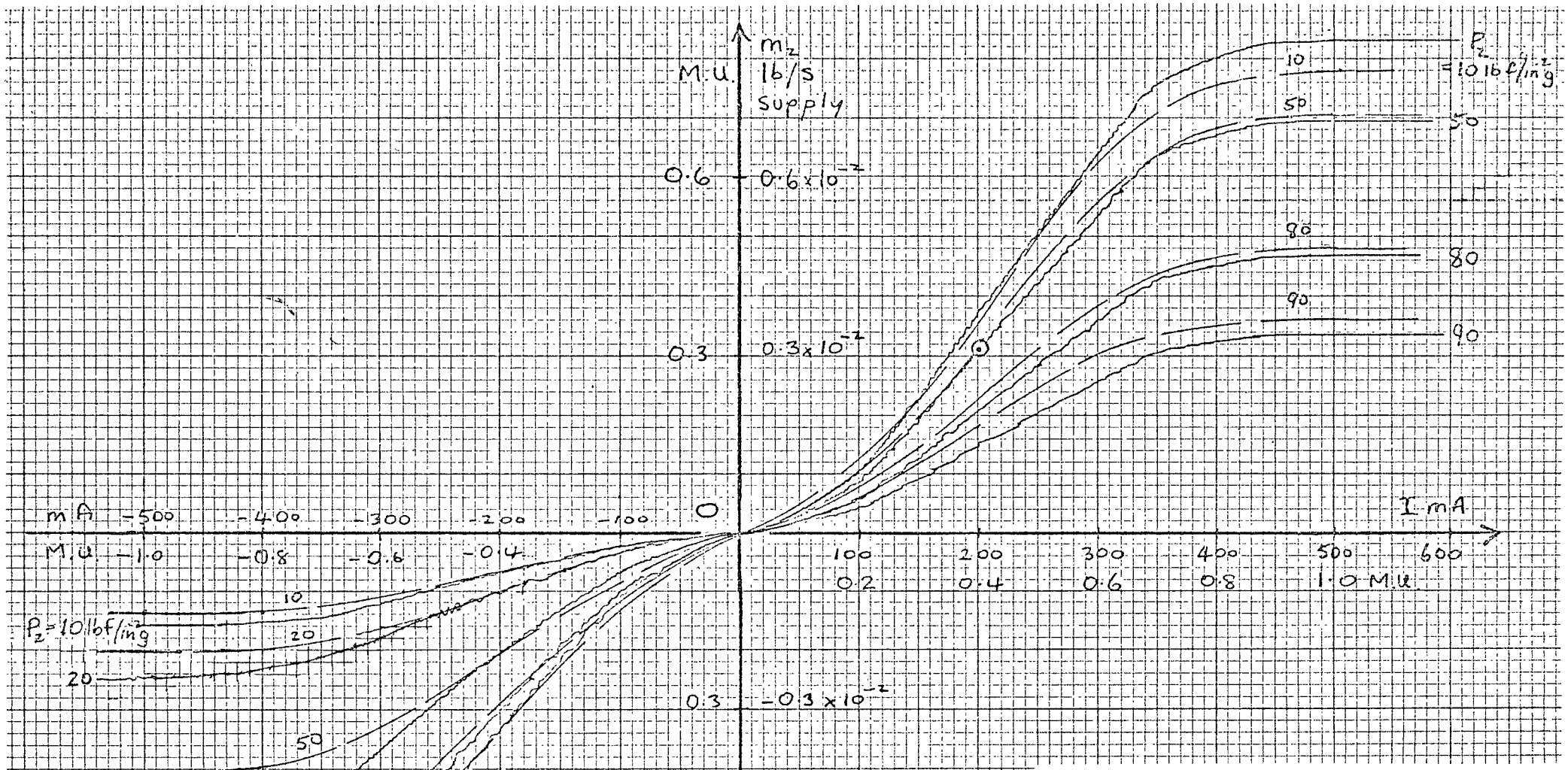

Fig. 6.8 Complete Computer Valve Characteristics

— — —valve curves displaced by 20mA to the left for comparison with:

——— computer traces.

(See note on fig. 6.7)

Eqns 6.1, 6.2 and 6.3 in scaled form become

$$\left[P_2 - P_1\right] = \frac{m_L}{A} \frac{150}{15 \times 10^3} \left[\frac{D^2 \gamma_o}{150}\right] + \frac{b}{A} \frac{5}{15 \times 10^3} \left[\frac{D \gamma_o}{5}\right] \qquad 6.6$$

$$\left[\frac{D^3 \gamma_o}{4000}\right] = \frac{1}{a'} \frac{1 \times 10^{-2}}{4000} \left[\frac{m_2}{1 \times 10^{-2}}\right] - \left(\frac{b' + e'}{a'}\right) \frac{150}{4000} \left[\frac{D^2 \gamma_o}{150}\right] - \left(\frac{c' + f'}{a'}\right) \frac{5}{4000} \left[\frac{D \gamma_o}{5}\right] \qquad 6.7$$

$$\left[\frac{I}{500}\right] = K_A K_p \cdot \frac{0.25}{500} \left(\left[\frac{\gamma_i}{0.25}\right] - \left[\frac{\gamma_o}{0.25}\right]\right) - K_{pr} \left(\frac{\tau_p D}{1 + \tau_p D}\right) \frac{15 \times 10^3}{500} \left[\frac{P_2}{15 \times 10^3}\right] \qquad 6.8$$

(b) Time scaling

The computer solution was slowed by a factor of 10 to enable a pen recorder to be used. To achieve this the integrator gains were reduced and fig. 6.1 shows the time and amplitude scaled circuit. All computer traces are marked in real time, for direct comparison with results from the servo.

6.1.7 Step Response Tests

The step response tests carried out as part of the full simulation are as listed for the servo step response tests in tables 5.1 and 5.2. The value used for V_{2a} in almost all cases was the final value of V_2, this being the mean value of the volume during the decaying transient oscillations (where such oscillations occurred). The exceptions were tests S26 to 33. In these cases, where small step commands were used, the mean value between initial and final piston positions was used (e.g. for tests S26 to 29 the position 1.125 in. was used to calculate V_{2a}). A value for the viscous friction coefficient (b) was decided on the basis of initial runs on tests FS1 and FS2. The value b = 6.7 lbf/(ft/s), derived in section 4.1.5 was tried initially. The analogue damping in this case was too light compared with that of the servo and therefore higher values were tried. A value, b = 13 lbf/(ft/s), gave a good match

between servo and analogue response. In fig. 6.9 the step response of the computer with these two values of viscous friction coefficient can be seen. (The lower traces are repeated in fig. 7.1 where the analogue and servo response can be compared.) The higher value of b was retained for the whole series of full and simple simulations. This point is discussed in sections 7.2.1 and 7.2.2. Complete records of the computer step response tests are included in Chapter 7, figs. 7.1 to 7.14. Attention is particularly drawn to fig. 7.3 in which the switching points for the valve simulation can be seen. In each case load displacement, pressure difference and valve current were recorded.

6.1.8 Potentiometer Settings

Potentiometer settings are shown algebraically in table A7.1, sample calculations for runs FS1 and FS2 and numerical potentiometer settings are given in Appendix 7.

6.1.9 Harmonic Response Tests

The closed loop harmonic response tests, detailed in table 5.3 for the experimental servo, were also conducted on the full simulation (tests FH1 to FH7). The resulting Bode diagrams are shown in figs. 7.15 to 7.21. Open loop Bode diagrams were derived from these plots using the Nichol's Chart as discussed in section 5.2.2. These diagrams are shown in figs. 7.22 to 7.28.

6.2 Simple Simulation

The results from the full simulation indicated that the complete equations developed in section 3.1.5 provided a good model of the operation of the servo over a wide range of inertial loads, step sizes, etc. These equations were linearized yielding the transfer operator of eqn. 3.42 and the purpose of the simple simulation was to investigate the validity of this much simpler model. This third order transfer operator was obtained by:

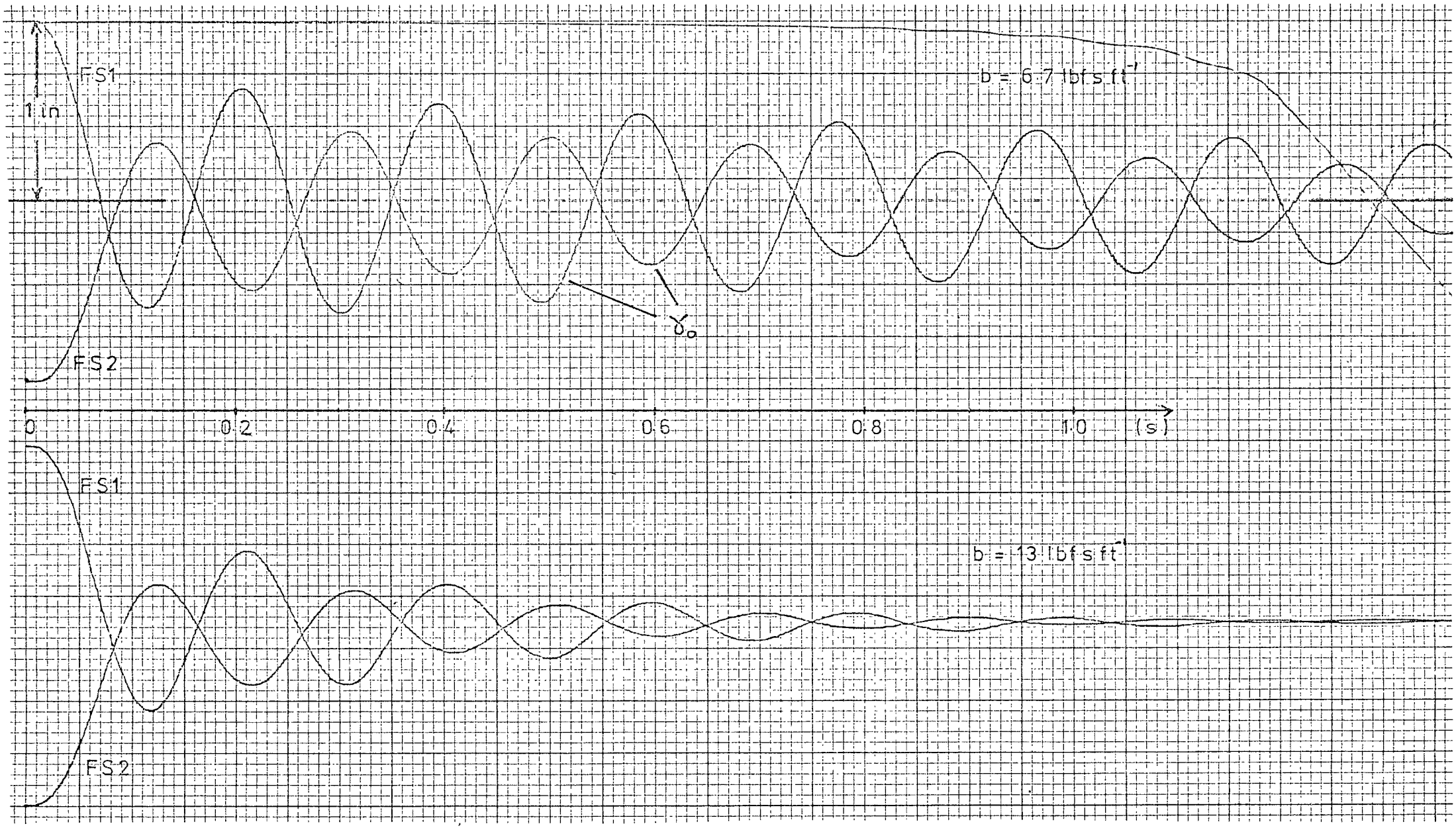

Fig. 6.9 Full Simulation Step Response with varying viscous friction

(a) Linearizing the valve characteristics

(b) Omitting the high pass filter in the pressure feedback path.

6.2.1 Linearizing the Valve Characteristics

The complete servo valve characteristics drawn in figs. 4.12, 4.13 and 4.14, in which flow rate is seen to vary with both valve current and pressure drop, can also be represented as a single, three-dimensional plot. This graph is drawn to isometric axes in fig. 6.10. The linearization of the valve characteristic described in section 3.1.7 can be regarded as the replacement of this three-dimensional surface by the plane surface shown in fig. 6.11. This plane is a representation of the linearised curves shown inset in fig. 6.11. Thus the selection of values for the valve coefficients c_1 and c_2 (eqn. 3.35) is the selection of slopes for these curves and for the plane in fig. 6.11. A value for c_1 was selected by drawing a straight line approximation to the quiescent pressure valve characteristic, as shown in fig. 6.12 and measuring its slope. The resulting value was

$$c_1 = 1.3 \times 10^{-5} \text{ (lb/s)/mA}$$

The selection of a value for c_2 was not so obvious, since the slope at the zero flow, quiescent pressure point is zero. The value actually selected was the measured slope of the -200mA exhaust flow curve at the quiescent pressure P_2 = 50 lbf/in^{2}g (fig. 4.14). If the +200mA supply flow curve had been used in the same way, the resultant value for c_2 would have been about 15% less. Thus for the simple simulation

$$c_2 = 20.3 \times 10^{-8} \text{ (lb/s)/(lbf/ft}^2\text{)}$$

The choice of c_1 and c_2 is further discussed in section 6.3.

6.2.2 Use of Simple Pressure Feedback

In order to minimize the complexity of the simple simulation,

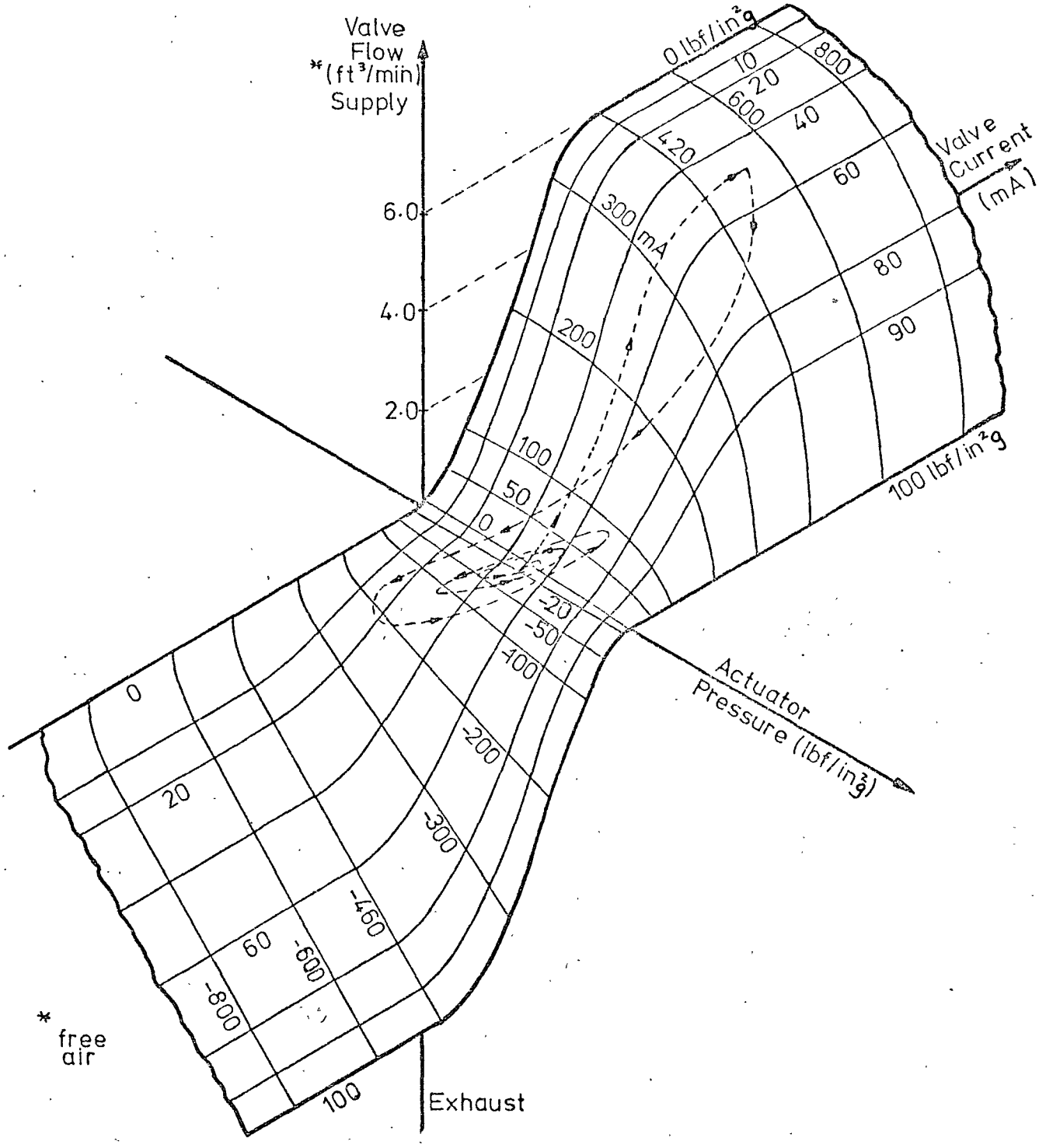

Fig. 6.10 Servo Valve Characteristics -

Three dimensional plot showing a typical trajectory for a step command signal (run FS12)

(a) Three dimensional representation - the "Valve Characteristic Plane"

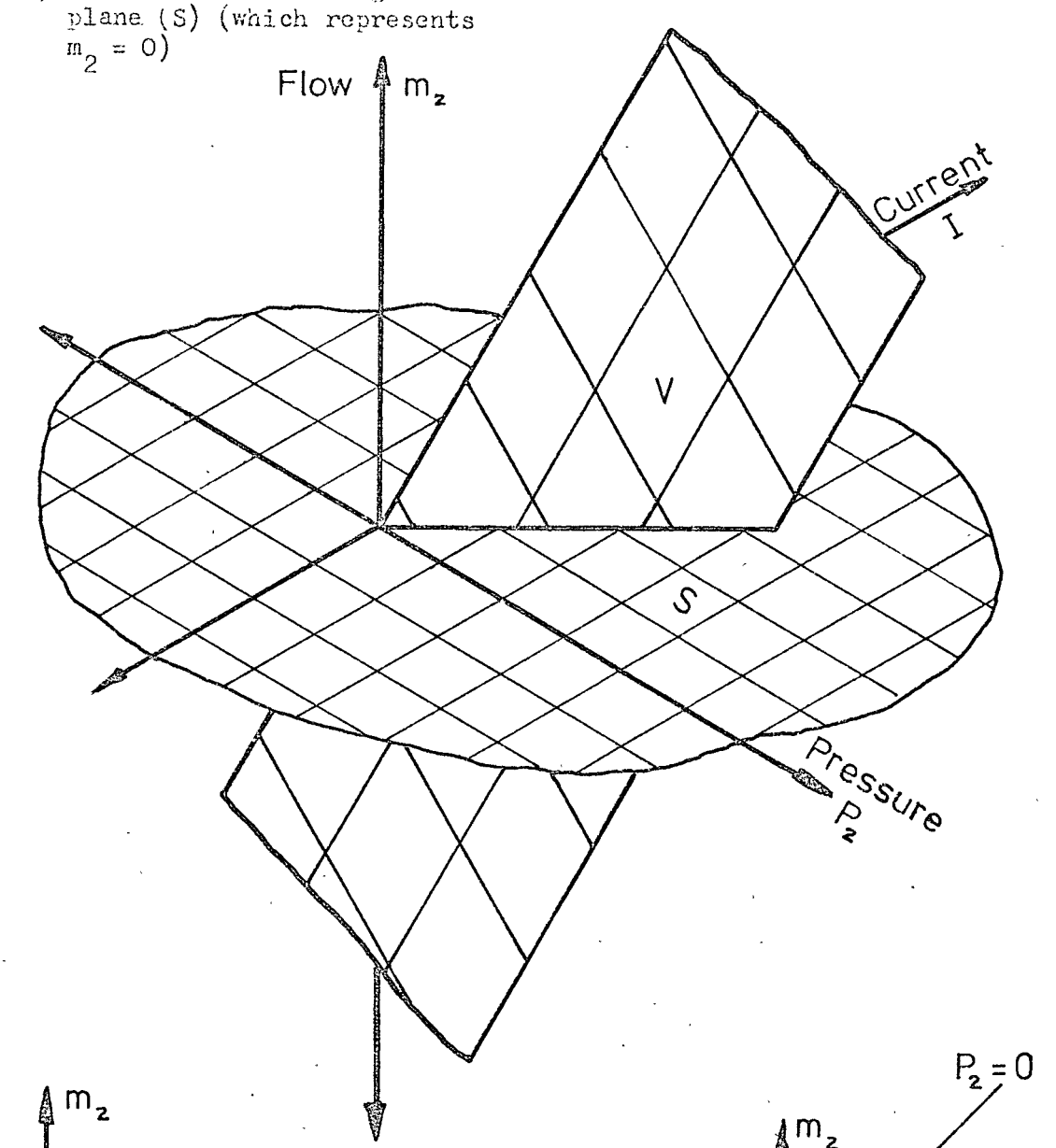

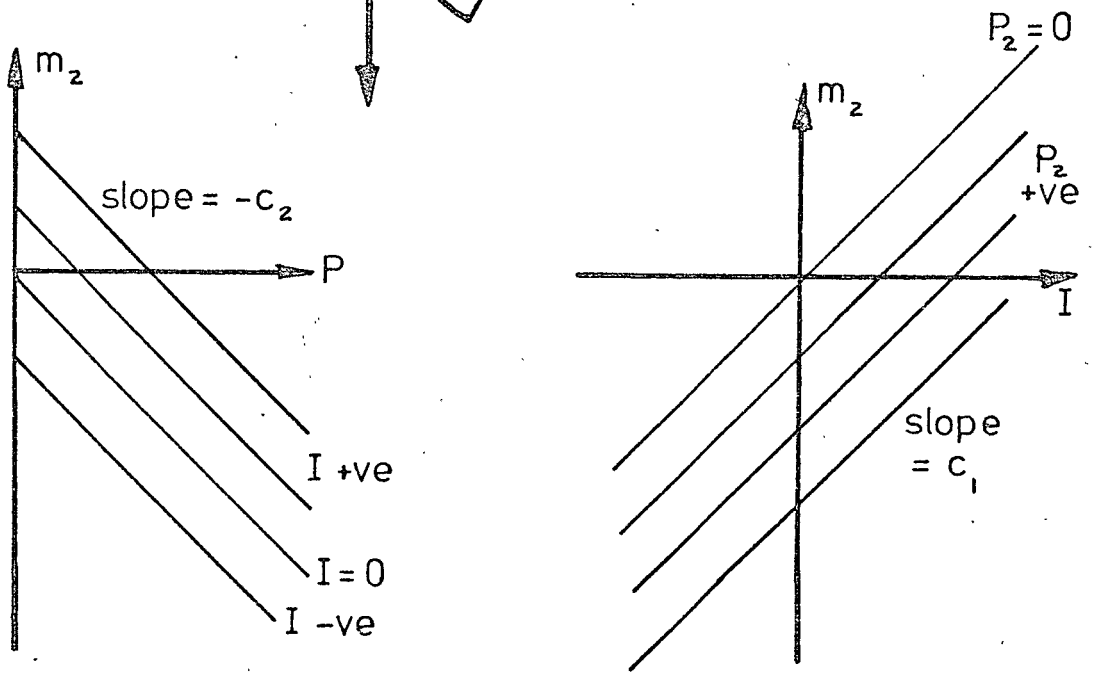

(b) Representation as two 'families' of straight lines

Fig. 6.11 Linearized Servo Valve Characteristics

i.e. graphical representations of eqn. 3.55:

$$\overline{m}_2 = c_1 \overline{i} - c_2 \overline{P}_2$$

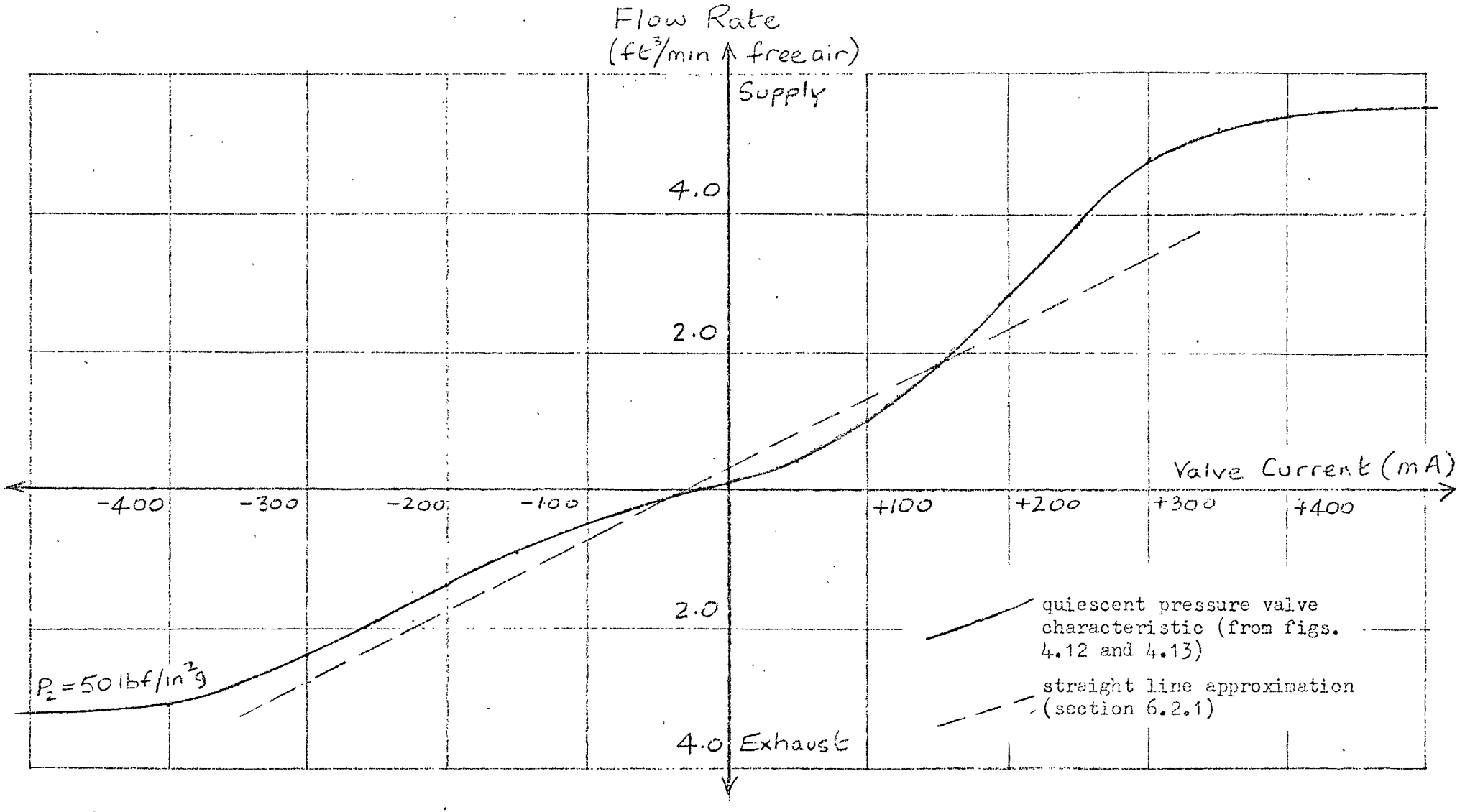

Fig. 6.12 Valve Characteristic Linearization

simple pressure feedback replaced transient pressure feedback.

Experience with the experimental servo suggested that the omission of the high pass filter in this way would not result in significant change in the response to step commands. Also the frequencies at which the filter would attenuate the pressure feedback were low and therefore on the flat portion of the closed loop Bode modulus plots, where the consequent damping reduction would be insignificant.

6.2.3 Scaled Equations

The same amplitude scale factors were used as for the full simulation (section 6.1.6).

Eqn. 3.42 in scaled form becomes

$$A'\left[\frac{D^2\bar{\gamma}_o}{150}\right] = -\int_o^{\infty}\left(B'\left[\frac{D^2\bar{\gamma}_o}{150}\right] + \frac{5C'}{150}\left[\frac{D\bar{\gamma}_o}{5}\right] + \frac{0.25D'}{150}\left[\frac{\bar{\gamma}_o}{0.25}\right]\right) - \frac{0.25D'}{150}\left[\frac{\bar{\gamma}_i}{0.25}\right] \qquad 6.9$$

As before, the time scaling was such that ten seconds on the computer corresponded to one second for the servo.

The computer circuit diagram is shown in fig. 6.13.

6.2.4 Step Response Tests

A number of the step response tests conducted on the experimental servo and on the full simulation were repeated. Details of the tests carried out are given in tables 5.1 and 5.2.

The viscous friction coefficient determined in section 6.1.7 was retained throughout the simple simulations.

In table 6.2 the individual values of all the coefficients (a', b', c' etc.) appearing in eqn. 3.41 are listed. This amount of detail is given as it enables the relative importance of individual terms to be estimated (see sections 6.3.2 and 7.2.2).

A pen recorder was used to record the computer response using

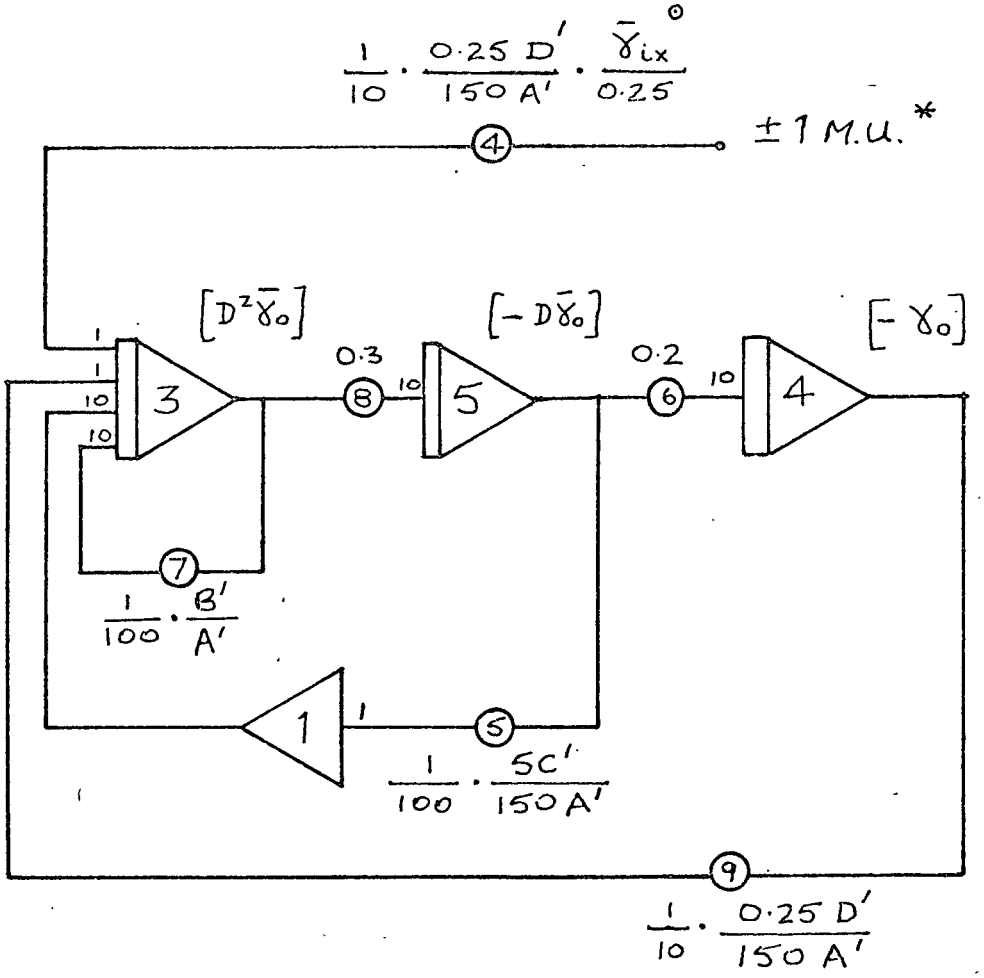

Fig. 6.13 Computer Circuit for Simple Simulation
(Time and amplitude scaled - see section 6.2.3)

[ ] indicates a scaled variable in machine units.

Specimen Potentiometer Settings:

For runs SS1/2, using the values of A' B' C' and D' listed in table 6.2, settings were P4 = 0.210, P5 = 0.111, P7 = 0.157 and P9 = 0.634.

* for step response tests

° $\bar{\gamma}_{i*}$ = amplitude of command signal in ft.

Table 6.2 Numerical Values for the Simple Simulation
(see Table 3.1 for symbols)

	Units	SS1/2	SS4/5 and SH1/2 and SO1/2	SS6/7	SS8/9	SS10	SS11	SS12
$a' = A'$	$lbft^{-1}s^2 x10^{-6}$	14.8	14.8	14.8	14.8	10.6	10.6	18.9
b'	$lbft^{-1}s x10^{-5}$	6.80	6.80	6.80	6.80	4.90	4.90	8.40
e'	"	1.03	1.03	1.03	1.03	1.03	1.03	1.03
g'	"	4.74	4.74	4.74	4.74	4.74	4.74	4.74
j'	"	10.6	57.5	22.4	57.5	10.60	57.5	10.6
$B' = b'+e'+g'+j'$	"	23.2	70.2	35.0	70.2	21.3	68.3	24.8
c'	$lbft^{-1}x10^{-3}$	4.14	4.14	4.14	4.14	4.14	4.14	4.14
f'	"	0.05	0.05	0.05	0.05	0.05	0.05	0.05
h'	"	0.22	0.22	0.22	0.22	0.22	0.22	0.22
k'	"	0.49	2.65	1.03	2.65	0.49	2.65	0.49
$C' = c'+f'+h'+k'$	"	4.90	7.06	5.44	7.06	4.90	7.06	4.90
$d' = D'$	$lbft^{-1}s^{-1} \times 10^{-2}$	5.60	5.60	9.35	9.35	4.36	4.36	4.36
$\tau_o = \frac{C'}{D'}$	s	0.087	0.126	0.058	0.075	0.112	0.160	0.112
$f_{no} = \frac{1}{2\pi}\sqrt{\frac{C'}{A'}}$	Hz	2.90	3.48	3.06	3.48	3.42	4.10	2.57
$\zeta_o = \frac{B'}{2\sqrt{C'A'}}$	-	0.445	1.08	0.618	1.08	0.465	1.24	0.410

Table 6.2 Numerical Values for the Simple Simulation
(see Table 3.1 for symbols)

continued on the following page

Table 6.2 continued

	SS13	SS16/18 and SH5 and S05	SS20/21 and SH3/4 and S03/4	SS * 22/23	SH6/7 and S06/7 (also SS24/25*)	SS * 26/27	SS * 28/29
A'	18.9	7.68	7.68	7.68	1.37	1.13	1.13
b'	8.40	6.80	6.80	6.80	6.80	5.60	5.60
e'	1.03	0.54	0.54	0.54	0.10	0.10	0.10
g'	4.74	2.46	2.46	2.46	0.44	0.44	0.44
j'	57.5	5.53	29.9	0.00	2.94	0.00	0.00
B'	71.7	15.3	39.7	9.80	10.3	6.14	6.14
c'	4.14	4.14	4.14	4.14	4.14	4.14	4.14
f'	0.05	0.05	0.05	0.05	0.05	0.05	0.05
h'	0.22	0.22	0.22	0.22	0.22	0.22	0.22
k'	2.65	0.49	2.65	0.00	1.52	0.00	0.00
C'	7.06	4.90	7.06	4.41	5.93	4.41	4.41
D'	4.36	4.36	4.36	4.36	4.60	12.8	4.45
τ_o	0.160	0.112	0.160	0.101	0.130	0.034	0.990
f_{no}	3.08	4.04	4.80	3.80	10.5	9.90	9.90
ζ_o	0.980	0.380	0.850	0.267	0.535	0.438	0.438

* These values are included for comparison though simple simulation results are not presented in Chapter 7

exactly the same X and Y sensitivities as were used for the full simulation records. These traces were then photo-copied to produce the transparent overlays in figs. 7.1 to 7.6, 7.8 and 7.9.

6.2.5 Harmonic Response Tests

Some of the closed loop harmonic response tests conducted on the experimental servo and on the full simulation were repeated (SH1, 2 and 5). The simple simulation did not display the amplitude dependence of the servo and the full simulation, so that the simple simulation measurements for test SH1 were also appropriate to test SH2. Bode diagrams appear in Chapter 7, figs. 7.15, 7.16 and 7.19.

The open loop Bode plots appearing in figs. 7.22 to 7.28 (nos. S01 to S07) were derived from the figures for τ_o, f_{no} and ζ_o in table 6.2, together with standard "second order" curves.

6.3 Discussion of Valve Simulation

6.3.1 Full Valve Simulation

The overall effectiveness of the full valve simulation can be judged from figs. 6.7 and 6.8. These compare the experimental static flow characteristics with those from a computer circuit incorporating McNaughton's expression and valve dither. A number of points emerge:

(a) On the supply side in fig. 6.7, the general shapes of the curves differ in the manner indicated by fig. 4.15.

(b) An alternative "matching" technique would have been to make the maximum flow value correct, for say I = +200mA. Reference to fig. 4.15 shows that in fig. 6.7 this strategy would have resulted in maximum error between the experimental points and the computer characteristic for pressure ratios between 0.4 and 0.8. This was not done since the valve operates with such pressure ratios for a large proportion of the time.

(c) If this curve matching had been adopted there would have been good agreement at maximum flows for all large openings (fig. 6.7), but the analogue indicates excessively low flows for small openings (e.g. ±100mA). This can be seen in a slightly different way in fig. 6.8 where the slope of the analogue curves is less than that of the valve curves, on either side of the origin. This effect would be caused by underlap in the valve (a little was observed in section 4.2.1) or by non-sinusoidal valve dither displacement.

(d) From fig. 6.8, it can be predicted that system disturbances resulting only in small valve currents would be less well modelled by these characteristics than larger disturbances (see section 7.2.1).

(e) Static valve characteristics were used on the assumption that these apply to the dynamic situation. This point is discussed in Chapter 7 where the dynamic response of the servo and the computer are compared. Shearer [3] modelled the static characteristics of the four-way valve in his high-pressure pneumatic system, using an electro-mechanical function generator which incorporated a stylus running over a three-dimensional "sculpture" of the flow curves.

6.3.2 Linear Simulation

Superimposed upon the three-dimensional valve characteristic (fig. 6.10) is a typical trajectory* for a step command signal to the closed loop system. This highlights the difficulty which arises in selecting single values for the valve coefficients c_1 and c_2 to represent large swings of pressure, current and flow. The linearization was based upon the assumption of small perturbations and if this were the case the problem would be less severe.

* Data from run FS12 used

A figure for c_1 was used for both supply and exhaust flow. Examination of fig. 6.12 shows that for any given opening of the servo valve the supply flow was about 1.5 times as great as the corresponding exhaust flow. This was due to the flow choking which occurred in the valve. The areas for exhaust and supply flow in this valve were equal, since it was designed for control of hydraulic oil where flow is simply a function of opening and pressure difference. In order to correct this inequality, the exhaust port area of a pneumatic valve can be made greater than the supply port area. A figure of 2:1 is often quoted for this purpose, but measurements from the valve characteristics (figs. 4.12 to 4.14) suggest that a figure of between 1.5 and 1.6 is suitable either with dither operating or without (i.e. valve fully open).

In the absence of dither the curve in fig. 6.12 would comprise two straight lines meeting at the origin, as in fig. 6.4. As discussed above, these two lines would have the same slope if the supply and exhaust areas were adjusted. In this case again, selection of c_1 would be obvious. The corresponding characteristic, linearized by Shearer [1], was made up of two straight lines of almost equal slope, with a small dead zone. Cutland's [23] valve had unequal supply and exhaust areas to equalize flows, though the characteristic was slightly s-shaped due to the occurrence of gradual saturation at full openings.

The selection of c_1 has considerably more influence on the behaviour of the simple simulation than does c_2. This is because c_1 appears in the term D', which is a coefficient in eqn. 3.42, while c_2 appears in g' and h' which are both added to other terms to make coefficients B' and C'. Reference to table 6.2 shows that c_2 has a negligible effect on C' but is sometimes an important influence on B'. The use of an unsuitable value for c_1 will show

up in the open loop integrating time constant (τ_o) in the Bode diagrams, while c_2 affects the open loop damping ratio (ζ_o) (see eqns. 3.45 and 3.46). This and other points from table 6.2 are further discussed in Chapter 7.

CHAPTER 7 THE ELECTRO-PNEUMATIC SERVO - COLLECTED RESULTS AND DISCUSSION

7.1 Collected Results

The results of the step response tests described in sections 5.1, 6.1.7 and 6.2.4, on the experimental servo and the full and simple simulations respectively, are shown in figs. 7.1 to 7.14. The collected results of the closed loop harmonic response tests are shown in figs. 7.15 to 7.21. Open loop Bode Plots are given in figs. 7.22 to 7.28.

7.2 Observations on the Computer Simulations

7.2.1 Full Simulation

Good general agreement between experimental results and those from the full simulations can be seen in figs. 7.1 to 7.28. In many of the step responses the damping of the models was slightly high. This would be improved if a lower figure for the viscous damping coefficient (b) was used. This point is further discussed in section 7.2.2.

In tests S6 to S15 the servo valve saturated owing to the large size of the step command. Flow saturation was built into the valve simulation and consequently the behaviour of the model follows that of the actual system closely. The largest pressure swings occurred in tests S0 to S13 where large inertia loads were present, while the largest chamber volume changes were in tests S10 to S15. At certain points in the full simulation equations, constants V_{2a} and P_{2a} replaced variables V_2 and P_2. These approximations would be most likely to lead to errors in the above-mentioned cases. However, again agreement is generally good though in some cases the computer pressure fluctuations were not as large as those occurring in the servo.

KEY TO FIGS. 7.1 TO 7.28

Step Response Results, figs. 7.1 to 7.14

(a) In these cases the actual pen-recorder traces from the Full Simulation (FS) are reproduced. The Servo response (ES) was recorded on u-v sensitive paper and these traces have been redrawn to the same scales as the FS traces, in figs. 7.1 to 7.14.

———————— Full Simulation (FS)

— — — — — Servo (ES)

(b) The transparent overlays are photographic reproductions of the pen-recorder traces for the Simple Simulation (SS). (Slight distortion in the reproduction is responsible for any misalignment of the grids, since the scale factors and time scales of FS and SS traces were identical.)

(c) Full details of parameters appear in tables 5.1 and 5.2.

(d) The scale shown for the γ_o traces refers to that shown in fig. 3.1.

(e) Referring to fig. 6.1, the Full Simulation traces were measured at amplifiers 9, 6 and 13 respectively. In the case of amplifier 6, $P_2 - P_1$ was actually recorded but since P_1 was constant, and allowing for this constant offset, the FS traces have been labelled P_2 for comparison with ES traces.

Closed Loop Harmonic Response, figs. 7.15 to 7.21

(a) Servo results are shown: —o——o——o—

Full Simulation: —×——×——×—

Simple Simulation, where applicable: ··o·····o·····o····

(b) Full details appear in table 5.3.

Open Loop Harmonic Response, figs. 7.22 to 7.28

Servo results: —o——o——o—

Full Simulation: —×——×——×—

Simple Simulation, derived from standard curves using parameters in table 6.2: ·····

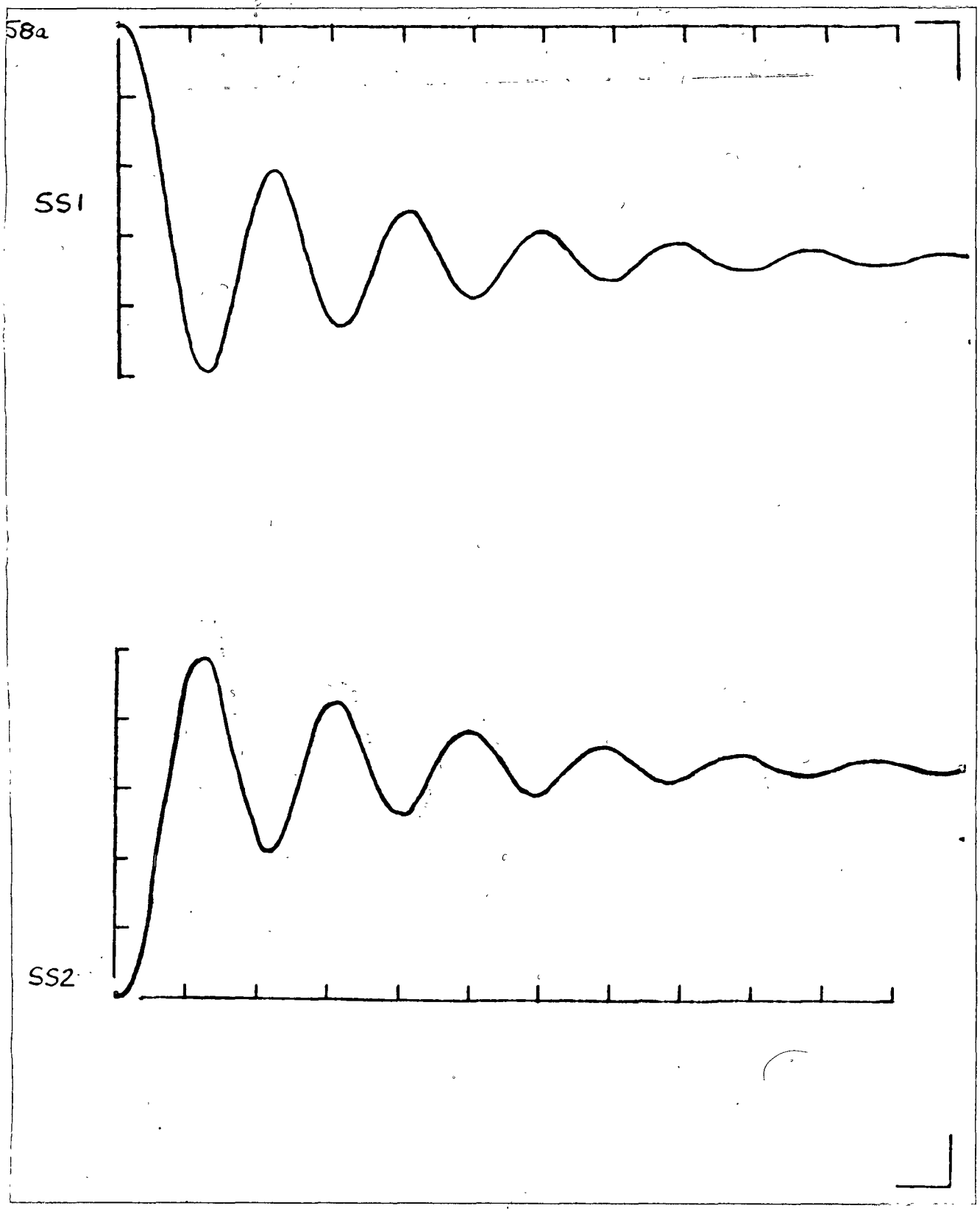
58a
SS1
SS2

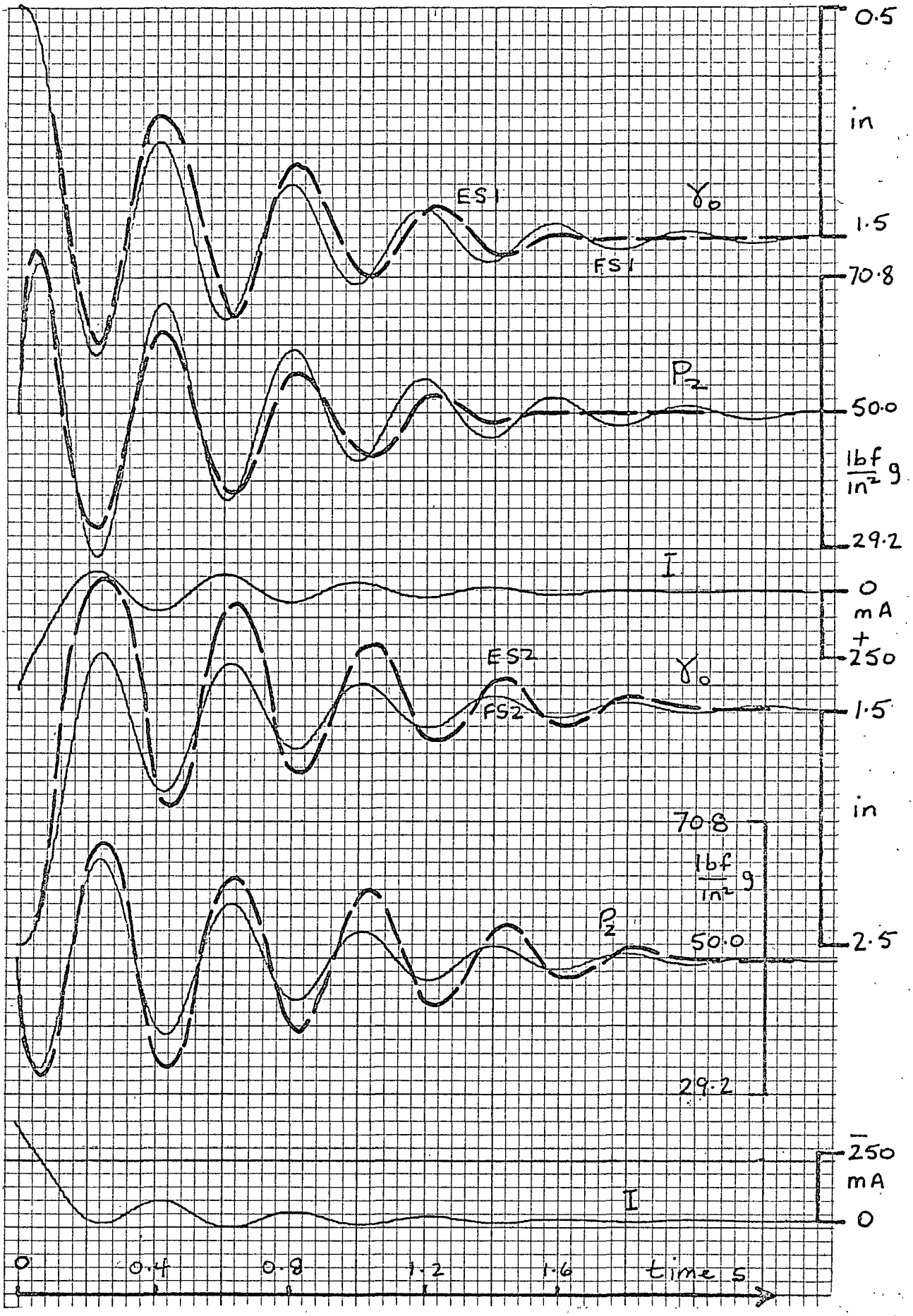

Fig. 7.1 Step Response Results

Showing 1 in steps towards piston mid-position, from left to right (test S1) and from right to left (S2), with large inertial load (93.7 lb)

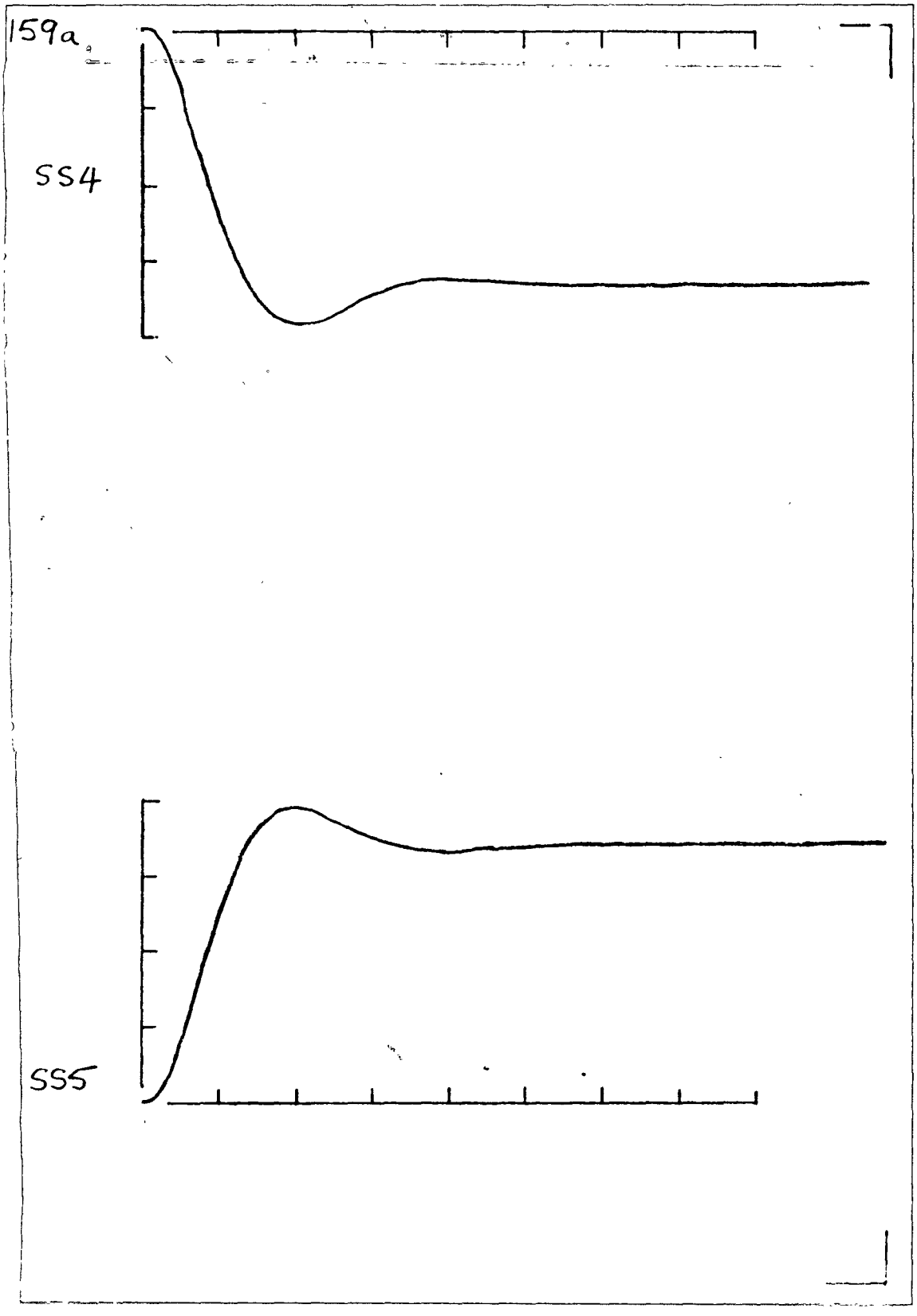
159a
554
555

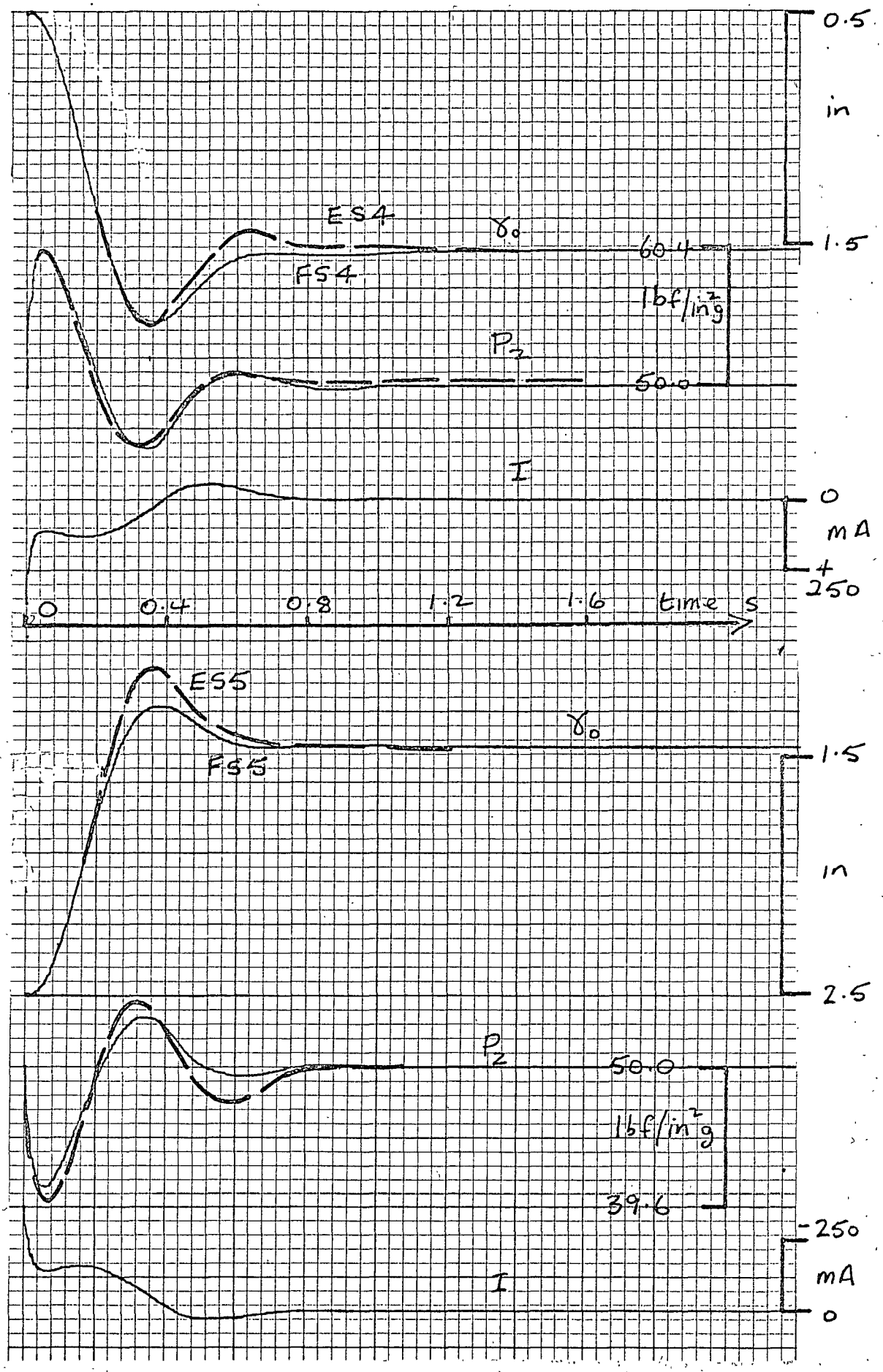

Fig. 7.2 Step Response Results

As fig. 7.1 but with increased transient pressure feedback.

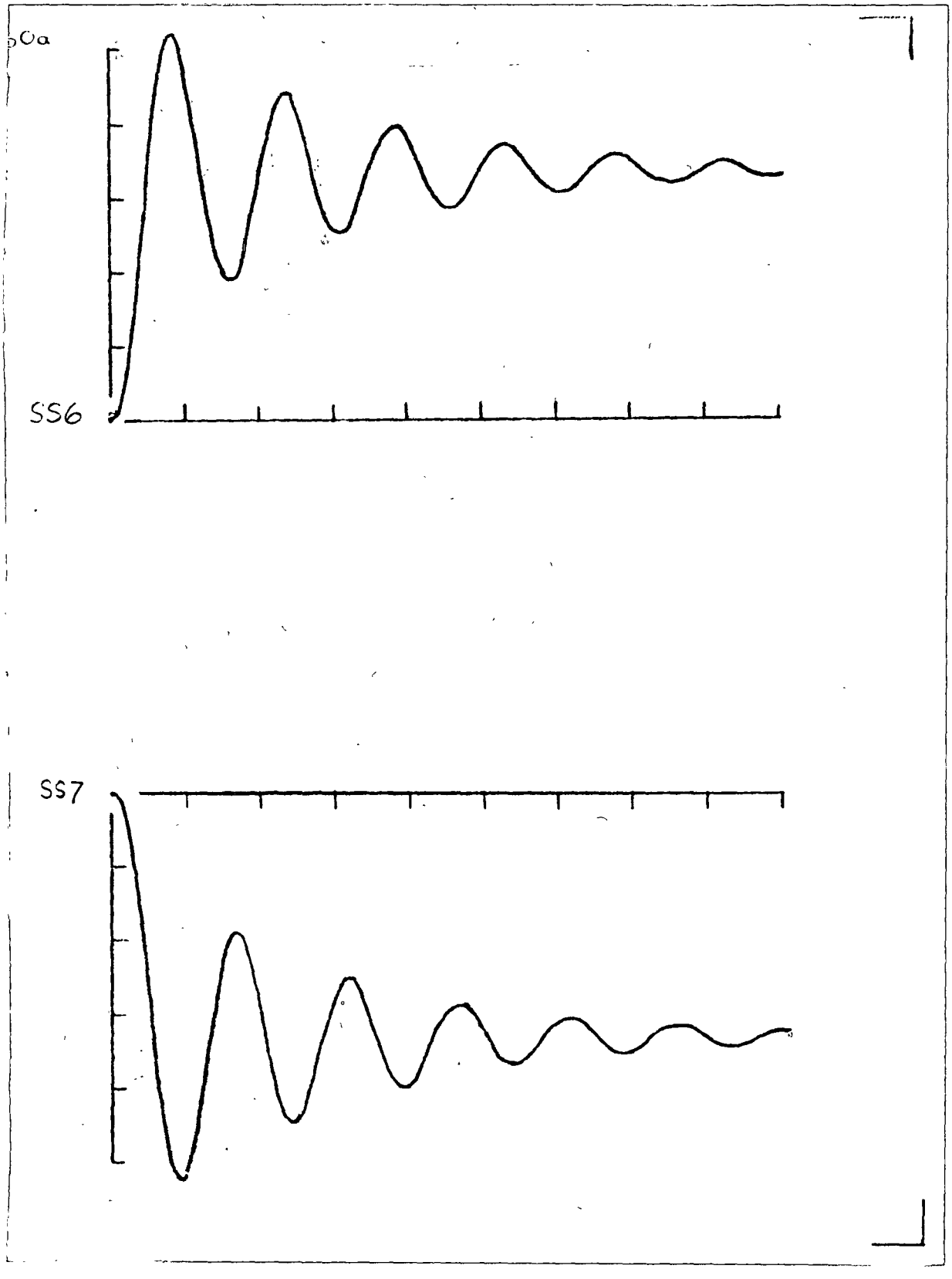
SS6
SS7

Fig. 7.3 Step Response Results

Showing 1 in steps towards piston mid-position from left to right (S6) and from right to left (S7), with large inertial load and with open loop gain set at maximum value to just maintain stability.

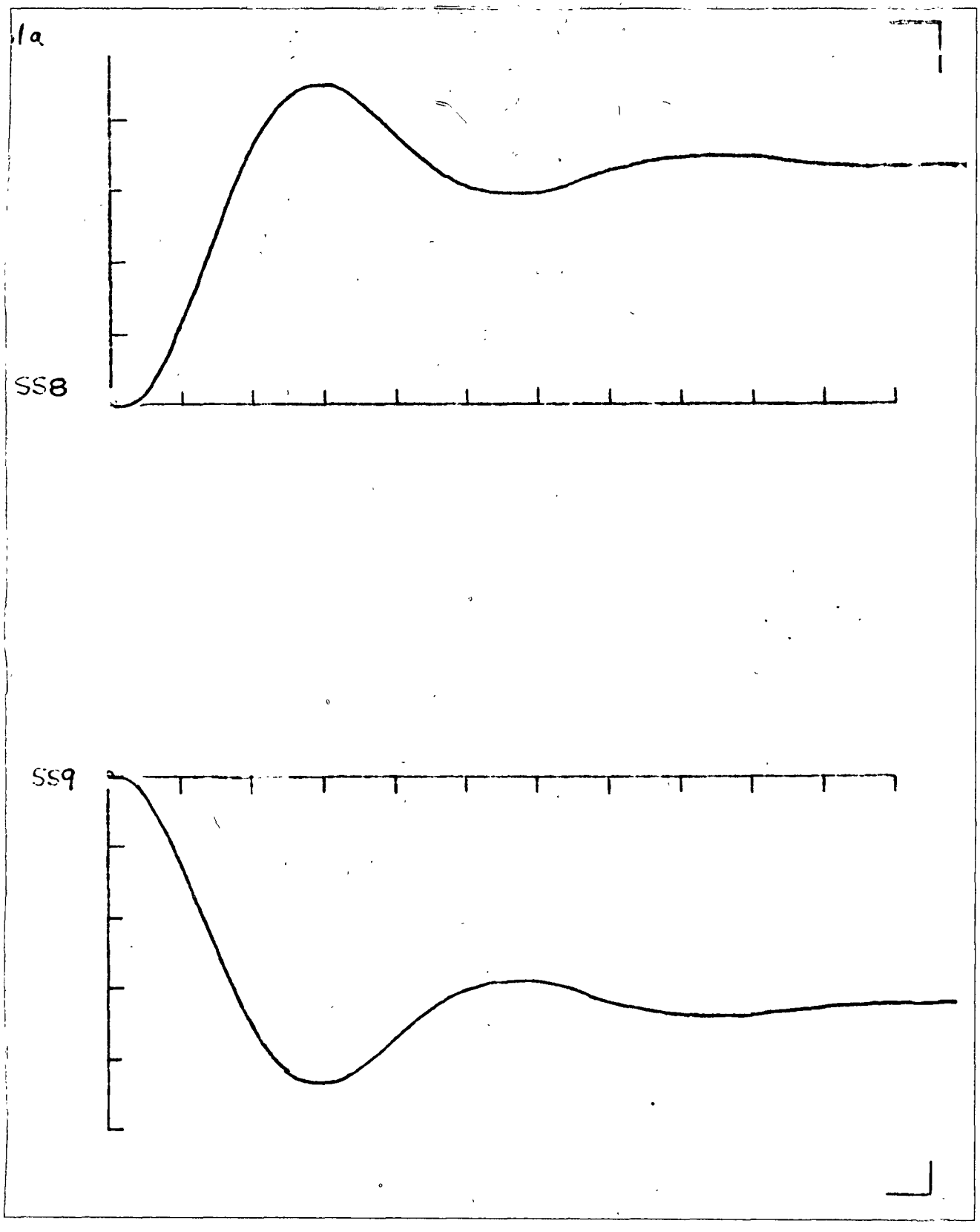
1a
SS8
SS9

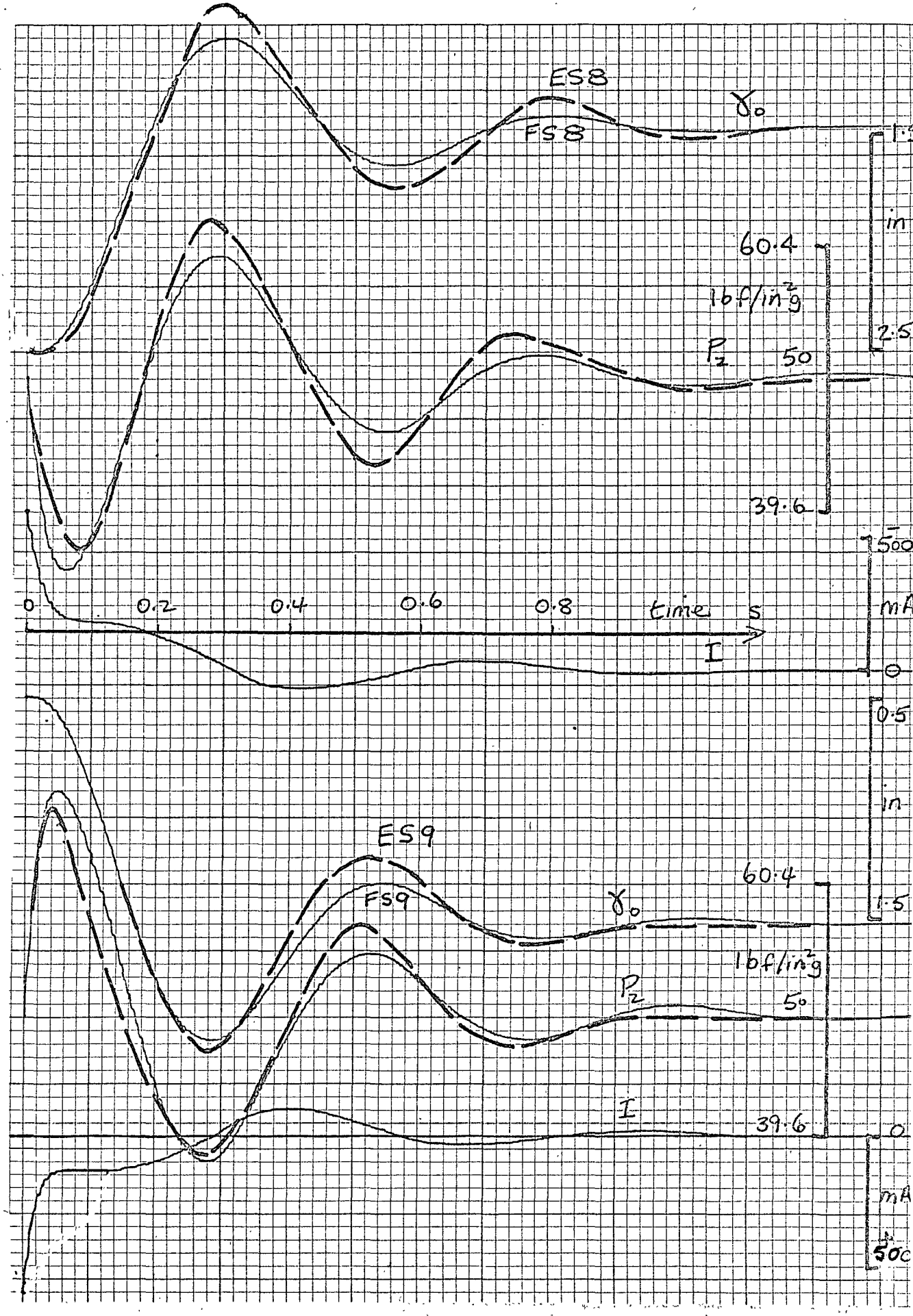

Fig. 7.4 Step Response Results

As fig. 7.3 but with increased transient pressure feedback.

62a

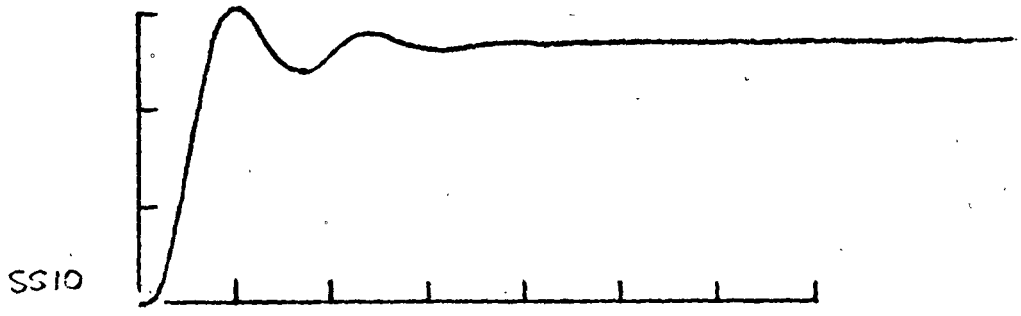

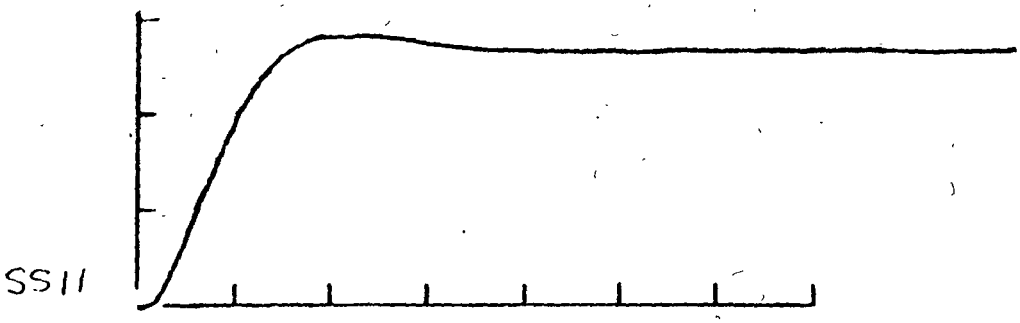

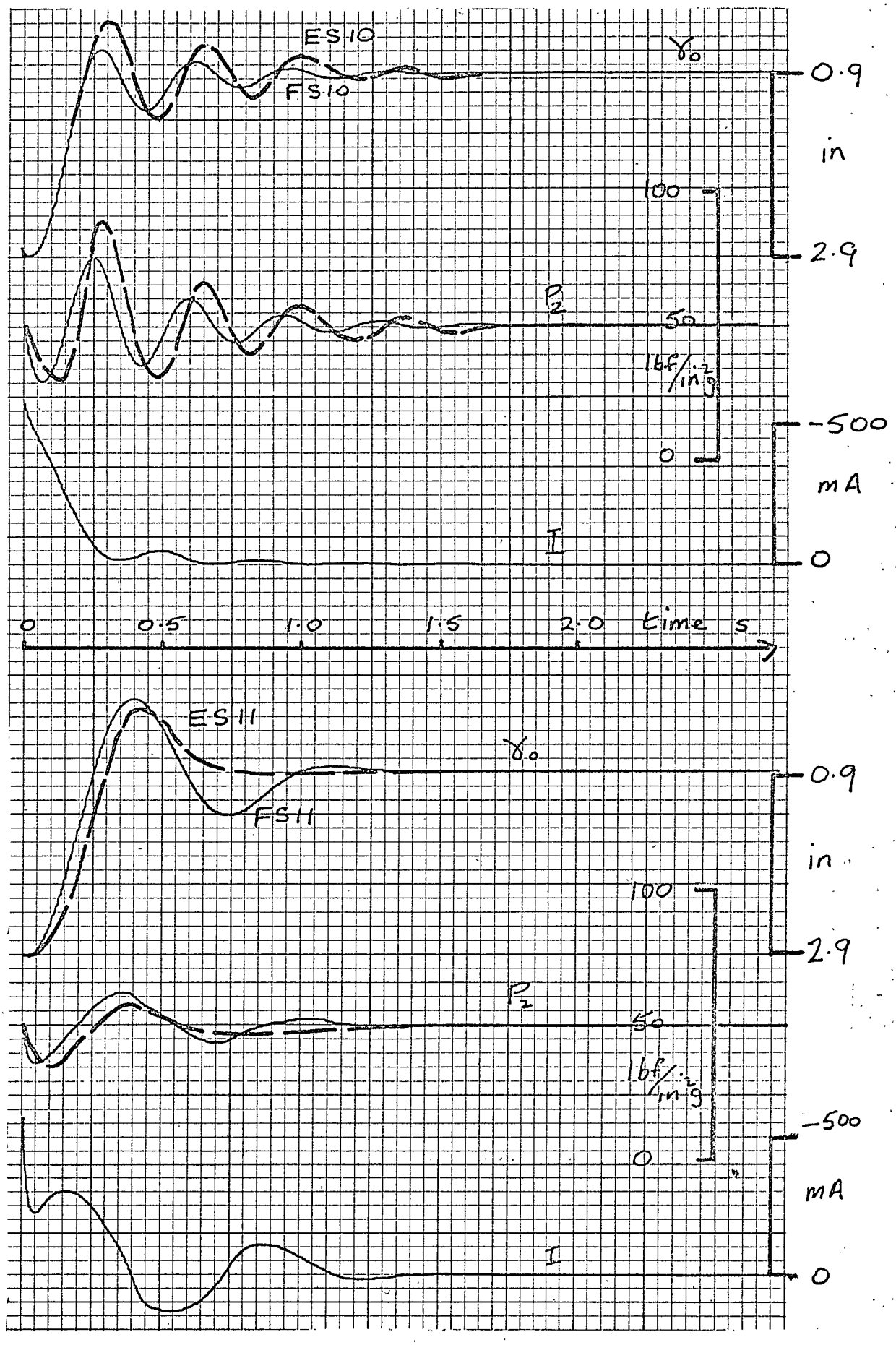

Fig. 7.5 Step Response Results

Showing large steps (2 in) with large inertial load (93.7 lb) with small (S10) and large (S11) amounts of transient pressure feedback.

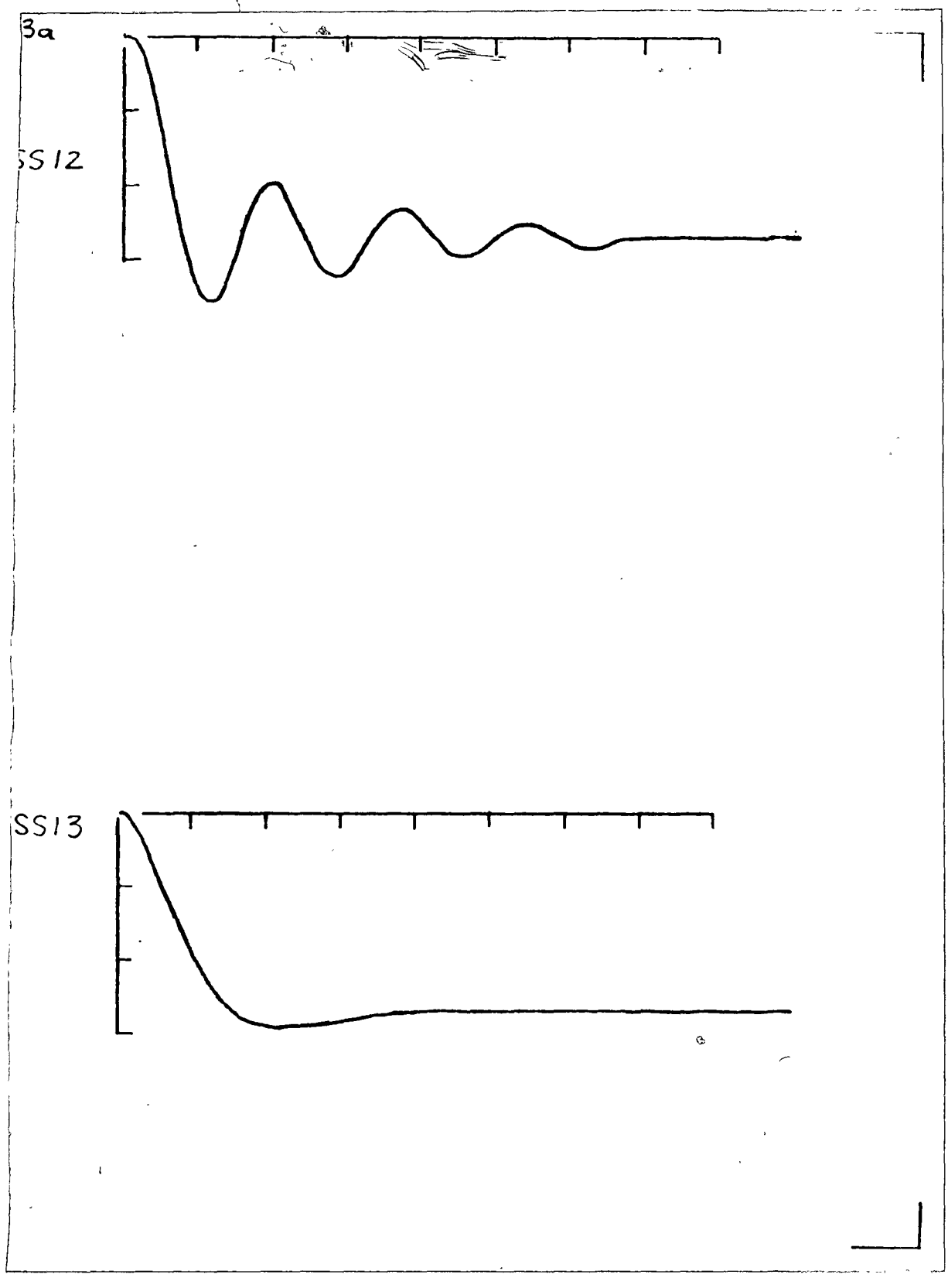
3a
SS12
SS13

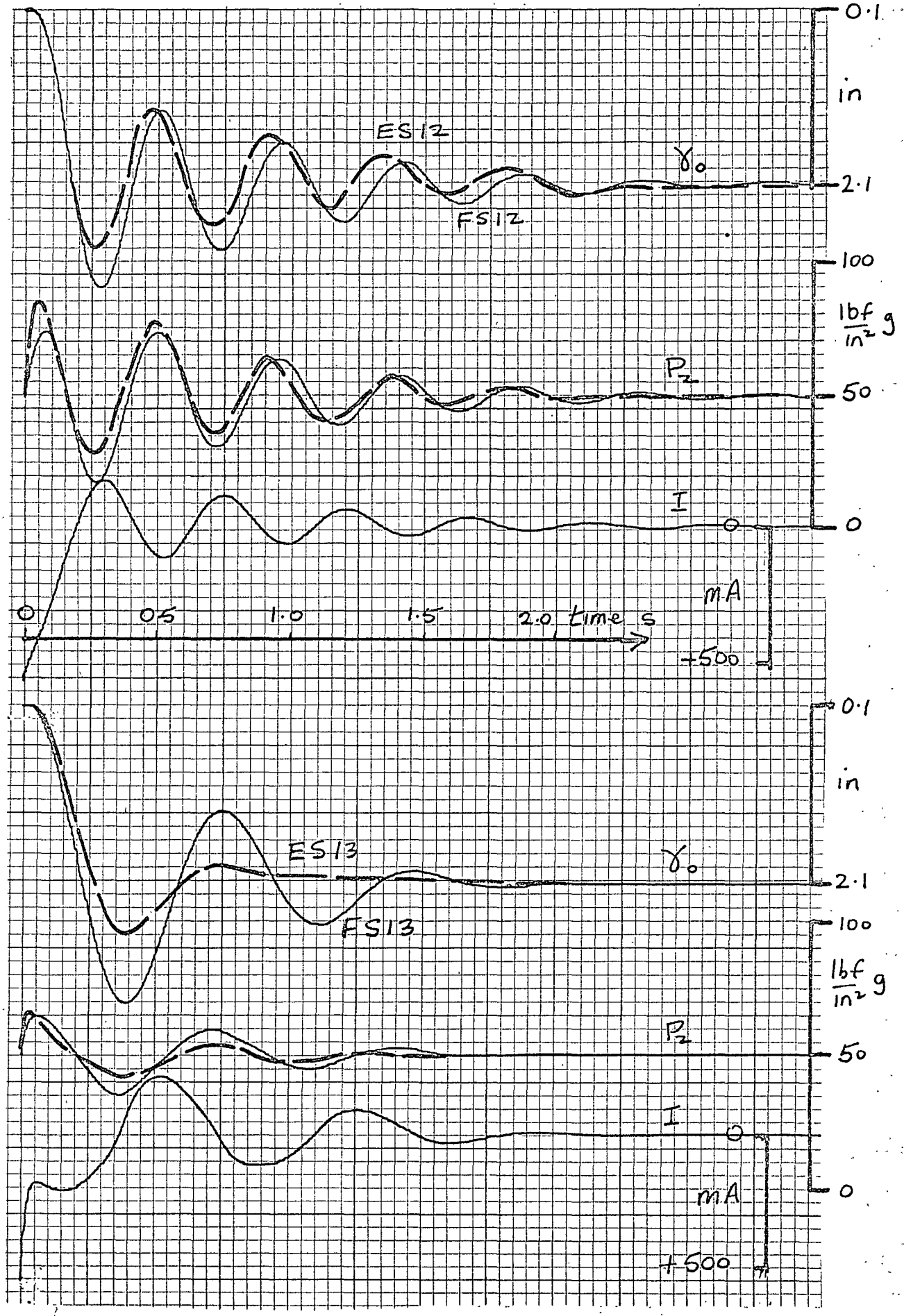

Fig. 7.6 Step Response Results

As fig. 7.5 but for left to right commands.

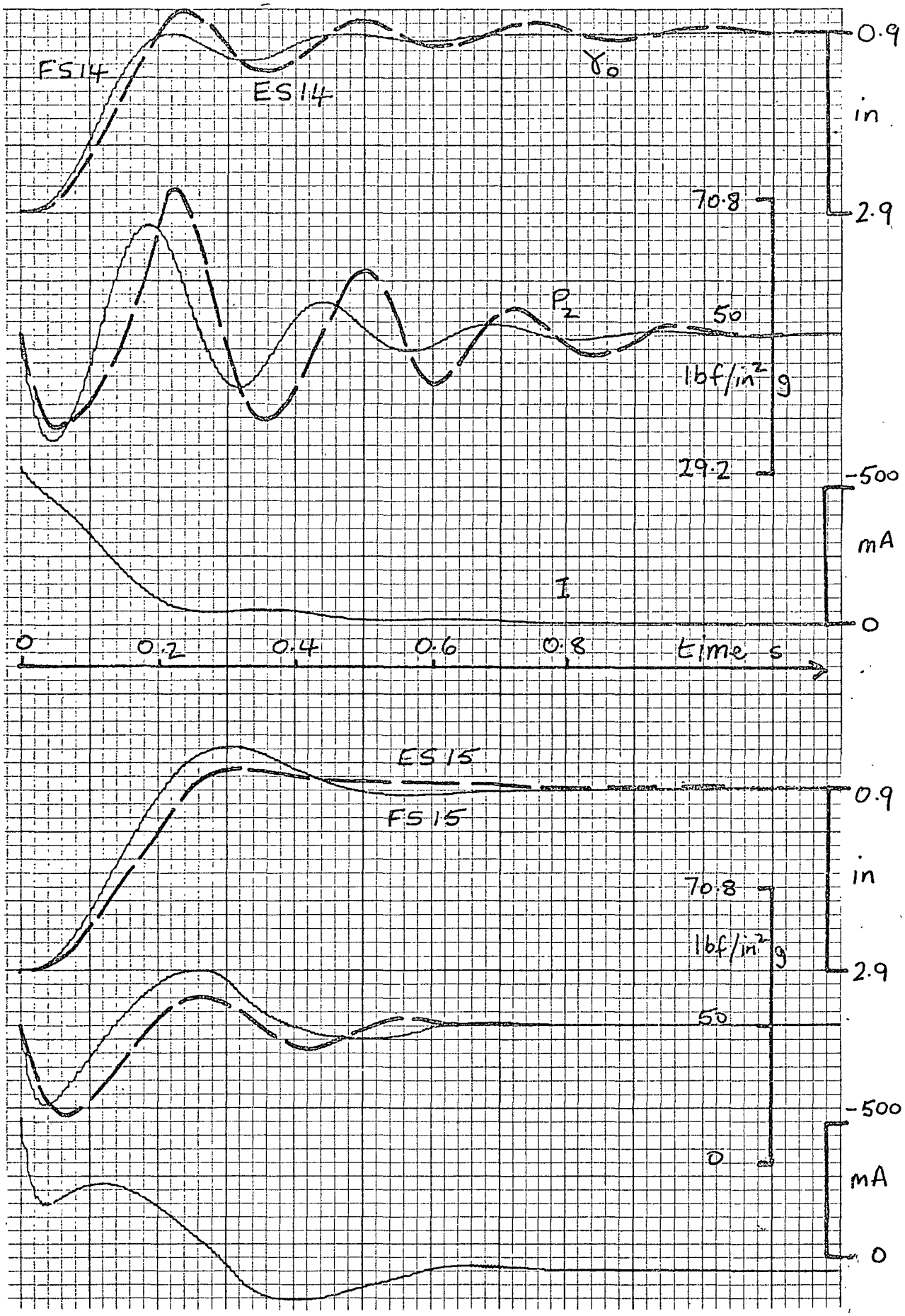

Fig. 7.7 Step Response Results

Repeat of tests S10 and S11 (fig. 7.5), with load mass approximately halved (m_L = 48.7 lb).

165a

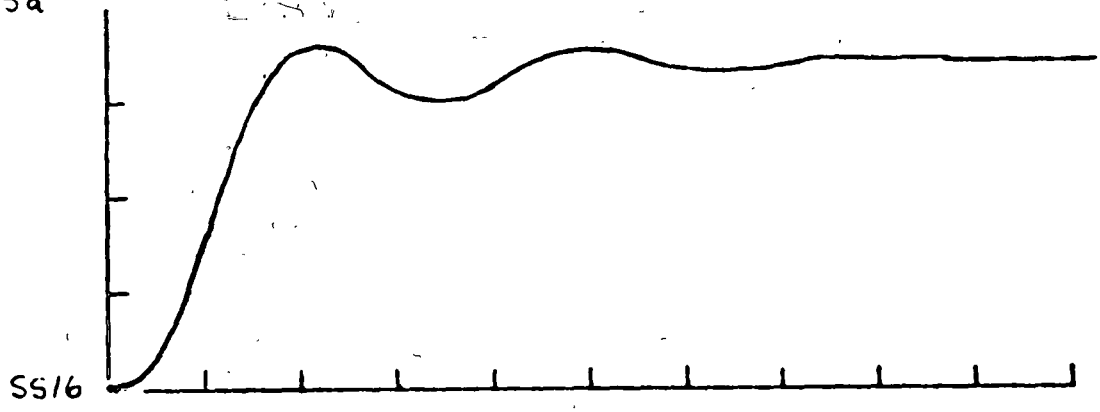

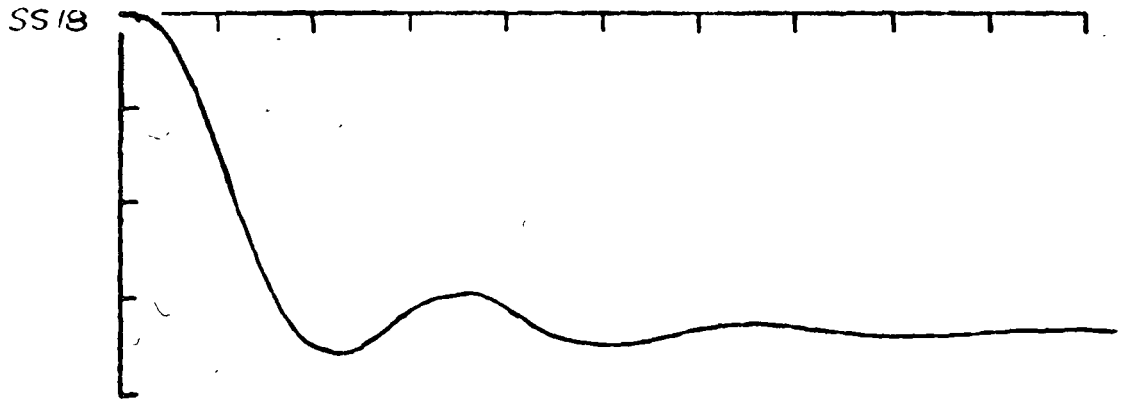

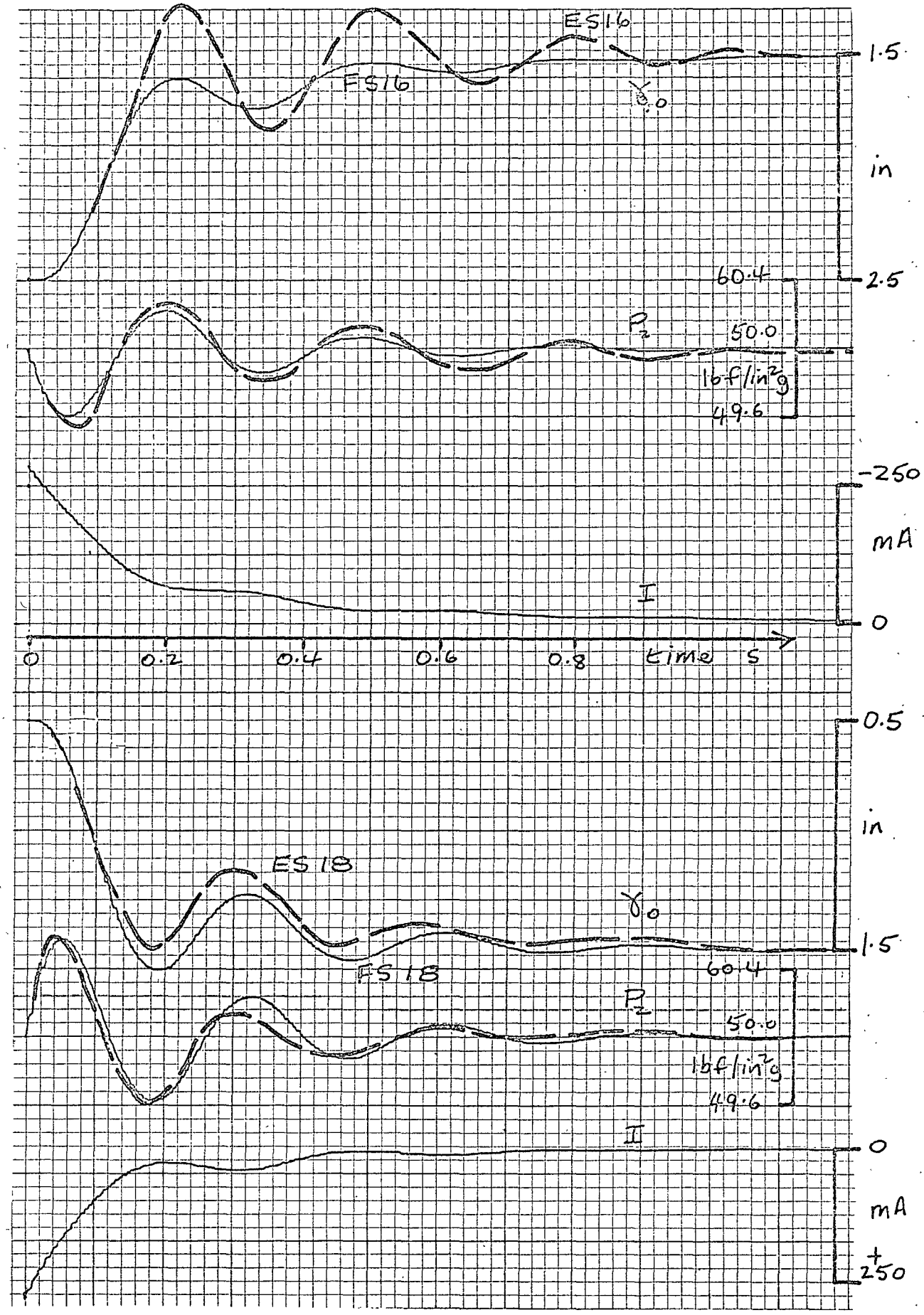

Fig. 7.8 Step Response Results

Showing 1 in steps towards piston mid-position from opposite directions, for load mass of 48.7 lb with small amount of transient pressure feedback.

66a

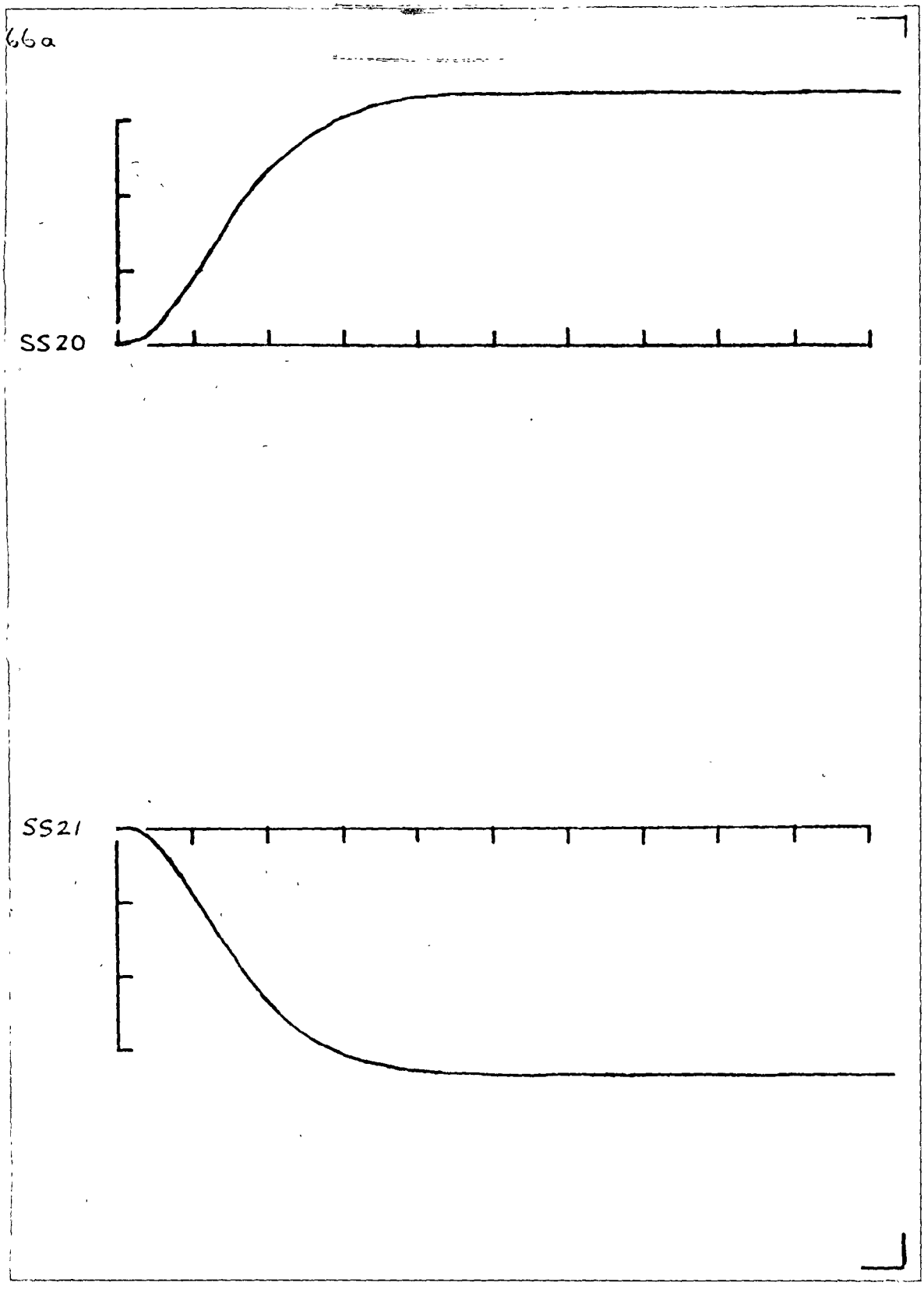

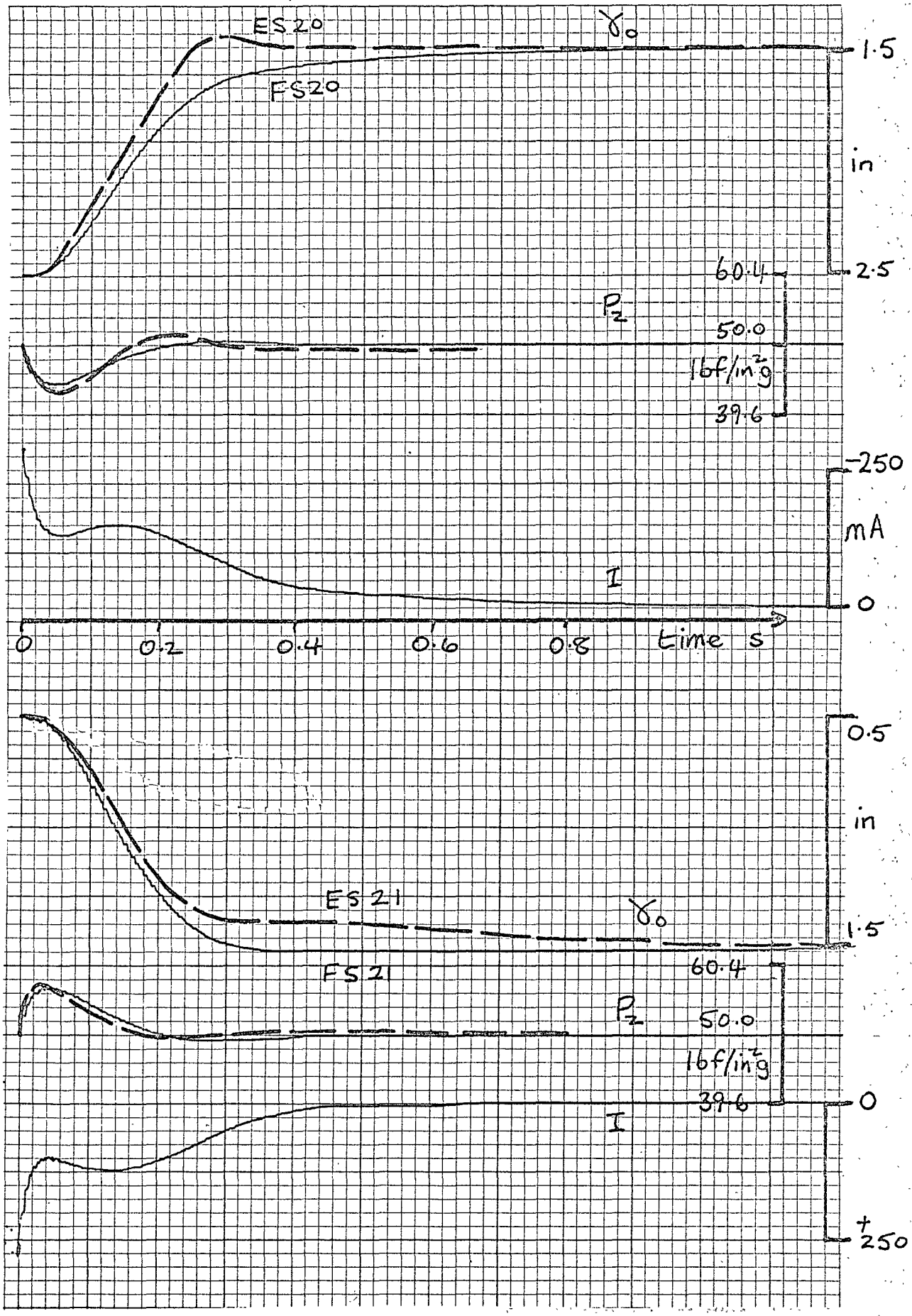

Fig. 7.9 Step Response Results

As fig. 7.8 but with increased transient pressure feedback.

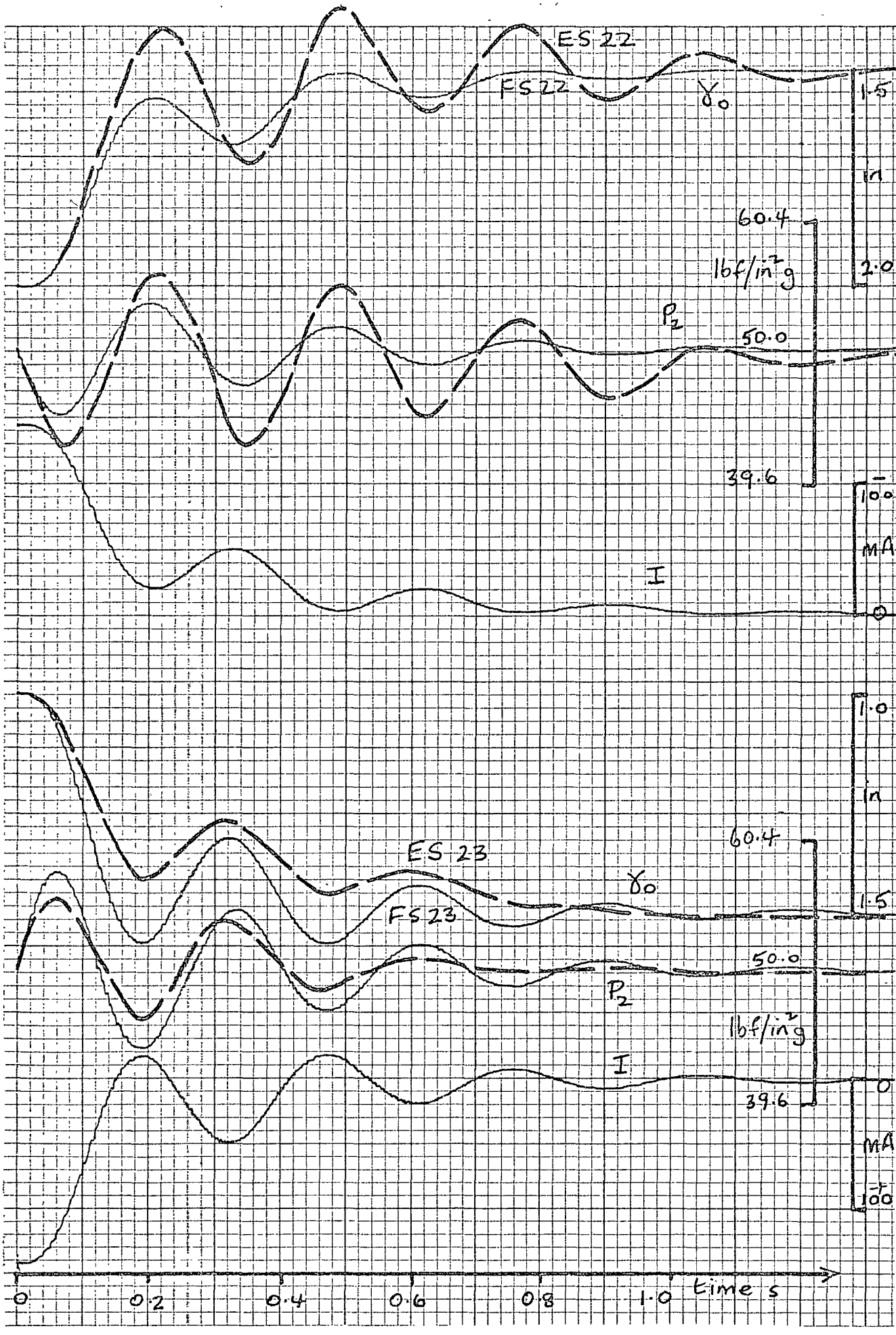

Fig. 7.10 Step Response Results

Showing $\frac{1}{2}$ in steps towards piston mid-position from opposite directions, with m_L = 48.7 lb and zero transient pressure feedback.

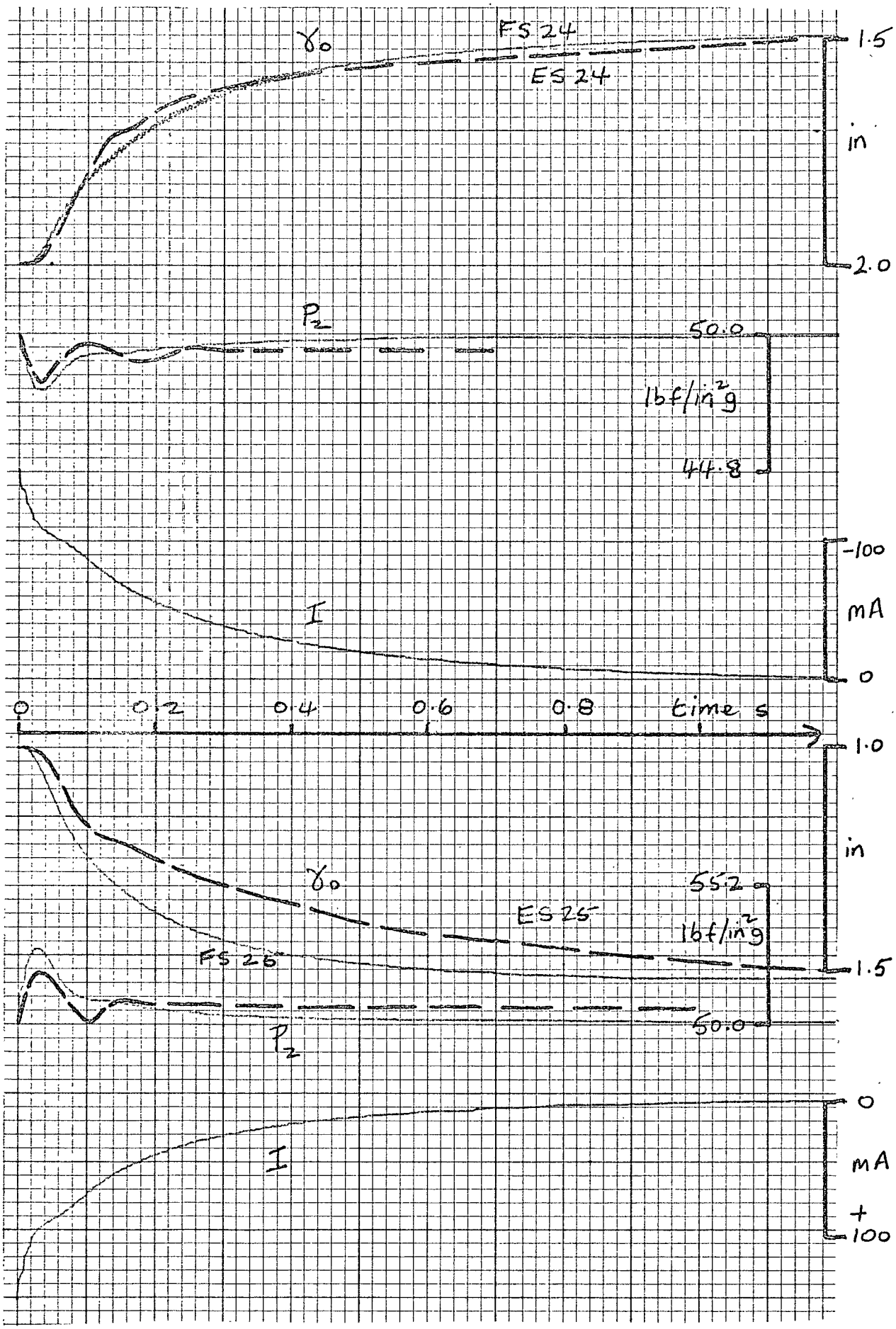

Fig. 7.11 Step Response Results

Showing $\frac{1}{2}$ in steps from opposite directions towards piston mid-position, for a light load (8.7 lb) with heavy transient pressure feedback damping.

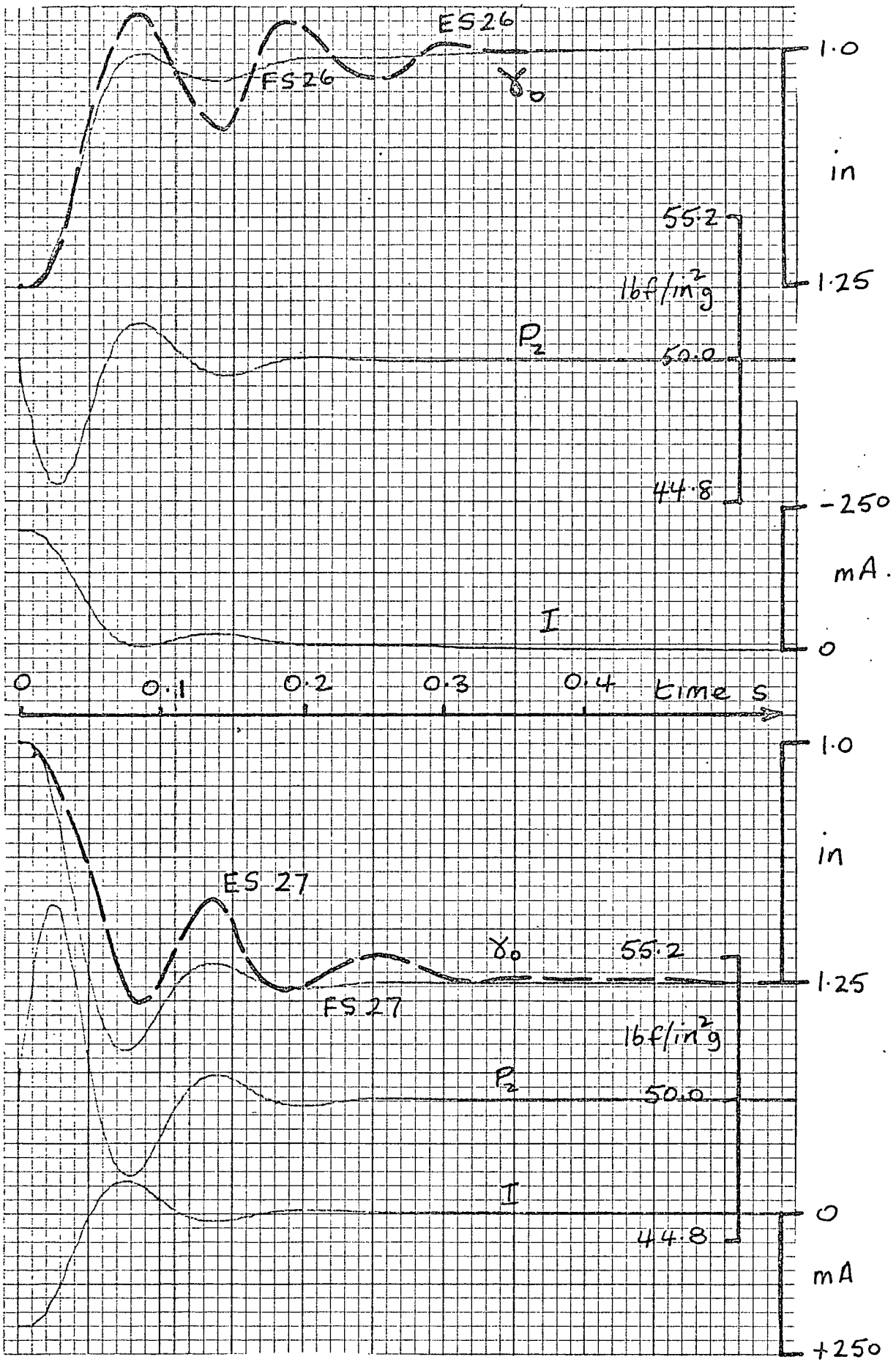

Fig. 7.12 Step Response Results

Showing small steps ($\frac{1}{4}$ in) from opposite directions with a light load (8.7 lb).

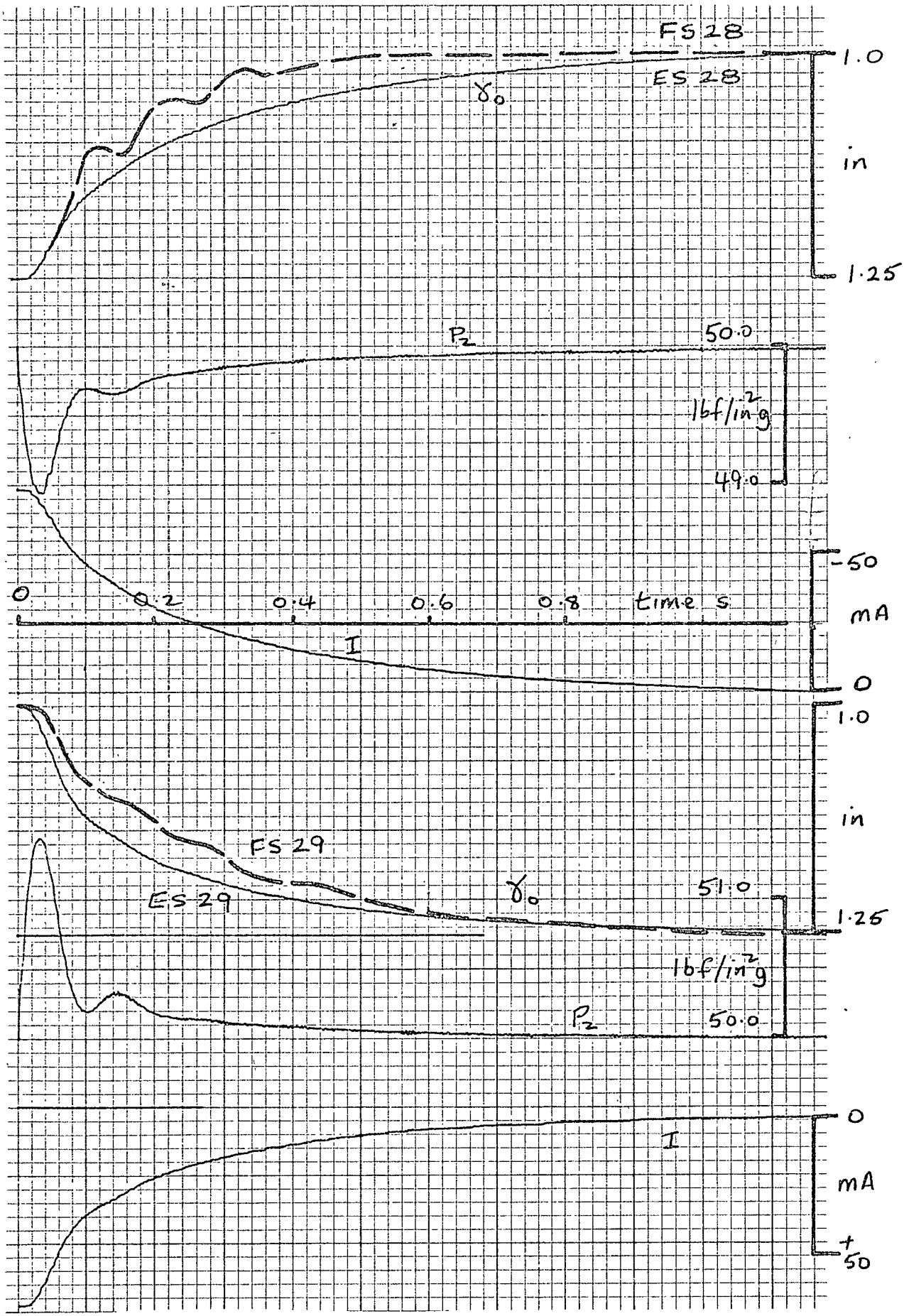

Fig. 7.13 Step Response Results

As fig. 7.12 but with open loop gain reduced by a factor of 2.9.

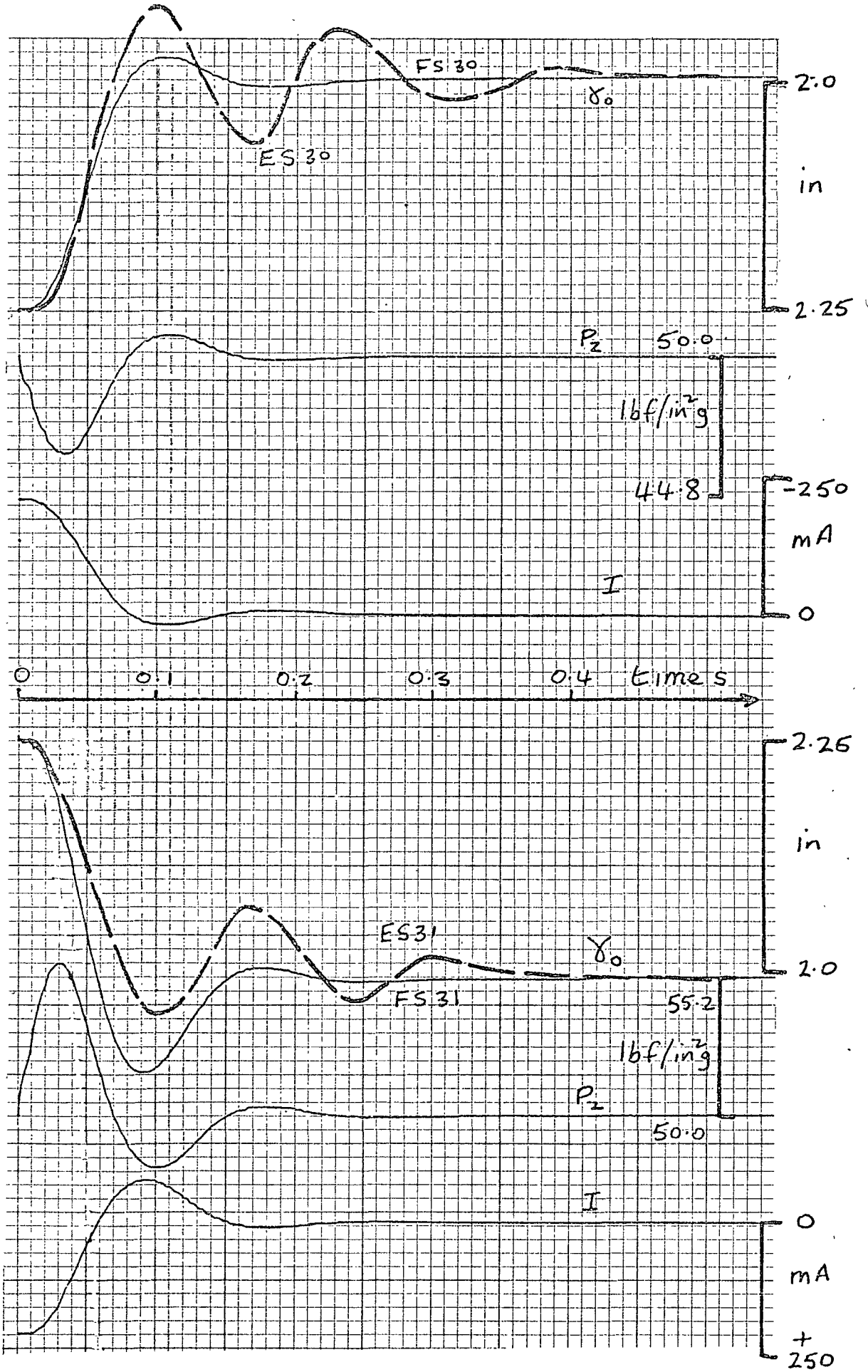

Fig. 7.14 Step Response Results

As fig. 7.12 but with equilibrium positions moved by 1 in. (i.e. volume V_2 increased).

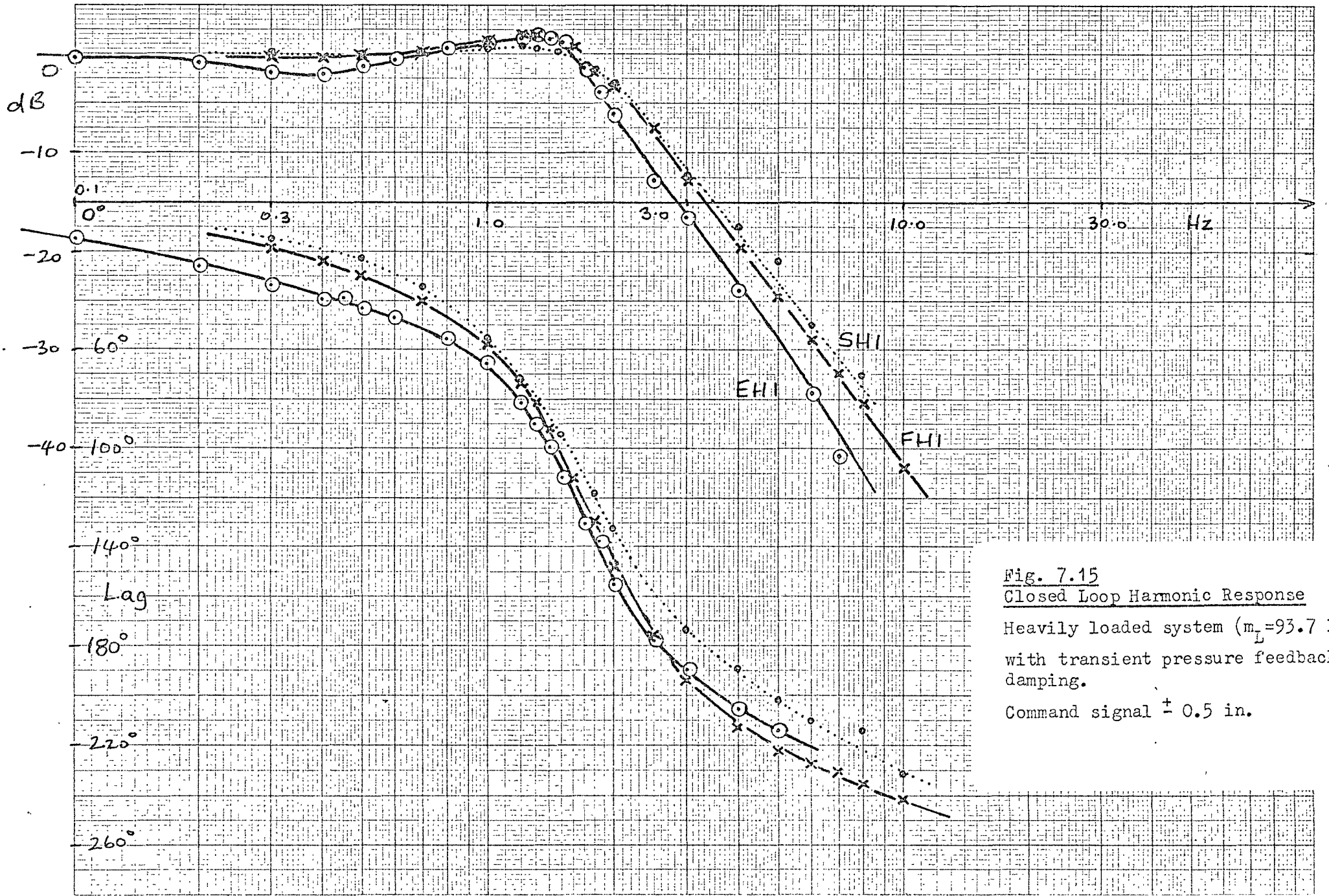

Fig. 7.15
Closed Loop Harmonic Response

Heavily loaded system (m_L=93.7 lb) with transient pressure feedback damping.

Command signal ± 0.5 in.

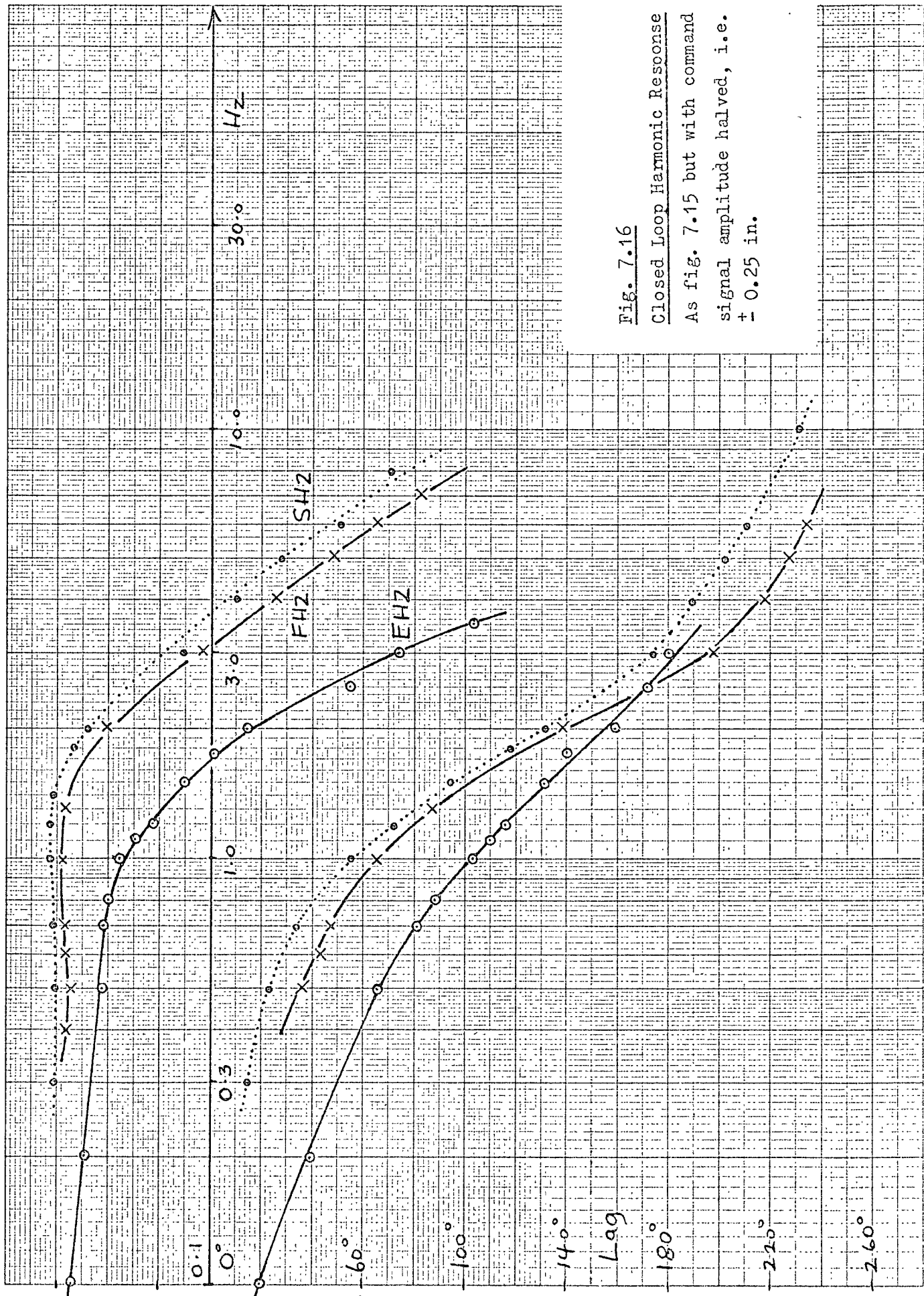

Fig. 7.16

Closed Loop Harmonic Response

As fig. 7.15 but with command signal amplitude halved, i.e. ± 0.25 in.

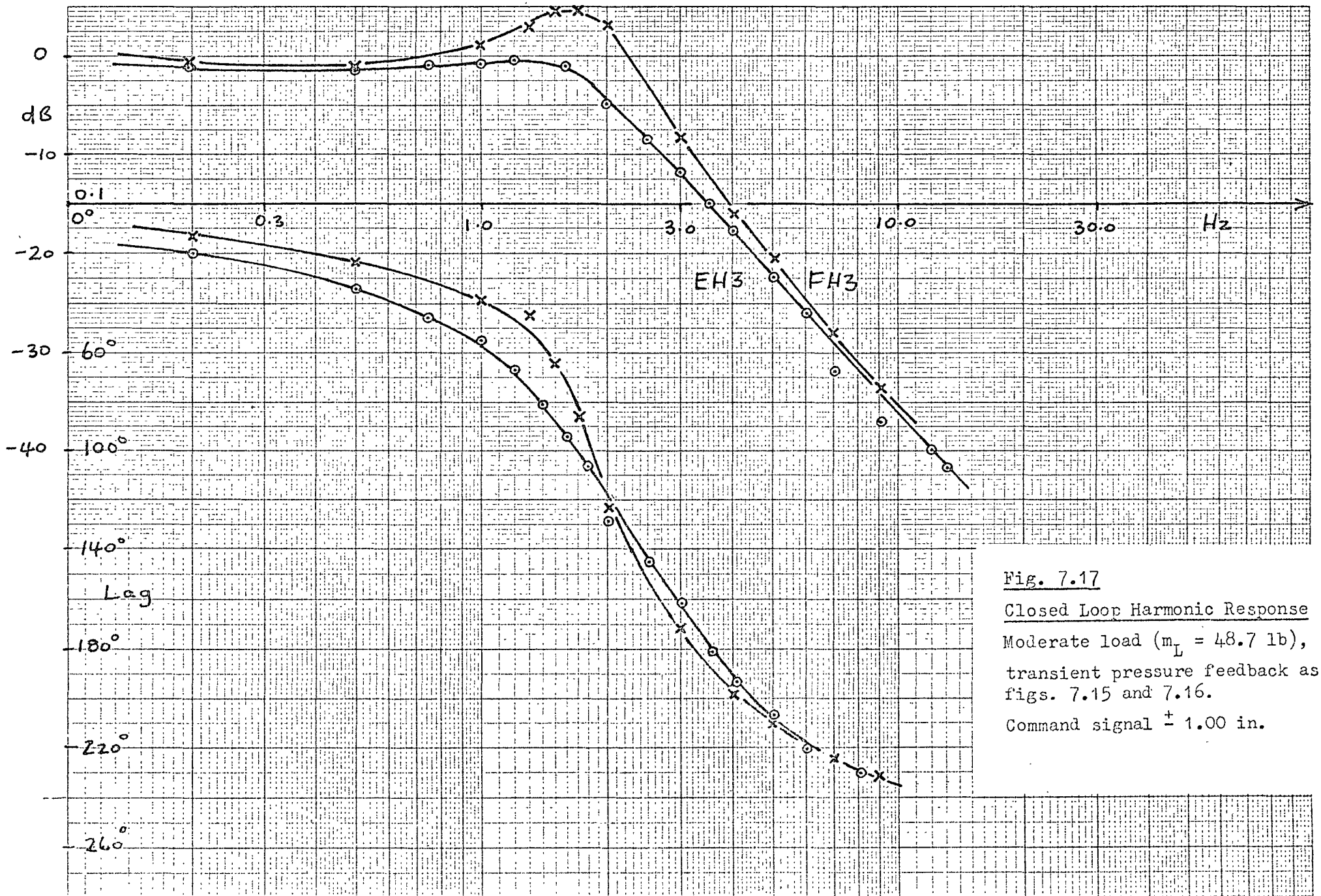

Fig. 7.17

Closed Loop Harmonic Response

Moderate load (m_L = 48.7 lb), transient pressure feedback as in figs. 7.15 and 7.16.

Command signal $\pm$ 1.00 in.

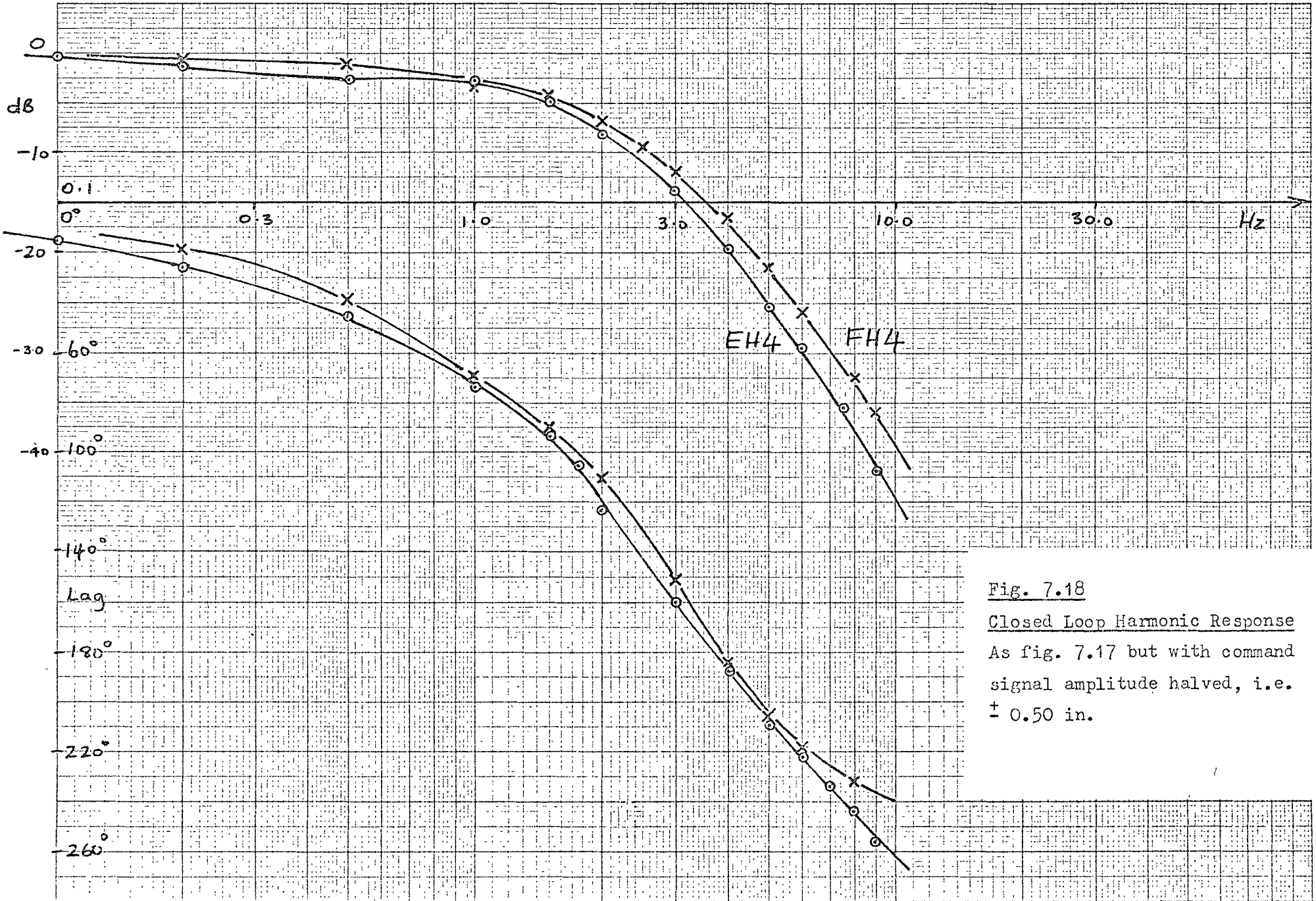

Fig. 7.18

Closed Loop Harmonic Response

As fig. 7.17 but with command signal amplitude halved, i.e. ± 0.50 in.

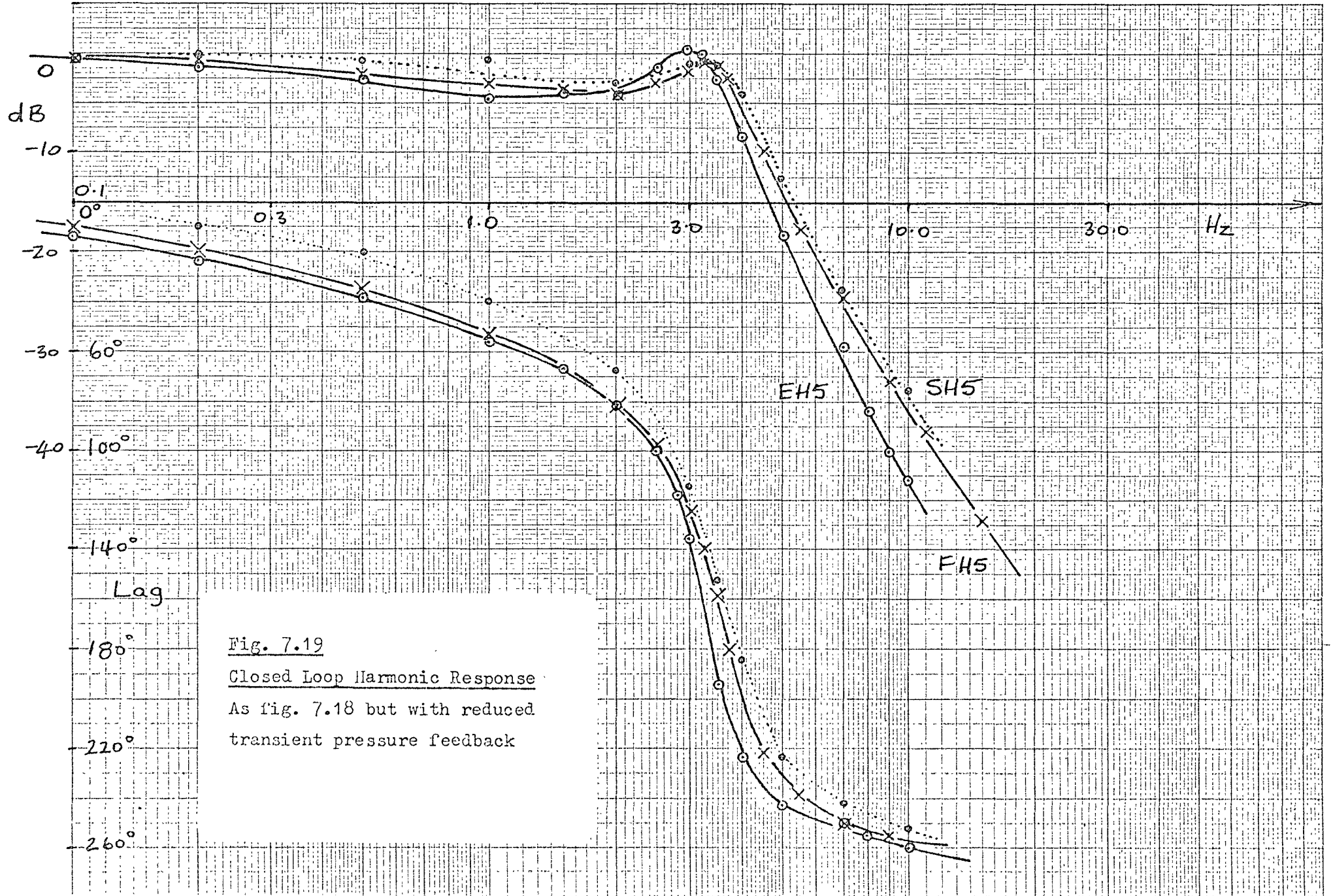

Fig. 7.19

Closed Loop Harmonic Response

As fig. 7.18 but with reduced transient pressure feedback

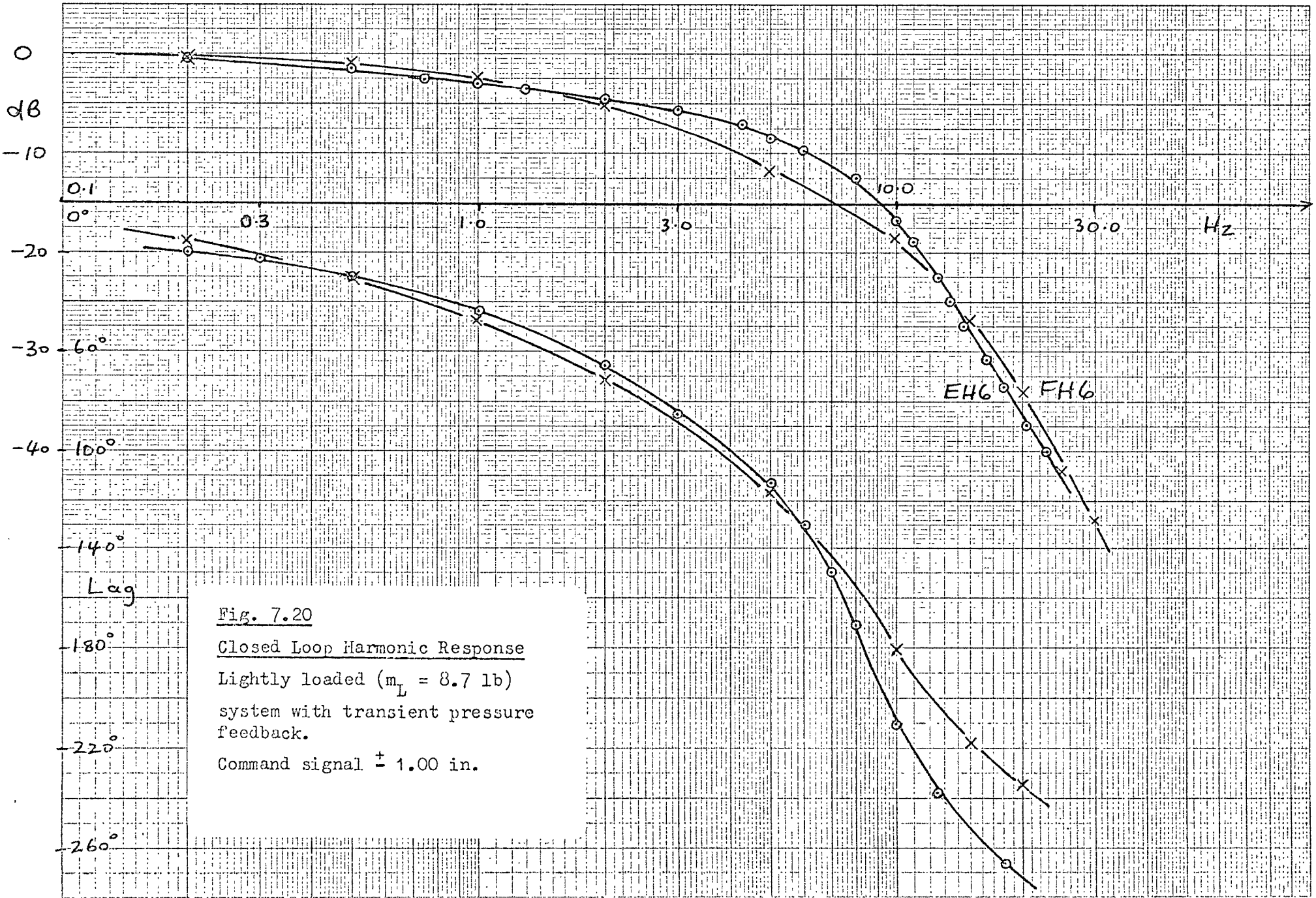

Fig. 7.20

Closed Loop Harmonic Response

Lightly loaded (m_L = 8.7 lb) system with transient pressure feedback.

Command signal $\pm$ 1.00 in.

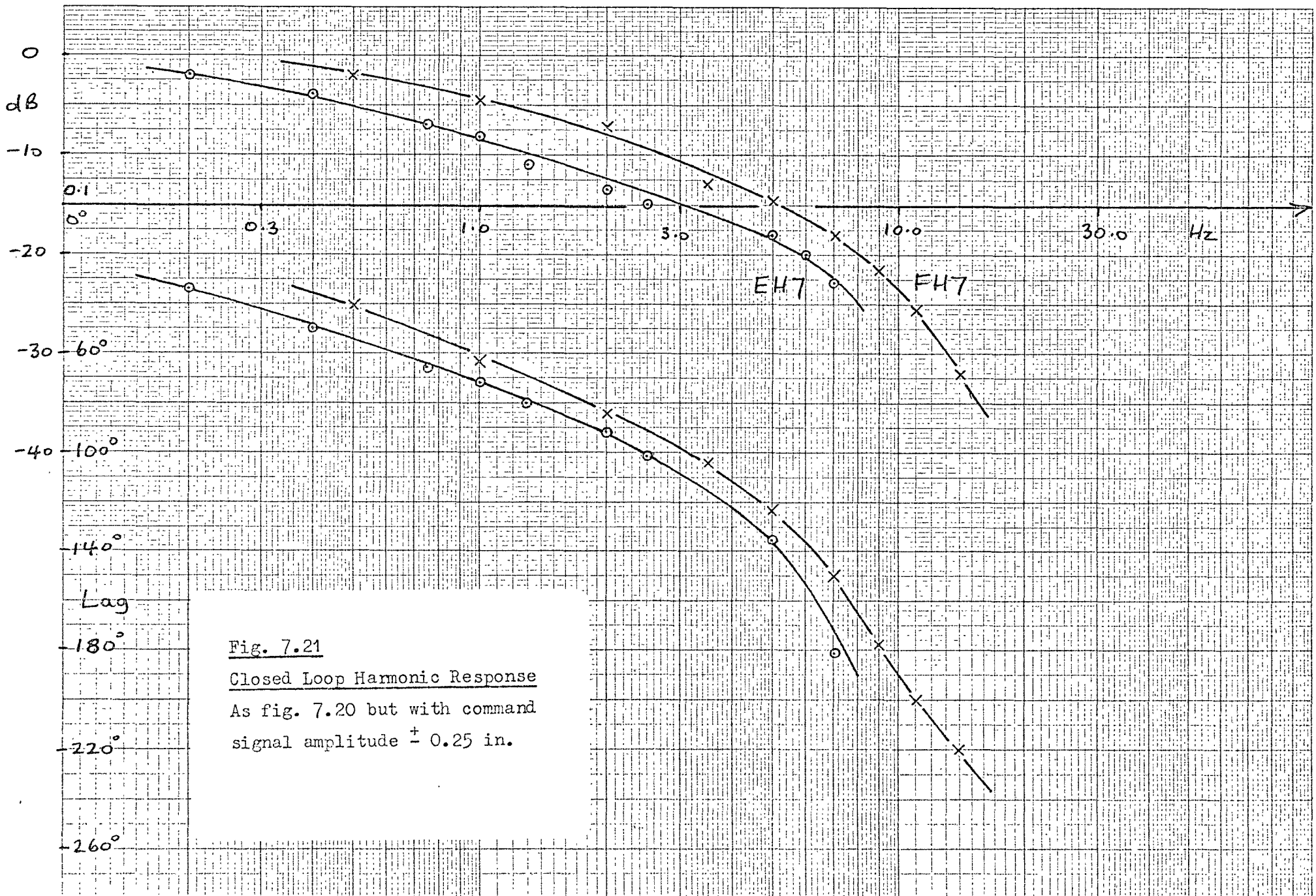

Fig. 7.21

Closed Loop Harmonic Response

As fig. 7.20 but with command signal amplitude ± 0.25 in.

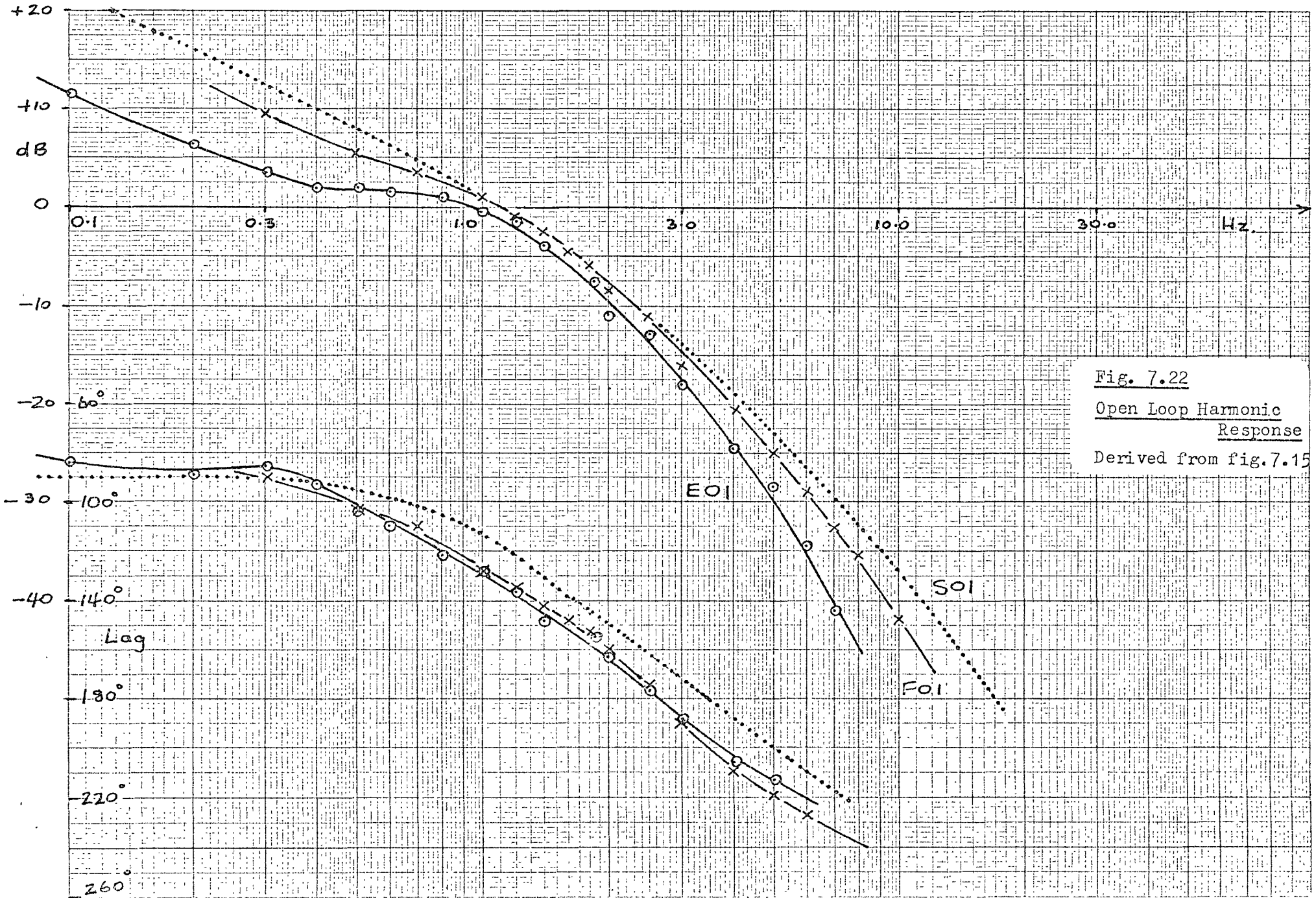

Fig. 7.22

Open Loop Harmonic Response

Derived from fig. 7.15

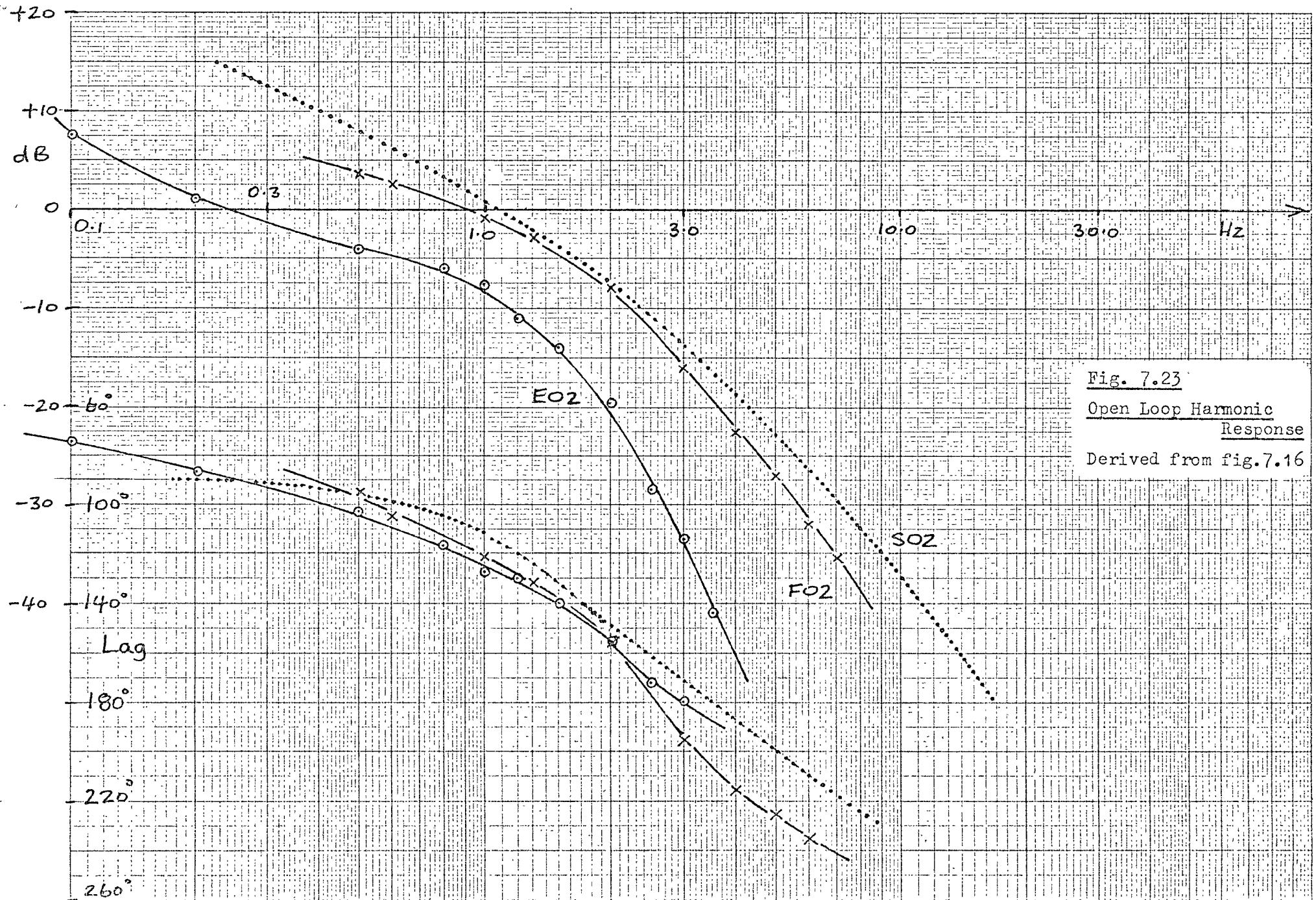

Fig. 7.23

Open Loop Harmonic Response

Derived from fig. 7.16

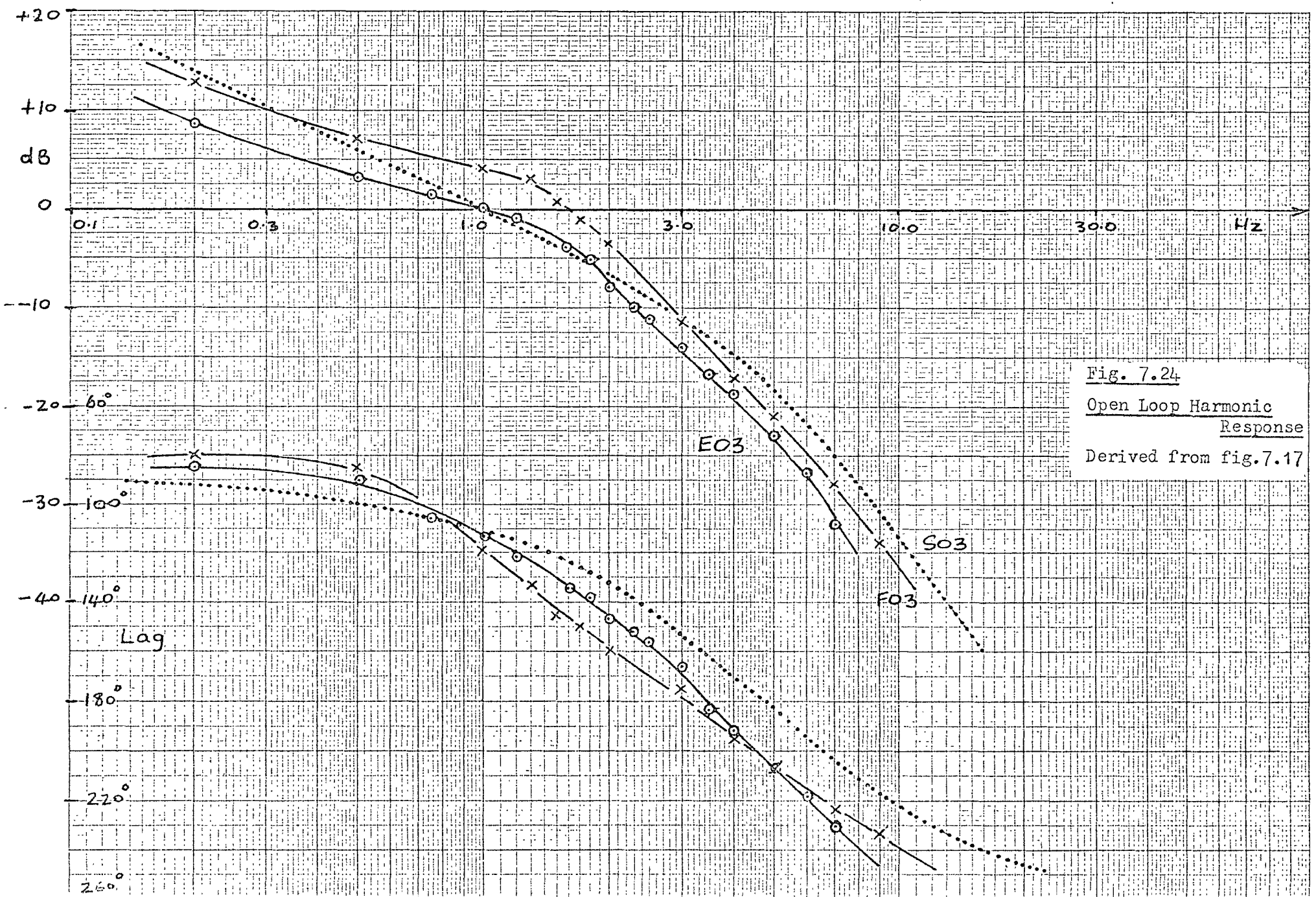

Fig. 7.24

Open Loop Harmonic Response

Derived from fig. 7.17

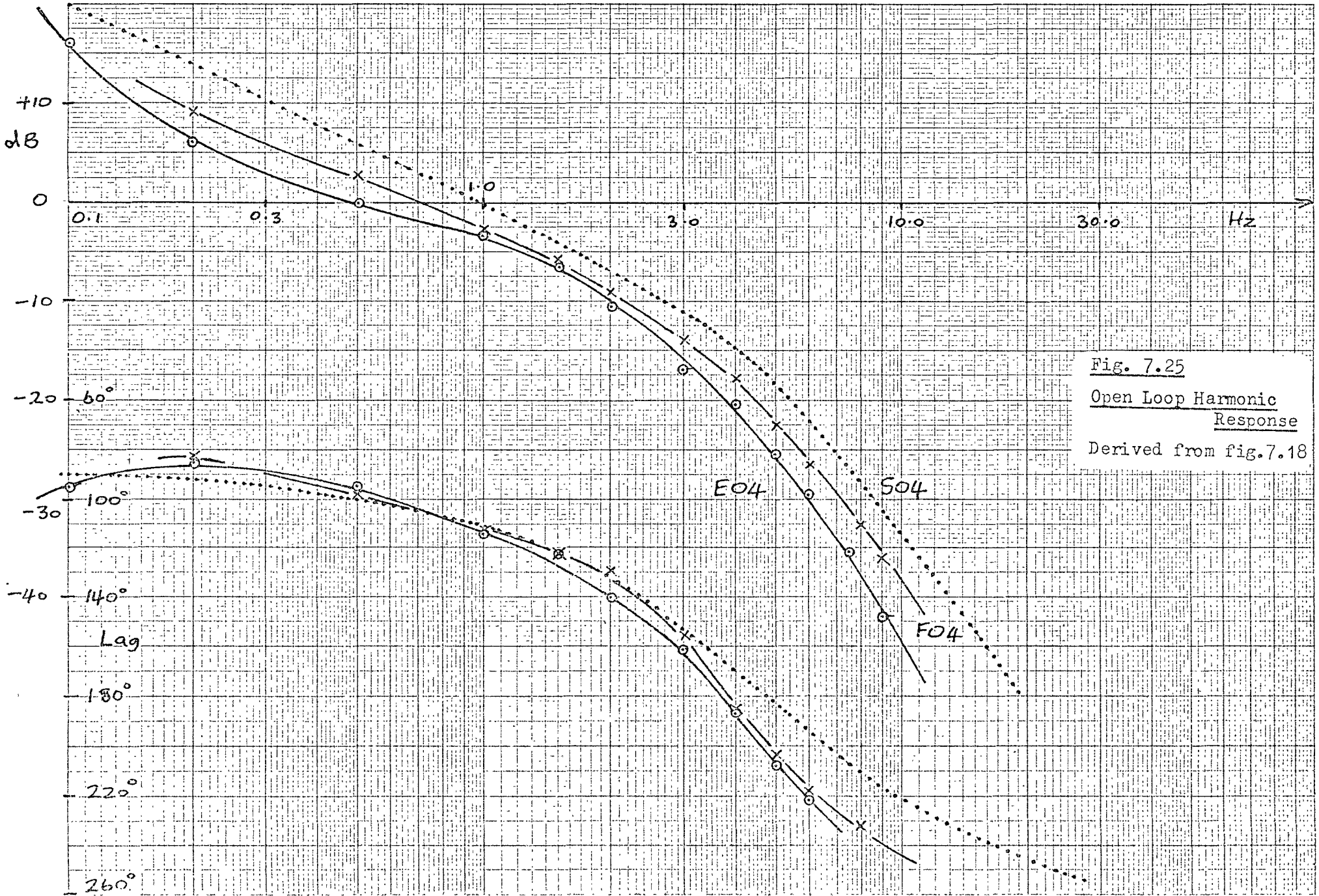

Fig. 7.25

Open Loop Harmonic Response

Derived from fig. 7.18

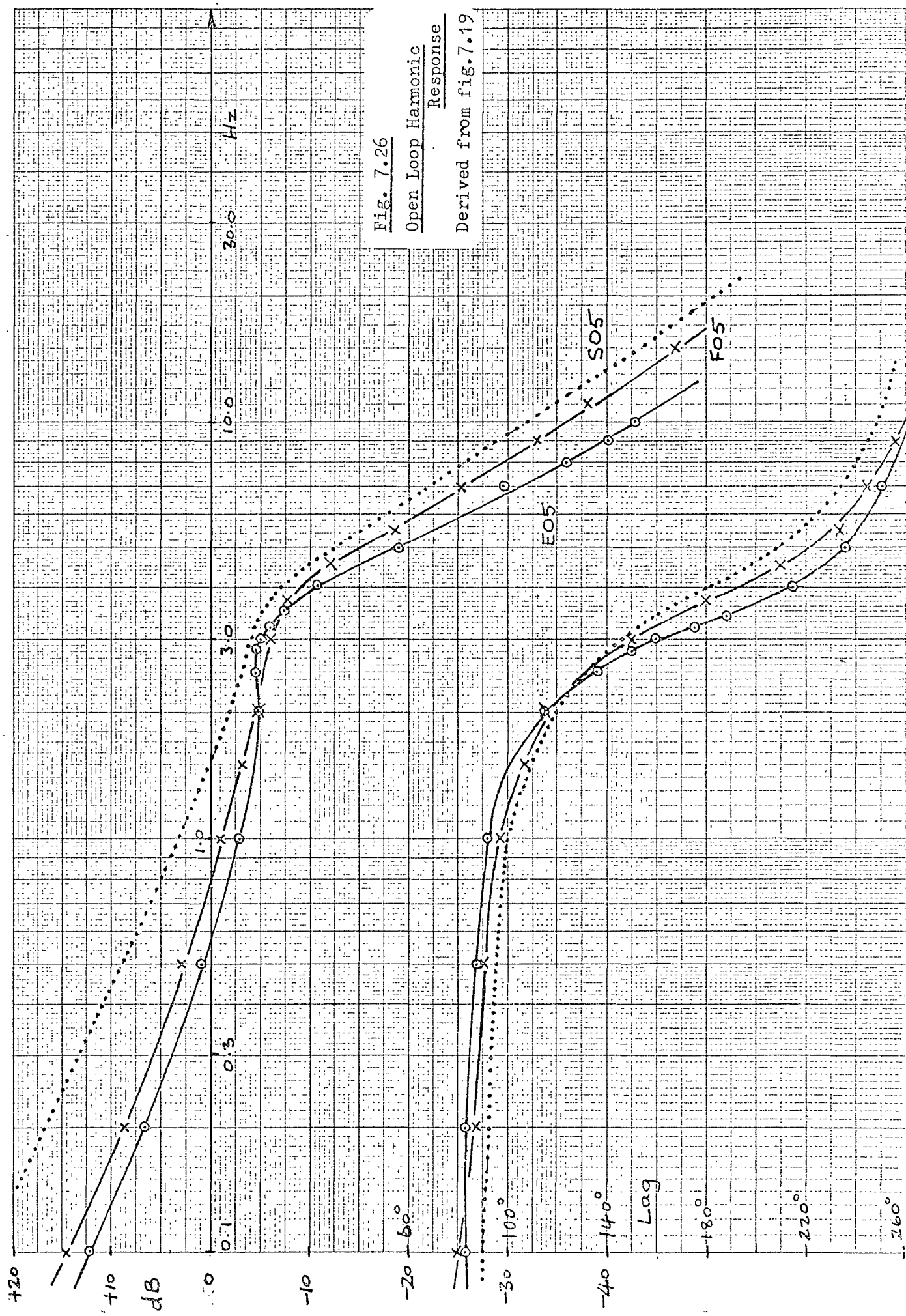

Fig. 7.26
Open Loop Harmonic Response
Derived from fig. 7.19

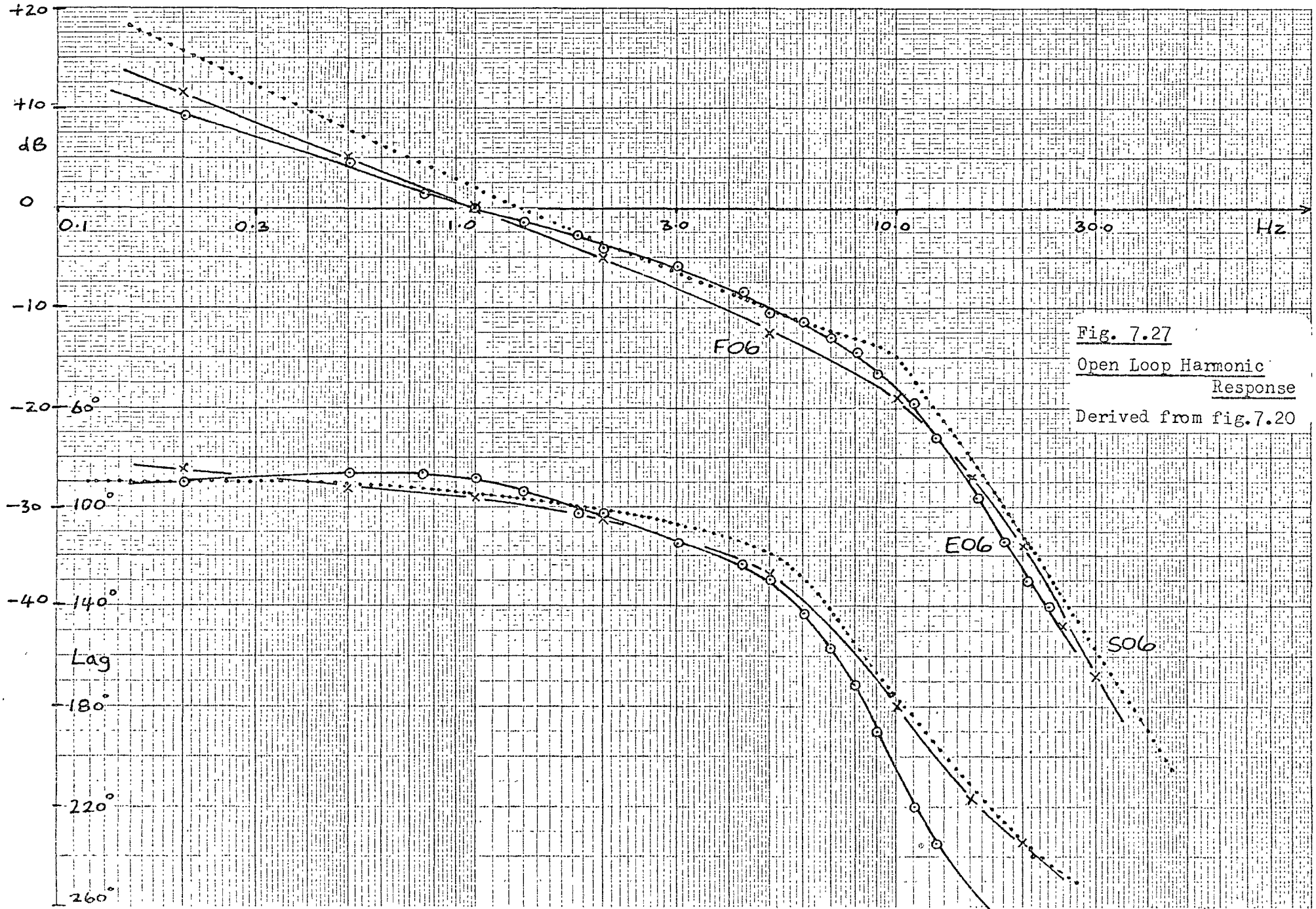

Fig. 7.27

Open Loop Harmonic Response

Derived from fig. 7.20

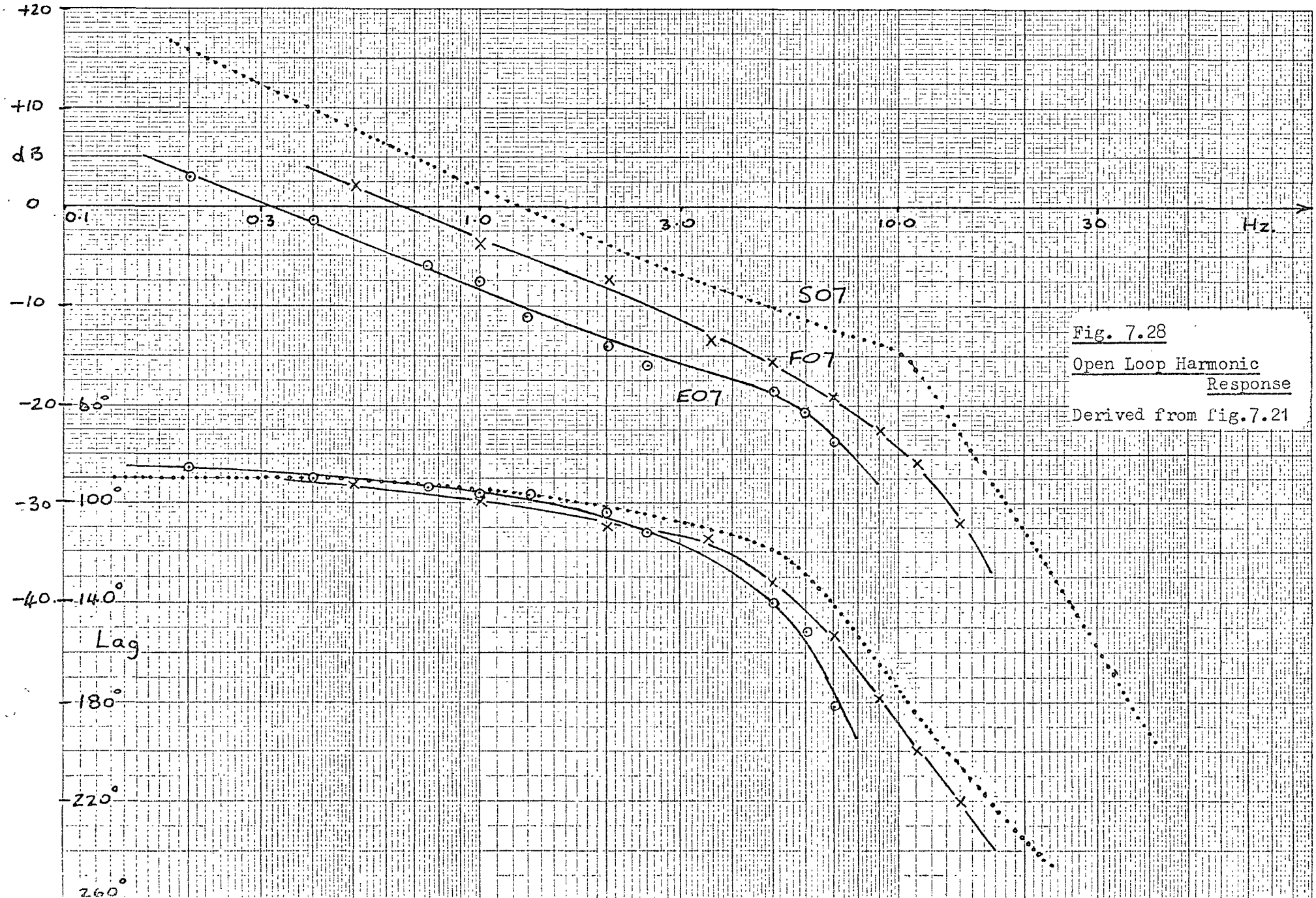

Fig. 7.28

Open Loop Harmonic Response

Derived from fig. 7.21

At the other extreme, in tests S29 and S28 and 02 and 07, relatively small perturbations of variables occur, for example in the two step response tests mentioned, the valve drive current did not exceed 75mA. It was in these cases, where only low valve flow rates occurred, that correspondence between model and system behaviour was poorest. Comparing the open loop plots 01 with 02 and 06 with 07, the full simulation is seen to be better for large amplitude (01 and 06) than for small. This is because there was considerably less change in the behaviour of the model as the amplitude was reduced than there was in the actual system. The difficulty in simulating small perturbations was predicted in section 6.3.1 and arises because it is under these conditions that small errors in the valve characteristic, and effects such as valve lap, become significant proportions of the total fluctuations. Throughout the step response tests and in those closed loop Bode plots where it can be determined, there is close agreement on the closed loop natural frequency between the analogue and the experimental system.

In section 5.4.5 it was noted that the response of the servo to step commands from different directions, but to a common final position, was not as expected. The behaviour of the full simulation, on the other hand, in which left to right responses were slightly faster than those from right to left, can be explained. This was due to the fact that the flow gain of the valve for supply flow was greater than that for exhaust. No explanation is advanced for this inconsistency between servo and full simulation. (The linear simulation was essentially symmetrical and therefore exhibited no directional effect.)

7.2.2 The Simple Simulation

The step response of the simple model closely resembled that

of the experimental servo and was never greatly different from that of the full simulation. In almost all cases, however, the full model was slightly the better. A reduction in the damping of the simple model would have improved agreement with the servo and table 6.2 can be used to illustrate this and other points.

In table 6.2 it can be seen that where transient pressure feedback was used, it made a very significant contribution to the damping term, (B'), sometimes far outweighing the other terms. Thus if the viscous damping coefficient were reduced, even to half the value actually used for the computer simulations, the effect on the term B' and consequently upon the behaviour of the model would be in many cases quite small. It can therefore be argued that better all-round correspondence between servo and models would have been obtained if the value for viscous friction coefficient, (b = 6.7 lbf/(ft/s)) established in section 4.1.5, had been used. The figure actually used (b = 13.0 lbf/(ft/s)) was adopted in section 6.1.7. There is also slight evidence to support the use of a load dependent damping coefficient, as discussed in section 4.3.3, in that the computer results for large load masses were slightly better than those for small loads. Another point which emerges from table 6.2 is the trivial effect on the system's dynamic behaviour of the relatively high piston leakage which occurred in the experimental servo.

The importance of correct selection of valve coefficients for a linear simulation can also be illustrated with the aid of table 6.2. Clearly the value of c_1 directly influences the open loop gain and therefore the system's stability and speed of response. On the other hand c_2, which occurs in the terms h' and g', could be estimated wrongly or even omitted altogether, without seriously decreasing the usefulness of the model. Inspection of fig. 6.12 shows that the value for c_1 selected, favoured moderate and even large

fluctuations of valve opening and flow rate. To simulate smaller perturbations a lower value of c_1 would be necessary. A reduction in open loop gain in this way would improve the agreement between the simple simulation and the servo for the small amplitude harmonic response tests. In that case, curve S02 would approach E02 and curve S07 would approach E07.

As explained in section 5.2.2, the open loop Bode plots for the servo and for the full simulation were derived from closed loop results, and therefore the deviation ($\gamma_i - \gamma_o$) amplitude was not constant throughout. This does not affect comparisons between FO and EO curves, but explains the relatively large deviations between the simple simulation (SO) and the servo (EO) Bode plots at low frequencies. In these cases the servo was operating with extremely small deviations and therefore small valve openings. Under these circumstances a smaller value of c_1 applies and consequently the SO curve at low frequencies should be lowered, thus improving agreement with the servo behaviour.

The linear model might have been expected to break down when valve flow saturation occurred. Inspection of the relevant step responses, SS6 to SS15, shows that in these cases correspondence with servo response was still close. This suggests that simulation of a system with extreme valve saturation could be effected, if the linear model were simply modified by the addition of limiting for large valve input signals. An example of a system which would require this modification if the rotation of a powered limb joint through say 100°, in which the valve would be fully open for perhaps 95° while acting continuously for deviations of $\pm 5^{\circ}$. In section 3.3.1(f) the effect of large steady load forces was discussed. In such cases it would be necessary to allow the valve coefficient c_1 to have different values for exhaust flow and for supply flow.

This modification could easily be introduced to the simple model.

Both Shearer [3] and Burrows and Webb [37] justified the use of linearization by reference to the fact that pressure fluctuations in their systems were always small. In view of the large pressure fluctuations which occurred during the present step response tests, the accuracy of the simple simulation is of particular significance. It was noted in section 5.1 that the maximum pressure variation in the controlled chamber was almost 80% of the possible variation. In the step response tests described in ref. 37 the corresponding figure was approximately 20%, and in the frequency response tests in ref. 3 the pressure variation was about 25% of the maximum value. Large pressure variations cause departure from linearity in two ways:

(i) The operating point on the valve characteristic moves well away from the quiescent pressure curve (i.e. term d' in eqn. 3.41), and

(ii) The "bulk modulus" or "stiffness" of the air departs from its quiescent value (term c' in eqn. 3.41).

The observation that the linearized equations cope effectively with large pressure swings indicates that full simulation of the valve characteristics will rarely be necessary.

7.2.3 The Use of Static Valve Characteristics under Dynamic Conditions

In section 4.2 the measurement of the steady state valve characteristics is described. These figures were obtained in the presence of sufficient dither to reduce hysteresis to negligible proportions. These characteristics were simulated as closely as possible for the full simulation and were used for the measurement of appropriate values of c_1 (shown in figure 6.12) and c_2 for the simple simulation. The close fit between servo behaviour and the behaviour of both models suggests that the dynamic behaviour of the

valve is very similar to its static behaviour, over the frequency range encountered. This runs counter to the conclusions in the paper by Burrows and Webb [37] and in Burrows' thesis [25], that static characteristics did not apply under dynamic conditions. This conclusion was reached because, in a small perturbation analogue computer model, the valve coefficient (c_1) had to be reduced to between $^1/_3$ and $^1/_5$ of the statically measured value, to achieve a reasonable fit with the actual behaviour of a low pressure on/off pneumatic servo. An alternative explanation for this discrepancy is advanced below.

A four-way, open-centre flapper/nozzle valve was used in their case and it appears likely that its flow characteristic was unsymmetrical about the quiescent position*. This means that a very much lower figure for the valve coefficient c_1 would be appropriate for flow from the actuator to the exhaust, than that for flow from the supply to the actuator. In the absence of exhaust flow characteristics, the supply flow curves were probably used in isolation and consequently the higher figure for c_1 was selected. An average figure for c_1 between the exhaust and supply values would probably be about one third of that actually used and, as mentioned above, this is the order of the correction required to explain the discrepancy encountered.

* This can be seen in fig. 6.6 of ref. 25. The quiescent (zero flow) actuator pressure was 54 lbf/in^{2}g, i.e. the quiescent air gap was almost 0.010 in. Clearly a change of +0.005 in. results in a much smaller mass flow change than does a change of -0.005 in.

CHAPTER 8 THE EXPERIMENTAL FLUIDICALLY CONTROLLED POSITION SERVO

In the final phase of this project the electro-pneumatic servo, described in Chapter 2, was extensively modified. A control system using discrete fluidic elements, to give pulse width modulated output signals, was developed. The P.W.M. output was chosen in preference to an analogue output signal in order that the servo-valve, the most expensive item in the original servo, could be omitted. In fact, two pneumatically-signalled, two-way on/off valves replaced the electrically-signalled three-way spool valve. The load position was measured using a specially developed fluidic displacement sensor, with analogue pressure output. The low friction linear actuator and load carriage used were similar to those used for the electro-pneumatic servo.

The general layout of the fluidic servo is shown in fig. 8.1 and individual components are described below.

8.1 The Displacement Sensor

A sensor operating on the interacting-jets principle was used to measure the linear displacement of the load carriage. The output from the sensor was a fluidic pressure in analogue form and displacements up to almost 3 in. were measured.

Fig. 8.2 illustrates the interacting-jets principle which is commonly used in devices which simply detect the presence or absence of an object at a particular location. Two in-line opposed air jets interact in a plane near the discharge nozzle of the weaker jet, causing a relatively high back pressure at that nozzle. An obstruction between the jets upsets the jet interaction allowing air from the right hand nozzle to escape more easily, resulting in the output signal pressure dropping almost to zero. One advantage of this type of sensor

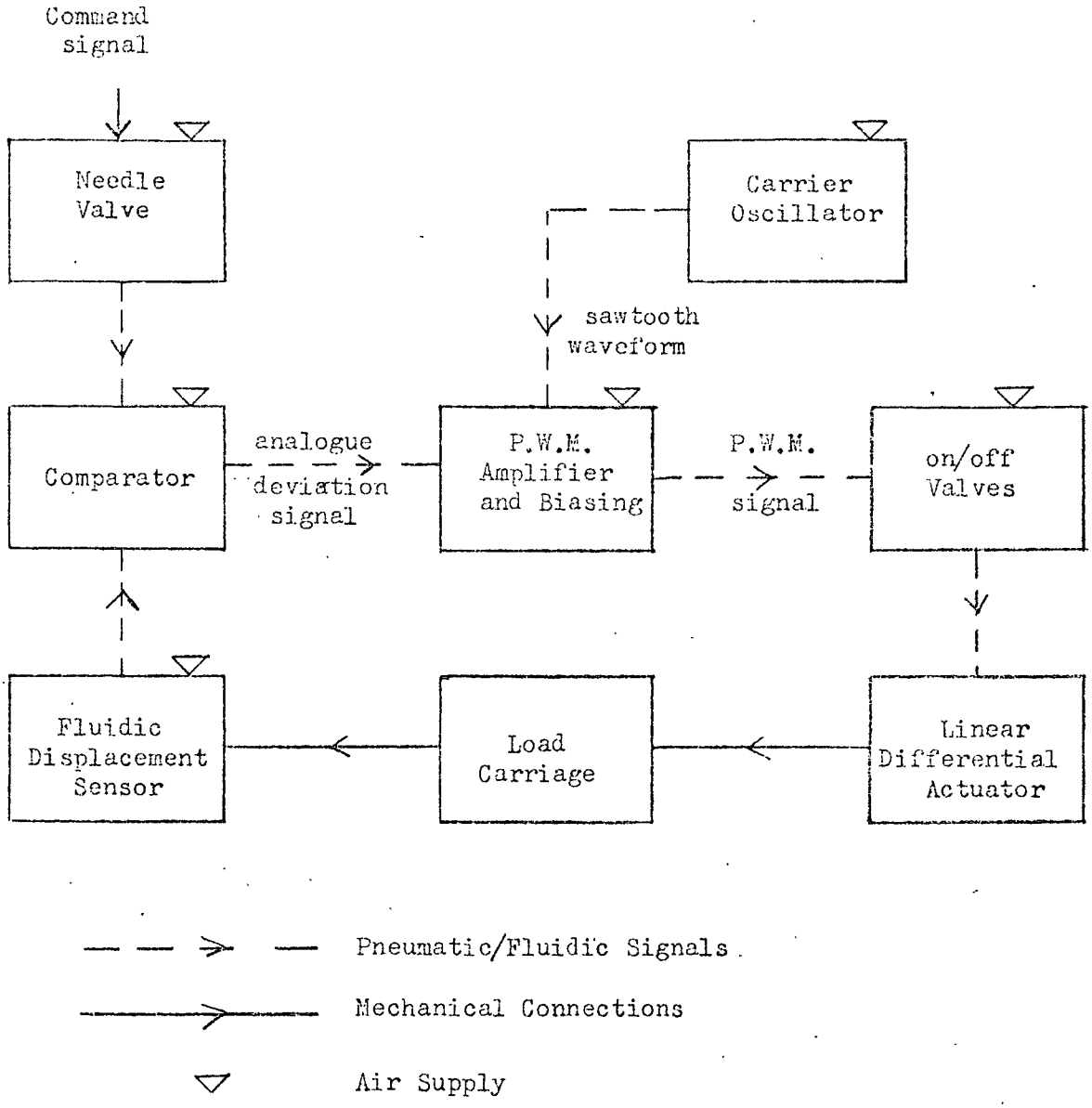

Fig. 8.1 Block Diagram of the Fluidically Controlled Position Servo

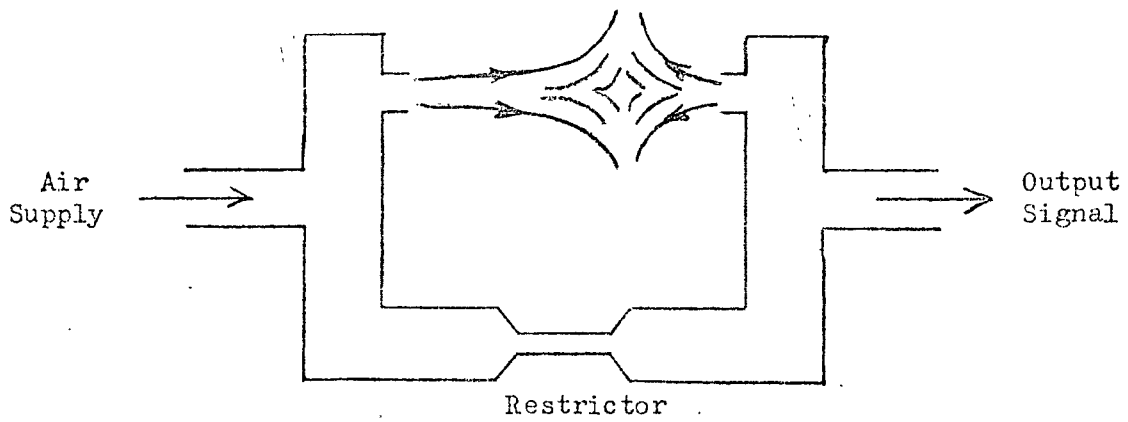

Fig. 8.2 Interacting Jets Sensor

is that the output signal is composed entirely of filtered supply air whereas with other designs the output air can become contaminated with particles from the environment of the sensor.

The 'Wedge' Sensor developed for the fluidic servo consisted of two components:

(a) A standard commercial interacting-jets object detector, of the type shown in fig. 8.2, which was held in a fixed position, and

(b) A steel plate, with one edge slightly inclined to the horizontal, which was attached to the actuator piston rod whose horizontal displacement was to be measured.

This plate or wedge was positioned in the gap of the sensor so that movement of the plate resulted in progressive interruption of the jets. This principle is illustrated in fig. 8.3. The sensor was moulded from Araldite and the nozzles were nominally rectangular. The inclination of the wedge and the height of the sensor body were adjustable, enabling the sensitivity and range of the device to be altered. Fig. 8.4 shows a photograph of the complete sensor.

Details of the sensor and calibration curves appear in section 9.1.1

8.2 The Oscillator

A Pulse Width Modulator, standard in electronic circuits, uses a continuous input signal to control the widths of a train of constant frequency pulses, which constitute its output. Thus ideally the mark/space ratio of the output varies from zero to infinity as the input varies from maximum to minimum. Such a device requires a constant frequency oscillator to provide a triangular carrier wave which is then modulated by the input signal. The linearity of the device is a function of the linearity of this triangular carrier.

A very simple fluidic oscillator can be constructed using

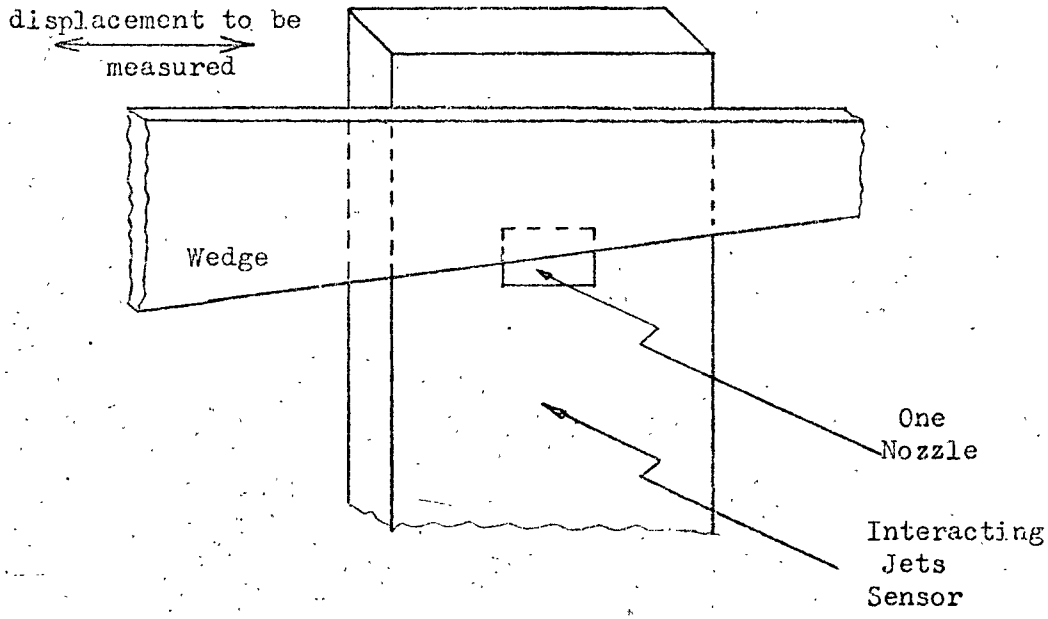

Fig. 8.3 Wedge Sensor Principle

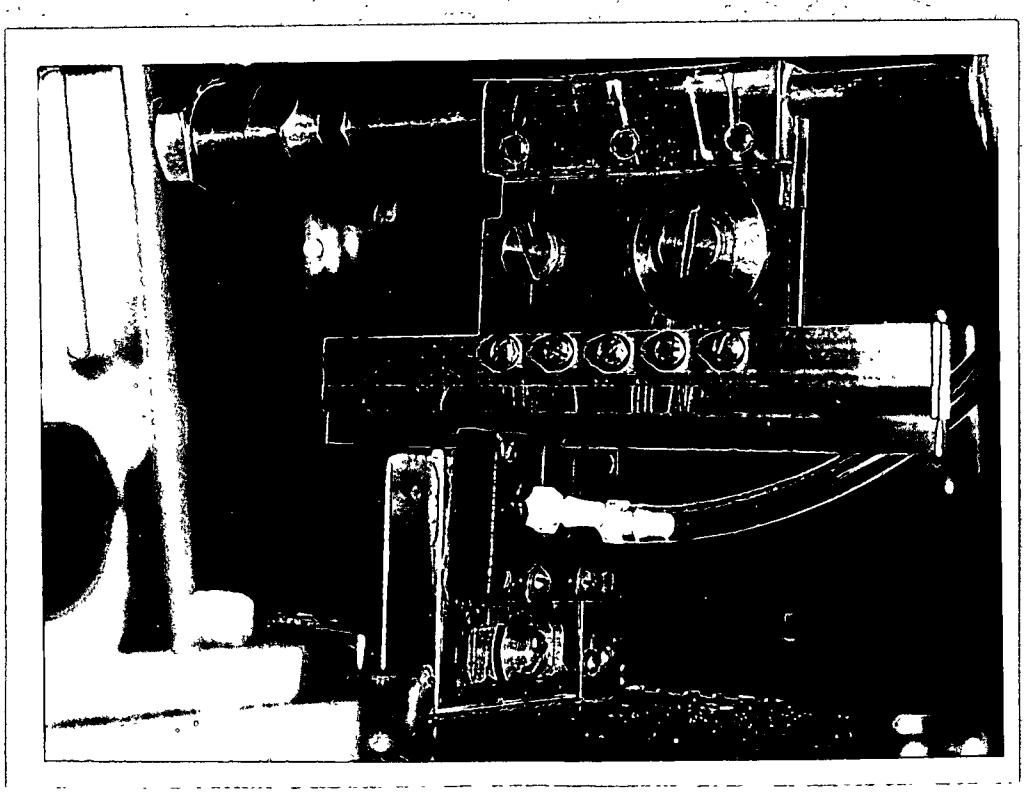

Fig. 8.4 Photograph of Wedge Sensor showing the inclined plate attached to the piston rod with the interacting-jets sensor in fixed position.

an or/nor gate and a capacitor as shown in fig. 8.5. With no signals at the control ports, air flows to the 'nor' output, 'charging' the capacitor C. Thus the control signal pressure increases until it is sufficiently high to switch the flow through the element to the 'or' port. At this point the capacitor 'discharges' until the control port pressure is sufficiently low to allow the flow to switch back to the 'nor' output. Thus the oscillator functions because of inherent hysteresis in the element. The maximum and minimum pressures of the output waveform are controlled by the switching levels of the element and the frequency depends upon the volume of C and the sizes of the interconnecting pipes.

The results of tests on this oscillator appear in section 9.1.2 but it was not used for the fluidic servo, as the mean pressure level of the output waveform proved to be too low for compatibility with the remainder of the control system.

The alternative oscillator design, which was adopted, is shown in fig. 8.6. In this case a bistable element and two feedback capacitors, C_1 and C_2, were used. In this case the flow through the bistable element switched when the differential pressure across its control ports reached a certain value. Again the operation depended upon hysteresis in the fluidic element and the frequency of oscillation was controlled by the sizes of the capacitors and pipes.

Beam-deflection elements moulded in Araldite were used in both oscillators and details of these and the capacitors are included in Appendix 4. The elements and a capacitor can be seen in fig. 8.8.

8.3 The Amplifier

Fig. 8.7 shows the complete fluidic control system, including the P.W.M. amplifier which comprised a comparing element, a signal biasing stage and two Schmitt triggers. (Component data appears in

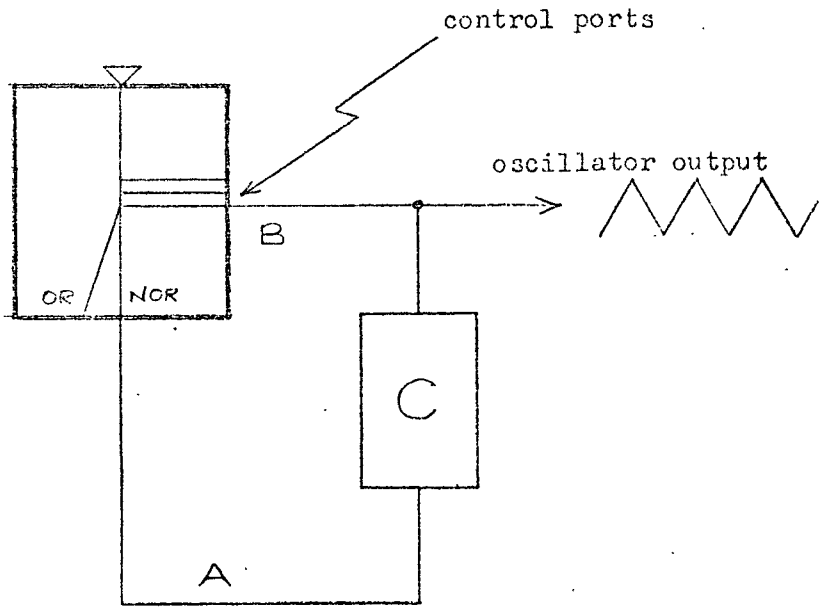

Fig. 8.5 Simple Fluidic Oscillator using an Or/Nor Element ('NOR' Oscillator)

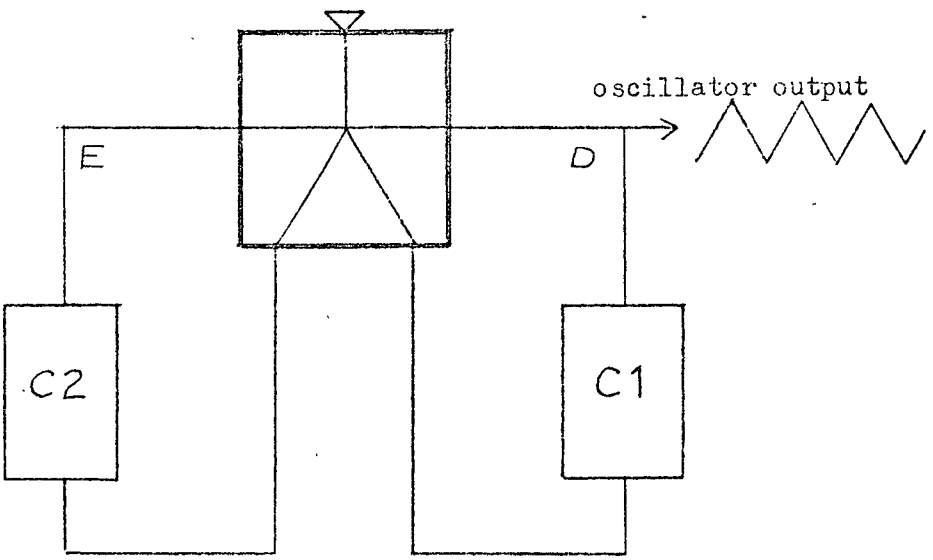

Fig. 8.6 Oscillator used for Fluidic Servo ('Bistable' Oscillator)

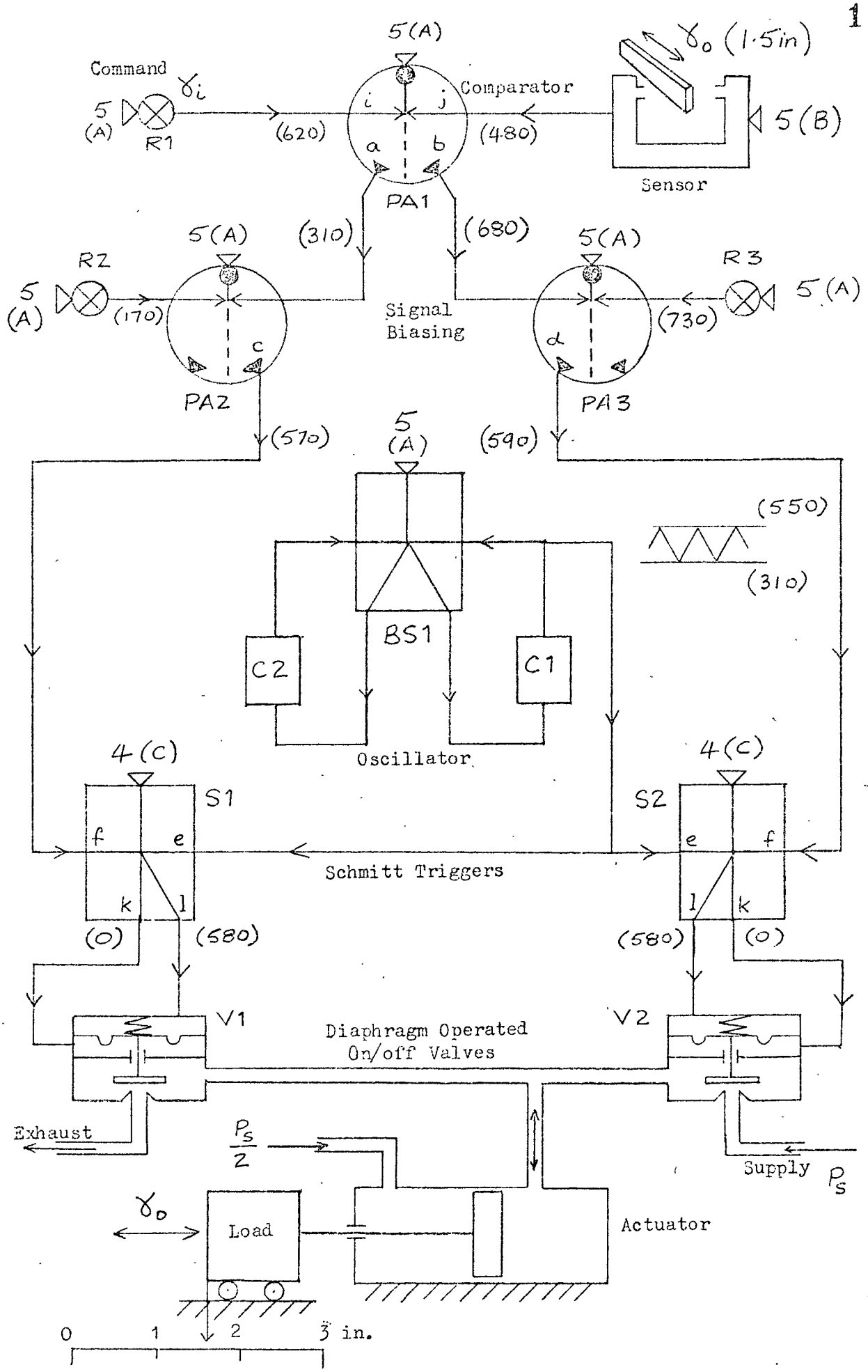

Fig. 8.7 Fluidically Controlled Servomechanism

Supply pressures are in lbf/in^{2}g. (A), (B) and (C) refers to reservoirs (see section 8.6).
( ) shows approximate null pressure levels in mm W.G. for the closed loop tests.

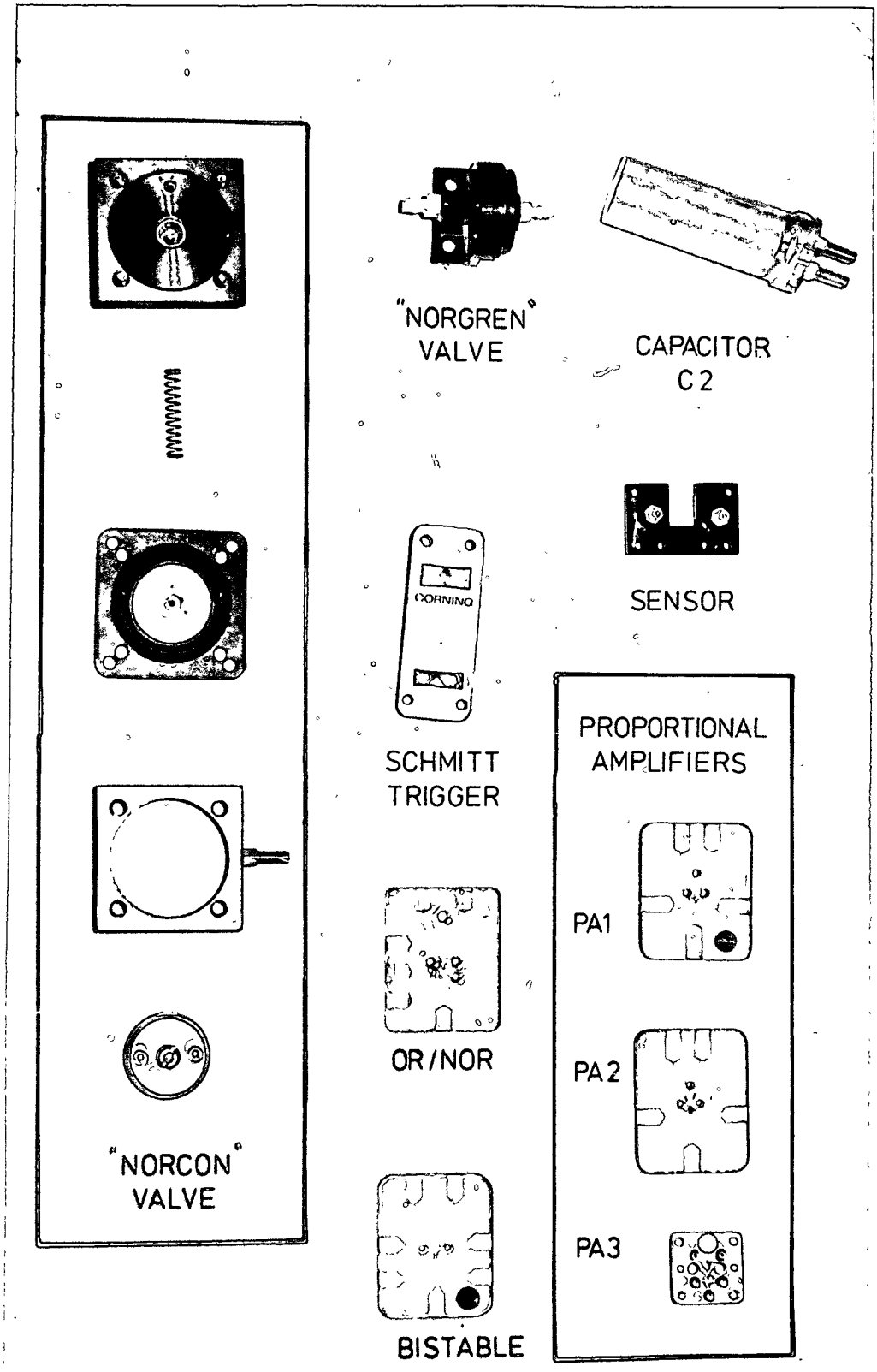

Fig. 8.8 Components of the Fluidic Servomechanism.

Appendix 4.) The comparing and signal biasing stages were constructed from three single-stage beam-deflection proportional amplifiers. The purpose of the first proportional amplifier PA1 was to generate the deviation signal on which the system's operation depended and the biasing stage enabled the valve overlap and underlap to be adjusted or eliminated, as required. At the Schmitt triggers the output signals from the biasing amplifiers were compared with the triangular carrier wave from the oscillator, so that when the pressure at port f exceeded that at port e, the output port 1 was pressurised, while when the pressure at f fell below that at e, port 1 was exhausted and port k pressurised.

Initial setting of the system was as follows:
With the command position and actual position set equal, valve R_2 was adjusted so that the pressure at input f of Schmitt trigger S1 was just greater than the maximum level reached by the carrier signal at e. Similarly R3 was adjusted to make the pressure at port f of S2 just exceed the carrier signal peak pressure at e. Thus in this condition both on/off valves remained closed.

Examining the behaviour of the supply side, a small increase in the command signal pressure to PA1 resulted in a fall in the pressure to port f of Schmitt trigger S2 to a level between the maximum and minimum pressures reached by the carrier signal at e. Thus the Schmitt trigger output switched from 1 to k as the carrier signal pressure exceeded the pressure on port f and the diaphragm valve V_2 opened. Each time the carrier signal fell again, the Schmitt output switched from k to 1 and the valve closed. Thus the time for which the valve remained open (assuming instantaneous valve movement) varied linearly with the pressure on f, provided that this pressure was between the maximum and minimum pressures reached by the carrier wave. In the presence of a large command signal pressure to PA1, the

output pressure from port d of PA3 fell below the minimum level of the oscillator output and port k of S2 remained pressurised continuously. In this case the supply valve V2 remained open and the system was saturated. In a similar way the exhaust valve (V1) opening was modulated when the command signal fell below its equilibrium position. Referring to fig. 8.7, in the closed loop system the sensor was connected so that its output signal pressure increased when the load carriage moved to the left, i.e. negative feedback was ensured. The amplifiers and a Schmitt trigger are shown in fig. 8.8.

8.4 The Valves

Two single stage valves were employed to control the supply and exhaust flow to the differential actuator. The valve-actuators were diaphragms which operated against light springs, enabling them to be operated by very low pressure signals. Positive action was ensured by switching the control pressure from one side of the diaphragm to the other, while the first chamber exhausted to atmosphere, when reversal was required. The valves were of the poppet type with spherical plugs and seats. Data on these valves appears in Appendix 4 and fig. 8.8 shows a photograph of a valve.

8.5 The Actuator and Load

A low friction differential actuator and load carriage, of similar design to those described in Chapter 2 and shown in fig. 2.2, were used.

8.6 Air Supplies

Low pressure air was supplied to the control system from three separate circuits, indicated (A), (B) and (C) in fig. 8.7, in order to eliminate unwanted interaction. These circuits each included

a regulator and a reservoir of approximately 300 in^3 capacity.

The actuator air supply arrangements were as described in section 2.2.5 but in this case the compressor worked at 100 lbf/in^2g.

8.7 Pressure Transducer

A strain gauge pressure transducer together with a preamplifier and a storage oscilloscope fitted with a Polaroid camera were used for dynamic pressure recordings. This was a low volume transducer using semiconductor strain gauges for maximum sensitivity and details are included in Appendix 4. This was not the ideal transducer for low pressure measurements such as are encountered in fluidics, but a more suitable device, such as a pressure sensitive transistor, was not available. The noise content of the pressure recordings which can be attributed to the pressure transducer itself can be judged from many of the figures in Chapter 9, in which atmospheric pressure traces are included (e.g. figs. 9.2, 9.3 etc.).

CHAPTER 9 THE FLUIDICALLY CONTROLLED SERVO - TESTS, RESULTS AND DISCUSSION

Tests on individual components, sections of the system and finally on the complete system are described and the results are presented and discussed.

9.1 Tests and Results

9.1.1 The Wedge Sensor

The displacement sensor incorporated a Plessey type IJ-1* object detector. The thickness of the interrupting wedge was 0.12 in. and its angle of inclination with the horizontal was 3.3×10^{-3} radians. This represented a height of about 0.01 in. in a stroke of 3 in. The gap between the sensor nozzles was 0.4 in. and the wedge was positioned approximately mid-way between them. The nozzles were nominally rectangular, 0.040 in. wide and 0.020 in. high, but examination under magnification showed that the exit orifices were very ragged and far from rectangular. The air consumption of the sensor, when loaded by amplifier PA1, was 0.20ft^3/min (free air) with the supply pressure at 3 lbf/in^{2}g.

(a) Static calibration

The displacement sensor was calibrated in position, with the remainder of the fluidic circuit connected as in fig. 8.7. The valves were not connected and the load carriage was simply positioned by hand.

Fig. 9.1 shows the static calibration curve with the supply pressure at 5 lbf/in^{2}g and with the command pressure on PA1 maintained at 630 mm W.G. throughout. In addition curves for supply pressures of 7 and 2.5 lbf/in^{2}g are shown, though only a few, more widely spaced points are included in these cases. Continual adjustment of valve R1 was necessary to maintain constant command pressure as the sensor

* Now marketed by British Fluidics & Controls

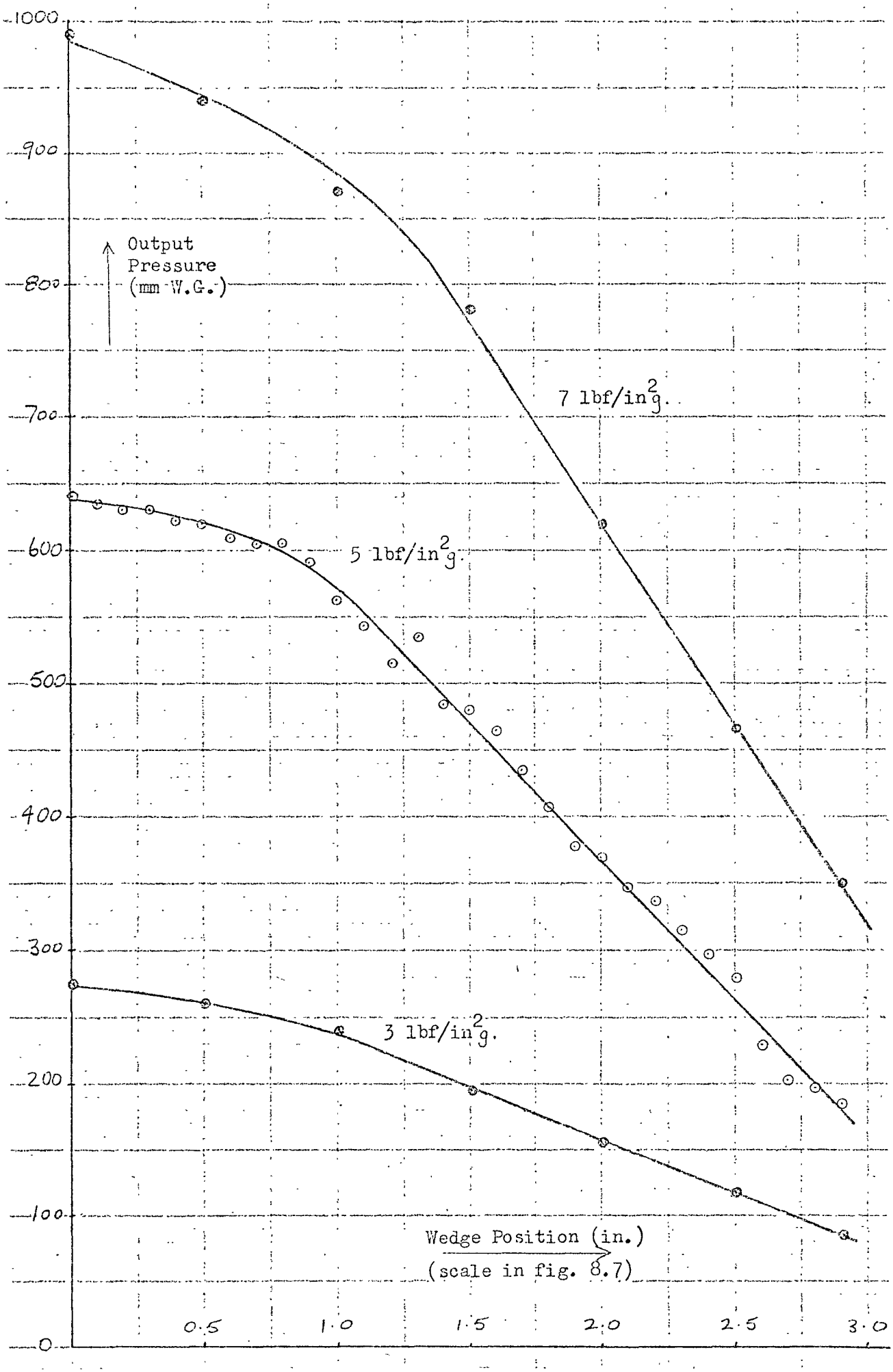

Fig. 9.1 Wedge Sensor Static Calibration Curves

displacement varied. (For example, in one case the command pressure was set at 630 mm W.G. with the load carriage in its extreme right hand position. The carriage was then moved to the extreme left hand position and unless R1 was adjusted, the command pressure rose to 730 mm W.G.) No hysteresis could be detected in the operation of the sensor.

(b) Dynamic response

The dynamic behaviour of the wedge sensor is illustrated by the recordings shown in fig. 9.2. Fig. 9.2(a) shows the output pressure from the sensor when a plate was first interposed quickly by hand, between the sensor nozzles, and then removed again. It can be seen that in the first case the rise time was about 15 ms. while for output pressure increase, the rise time was less than 5ms. A high frequency ripple is evident on the sensor signal in the absence of the plate between the nozzles. This is caused by the interaction of the two jets and closer examination showed that a major component was at a frequency higher than 1 kHz. There was also a considerable random content.

For figs. 9.2(b) and (c) a twin-beam oscilloscope was used to give simultaneous recording of the Wedge Sensor output pressure and the wiper voltage from a potentiometric displacement sensor (of the type described in section 2.2.3). In case (b) the load carriage (to which both sensors were connected) was moved approximately 1 inch, as quickly as possible, by hand. In case (c) the trolley was moved, again by hand, in roughly a sinusoidal manner. As is to be expected from recording (a) and the static characteristic in fig. 9.1, the fluidic sensor output corresponds closely to that of the potentiometric sensor, apart from the presence of the noise discussed above. The third trace in fig. 9.2(b) shows the output from the wedge

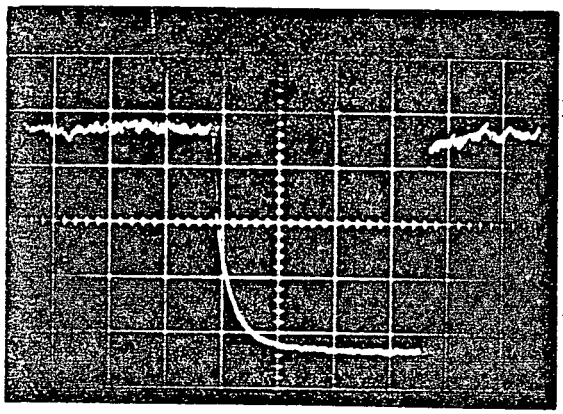

50 ms/division

(a) Sensor output pressure when plate suddenly interposed between nozzles and then removed

calibration
180 mm W.G./division (approx.)

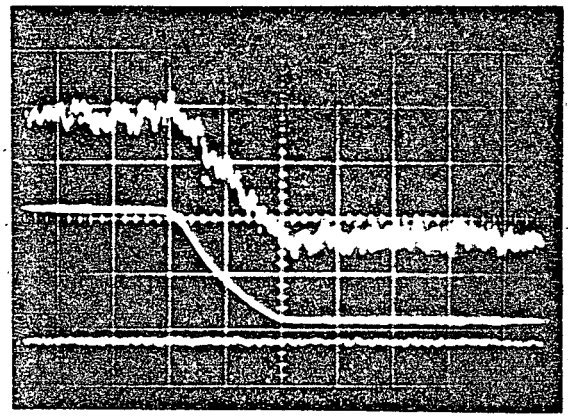

100 ms/division

(b)

(b) and (c) Responses of wedge sensor and potentiometric sensor compared.

calibration
upper traces: 90 mm W.G./division (approx.)
lower traces: 0.5 in./division

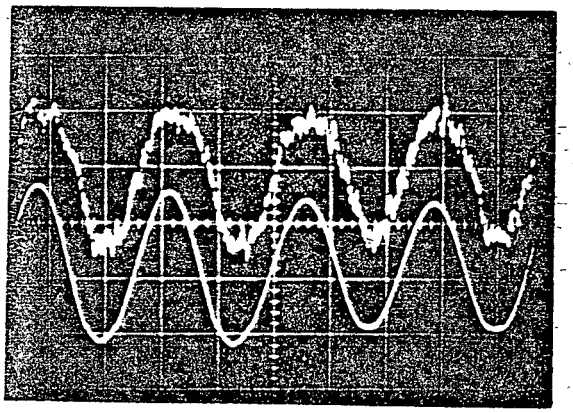

100 ms/division

(c)

Fig. 9.2 Dynamic Response of the Wedge Sensor

sensor when measuring atmospheric pressure. (In this case the vertical positioning is not significant since the oscilloscope shift control was used to position the trace.)

9.1.2 The Oscillator

The two oscillator designs described in Chapter 8 were tested while driving Schmitt triggers as in fig. 8.7.

(a) The 'Bistable' Oscillator

The output pressure from the oscillator shown in fig. 8.6 was recorded for supply pressures 5, 4 and 3 lbf/in^2. The waveforms are shown in fig. 9.3. It can be seen that the output amplitude decreased and the frequency increased as the supply pressure was lowered. Reference to the atmospheric pressure level, included in each case, shows that the mean pressure of the output oscillation also fell with the supply pressure. A supply pressure of 5 lbf/in^{2}g was used for the oscillator in later tests on the complete fluidic servo and fig. 9.4(a) is a second recording at this pressure, showing more cycles of the output waveform to enable study of its long term stability. This point and others are discussed in section 9.2.2.

(b) The 'NOR' Oscillator

Fig. 9.4(b) and (c) shows the behaviour of the simple oscillator of fig. 8.5 for 5 lbf/in^{2}g supply pressure, when fitted with two different feedback capacitors. Again an atmospheric pressure trace is shown in each recording and it can be seen that the mean pressure levels are considerably lower than for the 'Bistable' oscillator (e.g. fig. 9.4(a)).

9.1.3 Proportional Amplifiers

Three different proportional amplifiers were used in the comparing and signal biasing stages of the control system. Amplifiers PA2 and PA3 were required to operate with one of the control pressure signals constant, and were tested in that condition, the control

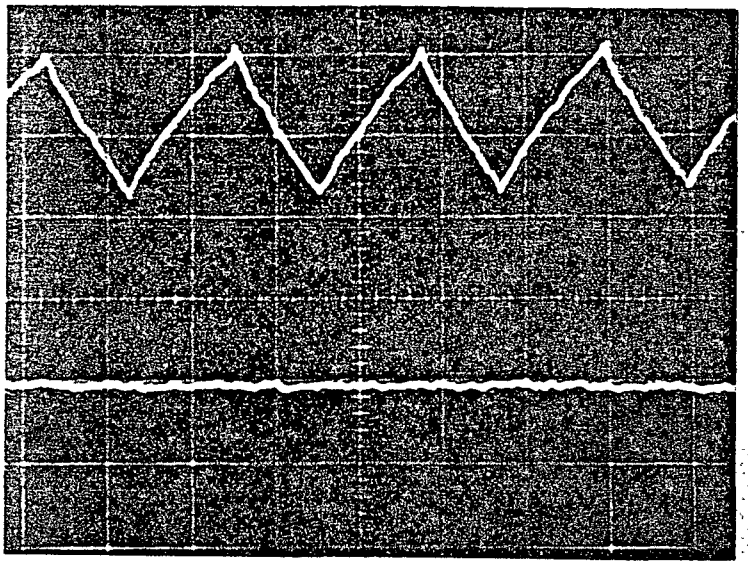

(a)

frequency: 20 Hz

supply pressure: 5 lbf/in^{2}g

Calibration for (a), (b) and (c)

Time: 22 ms/division

Pressure: 133 mm W.G./ division

(Second trace shows atmospheric pressure in each case)

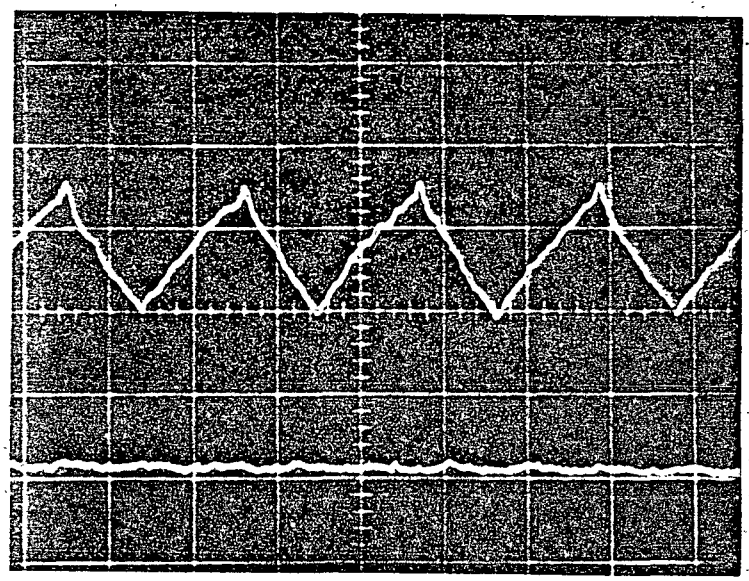

(b)

frequency: 21.3 Hz

supply pressure: 4 lbf/in^{2}g

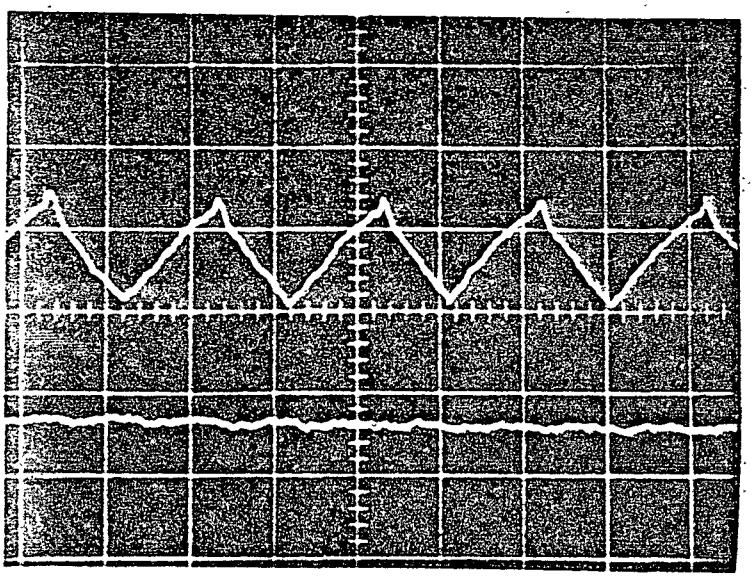

(c)

frequency: 22.9 Hz

supply pressure: 3 lbf/in^{2}g

Fig. 9.3 'Bistable' Oscillator Output Pressure Waveforms

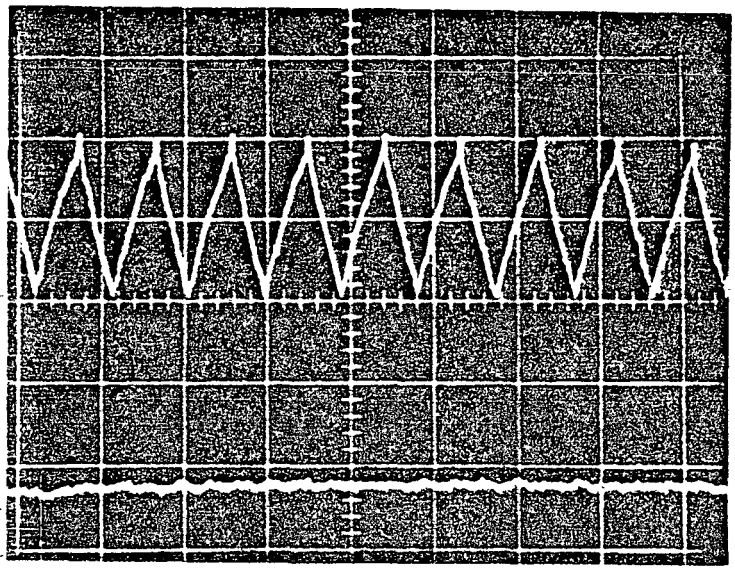

(a) 'Bistable' Oscillator

output: 425 ± 120 mm W.G. at 20 Hz

calibration

time: 55 ms/division

pressure: 133 mm W.G./division

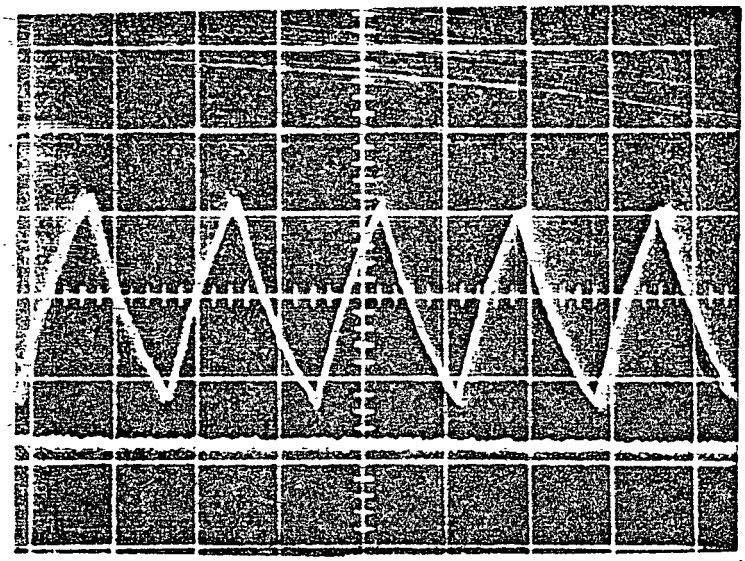

(b) and (c)
'Nor' Oscillator.

calibration

time: 50 ms/division

pressure: 133 mm W.G./division

(b)

output: 220 ± 165 mm W.G. at 11.4 Hz

feedback capacitor volume: 127×10^3 mm^3

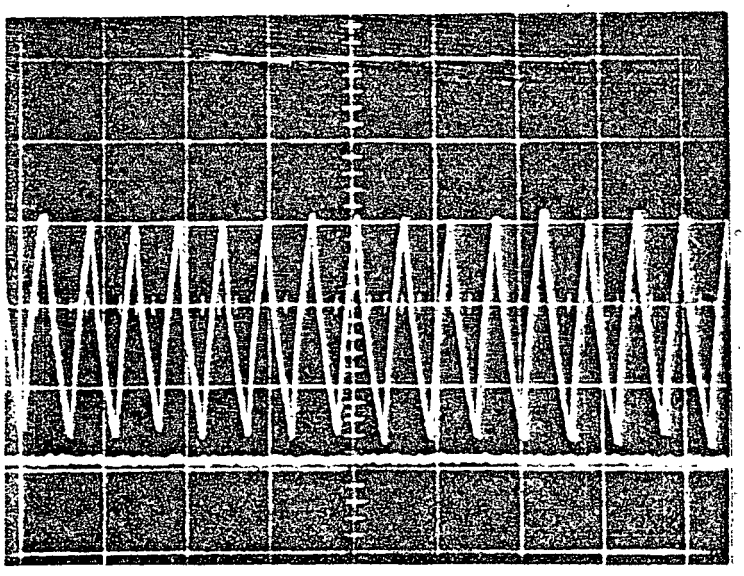

(c)

output: 215 ± 175 mm W.G. at 27.3 Hz

feedback capacitor volume: 31.2×10^3 mm^3

Fig. 9.4
Oscillator Output Pressure Waveforms
(second trace shows atmospheric pressure in each case)

pressure being adjusted by displacement of the load carriage. The resultant static characteristics are shown in fig. 9.5.

The requirement for PA1 was more demanding since, in that case, both control signals could vary. The input differential pressure level for the static calibration test on PA1 (fig. 9.6) was varied by moving the displacement sensor blade and when necessary, by adjusting restrictor R1 also. The Common Mode Rejection of PA1 was not studied in detail but it was observed that the output pressures at ports a and b did not remain constant when the input differential pressure was maintained constant, (by adjusting R1) for different sensor blade positions. The implication of this is that the two curves in fig. 9.6 are only typical curves and in fact, two "families" of curves could be drawn, each pair corresponding to a different constant control pressure on (say) port i.

9.1.4 Schmitt Triggers

Two identical Schmitt triggers were used to generate the output pulse trains which were used to signal the control valves. No hysteresis could be detected in the Schmitt triggers, using water columns for pressure measurement. Switching actually occurred when the pressure on port f was slightly lower than that on e, in both S1 and S2. The performance of a single Schmitt trigger was investigated as follows:

A Schmitt trigger was connected to the oscillator as shown in fig. 8.7, but a variable pressure controlled by a restrictor was fed to the second control port (f). The output pressure pulses at port 1 with the Schmitt trigger output dead-ended (i.e. connected to a pressure transducer only) were recorded for various settings of the restrictor. The mark-space ratio of this output was measured in each case. As the pulses were not perfectly square and the pulse width showed slight variation from cycle to cycle, the technique adopted

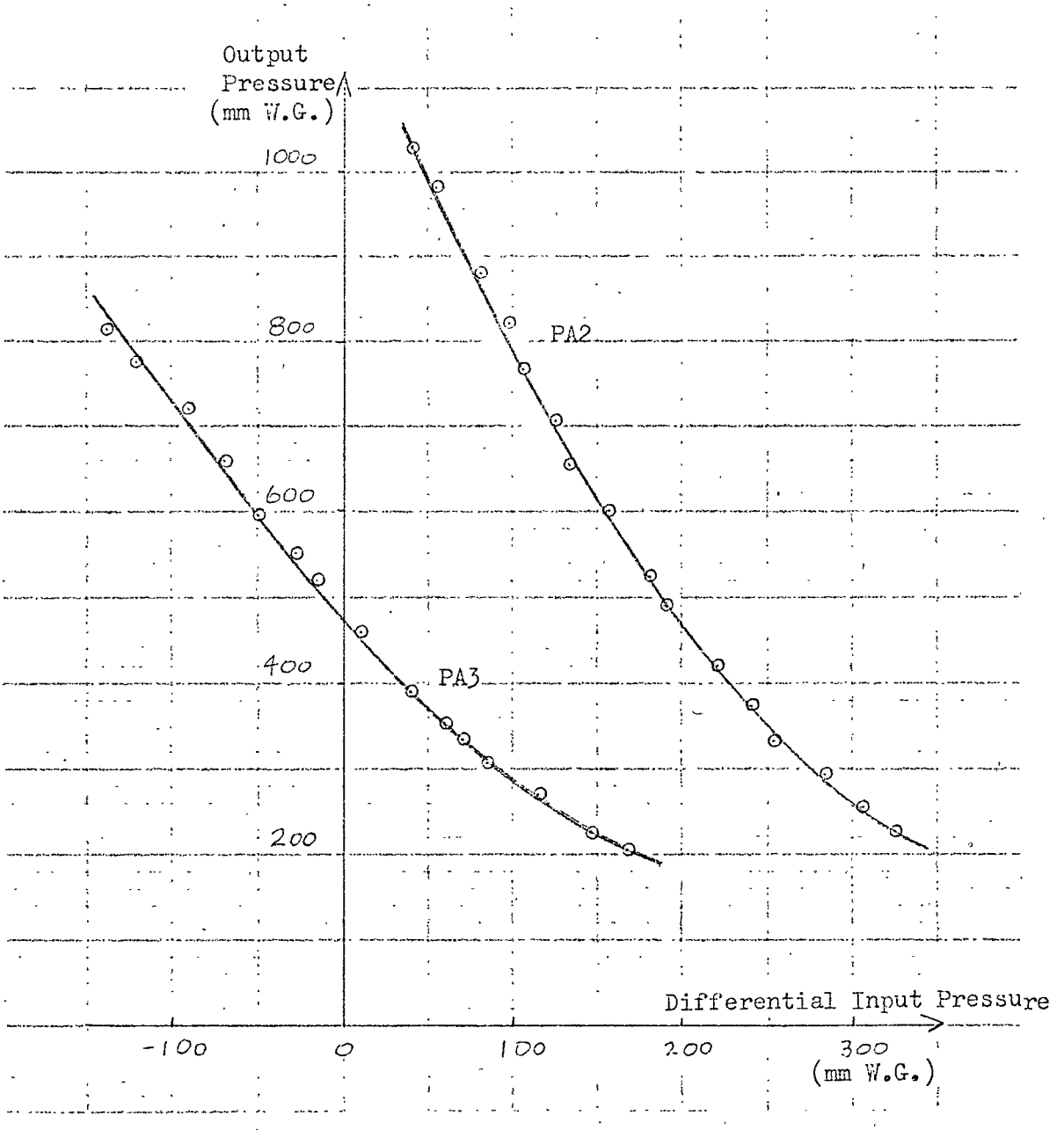

Amplifier PA2

Output: port c (fig. 8.7)

Bias pressure: 170 mm W.G. (R2)

Input: positive if control pressure (a) > bias

Supply: 5 lbf/in^{2}g

Amplifier PA3

Output: port d (fig. 8.7)

Bias pressure: 730 mm W.G. (R3)

Input: positive if control pressure (b) > bias

Supply: 5 lbf/in^{2}g

Fig. 9.5 Static Characteristics of Proportional Amplifiers

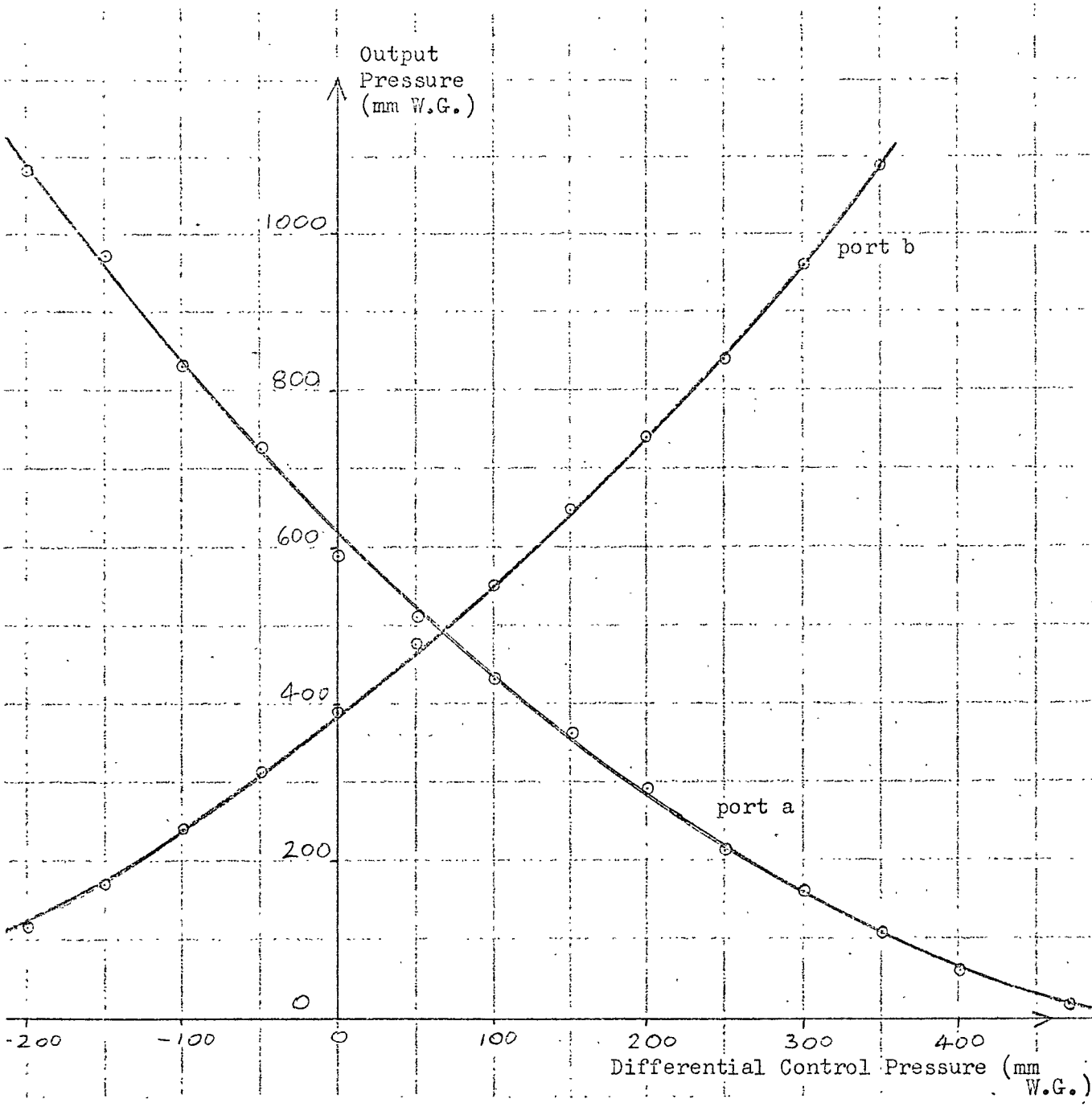

Control: positive if pressure at port i (fig. 8.7) exceeds pressure at port j. Both pressures adjusted during test (see note on common mode rejection in section 9.1.3)

Supply: 5 lbf/in^2g

Fig. 9.6 Static Characteristic of Proportional Amplifier PA1

was to take the average width at mid-height for several successive pulses. The results of these tests are plotted in fig. 9.7(a) and in (b) specimen recordings of the output waveform are shown.

9.1.5 Complete PWM Amplifier

Initial setting of pressure levels in the system was described in section 8.3. Fig. 9.6 shows that the outputs from amplifier PA1 were unsymmetrical and equilibrium pressures were selected in this case, so as to utilise the most linear portions of the characteristics. Approximate initial pressure levels at these and other points throughout the system are shown in fig. 8.7. These levels, at which both valves were just held in the 'off' position, were used for the tests described below.

To investigate the behaviour of the complete amplifier, the pressures at ports 1 of the two Schmitt triggers were recorded in turn, for a number of positions of the wedge sensor blade. The setting of valve R1 remained constant throughout. For these tests the only load on the Schmitt trigger under test was the pressure transducer, i.e. the output 1 was dead-ended and output k was open to atmosphere. Specimen output pressure waveforms from the Schmitt triggers are shown in fig. 9.8 and the mark-space ratio was measured in each case. The technique described in section 9.4 was adopted for this measurement and the results are shown in table 9.1. The variation of mark-space ratio with the differential pressure across PA1 is shown in fig. 9.9.

When the sensor was included in the system, the dependence of mark-space ratio upon sensor position was as in fig. 9.10. The reasons for the shapes of these characteristics and for the degradation of fig. 9.10 relative to fig. 9.9 are discussed in section 9.2.5.

9.1.6 Valves

The "Norcon" valves used in the fluidic servo (fig. 8.7) had a flow capacity slightly less than that of the servo valve in the

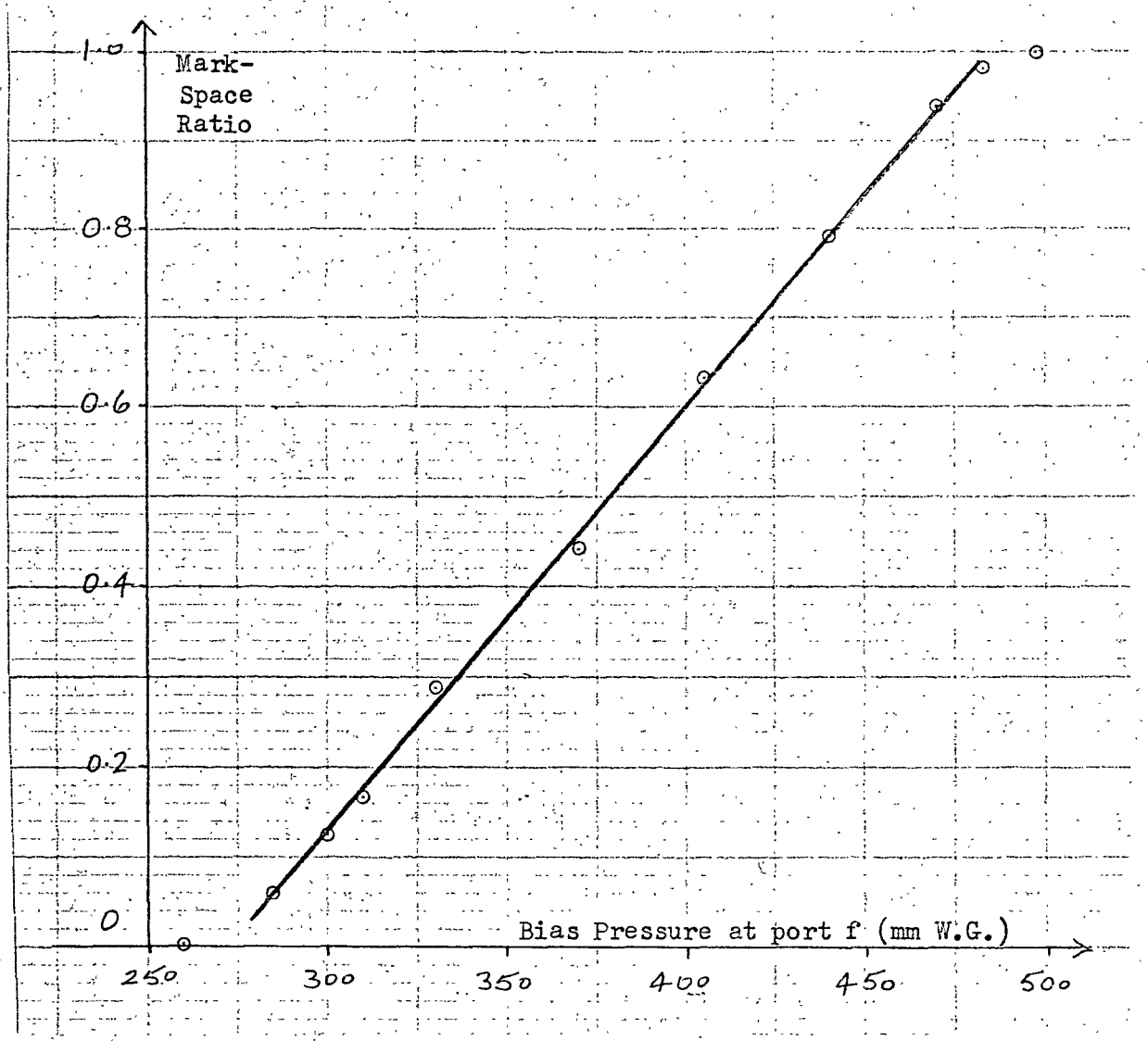

(a) Variation of Mark-Space Ratio with Bias Pressure at f.
Circuit as in fig. 8.7.
M/S ratio of 1.0 means port 1 pressurised continuously.

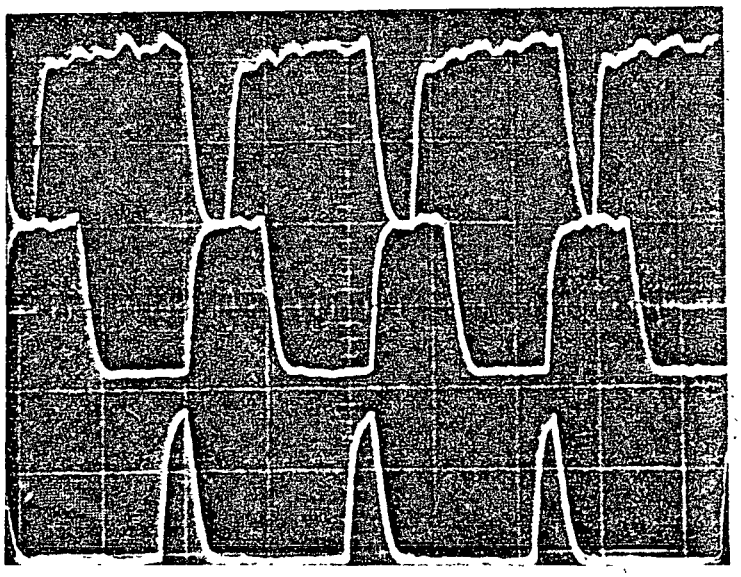

(b) Output Waveforms

Bias pressures: 440, 370 and 310 mm W.G. respectively

Calibration

Pressure: 270 mm W.G./ division

Time: 22 ms/division

Fig. 9.7 Schmitt Trigger Performance

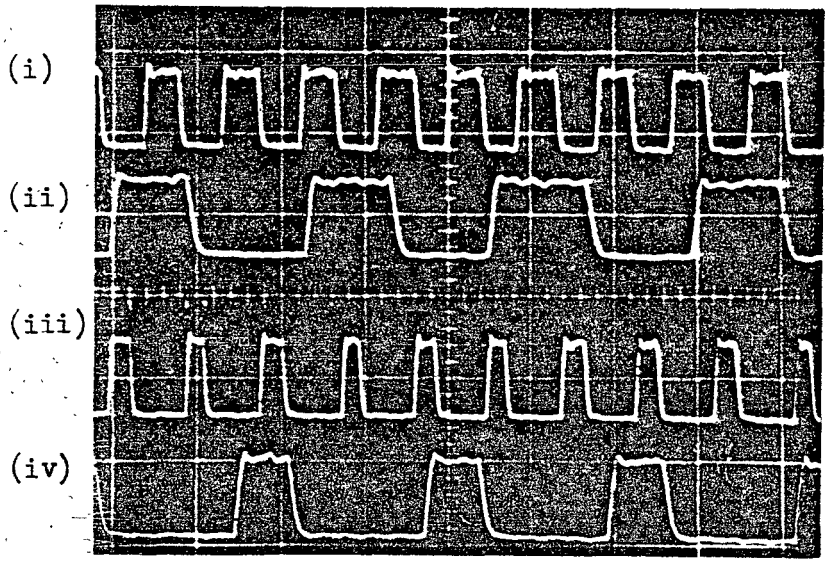

(a) Schmitt trigger S2 - dead ended

traces (i) and (ii): 1.90 in sensor position

traces (iii) and (iv): 2.00 in sensor position

Calibration for (a) and (b)

Pressure: 650 mm W.G./ division

Time: 55 ms/division for traces (i) and (ii)

and 22 ms/division for traces (iii) and (iv)

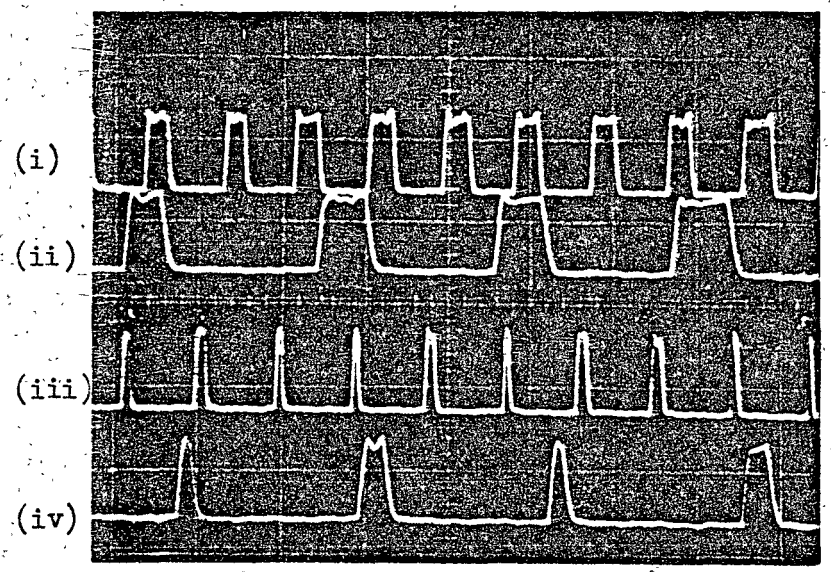

(b) Schmitt trigger S1 - dead ended

traces (i) and (ii): 1.12 in sensor position

traces (iii) and (iv): 1.03 in sensor position

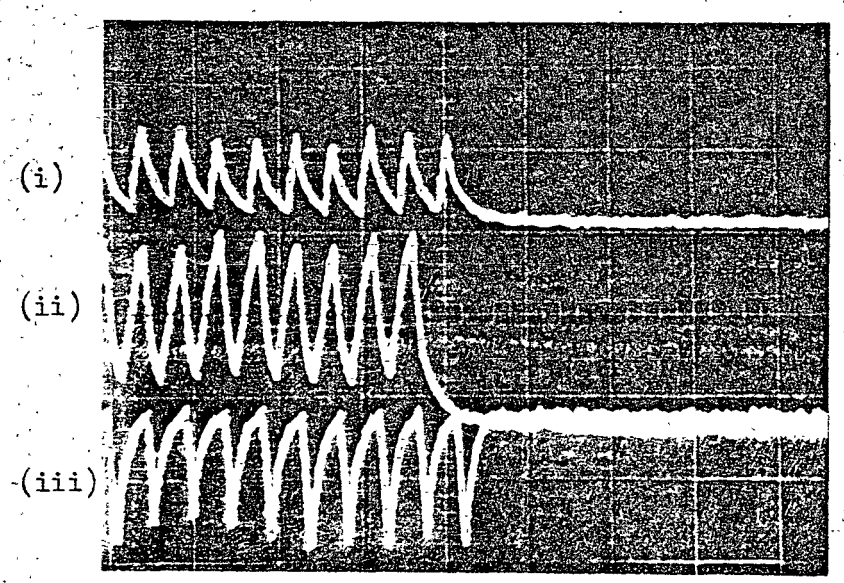

(c) Schmitt trigger feeding a Norcon Valve

for (i) low, (ii) moderate and (iii) high bias pressures

Calibration for (c)

Pressure: 133 mm W.G./ division

Time: 110 ms/division

Fig. 9.8 Complete P.W.M. Amplifier - Specimen Output Pressure Waveforms

Table 9.1 Test Results - Complete PWM Amplifier

Displacement Sensor Position (in.)	Displacement Sensor Output pressure (mm W.G.)	Command Pressure (mm W.G.)	Differential Pressure across PA1 Control Ports (mm W.G.)	Mark-Space Ratio of Schmitt trigger output (port 1)	
2.50	285	580	295	1.00	
2.40	300	585	285	0.99	
2.30	330	590	260	0.89	
2.20	345	592	247	0.80	
2.10	360	595	235	0.71	
2.00	365	600	235	0.71	Supply
1.90	387	600	213	0.50	Side
1.80	410	610	200	0.42	(S2)
1.70	435	615	180	0.24	
1.60	465	620	155	0.10	
1.50	480	620	140	0.00	
1.50	480	620	140	0.00	
1.40	490	620	130	0.00	
1.39	495	620	125	0.11	
1.37	507	622	115	0.22	
1.35	525	625	100	0.47	Exhaust
1.30	537	630	93	0.58	Side
1.20	525	630	105	0.41	(S1)
1.12	550	630	80	0.68	
1.10	560	630	70	0.81	
1.03	572	635	63	0.89	
0.92	582	640	58	0.99	
0.90	595	640	45	1.00	

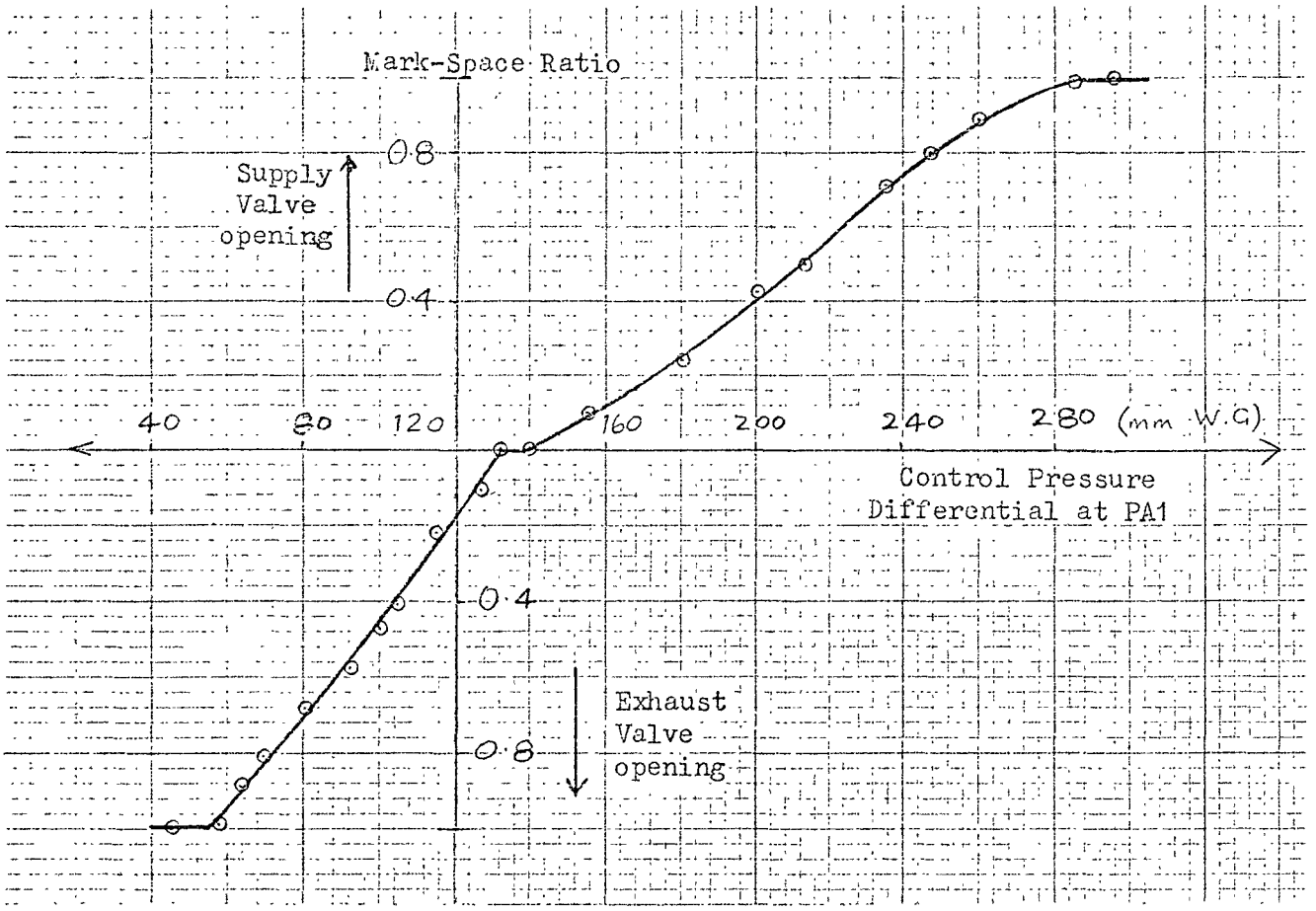

Fig. 9.9 P.W.M. Amplifier Performance, excluding the sensor. (columns 3 and 5, table 9.1)

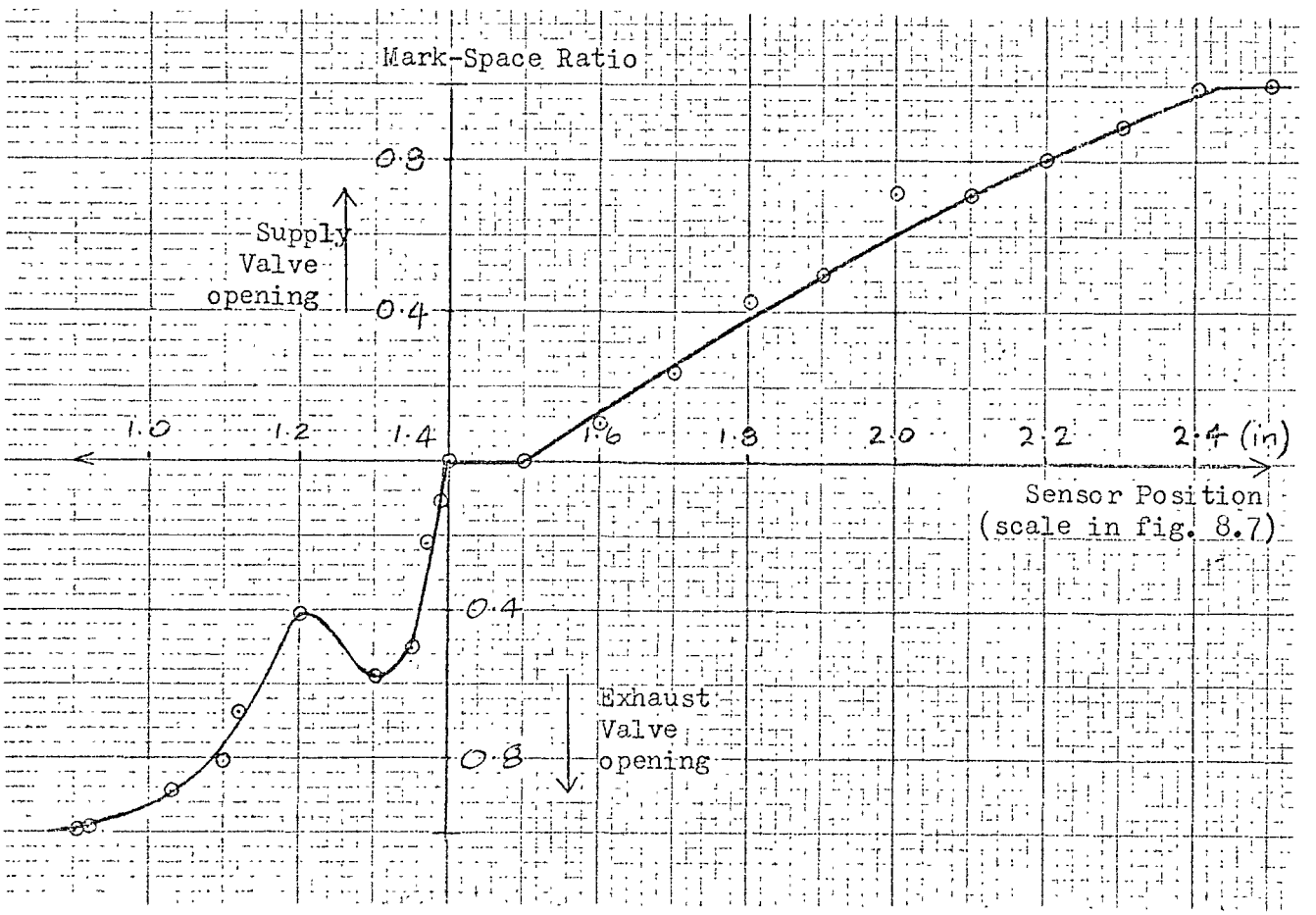

Fig. 9.10 P.W.M. Amplifier Performance, including the sensor. (columns 1 and 5 in table 9.1)

electro-pneumatic system described earlier. The diaphragm actuator springs were adjusted so that the valve switched when a pressure of approximately 250 mm W.G. was applied either to the top or bottom of the diaphragm. Operation was uncertain at pressures below this level. Further details appear in Appendix 4.

(a) Behaviour of the valve when signalled by Schmitt trigger

A valve, Schmitt trigger and the oscillator were connected as shown in fig. 8.7 and an independently controlled bias pressure was fed to port f of the Schmitt trigger. The Schmitt trigger supply pressure was 2 lbf/in^{2}g and this resulted in an output signal level of 360 mm W.G. The load presented to the Schmitt trigger by the Norcon Valve proved to be too great and the output pressure pulses were considerably degraded, compared to those observed when the Schmitt trigger output was dead-ended (e.g. fig. 9.8(a) and (b)). Fig. 9.8(c) shows the resulting pressure on the top of the valve diaphragm for low, moderate and high bias pressures (at port f) respectively. Also shown are reference pressure levels in each case (atmospheric pressure for traces (i) and (ii) and the maximum Schmitt trigger output pressure, i.e. 360 mmW.G. for (iii)). Thus there is approximate correspondence between (i) in fig. 9.8(c) and (iii) in fig. 9.8(b) and between (ii) in fig. 9.8(c) and (i) in fig. 9.8(a).

The step response of the Schmitt trigger/valve arrangement with the same supply pressure was observed separately and a rise time of approximately 60 ms. for the valve drive pressure signal was recorded. In view of this, the poor quality waveform, illustrated by fig. 9.8(c) for a carrier frequency of approximately 20 Hz, is not unexpected.

(b) Small Valve

The tests described above indicated that in order to utilize the output from the PWM amplifier, a valve actuator which demanded

considerably less flow from the Schmitt triggers was required. No suitable valve with flow capacity comparable to that of the Norcon valve was available but for comparison the behaviour of a small single-stage "Norgren" diaphragm-operated valve (see Appendix 4) was studied. In this case the diaphragm chamber volume was smaller and consequently the Schmitt trigger output waveform was hardly affected by it. A test similar to that conducted on the dead-ended Schmitt trigger (described in section 9.4) was performed with the "Norgren" valve connected to port 1. In this case the mark-space ratio of the valve input signal was not calculated but the resultant controlled flow through the valve was measured, using a float-type flow meter. For this test, air at an arbitrary pressure of 16 lbf/in^2g was supplied to the Norgren valve. The supply pressure to the Schmitt trigger was reduced to 0.9 lbf/in^2g in order to make its output pressure compatible with the valve. The meter float position fluctuated slightly in a random fashion but a mean flow rate was measured for several steady control pressure levels (on port f). These figures are plotted in fig. 9.11(a). Specimen waveforms for three different control pressures are shown in fig. 9.11(b).

9.1.7 The Complete Fluidic Servo

The closed loop system was connected as shown in fig. 8.7 with the supply pressure set at 80 lbf/in^2g but satisfactory operation was not achieved. The behaviour of the system for two different command positions was observed.

Carriage in 2.25 in. position

A command pressure of 480 mm W.G. was applied to PA1. The unloaded carriage did not maintain a steady position but oscillated randomly within a zone of $\pm$ 0.2 in. about the command value. A large and irregular component of this oscillation was at about 5 Hz. The valve V1 could be heard exhausting in a random fashion. When a step

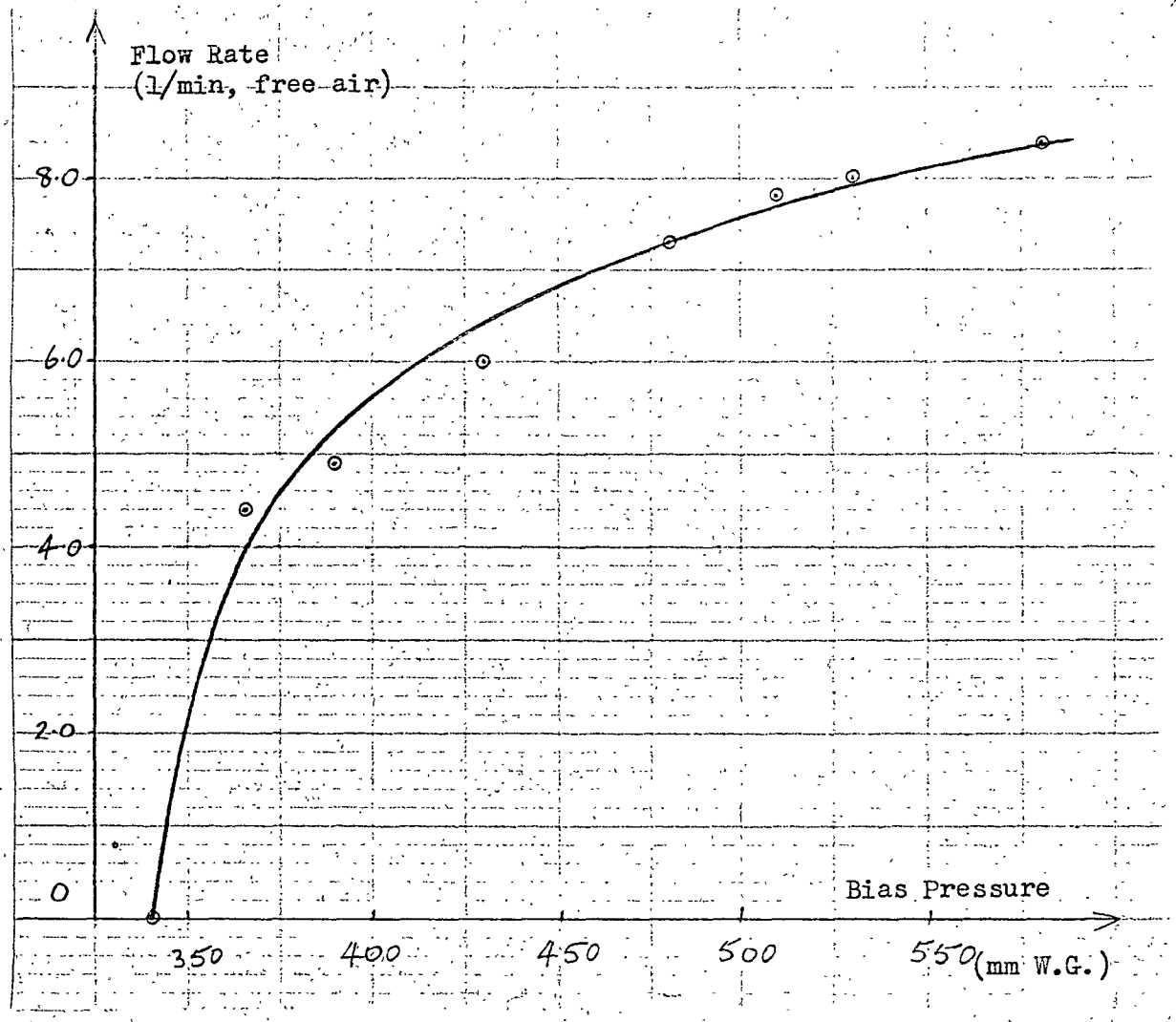

(a) Valve flow variation with bias pressure

(port f, fig. 8.7). Valve supply pressure: 16 lbf/in^{2}g

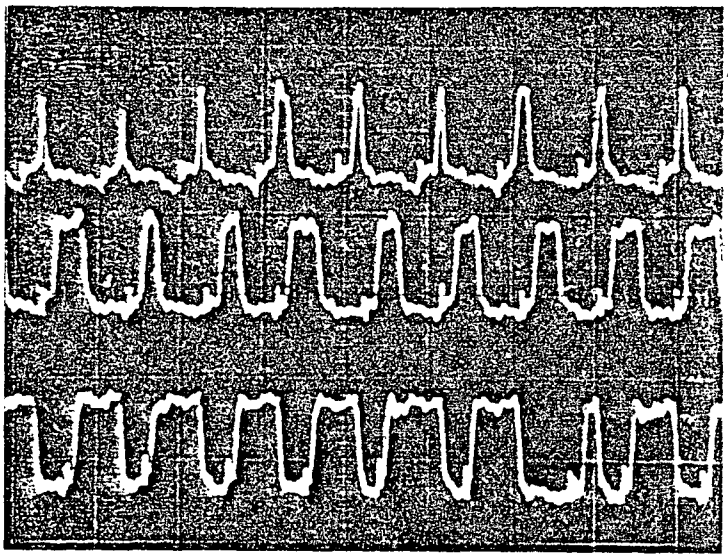

(b) Specimen Waveform

for bias pressures (port f) of 390, 430 and 480 mm W.G. respectively.

Calibration

Pressure: 133 mm W.G./ division

Time: 55 ms/division

Fig. 9.11 Schmitt Trigger Controlling Norgren Valve with a P.W.M. Signal

command was fed to the system requiring the carriage to return to this position from elsewhere in the stroke, it did so but on reaching the required position the random behaviour described above recurred. The stiffness, estimated by leaning on the load carriage, was high in both directions and the valve had approximately zero lap. The addition of a load of 5 kg. to the carriage resulted in large limit cycles.

Carriage in 1.4 in. position

When a command pressure of 610 mm W.G. was applied to PA1 the system behaved in an even less satisfactory manner. Large random oscillations about the desired position were observed and at times the unloaded carriage moved rapidly to the 0 in. position, striking the end stop violently in the process. On these occasions the carriage recovered its original position some seconds later. Although only the command signal pressure had been changed, a large dead zone, between the 0.9 in. and 1.7 in. positions, was now observed.

9.2 Discussion of Fluidic Servo Results

The tests described in Chapter 9 show that while the fluidically-controlled position servo using P.W.M., described in Chapter 8, is possible in principle, a certain amount of development and refinement is required for most of its components. The results of these tests are discussed below, and a number of suggestions are made for improving the performance of the system.

The selection of supply pressures for the various components was to some extent arbitrary though certain minima were set by the components selected, e.g. the valve operating pressures. Another factor operating in this case was the absence of pressure transducers capable of monitoring very low pressures. It is quite possible that

lower pressures might be used if minimisation of air consumption and/or audible noise were required.

9.2.1 Displacement Sensing

When development of this fluidic servo commenced, no existing fluidic analogue displacement sensors could be located. Since then, however, a number of devices have been marketed [33] and others have been developed and tested [29].

The scatter of experimental points on the Wedge Sensor characteristic in fig. 9.1 was probably due to the irregular shape of the sensor nozzles, a feature which is of no consequence in the normal operation of the device as a two state object detector. No investigation of the flow pattern around the sensor blade was conducted but the good repeatability and absence of hysteresis which was observed suggest that the flow is stable. It is likely that good linearity would be achieved with carefully made and suitably shaped nozzles.

A more sensitive pressure transducer would be required for further investigation of the noise content of the sensor output signal, but its frequency is sufficiently high to cause no embarrassment in most applications.

The Venturi Back Pressure Sensor described in reference 29 showed great promise and in view of its air consumption, which was less than 20% of that of the Wedge Sensor, it may be that further development of that device would be more rewarding.

9.2.2 Oscillators

The shape of the waveform from the 'Nor' oscillator was of similar quality to that from the 'Bistable' oscillator but the former was not used in the P.W.M. system as its minimum output pressure was almost as low as atmospheric pressure. This would have meant the proportional amplifiers being required to operate at these low pressures, i.e. well outside their linear ranges. This low pressure output signal

was a function of the switching pressures of the particular OR/NOR element used and might be corrected by the use of an alternative design.

Capacitors for the 'Bistable' oscillator were selected from those available, so as to give an operating frequency of about 20 Hz. The use of unequal capacitors resulted in the slight lack of symmetry for increasing and decreasing pressures, seen in fig. 9.3.

The selection of carrier frequency for a P.W.M. servo has to be a compromise. A high frequency is desirable so that the actuator will not respond to the pulsations in supply and exhaust flow, and yet the operating frequency must be within the dynamic range of the valves used. For example, in fluidic missile direction control systems, where pairs of opposing jet reaction nozzles emit pulse-width modulated gas flows, it has been suggested that the missile inertia smooths out the carrier ripple if the carrier frequency is more than twice the natural frequency of the missile [69].

It can be seen from figs. 9.3 and 9.4 that the output waveforms from the two oscillators tested were not truly triangular. A lumped-parameter, R-C approximation suggests that charging and discharging in such systems is exponential. The oscillator output signals shown in figs. 9.3 and 9.4 give the general impression of being made up of the initial segments of a series of exponential curves.

The behaviour of the 'Nor' oscillator in fig. 8.5 was also observed in the presence of a variable restrictor either in line A or in line B. In each case the shape of the output oscillation was progressively worsened and its frequency decreased as the restrictor was closed. In fact, the output became less triangular and more obviously 'exponential' as the restrictor was closed. Oscillation ceased altogether when excessive restriction was introduced. These effects are as expected for the linearized model described above and

are also evident in results presented by Flood [32]. In that case restrictors were introduced to a 'Bistable' oscillator, similar to that shown in fig. 8.5, at points D and E. The purpose of these restrictors was to attenuate a large unwanted high frequency component (about 250 Hz) which was present in the output signal. The restrictors had the desired effect but in fig. 5 of reference 32, the 'side' effects on output shape and frequency mentioned above are also evident.

The high frequency distortion referred to above was not present in the output signals from either the 'Nor' or the 'Bistable' oscillator. Some noise is present in the recordings in figs. 9.3 and 9.4 but reference to the atmospheric pressure traces therein shows that this was probably due to such effects as "pick-up" on connecting leads. This was minimised but was inevitable in view of the low sensitivity of the pressure transducer used (see section 8.7). Independent tests on the transducer showed that pressure fluctuations of the magnitude and frequency observed by Flood would certainly have been detected had they been present. A possible explanation for the purer waveform observed in the present case lies in the fact that the components used in the two cases were different. For example, the amplitude of the triangular waveform presented in reference 30 was over three times greater than that shown in fig. 9.3 while the supply pressure was lower in the former case. Thus the loading conditions of the fluidic elements were different and the reduced bore at the element control ports and capacitor connectors may have served the purpose of 'shaping' resistors in the present case.

The waveforms shown in figs. 9.3 and 9.4 have a good basic shape but there is some inconsistency in amplitude, from cycle to cycle. This can, alternatively, be regarded as a random frequency variation and was found to amount to approximately $\pm 4\%$ around a mean frequency,

in the tests on the 'Nor' and 'Bistable' oscillators. Remedies for this were sought including the use of various supply pressures, replacement elements, various restrictor and capacitor combinations, buffer elements and two stage oscillators, but no improvement resulted. A similar fluctuation was noted by Flood. The supply pressure was also examined but found to be free of distortion. It therefore appears that the cause was poor repeatability in the performance of the fluidic elements making the control pressure levels at which switching occurred vary. In a P.W.M. application small carrier amplitude variations may be acceptable, provided long term stability is maintained, since P.W.M. is essentially an averaging process.

9.2.3 Proportional Amplifiers

Improving the performance of the PWM amplifier depends upon improving the linearity and particularly the common mode rejection of the comparing and signal biasing stages. Poor common mode rejection at amplifier PA1, as observed in section 9.1.3, affects the performance of the closed loop servo adversely. Suppose the system were set up for zero valve lap, with the command and actual positions equal at some particular value. If, when command and actual positions are again equal but at some new value, the output signals from PA1 have decreased instead of remaining constant, the result is that there will now be valve overlap. This explains one aspect of the behaviour of the fluidic servo described in section 9.1.7. Also the open loop gain of the system will vary according to command and actual position, if the output pressures from the comparison stage depend on anything other than the applied differential pressure.

These problems may be solved by the substitution of a multi-stage Operational Amplifier, of the type that is now commercially available, for the proportional amplifiers in the fluidic servo. Such

a device could be expected to have a more linear characteristic than the proportional amplifiers used here and also to suffer less from interaction between input signals. A single operational amplifier could be arranged to compute the deviation and add the carrier signal to it, leaving the Schmitt triggers for bias adjustment. Operational amplifiers of this type are however expensive. The method of using two separate output pressure signals from amplifier PA1 contributes to the common mode rejection problem and this would be improved, though not eliminated, in a system using only the differential pressure across the output ports.

9.2.4 Schmitt Triggers

These particular bistable elements were chosen because of their negligible hysteresis. Hysteresis limits the linear range of mark-space ratio with input signal [32] and fig. 9.7 shows that this linear range, for the Schmitt trigger alone, was certainly from 0.05 to 0.95 and probably better.

9.2.5 The Complete PWM Amplifier

The behaviour of the complete amplifier is shown in fig. 9.9. A number of factors contribute to the deviation of this curve from the ideal, i.e. a straight line passing through the origin, limiting at a mark-space ratio of 1.0.

(a) The dead zone at the origin could be eliminated by careful adjustment of the bias on restrictors R_3 and R_2.

(b) The characteristics of all three amplifiers in the system showed a characteristic 'S' shape which is reproduced in the overall behaviour.

(c) The slope of the characteristic of the exhaust side amplifier (PA2) at its operating point was considerably steeper than that for PA3 (supply side). This resulted in the higher gain for the exhaust side seen in fig. 9.8.

The use of matched amplifiers (PA2 and PA3) over only a limited part of their characteristics would result in a great improvement in overall linearity.

The variation in output pulse width from cycle to cycle which was observed was probably largely due to the fluctuation in the oscillator frequency discussed earlier. This explanation could be verified by simultaneous observations of these two signals.

The above observations apply also to fig. 9.10 but an additional factor contributing to the erratic nature of these readings was the behaviour of the sensor itself. As discussed earlier, the sensor static test results showed considerable scatter about a mean curve. A particularly noticeable discontinuity occurred at a carriage position around 1.2 in. to 1.4 in. in fig. 9.1 and this has a clear effect in fig. 9.10.

9.2.6 Valves

A serious deficiency in the fluidic control system was the poor dynamic performance of the on/off valves when signalled by the Schmitt triggers.

The Norcon valves were chosen for their low operating pressures and small diaphragm chamber volumes but the latter proved to be too large for the relatively low air flow generated by the Schmitt triggers. This is illustrated in fig. 9.8 where recordings (a) and (b) show the Schmitt trigger output pressures when operating into a pressure transducer of approximate volume 0.25×10^3 mm^3 while (c) shows the extent to which the pulses are degraded when a Norcon valve is being driven by the Schmitt trigger. In this case two valve actuator chambers of approximate volume 11×10^3 mm^3 and 6×10^3 mm^3 respectively were being alternately pressurised and exhausted.

A low pressure actuator has recently been developed for an existing range of pneumatic on/off valves by Kay [22]. Particular

attention was paid in the design to minimising the diaphragm movement and air space, and very good dynamic response is claimed. The valve is a two-stage device in which the low-pressure diaphragm positions a poppet-type pilot valve which controls the high pressure air which in turn is used to position the main spool. Reference 22 also describes a compatible, bi-stable switching arrangement (known as a "Jet Receiver" and "Venturi Block"). With this system, rapid switching of the valve pressure from positive to sub-atmospheric levels is possible, in response to fluidic input signals. In this case only one side of the valve diaphragm is signalled.

A Kay valve of this type has been examined and the volume of the appropriate diaphragm chamber was found to be approximately 4.0×10^3 mm^3 and the diaphragm diameter was 50 mm. This valve was designed to operate at extremely low signal pressures, i.e. between 50 and 500 mm W.G. Thus if such valves were operated from the existing Schmitt triggers, from which very much greater signal pressures are available, the area of the actuator diaphragms could be reduced by a factor of about ten. Thus a reduction in chamber volume to the level of that in the small Norgren valve (see section 9.1.6(b)) is possible. The volume of the second actuator chamber was found to be 18×10^3 mm^3. This could be reduced to a comparable size to the first chamber discussed above, by the use of the smaller diaphragm and other fairly simple modifications. Modified Kay valves could be incorporated into the present fluidic servo and a great improvement on the response typified by fig. 9.8(c) should result.

A quantitive estimate of this improvement in performance is not possible in the absence of a model of the process of pressure increase and decrease in the valve chambers. This process is

complicated by the facts that:

(a) The chamber volumes vary as the diaphragm moves.

(b) The Schmitt trigger flow/pressure characteristic is highly non-linear.

(c) The connection is via a pipe and connectors which constitute distributed non-linear resistance.

In Appendix 8 a very simple model is developed, based on a number of approximations. This model confirms that the resistance of the connection between the Schmitt trigger and the valves, and the volumes of the valve actuators, must be minimised. A compromise has to be reached between the conflicting requirements of small air space for low capacitance and large flow paths for low resistance. The model also shows that a low output impedance is desirable for the driving element. This means that the Schmitt trigger output pressure should be independent of the flow which is taking place. The mass of the moving parts of the valve should be minimised, and careful matching of the Schmitt trigger output pressure and the switching level of the valve is also necessary, in order to ensure that no more air than is absolutely necessary has to be evacuated when reversal is subsequently required.

A further possibility is to replace the Schmitt trigger by the switching arrangement designed by Kay. The dynamic behaviour of the complete Kay system has not been determined but in one application, where high speed valve switching was required, a valve was continuously cycled, with full opening and closing, at 150 Hz. In order to achieve this, the valve was modified so as to restrict its movement and the diaphragm was supplied with air at 0.5 $lbf/in^2 g$ pressure from a specially designed jet-pipe type valve. The jet-pipe was oscillated mechanically through a crank driven by a synchronous motor [66b]. It therefore seems possible that

oscillation at the frequencies required for a P.W.M. servo, i.e. 20 to 40 Hz say, may be achieved using modified Kay valves and possibly by replacing the Schmitt triggers with the compatible switching arrangement mentioned above, or with some development of it.

The results of the tests on the small Norgren Valve, shown in fig. 9.11(a) illustrate an important point. Distinct saturation of this mark-space ratio/bias pressure curve is evident while, on the other hand, the Schmitt trigger is shown by fig. 9.7(a) to have a linear characteristic. The explanation of this difference lies in the non-linear flow/opening characteristic of the valve itself. The sensitivity for small openings for a poppet valve is high, i.e. a large proportion of the maximum flow occurs for small openings. Thus for short opening times, when the pulse shape deteriorates, the valve does not even reach the fully open position yet considerable flow occurs. At the other extreme, when the valve is open for most of the time, it never reaches the fully closed position. This small valve movement at the insensitive end of its flow characteristic reduces the net flow very little.

The random dithering of the flow meter reading in this test, mentioned in section 9.1.6, was probably caused by fluctuation of the nominally constant mark-space ratio of the valve drive signal which in turn was due to oscillator waveform variations. This fluctuation can be seen in the specimen trace, fig. 9.11(b). The fact that this random flow fluctuation could be detected may mean that a higher carrier frequency will be required for the servo. This of course depends upon the nature of the actuator and the load which is to be positioned.

Using a P.W.M. amplifier derived from that shown in fig. 8.7, together with a similar small Norgren valve, Sieh and Creek [70]

controlled the velocity of a small commercial linear actuator. Using a carrier frequency of about 30 Hz they found that the unloaded piston moved smoothly at a constant speed, which could be accurately pre-set by a bias restrictor. This indicates that the smoothing effect of this loading arrangement was sufficient to eliminate all trace of the 30 Hz valve pulsation, as well as any random content as described above, from the final piston speed.

9.2.7 The Closed Loop System

The behaviour of the complete fluidic servo was unsatisfactory but this was not unexpected, in view of the shortcomings in the performance of almost all its component parts, which are discussed above. In fact, the closed loop observations in section 9.1.7 reveal only that the concept of the system is sound. The occasional eccentric behaviour of the system, in lurching suddenly to one end of its stroke, mentioned in section 9.1.7, illustrates a general point. A feature to be avoided in designing a component for a feedback system is any reversal of slope in its characteristic. For example, when beam-deflection proportional amplifiers were being developed, it was found that in early designs the input-output curve "turned over" at its extremes, i.e. had a negative gradient after the inevitable saturation. If a component is allowed to operate under such a regime, the result is positive feedback. The characteristic of the Wedge Sensor (fig. 9.1) includes such a reversal of slope for carriage positions between 1.2 in. and 1.4 in. The eccentric closed loop behaviour mentioned above, occurred when the load carriage was in the vicinity of this discontinuity.

The signal biasing stage (PA2 and PA3) in fig. 8.7 was not used to amplify the deviation signal, but only to adjust the signal level in order to control the valve lap. With careful selection of operating pressures these two amplifiers could be omitted, at the

expense of reduced versatility in the system.

h) Stabilization

A further problem which will have to be solved before a fluidic servo becomes operational is that of stabilization. For example, Kent and Lenaerts [27] noted that excessive friction in their fluidic servo detracted from its performance. On the other hand, had an actuator and displacement sensor with less friction been used, stability would have been inadequate.

A number of approaches are possible. The digital compensator proposed by Taft and Nawaz [31] is particularly attractive since in the present system a pulse width modulated signal is already available. This method, which modifies the pulse train, can easily provide certain forms of compensation which would be difficult to produce in any other way [71]. Alternatively, shaping can be carried out on the analogue signal using passive pneumatic R-C circuits. Transient pressure feedback as used for the electro-pneumatic servo, described in the early chapters of this thesis, should be relatively simple to arrange. Bleed signals from the actuator chambers, suitably shaped by a C-R circuit could be used, particularly if an operational amplifier were included, for summation of command and feedback signals.

CHAPTER 10 FINAL DISCUSSION AND CONCLUSIONS

10.1 Final Discussion

Discussions of many points have been included in Chapters 3 to 7 and 9 and these will not be repeated here.

In Chapter 3, it was established that findings from the experimental servo, incorporating a three-way valve and differential actuator, were applicable to a four-way valve/balanced actuator system. The only exception was that there was no configuration of a three-way valve system equivalent to a four-way valve system with off-centre piston. However, linearized equations for an equivalent four-way valve system, for variable piston position, were developed and it is known that the mid-position represents the worst stability case.

A number of methods of stabilizing pneumatic systems were discussed, including some which reduce the static stiffness of a system. Such methods may be acceptable in hydraulic systems, where the high bulk modulus of the working fluid contributes to the stiffness of the system. They would not, however, be useful in a pneumatic system, where one purpose of the stabilization is to enable the use of high loop gains, in order to increase the system stiffness [10].

The Impulse Tests and other tests, described in Chapter 4, yielded information about the behaviour of individual components, which was subsequently used in the computer simulations and also suggested areas in which improvements in performance could be sought. Two approaches exist for dealing with friction in pneumatic systems. First, friction can be minimised in a number of ways. These include the omission of sliding piston seals, the use of air bearings or recirculating ball bearings, the development of PTFE type seals and the use of rolling seal piston diaphragms. Alternatively, a good

and simple model for the remainder of a pneumatic system has now been developed, enabling attention to be focused on the simulation and study of the effects of unavoidable friction, for example in systems where air leakage is completely unacceptable.

The use of dither complicates what can otherwise be a very simple system and also adds a significant non-linearity to the valve characteristic. Only one other commercially available servo-valve has been found. This is the valve used in reference 27 and manufactured by The Glarban Corporation U.S.A. This is a single-stage flapper-nozzle valve suitable for hydraulic or pneumatic use and is available with fluidic or electric actuation. Little information on the performance of this valve, and particularly of its hysteresis, is known. This type of valve can only be used if valve leakage can be tolerated. Improved servo-valve design would contribute a significant advance. Pulsed operation of electrically or pneumatically signalled on/off valves offers another alternative.

The behaviour of the experimental servo under various conditions was recorded and discussed in Chapter 5. In almost all cases this behaviour could be simply explained by reference to linear equations and root loci. Transient pressure feedback was found to be more effective for stabilization than velocity feedback. The time constants of the pressure feedback high pass filter used for the tests in section 5.1 and 5.2 were large and the values used for the tests described in sections 5.3.1 and 5.3.3 are probably more practical values. This gave a fairly rapid recovery after load force application as shown in fig. 5.6.

The form of the static valve characteristics and effective methods for their simulation were discussed in Chapter 6. The three-dimensional surface of fig. 6.10 offers a useful aid to

visualization particularly in view of the conclusion reached in Chapter 7, that this also represents the valve's behaviour under dynamic conditions.

One of the most important equations developed in Chapter 3 is eqn. 3.41 (see also table 3.1). This linearized equation, which takes account of many system parameters, was shown in Chapter 7 to give a good representation of the behaviour of the experimental servo over a wide range of operation conditions. The form of this equation is particularly useful in indicating the effects of various system parameters. This is illustrated by table 6.2 in which coefficients, evaluated for the purpose of the simple simulation, can be compared and their relative importance assessed. This equation can be used with confidence for subsequent studies of the effects of such things as stabilizing strategies, actuator friction and valve saturation.

It was noted in Chapter 7 that the least effective aspect of the present simulation was its representation of small perturbations about the equilibrium position. It has been pointed out that a servo system spends most of its life dealing with small movements [72] and this is a topic which has received considerable attention in connection with hydraulic servos [72, 73, 74]. Martin [74] found it necessary to use a digital computer for his investigation of the threshold behaviour of hydraulic servos, to eliminate unwanted machine effects which were introduced by analogue computer simulation. The behaviour of pneumatic servos under these threshold conditions is worthy of further study. The relatively high piston leakage in the experimental servo made a negligible contribution to damping, but its effect on steady state errors was not investigated, though this would be of interest.

In the experimental electro-pneumatic servo, valve laps were

set close to zero throughout. In a computer study, Botting et al [10] showed that careful selection of supply underlap together with exhaust overlap, in the presence of some quiescent exhaust leakage, improved the performance of a pneumatic servo in a number of ways.

(a) The quiescent pressure in the actuator chambers was increased, with resultant increase in natural frequency and bandwidth.

(b) Provided that the inlet underlap and exhaust overlap were not excessive, the static stiffness at the actuator was not reduced too much.

(c) Quiescent power loss was held within reasonable limits by the exhaust overlap.

(d) Limit cycling due to stiction was damped out, probably due to the resultant reduction in the slope of the valve characteristic over the region of the limit cycle amplitude.

It was concluded that the best compromise between (a) and (b) was achieved when quiescent actuator pressures between 0.5 and 0.8 of supply pressure were used.

For the fluidic servo described in Chapter 8 two major changes were made. First, all electrical elements were replaced and secondly pulse-width modulation of on/off valves was used. These two changes were independent and indeed the use of P.W.M. with electrically operated on/off valves may offer the most satisfactory compromise in view of the absence of an adequate, commercially available servo-valve and the ease with which electrical signals can be processed.

It has been said [58] that "compelling reasons" must exist for the preference of fluidic systems over alternatives, in view of their relatively high weight and low efficiency. The latter results

from the continuous flow which fluidic devices demand. In cases where fluidic systems have been preferred, it has usually been as a result of their good environmental stability or high reliability or where simplicity due to the elimination of interfaces has resulted.

The performance of the fluidic servo was discussed in Chapter 9, and it is clear that a considerable amount of further work is required before an operational fluidic servo is produced. A number of the developments suggested in Chapter 9, and summarized in this Chapter under "Conclusions", can be investigated at fairly low cost. In the light of those results, a decision on whether further work is justified will be possible.

10.2 Conclusions

A low pressure electro-pneumatic linear motion servomechanism has been built and tested, enabling effective models of many aspects of the behaviour of such systems to be constructed. The results from the experimental system, which included a three-way valve and differential actuator, have been shown to be relevant to systems using four-way valves and balanced actuators.

Two distinct models were studied, using analogue computers. In one case the valve characteristic was simulated using an empirical expression by MacNaughton. This was better for this purpose than the theoretical isentropic expression, in addition to being more easily simulated. In the second case a single straight line was substituted for the family of non-linear curves, which constituted the full valve characteristics. The linearised equation (eqn. 3.41) for the system which resulted, was presented in a form which is particularly convenient for assessing the effects of individual parameters on performance (table 3.1). Step and harmonic response tests

were conducted in which wide variations in system parameters occurred. Both the simple and full simulations modelled these fluctuations closely. On the evidence of these results, the simpler model is sufficiently accurate for many purposes. Thus the very simplest analogue computer can be used. Care must be taken over the selection of the valve flow coefficient (c_1) and it will improve accuracy if this quantity is varied under certain conditions, for example for small perturbations of the system. The possibility of adding a limiter, for simulation of systems in which flow saturation occurs for long periods, has been discussed.

Transient pressure feedback was found to be very effective in stabilizing the experimental servo. Velocity feedback was much less useful since it resulted in sluggish behaviour. These effects have been explained by reference to the root locus diagrams of linearized models.

The agreement between system and models demonstrated that valve characteristics determined under static conditions can confidently be used to represent the dynamic situation. An instructive model of the valve characteristics, as a three-dimensional surface drawn to isometric axes, was developed.

The experimental servo was carefully designed to minimise friction and to focus attention on other aspects of the system's behaviour. Tests on the actuator and load, and also the simulation studies on the closed loop servo, showed that in this case an assumption of viscous friction gave a good representation of actual conditions. One of the ways in which friction was minimised was by allowing some air leakage past the piston and piston rod. If this is tolerable, friction is greatly reduced. Existing pneumatic actuators are mostly constructed for rugged industrial duties and such devices are totally unsuitable for position control, due to

their high and inconsistent friction forces. In cases where leakage is intolerable, the investigation of composite PTFE seals is proposed. Actuators with rolling seals have been shown to have low friction and good durability and further investigation of these devices for servo applications is recommended.

Current models for friction in sliding seal actuators are inadequate. The existence of simple and effective models for the remainder of the pneumatic system enables attention to be directed at this problem in future.

The loaded actuator was isolated from the valve for "Impulse" Tests. A value for the polytropic exponent of expansion and compression ($n = 1.28$) was established from these tests, enabling earlier models, based upon the assumption of either isothermal or adiabatic conditions, to be further refined.

The electro-pneumatic servo-valve used showed an intolerable amount of hysteresis. For this reason a large high frequency dither signal was introduced which had the effect of adding a significant non-linearity to the valve characteristic.

An alternative all-pneumatic system in which the servo-valve was replaced by on/off valves driven by pulse-width modulated signals was built. Tests showed that satisfactory operation of such a fluidically controlled servo depends upon the solution of a number of problems.

(a) A displacement sensor with a linear characteristic is required. This may be accomplished by further development of the interacting-jets ("Wedge") sensor used in these tests, or by using an existing back-pressure sensor [29].

(b) A number of aspects of the performance of the fluidic control system would be improved if a multi-stage

operational amplifier replaced the single-stage proportional amplifiers which were used. A more linear system without interaction between command and feedback signals should result. Also the dependence of valve lap upon load position should be reduced or even eliminated.

(c) Improved valves are required. This is a serious problem which may be solved by the use of an alternative valve design in which the valve-actuator volume and also the inertia of moving parts have been minimised.

(d) The existing Schmitt triggers are adequate but, depending on the action taken on (c) above, an alternative bistable switching arrangement by Kay [22] may improve performance.

(e) Random fluctuation of the amplitude of the oscillator output signal is acceptable provided that it is effectively smoothed by the servo load. If this is not the case alternative digital elements, having more stable switching levels, will have to be sought.

(f) Stabilization will be required and analogue and digital techniques which may achieve this, have been suggested.

A number of these developments can be fairly easily investigated to enable a decision to be taken on the advisability of undertaking further work.

The production of an electrically or fluidically controlled, low pressure pneumatic position servo, with adequate performance and reliability, for example, for industrial applications, requires the development of improved components.

ACKNOWLEDGMENTS

It is a pleasure to acknowledge the help given by my wife, Anne, and by my friends, particularly Professor T. H. Lambert, Mr. M. R. E. Bloyce, Mr. P. T. Gleeson, Mr. A. J. Huber and Mr. H. Wolanek.

I gratefully acknowledge the assistance given by the London Borough of Barnet Education Committee and the kind co-operation of Dr. E. P. Booth, Head of the Department of Mechanical Engineering, Hendon College of Technology (Middlesex Polytechnic).

APPENDIX 1 REFERENCES

1. SHEARER, J. L. 'Study of pneumatic processes in the continuous control of motion with compressed air' Pts. I & II, Trans. ASME Feb. 1956 p. 233-249

2. DEAVERS, C. J. Contribution to discussion of ref. 1.

3. SHEARER, J. L. 'Non linear analogue study of high pressure pneumatic servomechanism', Trans. ASME, Vol.79 April 1957 p.465-472.

4. SHEARER, J. L. 'Continuous control of motion with compressed air', Sc.D. Thesis, M.I.T. 1954. (a) App. 1, (b) p. 54, (c) p. 7.

5. LEVENSTEIN, H. 'Tie simplicity to power with pneumatic servomechanisms' Control Engineering, June 1955, p. 65.

6. CHELOMEY, V. N. 'A study of pneumatic and hydraulic servomechanisms', Avtomaticheskoye Upravleniye i Vychislitel'naya Tekhnika, Moscow 1958, p. 166-181. Translation by Foreign Technology Division, Air Force Systems Command, WP.AFB Ohio 1961, (FTD-TT-61-107/1 and 2).

7. EYNON, G. T. 'Developments in high performance electro-mechanical servomechanisms at the R.A.E., Farnborough', Proc. of Conf. on Recent Mechanical Engineering Developments in Automatic Control, I. Mech.E. 1960.

8. SUNG, C. B. and TAPLIN, L. B. 'Aerospace pneumatic control systems', J. Engng Ind., Trans. Am. Soc. Mech. Engrs 1963 85 (Series B), 135.

9. VAUGHAN, D. R. 'Hot gas actuators; some limits on the response speed', J. bas. Engng, Trans. Am. Soc. Mech. Engrs 1965 87 (Series D), 113.

10. BOTTING, L. R., EYNON. G.T., and FOSTER, K. 'The response of a high-pressure pneumatic servomechanism to step and sinewave inputs', Proc. I.Mech.E. 1969-70 Vol.184 (Pt.I) No.54.

11. HALL, M. J. and LAMBERT T. H. 'Artificial limbs - an engineering appraisal' The Hospital Engineer Feb. 1965 p.33.

12. PROCEEDINGS of a symp. on powered prostheses, Roehampton, Oct. 1965.

13. McWILLIAM, R., MONTGOMERY, S. R. and SANDERSON, D. D. 'The design and development of an experimental externally powered upper-limb prosthetic system'. Nov. 1970. M.R.C. Powered Limbs Unit, West Hendon Hospital, London.

14. SIMPSON, D. C. 'An externally powered prosthesis for the complete arm', Proc. I.Mech.E. 1968/9, Vol. 183, Pt. 3J, 11-17.

15. RING, N. D. Report in B.R.A.D.U. Bulletin July 1971, p.53.

16. LORD, M. 'Pneumatic position control servomechanisms for arm prostheses' Dept. of Mech. Eng. University College London. April 1972.

17. JOHANSSEN, C., PERSSON, T. and ULEN, E. 'Report on development of pneumatically generated elbow joint and electrically controlled pneumatic valve'. July 1970. FOA 2 report C2407-54.

18. COOL, J. C. and HOOREWEDER, G. J. O. van. 'Hand prosthesis with adaptive internally powered fingers'. Med. & Biol. Eng. 1971, Pergamon Press, Vol. 9, p.33-36.

19. BOUSSO, D. 'A six degree of freedom experimental limb for thalidomide children', Biomed. Eng. July 1969, p.313-321.

20. BRANN, R. P. 'Linear analysis of a pneumatic differential actuator with position feedback for prosthetic control'. Control. Aug. and Sept. 1966.

21. BRANN, R. P. and KIRKWOOD, P. A. 'Transient testing of a pneumatic servomechanism for prosthesis control'. The Hospital Eng. July 1966, p.83.

22. KAY, F. X. 'Miniaturization in pneumatics' F.P.I. Conf. June 1972.

23. CUTLAND, M. J. 'Response of a pneumatic servomechanism', M.Sc. (Eng.) thesis, 1967, Univ. of London. (a) App. 1b, (b) App. 3, (c) p.79.

24. ANDERSEN, B. W. 'The analysis and design of pneumatic systems' Wiley 1967, (a) p.8, (b) p.106.

25. BURROWS, C. R. 'Non-linear pneumatic servomechanisms', Ph.D. thesis, 1969 Univ. of London .

26. SHARP, R., MACLEAN R. and McCLINTOCK A. 'Numerical position indication by fluidics' N.E.L. Report No. 410 1969 .

27. KENT, A. H. and LENAERTS, P. 'Development of an open loop damping fluidic stability augmentation system', R.A.E. contract No. K43A/94/CB. 43A1 1970.

28. KENT, A. H. and DYE, B.C. 'The design and development of a fluidic pick-off for a position gyro', R.A.E. contract No. K64B/88/CB. 64B 1971.

29. CHITTY, A., LENAERTS, P. and DYE, B.C. 'Analogue fluidic position sensors', F.P.I. April 1972.

30. LLOYD, G. F. H. 'A fluidic proportional amplifier using P.W.M. techniques', 4th Cranfield Fluidics Conf. (C.F.C.) 1970 Paper H4.

31. TAFT, C. K. and NAWAZ S. 'Fluidic pneumatic control system compensator', 4th C.F.C. 1970 Paper E2.

32. FLOOD, J. M. 'A fluidic pulse width modulator with separate oscillator', R.A.E. abstract. Oct. 1971.

33. CHITTY, A. and LENAERTS P. 'Fluidic displacement sensing', F.P.I. Feb. 1972.

34. AUGER, R. N. 'A fluidic prox. detector', 3rd C.F.C. 1968 Paper E7.

35. LeHUNTE, G. G. and RAMANATHAN, S. 'Dev. of a digital fluidic prox. sensor', 4th C.F.C. 1970 Paper S1.

36. SINCLAIR, C. G. and LETHERMAN, K. M. 'The static and dynamic characteristics of a reflected jet prox. detector'. 4th C.F.C. 1970 Paper S4.

37. BURROWS, C. R. and WEBB, C. R. 'Further study of a low-pressure on-off pneumatic servomechanism', Proc.I. Mech.E. 1969-70, Vol. 184, Pt. 1 p.849-858.

38. B.S. 1523: Pt. 1: 1967.'Glossary of terms used in automatic controlling and regulating systems'.

39. MAINE, A. E. 'A practical approach to fluidic control systems', 3rd C.F.C. 1968 Paper A2.

40. BAKER, P. J. and JACOBS, B.E.A. 'The dev. of fluidic sensors for application in steel handling'. 4th C.F.C. 1970 Paper R4.

41. PAVLIN, C. and FACON P. 'A fluidic chain for missile attitude control' 4th C.F.C. 1970 Paper L2.

42. REFERENCE manual of transistor circuits, Mullard 1961 p. 271.

43. BLACKBURN, J. F., REETHOF, G. and SHEARER, J. L. 'Fluid power control' Wiley 1960.

44. RAVEN, F. H. 'Automatic control engineering' McGraw Hill, 1968, p.550.

45. BURROWS, C. R. 'Effect of position on the stability of pneumatic servomechanisms', J. Mech. Eng. Sci. 1969 Vol. 11 (No.6) p.615.

46. MARTIN, K. F. 'Stability and step response of a hydraulic servo with special reference to unsymmetrical oil volume conditions', J. Mech. Eng. Sci. Vol. 12 (No.5) p. 331. 1970.

47. GUILLON, M. 'Hydraulic servo systems', Butterworth 1969.

48. LAMBERT, T. H. and DAVIES, R. M. 'Investigation of the response of an hydraulic servo with inertial load'. J. Mech. Eng. Sci. Vol.5 (No.3) p. 281 1963.

49. BELL, R. and de PENNINGTON, A. 'Active compensation of lightly damped electrohydraulic cylinder drives using derivative signals'. Proc. I.Mech.E. 1969-70. Vol.184 Pt.1.

50. WILLIAMS, B. (Elliott Bros. Ltd.) Personal communication 15th June 1972.

51. ANON. 'Controlled damping through dynamic pressure feedback'. Moog Technical Bull. 101, 1958.

52. ANON. 'Dynamic pressure feedback'. Aircraft Eng. June 1960, p.171.

53. BURROWS, C. R., MARTIN, D. J., and RING, N. D. 'Comparison of the experimental and theoretical responses of a pneumatically powered elbow joint'. I.Mech.E. Conf. 'Human Locomotor Eng.' Sept. 1971.

54. LORD, M. and CHITTY, A. 'Stabilisation of pneumatic prosthetic systems', I.Mech.E. Conf. 'Human Locomotor Eng.' Sept. 1971.

55. BURROWS, C. R. and WEBB, C. R. 'Use of root loci in design of pneumatic servo-motors'. Control, Aug. 1966.

56. WALTERS, R. 'Hydraulic and electro-hydraulic servo systems'. Iliffe Ltd., 1967, p.75.

57. SKINNER, C. K. and WAGNER, F. D. 'A study of the processes of charging and discharging constant volume tanks with air'. S.B. thesis, Dept. of Mech. Eng., M.I.T. 1954.

58. ROSE, R. K. 'Fluidic power control systems', 4th C.F.C. 1970, Paper L3.

59. HIRTREITER, A. B. 'Air springs', Machine Design, April 1 1965, p.104.

60. TOWILL, D. R. and CARNE, C. M. 'The polytropic stiffness of perfectly sealed pneumatic cylinders', The Royal Mil. Coll. of Sci. Eng., Physics Branch, Tech. note EP1, Sept. 1963.

61. ROGERS, G. F. C. and MAYHEW, Y. R. 'Eng. thermodynamics, work and heat transfer', Longmans, 1967, p.355.

62. UNPUBLISHED compressor test reports, Broom and Wade Ltd., High Wycombe, 1969/70.

63. RASHID, A. H. 'To investigate the friction characteristics and the wear of seals in pneumatic cylinders'. Middlesex Poly., Hendon Coll., Dept. of Mech. Eng., B.Sc. project rep. 1972.

64. PARNABY, J. 'Non linear effects in automatic control systems with particular reference to speed control'. Ph.D. thesis, Univ. of Glasgow, 1966.

65. PARNABY, J. 'Instability due to static and Coulomb friction in autonomous control systems'. 2nd Fl. Power Symp. Jan. 1971.

66. KAY, F. X. (Kay Pneumatics Ltd., Dunstable) Personal communication, (a) 15th March, 1972, (b) 20th Sept., 1972.

67. DAVIES, B. L. 'A portable power unit for prostheses'. M.Phil. Thesis 1971 Univ. of London .

68. MacNAUGHTON, J. D. 'Aids to the design of pneumatic servo valves'. Canadian Aero. J. Dec. 1959, Vol. 5 p.413-414.

69. FOSTER, K. and PARKER, G. A. 'Fluidics'. Wiley 1970, p.266.

70. SIEH, K. S and CREEK, J. 'The design and development of a fluidic servo amplifier'. Univ. Coll. London, Mech.Eng. Dept., B.Sc. special task report, 1972.

71. TAFT, C. K. Contribution to discussion of ref. 31.

72. CARRINGTON, J. E. and MARTIN, H. R. 'Threshold problems in electro-hydraulic servomotors'. Proc. I.Mech. E. 1965-66, Vol.180, Pt. 1.

73. MONTGOMERY, J. and LICHTAROWICZ, A. 'Asymmetrical lap and other non-linearities in valve-controlled hydraulic actuators'. Proc. I. Mech. E. 1968-69, Vol.183, Pt. 1, No. 33.

74. MARTIN, H. R. 'A theoretical study into peaking pressure reduction and its effects on hydraulic servo performance'. Ph.D. Thesis 1968 Nottingham Univ.

APPENDIX 2 NUMERICAL VALUES FOR PARAMETERS OF THE ELECTRO-PNEUMATIC SERVO AND DETAILS OF IDENTIFICATION CODE FOR TESTS IN CHAPTERS 5 AND 7

Piston Area	A =	$1.23 \times 10^{-2} ft^2$
Amplifier Gain	K_A =	590 mA/V
Feedback Potentiometer Gain	K_p =	2 x (applied voltage) V/ft
Inherent Piston Leakage	L_b =	1.3×10^{-7} $(ft^3/s)(lbf/ft^2)$ air volume measured at $64.7 lbf/in^2 a$
Polytropic Exponent	n =	1.28
Constant Chamber 1 Pressure	P_1 =	$64.7 lbf/in^2$ abs. = $9300 lbf/ft^2$ abs.
Valve Exhaust Pressure	P_e =	$14.7 lbf/in^2$ abs.
Valve Supply Pressure	P_s =	$114.7 lbf/in^2$ abs.
Gas Constant	R =	53.3 ft lbf/lbR
Average Air Temperature	T =	525 R
Air Density at $64.7 lbf/in^2$ abs.	P_{2a} =	$0.336 lb/ft^3$
Air Density at $14.7 lbf/in^2$ abs.		$0.076 lbf/ft^3$
Load Carriage Mass		8.67 lb.
Piston Diameter		1.5 in.
Piston Rod Area		$0.05 in^2$.
Left Hand Actuator Chamber Clearance Volume		$1.15 in^3$. = $0.67 \times 10^{-3} ft^3$ for closed loop tests (Chapter 5) and $0.73 in^3$. ≡ $0.422 \times 10^{-3} ft^3$ for Impulse Tests (Chapter 4)
Valve Dither Current		±110mA (peak) at 200 Hz.
Pressure Feedback Constants		K_{pr} and τ_p, variable. Four different settings of the variable feedback potentiometer (fig. 2.5) were used for the main step and harmonic response tests. These are shown in the table overleaf.

Table A2.1 Transient Pressure Feedback Data

Setting (arbitrary scale)	Potentiometer Resistance to be added to 19.5K Ω (K_Ω)	Coefficient - measured experimentally (K_{pr} mAft^2lbf^{-1}x10^{-2})	Time Constant - calculated (τ_p s)
0	93	3.47	1.69
5.5	31	7.30	0.75
7.5	15	10.6	0.55
10	0	18.75	0.293

Note on identification of tests and records in Chapters 5 and 7

Tests and records are identified as follows:

Electro-pneumatic Servo	E
Full Simulation	F
Simple Simulation	S
Step Response	S
Closed Loop Harmonic Response	H
Open Loop Harmonic Response	O
Individual Step Tests	1 to 33
Individual Harmonic Tests	1 to 7

For example, ES21, FS21, SS21 refer to step tests with the same parameters, conducted on the servo, the full and the simple simulation respectively.

Tables 5.1, 5.2 and 5.3 show full details.

APPENDIX 3 FURTHER WORK ON ACTUATOR AND LOAD FRICTION

A3.1 Drift Tests

The "Drift" method of measuring friction forces for a differential actuator, as outlined in section 4.1.6, is interesting as it enables measurements at very low velocities to be made, for which no easy alternative method is available. In particular it enables steady velocities to be achieved when forces less than the 'stiction' or starting friction forces are applied. This is because the arrangement (fig. 3.2) is 'self-balancing', i.e. the driving force falls as the velocity increases, in order to allow the necessary leakage flow past the piston (or through a by-pass channel). The method was used by Rashid [63] to obtain the friction characteristic of the actual actuator used in the electro-pneumatic servo, described in this thesis. A graph from reference 63 is reproduced here as fig. A3.1 illustrating the results obtainable by this method. The extremely low piston speeds used should be noted. Fig. A3.1 shows the results of tests on the actuator in which the only load was the piston and piston rod, and is therefore not directly applicable to the present tests in which a load carriage was attached.

This method would also be applicable to actuators with low inherent leakage, since a piston by-pass path can be deliberately introduced. It does, however, require the friction to be independent of piston position, in order that an equilibrium velocity can be reached, and this condition is unlikely to be met by mass produced, industrial actuators. It is intended that the 'Drift' method will be used with a number of prototype actuators currently under construction, in which various composite P.T.F.E./Rubber seals are being incorporated.

Fig. A3.2 shows the results of tests on the unloaded actuator

Fig. A 3.1

Friction characteristic for the author's pneumatic actuator, without load carriage (Reproduced from reference 63 p.31)

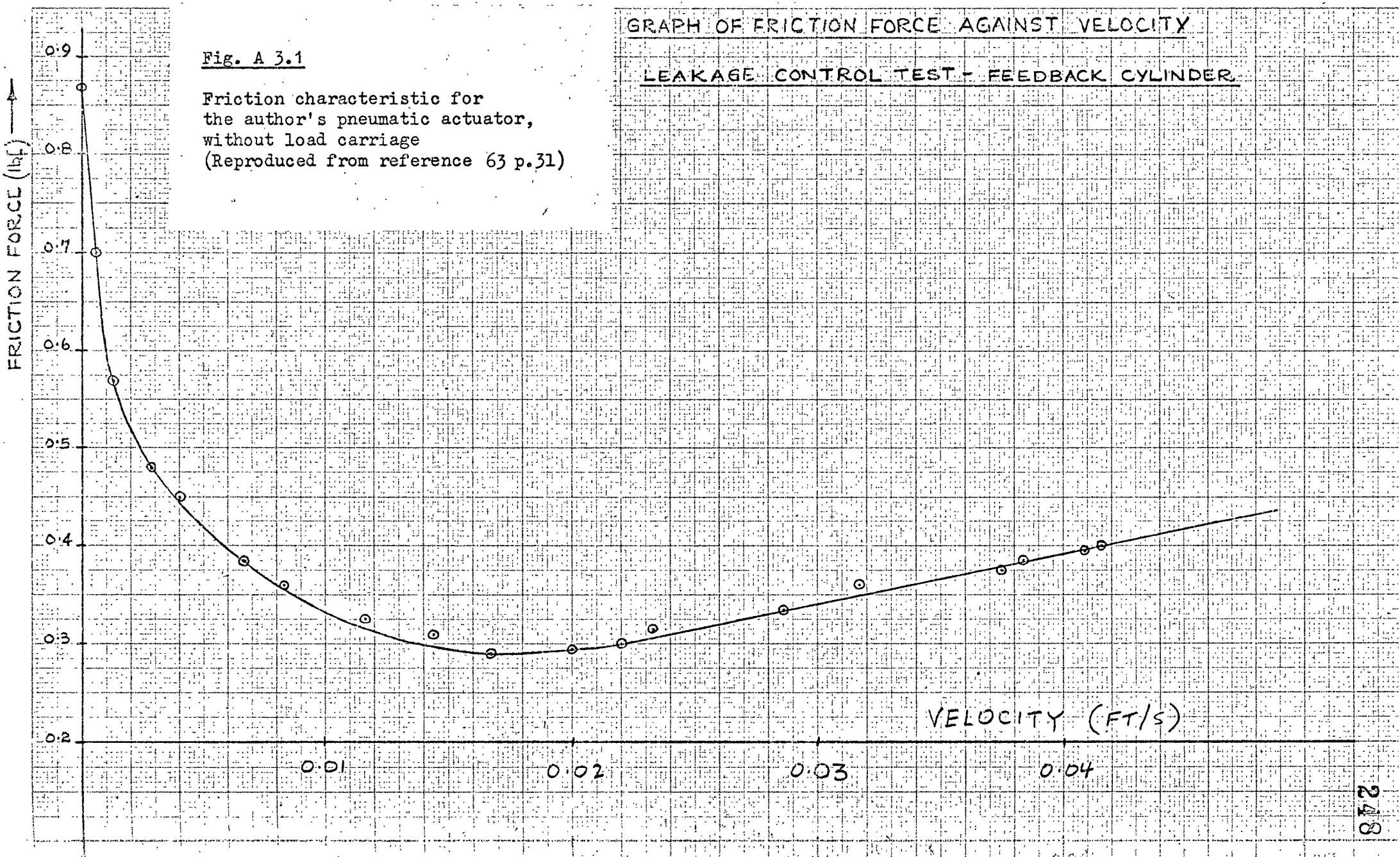

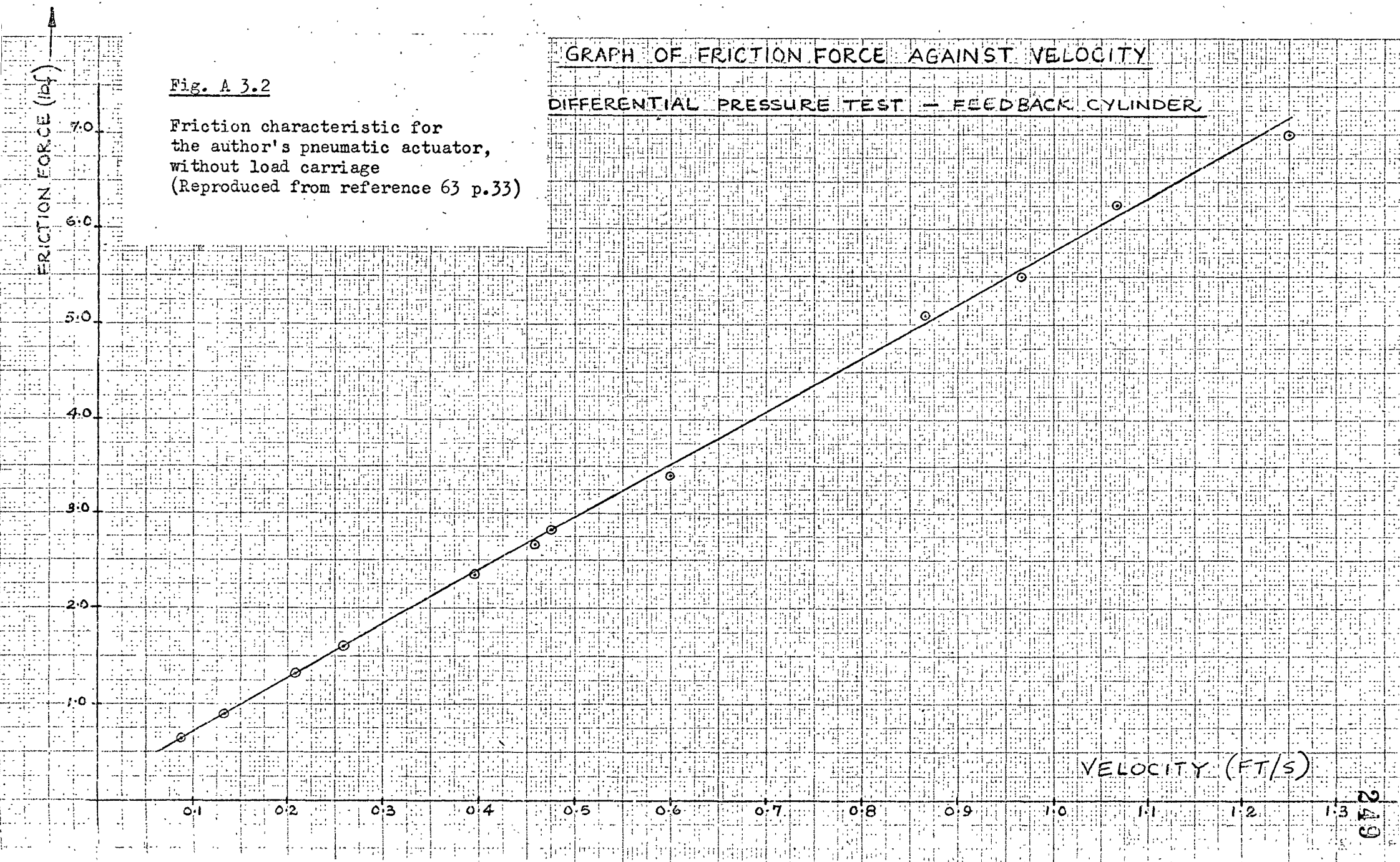

Fig. A 3.2

Friction characteristic for the author's pneumatic actuator, without load carriage (Reproduced from reference 63 p.33)

in which the saturation velocities of the piston were measured for various driving forces. Steady differential pressures were maintained across the piston to provide constant driving forces. It can be seen that the experimental points fall very close to a straight line and that therefore the assumption of viscous damping under these conditions is valid. From the straight line in fig. A3.2 the viscous friction coefficient for the actuator without any load can be calculated as 5.6 lbf/(ft/s).

A very good overall picture of the friction/velocity relationship can be obtained by combining the low velocity Drift Test results with those from Saturation Velocity Tests (i.e. by combining figs. A3.1 and A3.2).

A3.2 Commercial Actuators

Also in reference 63, a number of commercial actuators were compared with the low-friction actuator used by the present author in the electro-pneumatic servo. These results were not directly comparable since, due to the availability of equipment, the piston diameters were all different - i.e. 1 inch, $1\frac{1}{4}$ inch, $2\frac{1}{2}$ inch compared to $1\frac{1}{2}$ inch. The manufacturers of the actuators used were asked for friction figures for different sized actuators but were unable to offer any guidance. In order to introduce some comparability a crude correction can be applied as follows.

It is common industrial practice to allow a certain fraction, typically 15% or 20%, of the maximum thrust from an actuator, to overcome actuator friction. Thus the implication is that friction is proportional to piston area. The figures from reference 63, table 6.5, are therefore scaled in the inverse ratio of their areas, for comparison with the $1\frac{1}{2}$ inch diameter actuator. These figures appear in table A3.1. It is not suggested that these figures are other than

coarse approximations, but it is apparent that:

(a) If a little leakage is tolerable (actuator (i)) the friction in sliding piston actuators is greatly reduced.

(b) The relatively high friction forces for cases (ii) and (iii) are explained by the fact that these actuators were made for use on arduous industrial tasks and therefore the highest priority in design was given to efficient sealing, durability and low cost.

(c) If zero leakage is imperative, the rolling seal type actuator (iv) offers considerably less friction than sliding rubber seals (ii) and (iii). (The reliability of the rolling seal actuator was demonstrated by the fact that a wear test was stopped after over 9 million strokes at which point no seal damage was observable.)

Table A3.1 Friction figures from reference 63, table 6.5 - corrected (see text) for comparison with the actuator described in Chapter 2

Actuator	Seals	Piston Diameter (in.)	Approximate Corrected Figures for $1\frac{1}{2}$ in. diameter		
			Coulomb Friction (lbf)	Viscous Friction Coefficient (lbf)/(ft/s)	Static Friction (Stiction) (lbf)
(i) "Feedback" (actuator used by the present author)	Labarynth	$1\frac{1}{2}$	0.18	5.6	0.9
(ii) "Kay"	Neoprene, cup-type and '0' rings	$1\frac{1}{4}$	6	19	6
(iii) "Maxam"	High Nitrile Rubber, U-section	1	7	19	8
(iv) "Bellofram"	Neoprene, Rolling Diaphragm	$2\frac{1}{2}$	1.4	4	1.4

A3.3 Saturation Velocity Tests

These tests were conducted to investigate the effect of load mass variation on the total actuator and load carriage friction in the electro-pneumatic servo. A second test rig was used for these tests, since the original was no longer available (actually the fluidic servo test rig was used here). The only difference between the designs was that the actuator used for this test had slightly less friction at the rod bearing (a ball race replaced the original nylon bush).

Referring to fig. 3.1, a constant low pressure was applied to chamber 1, to which an additional large reservoir had also been connected. Chamber 2 was open to atmosphere. The load carriage was held at the extreme right hand position and then released. The load displacement and the pressure P_1 were recorded for the ensuing movement. The pressure in chamber 1 and the resultant saturation velocity were measured from the recordings. A specimen recording

Pressure in Chamber 1 at Saturation Velocity (in Mercury)	Load Mass (lb)	Saturation Velocity (ft/s)
8.4	0.44 (No carriage attached)	1.40
8.4	11.0	1.25
8.4	22.0	1.13
8.4	33.0	1.03
8.4	44.0	0.98
8.4	55.0	0.95
8.4	66.0	0.85
8.4	77.0	0.85
8.4	88.0	0.80

Table A3.2 Saturation Velocity Test Results

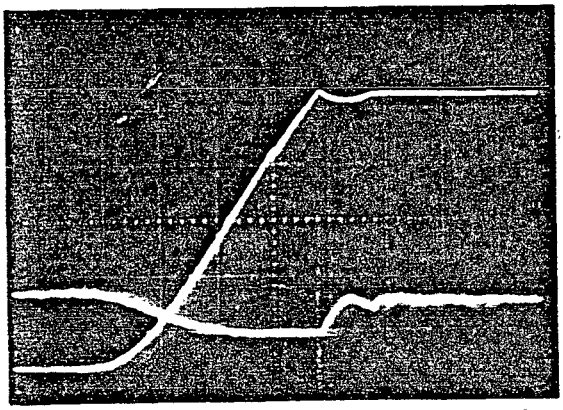

(a) Sample Record

showing (i) piston position
(ii) chamber pressure

(i)

Calibration

Position: stroke = 2.9"

Pressure: 1 in mercury/division

(ii) Time: 50 ms/division

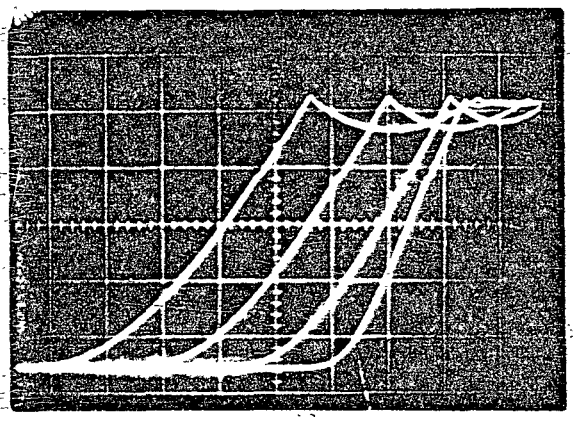

(b) Sample Record

showing piston position for loads of 88, 66, 44 and 11 lb respectively left to right

(c) Variation of Friction with Load Mass

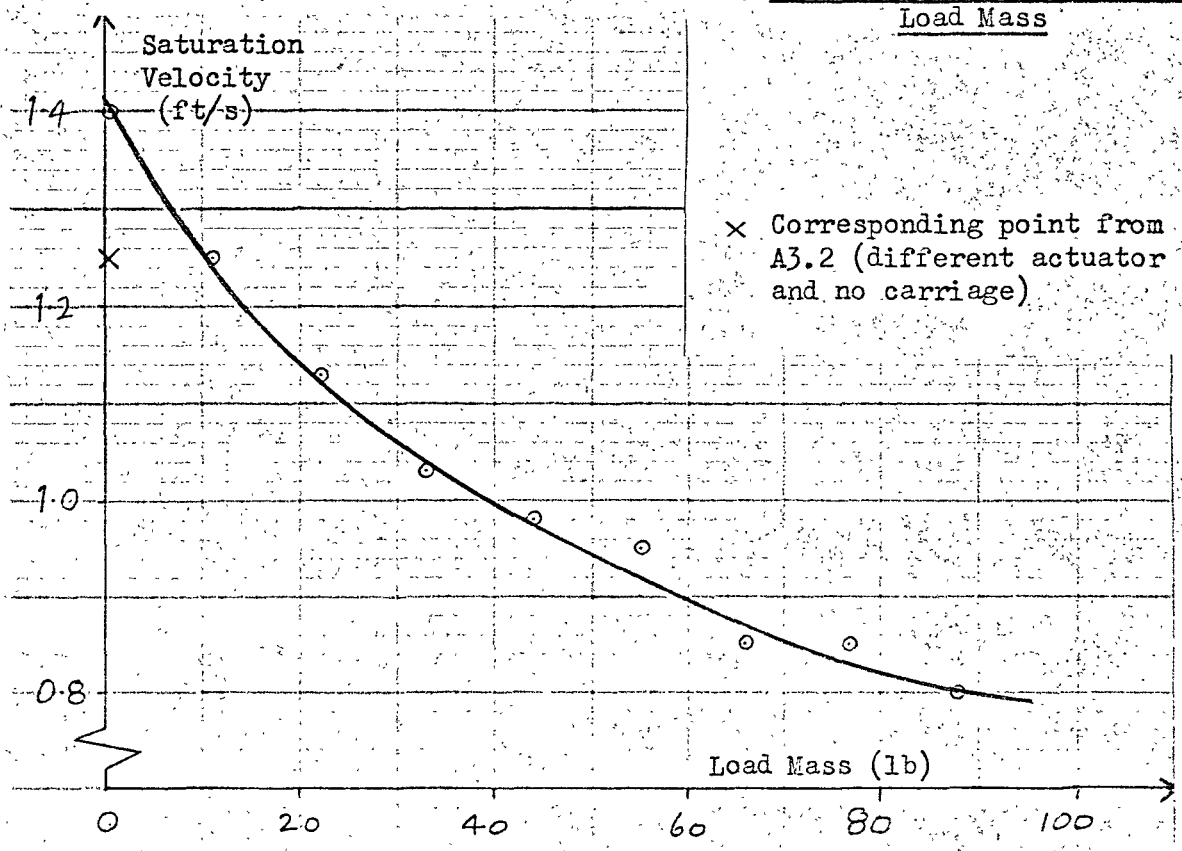

Fig. A3.3 Saturation Velocity Tests

is shown in fig. A3.3(a), and the effect of mass variation on saturation velocity can be seen in fig. A3.3(b).

In the case of the large load tests it was not certain that the carriage reached full saturation velocity before striking the end-stops, though inspection of fig. A3.3(b) shows that it probably did. It was however clear that there was a distinct difference between the maximum velocities for different loads and fig. A3.3(c) indicates this trend. Results are shown in table A3.2. It can be seen that the saturation velocity fell by about 35% from minimum to maximum loads.

A single point, replotted from fig. A3.2, is also shown in fig. A3.3(c). This illustrates that the present actuator had slightly less friction than the one used in the main experimental rig.

These results are discussed in section 4.3.3.

APPENDIX 4 DETAILS OF EXPERIMENTAL APPARATUS

A4.1 The Electro-Pneumatic Servo

(a) The Actuator was manufactured by Bristol Control Ltd. (since acquired by Feedback Ltd.) and had a modified piston rod seal. The ball race was replaced by a nylon bush.

(b) Pressure Feedback The pressure transducer was a Solartron Ltd., NT4 313.

A second transducer of the same type was used to monitor the pressure in chamber 1.

(c) The Servo-Valve was an Elliott Bros. Ltd. (MAC Division) type 610 and is shown in fig. A4.1. The valve was designed for use with hydraulic fluid and most of the following data, supplied by the manufacturer, relates to its use with oil.

Input:	±400mA d.c. (Valve coils in series), 3.2W.
Output:	2 gallons/min. at 1500 lbf/in^2 valve pressure drop (DTD 585 Fluid)
Ports:	Flow area varies linearly with spool movement
Filtration:	10 microns
Hysteresis:	6% of rated current) Dither recommended
Threshold:	2% of rated current) to reduce these
Valve Position Transducer:	Integrally mounted inductive "pick-off" (series 4000), of the inductive bridge type, giving an alternating output proportional to valve spool displacement when supplied with a.c.

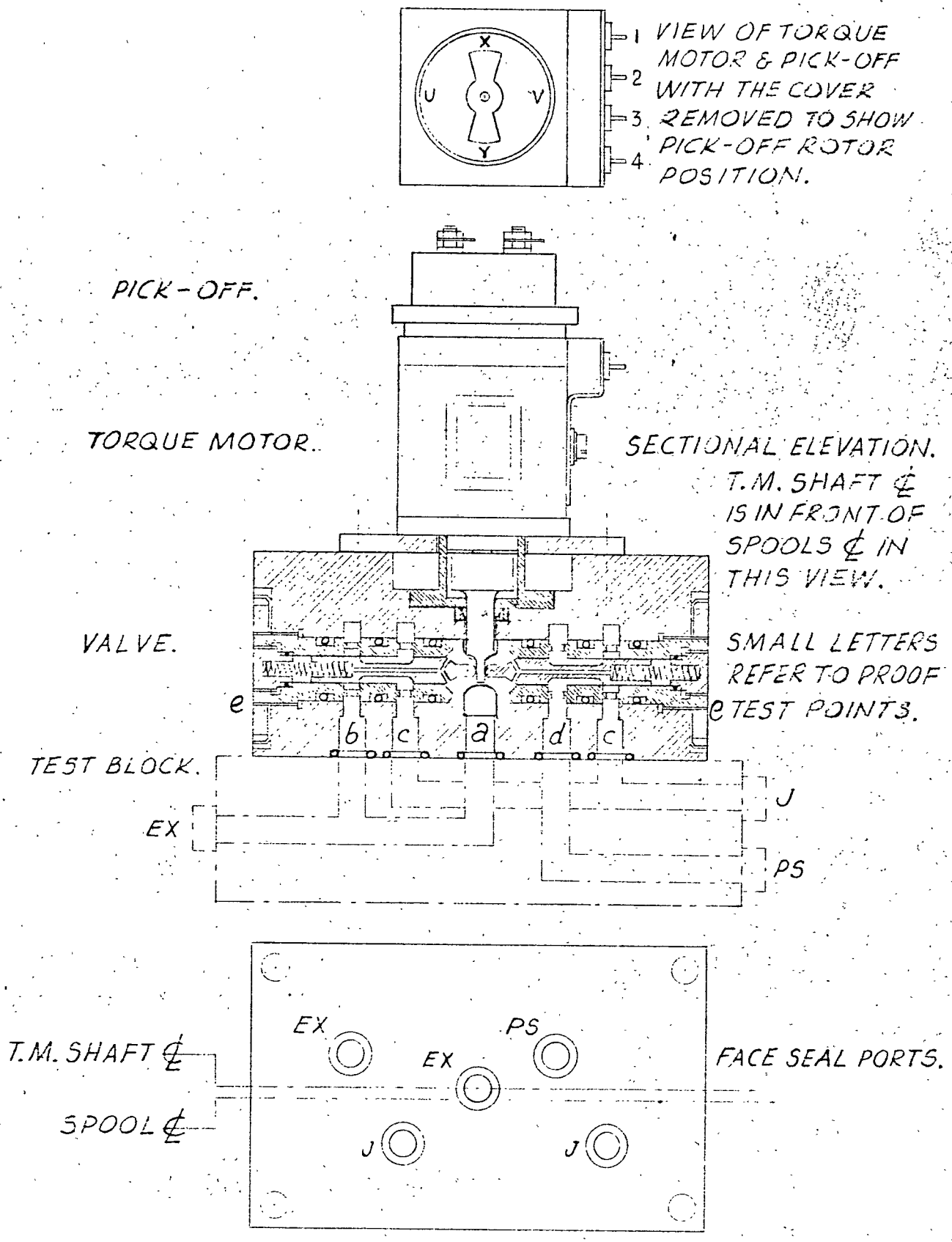

Fig. AA.1 The Electro-Pneumatic Servo Valve (Elliott type 610)

A4.2 The Fluidic Servo

(a) Fluidic Components (see figs. 8.5 to 8.8)

BS1 Bistable. Plessey Fluidics type BS.

PA1, PA2 Proportional Amplifiers, prototypes manufactured by Plessey T.R. Ltd., Taplow, Bucks. (Development now discontinued) Moulded Araldite type

PA3 Proportional Amplifier G.E. type AW 32.

OR/NOR Plessey type ON.

C1 Capacitor. Volume = 127×10^3 mm^3

C2 Capacitor. Volume = 31.2×10^3 mm^3

S1, S2 Schmitt triggers. Corning Fluidic Products, quoted hysteresis 0.5% of supply pressure. Characteristic shown in fig. A4.2.

Piping 4 mm i.d. throughout, except the Schmitt trigger inputs which were 3 mm i.d.

(b) Pressure Transducer and Amplifier

Sensitivity of transducer and amplifier: 7.5×10^{-3} mv/mm W.G. over the range 0 to 1000 mm W.G. i.e. 1 mv represented 133 mm W.G.

Type: Ether BP11 transducer (0-2000 lbf/in^2) and 3MX20 amplifier.

Dynamic Response: An independent test showed that the transducer responded completely to a sudden (faster than 1 ms) pressure change of 1000 mm W.G. in 2 ms or better.

(c) On/off Valves (figs. A4.3 and 8.8)

(i) Norcon Ltd. type 420 DP "Pilot Valves", modified by drilling out the orifice to 0.070 in. diameter in order to increase the flow.

Diaphragm diameter: 1.8 in.

Diaphragm movement: 0.015 in.

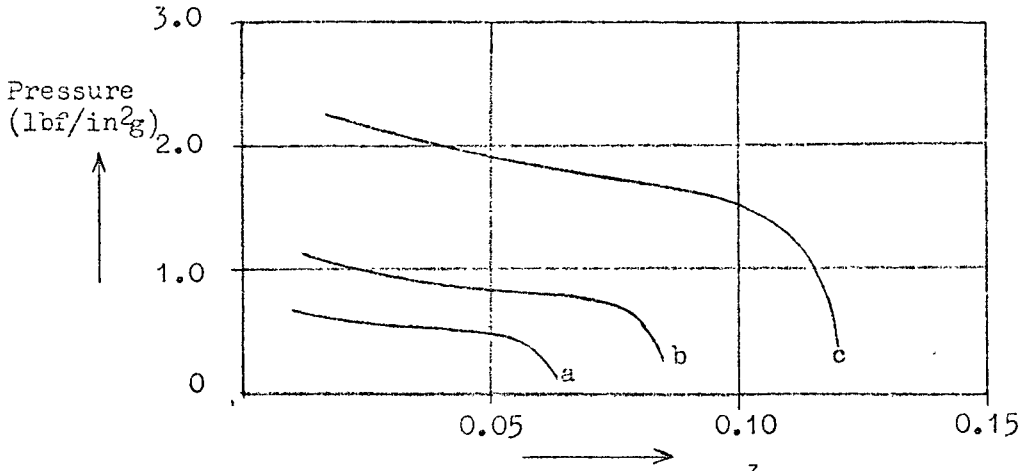

Supply Pressures: (a) 3 lbf/in²g

(b) 5 lbf/in²g

(c) 10 lbf/in²g

Fig. A4.2 Schmitt Trigger Characteristic

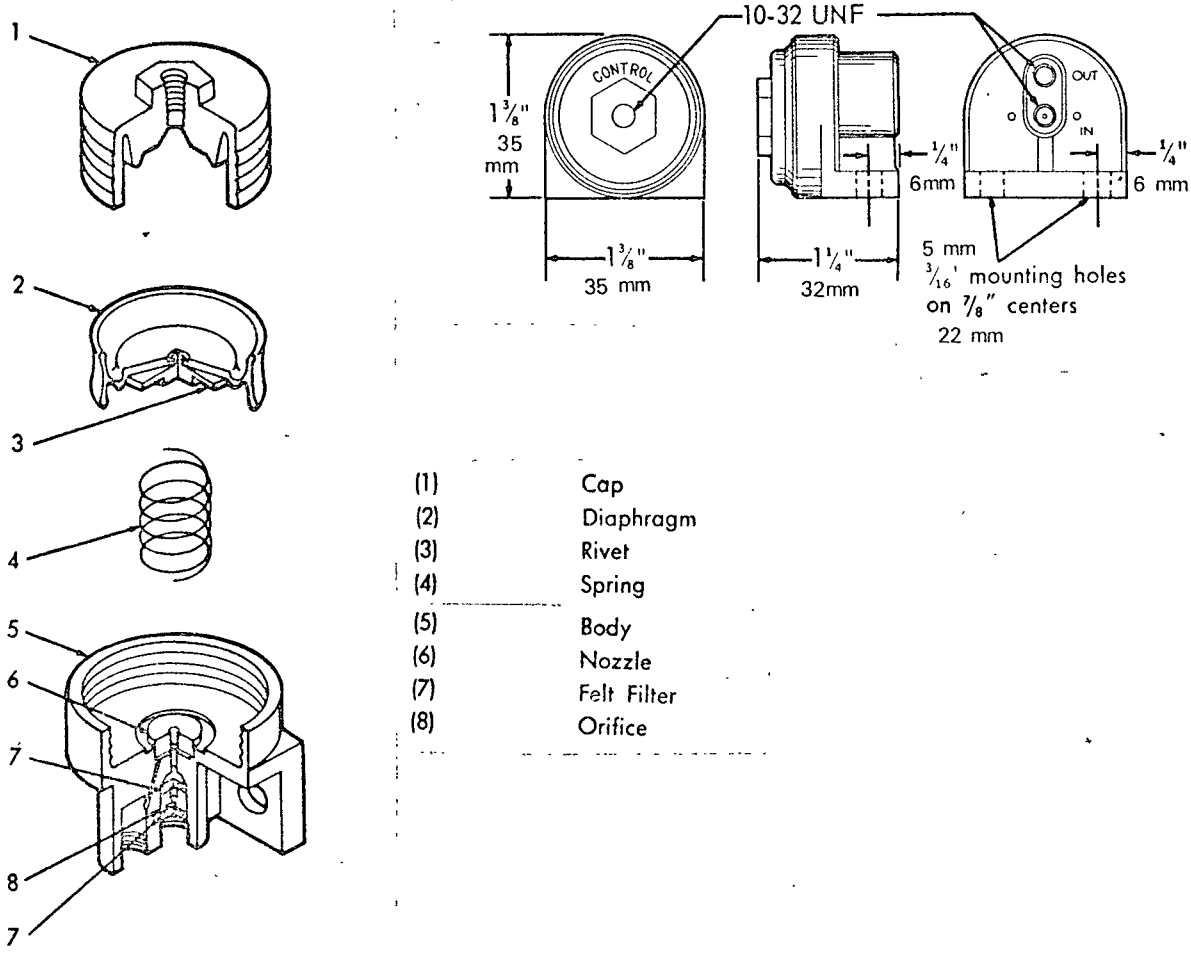

(1)	Cap
(2)	Diaphragm
(3)	Rivet
(4)	Spring
(5)	Body
(6)	Nozzle
(7)	Felt Filter
(8)	Orifice

Fig. A4.3 Norgren Valve

Flow: 3.0 ft^3/min, free air, with supply at 60 lbf/in^2g and exhausting to atmosphere.

Normal Use: As first stage of a fluidically signalled hydraulic directional control valve.

Chamber Volumes: The volume above the diaphragm (valve closes when pressurised) was approximately 11×10^3 mm^3 and below (valve opens when lower chamber pressurised) was approximately 6×10^3 mm^3.

Input: Differential pressure, adjustable according to spring fitted.

(ii) Norgren Fluidics Ltd. type 5DA 010.

Actuation pressure: 75 mm W.G.

Diaphragm chamber volume: 0.3×10^3 mm^3 (approximate)

APPENDIX 5 STATIC LEAKAGE TESTS

A5.1 The Pneumatic Actuator

In Chapters 3 to 6 a laminar piston leakage coefficient was used for the actuator which formed part of the electro-pneumatic servo. The evidence for this is presented below.

A5.1.1 Description of Tests

The circuit arrangement for these tests is shown in fig. A5.1.

Test I A constant pressure (P_1) of 50 lbf/in^{2}g was maintained in the right-hand chamber and the piston leakage flow rate was measured using float-type meters for different values of P_2, the pressure in the left-hand chamber. This test was carried out for two piston positions, on either side of the mid-position, i.e. the 1 in. and 2 in. positions on the scale shown in fig. A5.1 (and also in fig. 3.1). The resultant graph is shown in fig. A5.3 (line OA).

Test II The test was repeated with the piston in the two extreme positions, i.e. the 0 in. and 3 in. positions (lines OC and OB in fig. A5.3).

Test III Similar tests were carried out at the 1 in. position, for P_1 = 40 lbf/in^{2}g and P_1 = 60 lbf/in^{2}g (fig. A5.4).

Test IV The leakage flow rate was also checked with the pressure differential and flow in the opposite direction, i.e. $P_2 > P_1$. There was no measurable difference in leakage coefficient.

A5.1.2 Discussion of Results

(a) Reasonable, straight lines were drawn through the experimental points of figs. A5.3 and A5.4, i.e. leakage flow was shown to be approximately proportional to differential pressure.

(b) Leakage is approximately constant for two positions of the

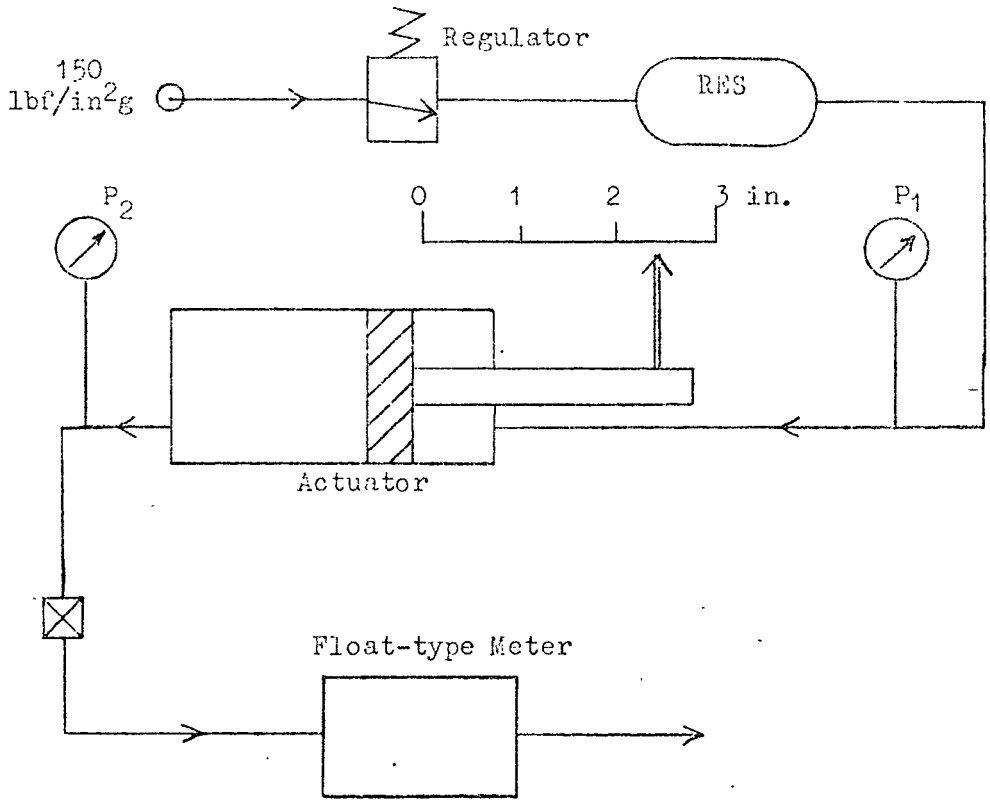

Fig. A5.1 Piston Leakage Test Circuit

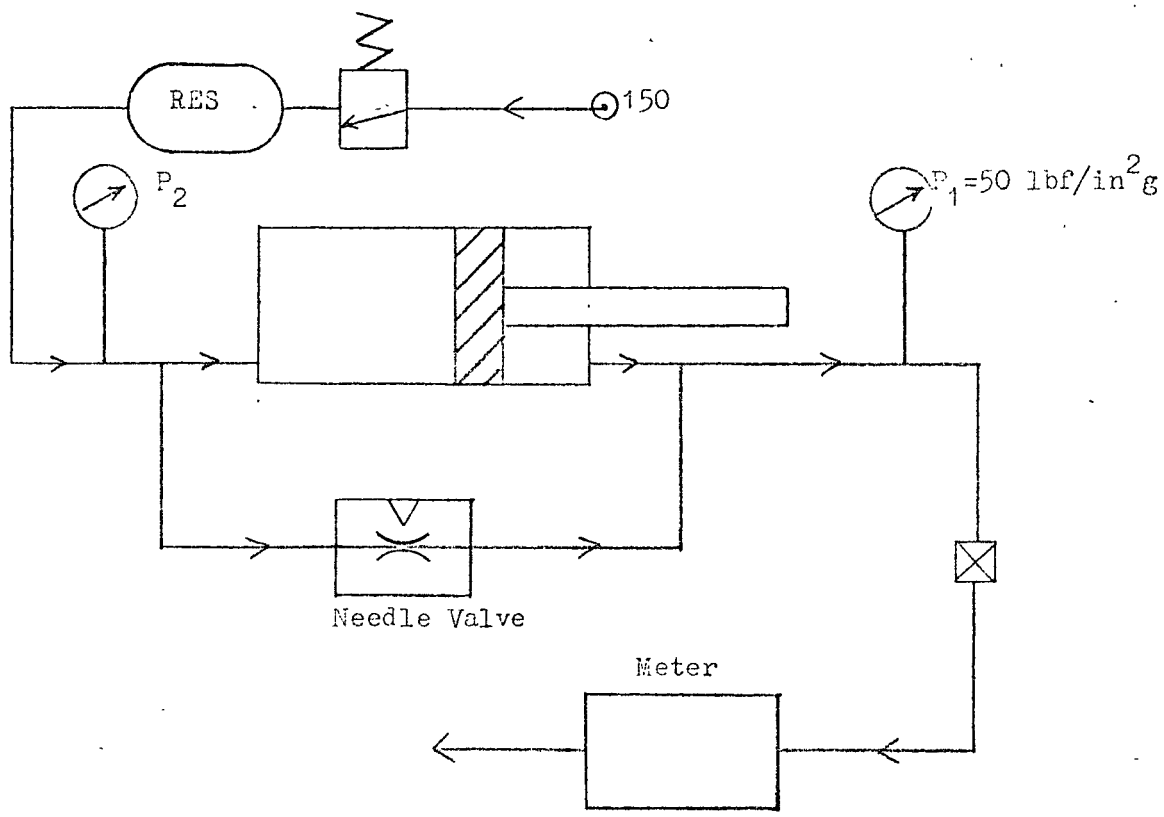

Fig. A5.2 Needle Valve Calibration Test Circuit

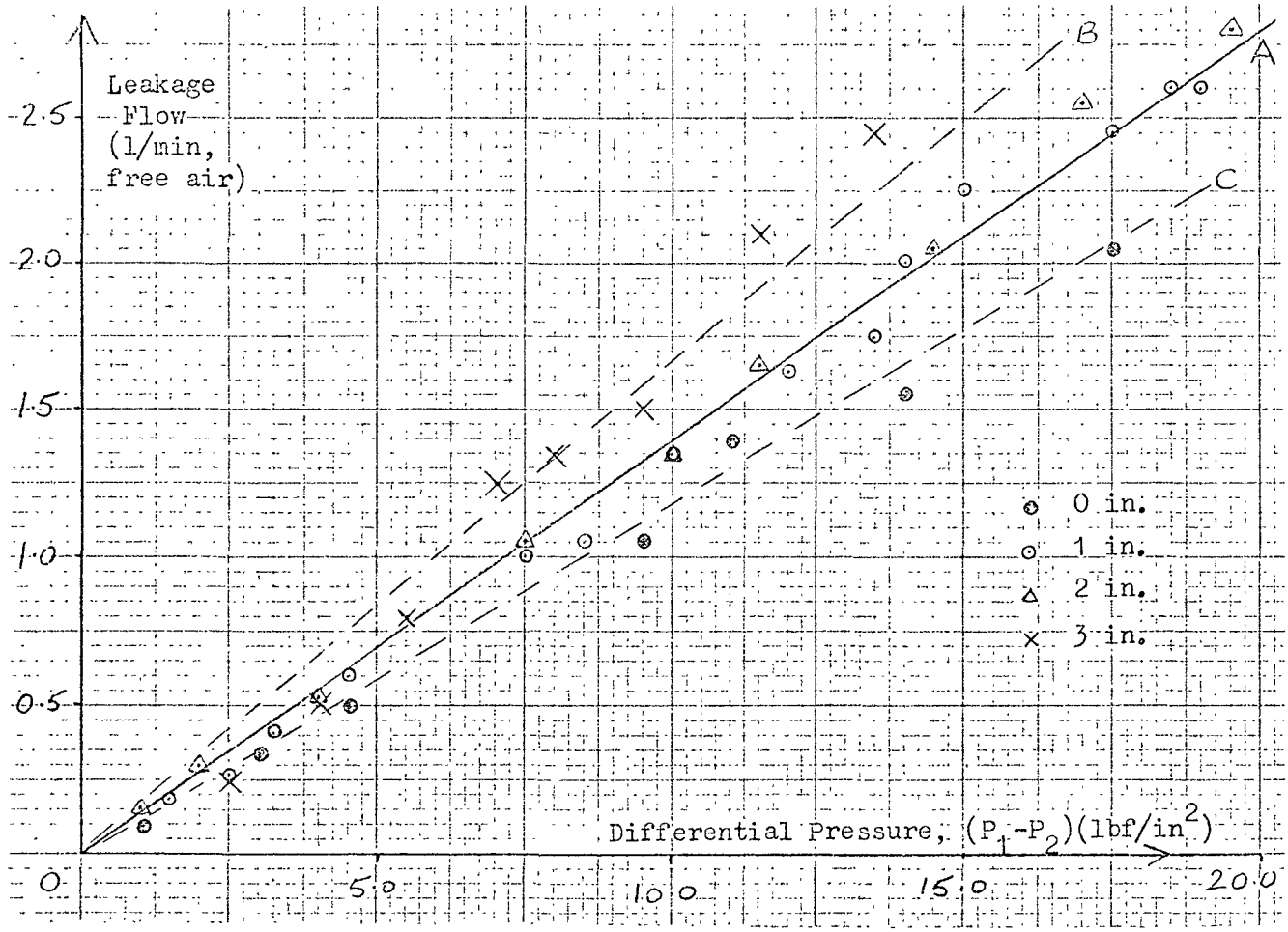

Fig. A5.3 Piston Leakage Tests for Varying Piston Position (Tests I and II)

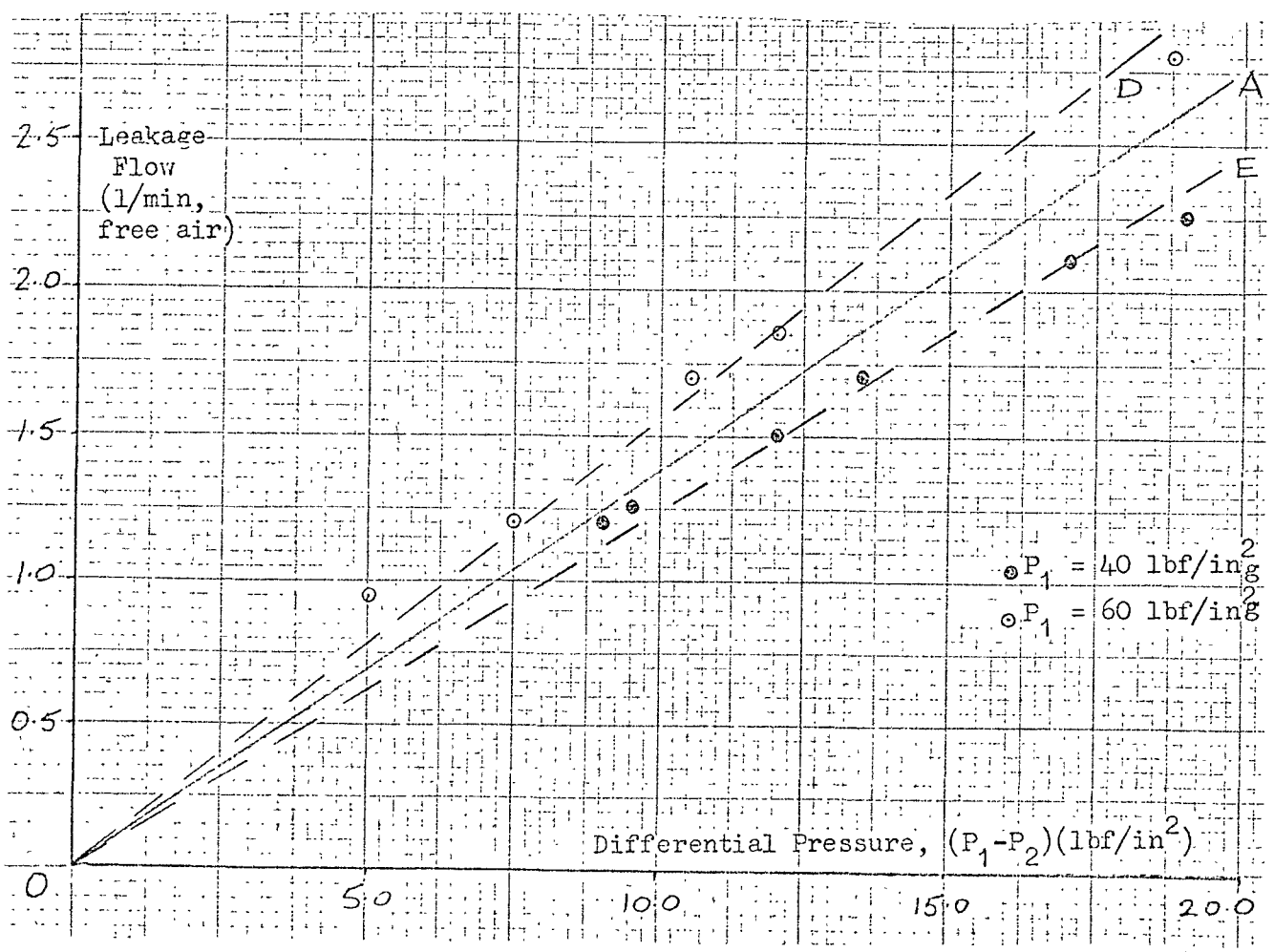

Fig. A5.4 Piston Leakage Tests for Varying Pressure (Test III)

piston around mid-stroke and deviates slightly for the two end positions. In fig. A5.3 the lines OB and OC are within ±15% of OA.

(c) The leakage coefficient varies with upstream pressure as shown in fig. A5.4. For absolute pressure changes of ±15% the change is less than ±10%(lines OD, OA and OE in fig. A5.4).

(d) As stated previously, the leakage coefficient can be considered to be constant for both directions of flow.

A5.1.3 Leakage Coefficient Calculation

Using line OA in fig. A5.3 as a representative average:

$$\text{Slope of OA} = 0.14 \frac{(\text{litres of free air/min})}{(\text{lbf/in}^2)}$$

$$\text{So} \quad L_b = \frac{0.14 \times 14.7}{28.3 \times 60 \times 144 \times 64.7} \ (\text{ft}^3/\text{s})/(\text{lbf/ft}^2)^*$$

$$\text{i.e.} \quad \underline{L_b = 1.3 \times 10^{-7} \ (\text{ft}^3/\text{s})/(\text{lbf/ft}^2)^*}$$

(* Air volume measured at 64.7 lbf/in^2)

where L_b is the leakage coefficient inherent in the actuator design.

A5.2 Additional Inter-chamber Leakage

A5.2.1 Description of Tests

The needle valve used to provide additional leakage in the Impulse Tests described in section 4.1.5(b) was calibrated statically using the arrangement of fig. A5.2.

The flow meter was used to measure the leakage flow rate (free air volume) for various settings of the by-pass needle valve. This needle valve was controlled by a screw thread and seven complete rotations of this screw were required to move the needle from fully closed to fully open. The flow rate measured was the flow past the piston plus the flow through the by-pass valve.

The results of these tests are plotted in fig. A5.5 and fig. A5.6.

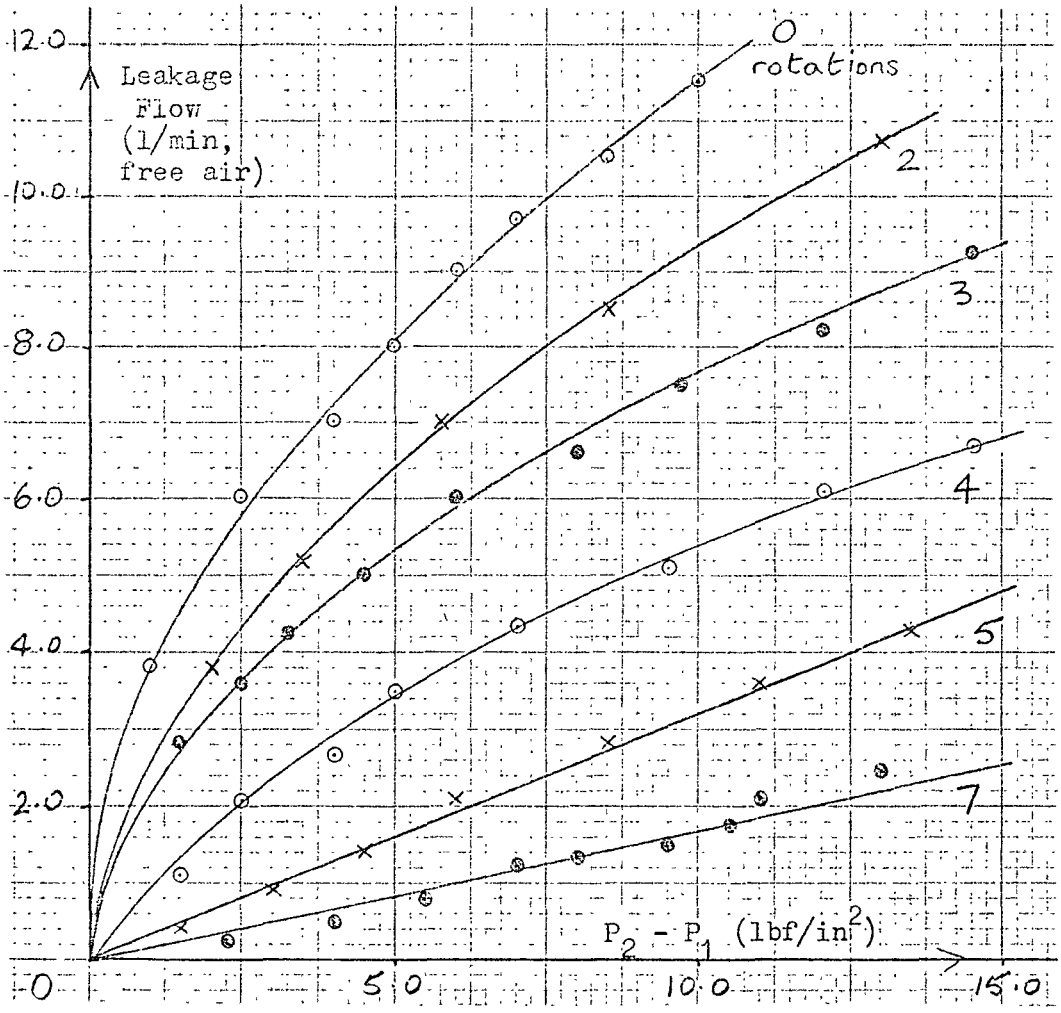

Fig. A5.5

Leakage due to Piston and Needle Valve

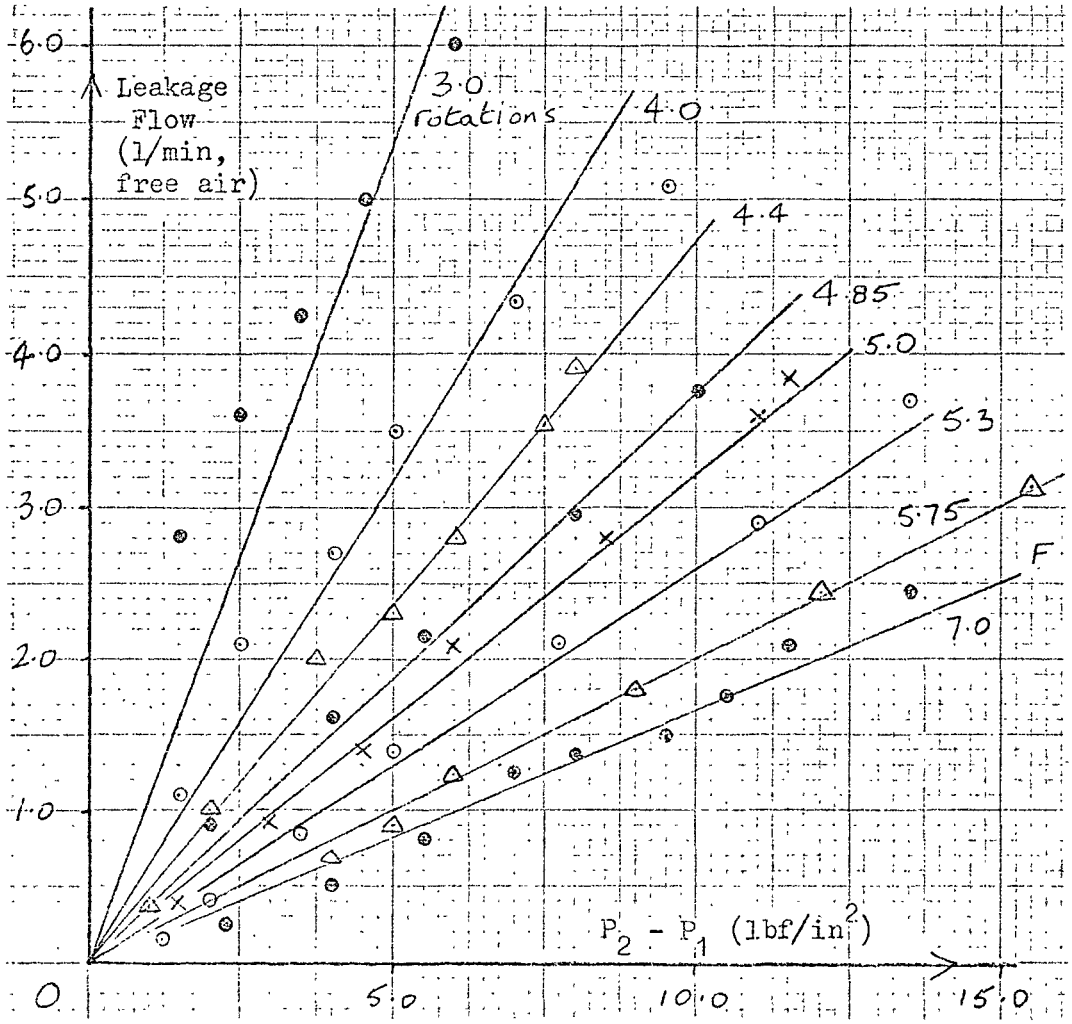

Fig. A5.6

Leakage due to Piston and Needle Valve (Linearized)

A5.2.2 Discussion of Results

Straight line approximations were drawn through some of the experimental points, over limited ranges of differential pressure, as shown in fig. A5.6. Calibration curves for the needle valve alone were produced by subtracting the "fully closed" curve (line OF) from the other curves in fig. A5.6. Values of leakage coefficients calculated from the slopes of these lines are shown in fig. A5.7.

A5.3 Conclusions (Appendix 5)

(a) A figure for the inherent laminar piston leakage coefficient, for the actuator used in the electro-pneumatic servo, was established:-

$$L_b = 1.3 \times 10^{-7} \ (ft^3/s)/(lbf/ft^2)$$ (Volume measured at 64.7 lbf/in^2)

This was applicable for the range of pressure differential encountered in the tests, i.e. ±18 lbf/in^2.

(b) It was shown that additional leakage, provided by a calibrated by-pass valve, could be regarded as laminar under certain conditions of flow and pressure difference (see fig. A5.6). The maximum additional laminar leakage was about $6\frac{1}{2}$ times the inherent jack leakage.

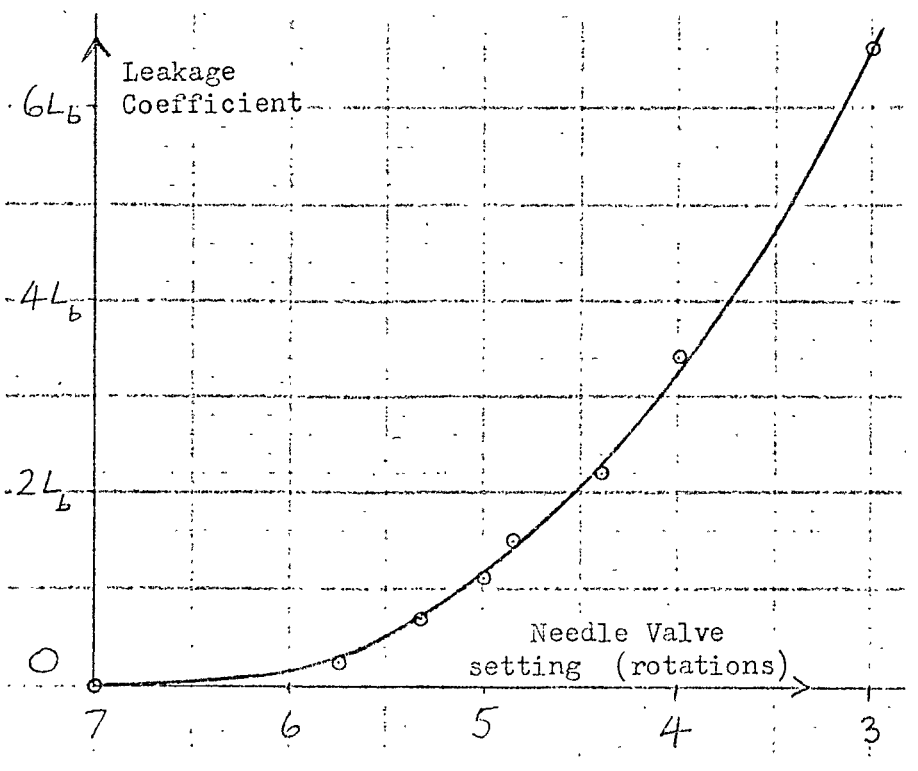

Fig. A5.7
Needle Valve Characteristic

APPENDIX 6 PRESSURE IN CHAMBER 1

The analysis leading to eqn. 3.23 includes the assumption that the pressure (P_1) in chamber 1 is constant. This assumption is investigated here. This pressure was recorded throughout the Impulse Tests of Chapter 4 and spot checks were made during the closed loop tests of Chapter 5.

A6.1 Analysis

To minimise fluctuation in pressure P_1, a large reservoir was connected, as shown in fig. A6.1, throughout the open and closed loop tests described in Chapters 4 and 5. This "sub-system" will be considered here.

The piping between chamber 1 and this reservoir offers a certain resistance to flow and three cases can be considered:-

(a) Infinite Resistance

In this case there is no reservoir and the pressure fluctuation amplitude, δP_1, will follow volumetric fluctuation, δV_1, according to

$$\frac{\delta P_1}{nP_1} = \frac{\delta V_1}{V_1}$$

(b) Zero Resistance

Now $\frac{\delta P_1}{nP_1} = \frac{\delta V_1}{V_1 + V_R}$ where V_R = Volume of reservoir 1.

Typically this pressure fluctuation would be 0.1% of P_1 for the parameters of the experimental rig.

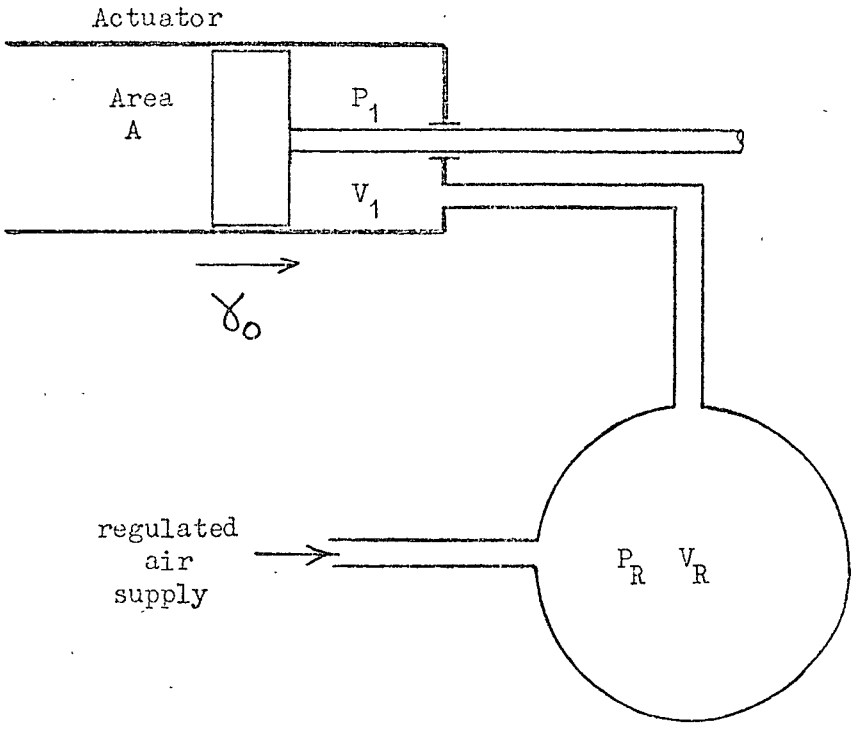

Fig. A6.1 Sub-system Consisting of Chamber 1 and Reservoir

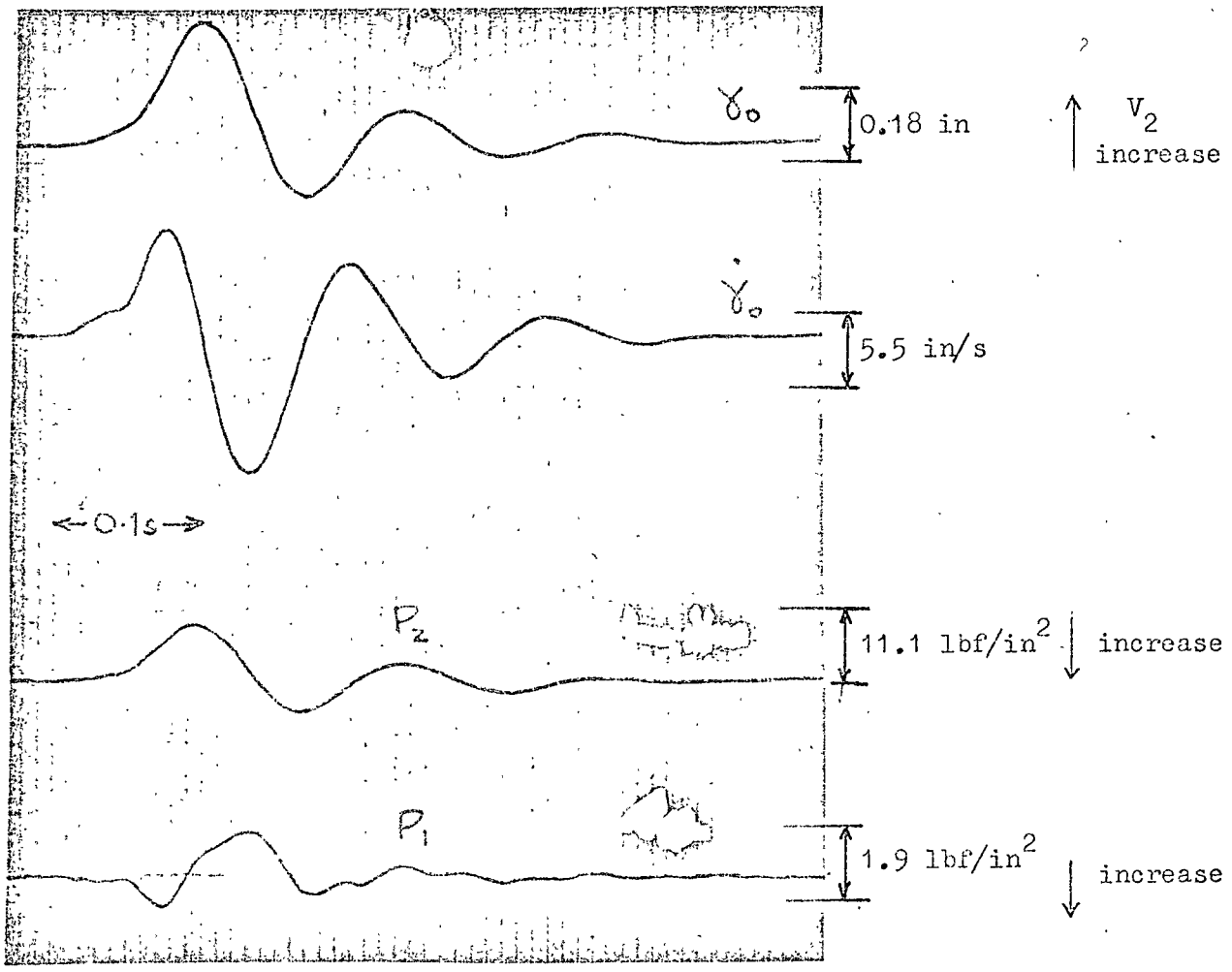

Fig. A6.2 Impulse Test Trace

(c) Finite Resistance

In practice the piping represents some finite resistance. Assuming laminar flow, the mass rate of flow of air along the interconnecting pipe = $\rho_1 C_5(P_1 - P_R)$ where

C_5 = constant.

And by a similar procedure to that used to derive eqn. 3.12 and ignoring leakage

$$\text{Rate of change of mass of air in chamber 1} = \rho_{1a}\left(A\frac{d\bar{\gamma}_o}{dt} - \frac{V_{1a}}{nP_{1a}}\frac{d\bar{P}_1}{dt}\right)$$

for small perturbations.

$$\text{Hence } \frac{\bar{P}_1 - P_R}{\bar{\gamma}_o} = \frac{AD}{\frac{V_{1a}}{nP_{1a}}D + C_5} \quad \text{where } D = \frac{d}{dt}$$

$$= \frac{K\tau D}{1 + \tau D} \qquad \text{A6.1}$$

where τ and K are constants.

This is the transfer operator of a high pass filter and indicates that at low frequencies of piston oscillation, there is very slight pressure fluctuation in chamber 1, and a phase difference of 90°, i.e. case (b) above, while at high frequencies, the interconnecting pipe acts as a "plug" or infinite resistance, i.e. case (a) above. The definition of "low" and "high" frequencies clearly depends on the volumes, resistances, etc. of the components in a particular case.

A6.2 Experimental Observations

In the Impulse Tests and the Closed Loop Step Response Tests, described in Chapters 4 and 5, the "sub-system" under consideration received a damped harmonic stimulus (γ_o).

A6.2.1 Impulse Tests

All the Impulse Test results recorded in table 4.1 were

studied, together with a number of others which were excluded from that table because of excessive pressure fluctuations in chamber 1 (see the note at the end of section A6.3 below). Fig. A6.2 shows a specimen trace of the latter type, while in fig. 4.1 a much smaller fluctuation is seen.

(i) The range of frequencies for the damped transient oscillations observed was between 2.5 Hz and 10 Hz.

(ii) In all cases pressure fluctuations were small, i.e. $\pm$2% or less in P_1 (64.7 lbf/in^2 abs.).

(iii) The maximum fluctuation ever to occur in P_1 was 15% of the corresponding fluctuation in P_2.

(iv) The phase difference between P_1 and piston displacement (γ_o) could not be measured accurately, but showed a phase lead of P_1 on γ_o of about 90^o in all cases where an estimate was possible (even with the minute fluctuation in fig. 4.1 a phase lead of about 90^o is just discernible).

(v) There was a slight tendency for the amplitude of pressure fluctuation to increase with frequency though no corresponding trend in phase could be detected.

A6.2.2 Closed Loop Step Response Tests

The pressure in chamber 1 was also checked for a number of the tests described in Chapter 5. The same observations as in section A6.2.1 above apply. In most cases, when the pressure in chamber 2 varied considerably, i.e. for larger load masses, the fluctuation in P_1 was very small. In fig. 5.1, (tests ES32/33) P_1 and P_2 are shown together and the amplitude of P_1 fluctuations was no greater, for larger step sizes and loads.

A6.3 Discussion

Referring to the approximate transfer operator (eqn A6.1), the above observations suggest that the frequency, $\frac{1}{\tau}$ rad/s is considerably higher than the frequencies used in these tests. Therefore the practical results are considerably nearer to the zero "resistance" case (case (b)) than to the infinite "resistance" case (case (a)).

The reliability of the phase information extracted from the experimental records is confirmed by the observation that, in all cases, the phase difference between load displacement (γ_o) and variable pressure (P_2) was about 180°. This is as expected for a system in which the load is predominantly inertial. (The phase difference would be exactly 180° if the load were solely inertial.)

The observed phase difference of 90° between γ_o and P_1 makes the effect of the already small pressure fluctuation, even less. In effect, the "stiffness" of the enclosed air in chamber 2 is increased over one half cycle of oscillation and decreased for the following half cycle, if P_1 is 90° out of phase with P_2. This "cancelling" over one complete cycle minimises the effect which this fluctuation in P_1 has on the "stiffness" and hence on the natural frequency of the actuator.

The variation (δP_1) in P_1 was also compared with the variation (δP_2) in P_2 for each Impulse Test (section 4.1.2) and a maximum value for ($\frac{\delta P_1}{\delta P_2}$ x 100) of 5% was arbitrarily adopted.

A6.4 Conclusions (Appendix 6)

1. The effect of variations in the pressure (P_1) in chamber 1 upon system behaviour was shown to be small and was therefore neglected.

2. For the range of transient frequencies and amplitudes under investigation, the fluctuations in pressure of chamber 1 were never greater than $\pm$ 2% of the equilibrium value.

3. A simple first order transfer operator was proposed for the relationship between piston position and chamber 1 pressure (eqn. A6.1) and results were consistent with this proposed transfer operator.

APPENDIX 7 FULL SIMULATION - SAMPLE CALCULATIONS
(see section 6.1.8)

Tests FS1 and FS2 - constants a', b' etc. defined in table 3.1.

$$V_{2a} = 1.23 \times 10^{-2} \times \frac{1.5}{12} + 0.67 \times 10^{-3} = \underline{2.21 \times 10^{-3} ft^3}$$

$$a' = \frac{2.21 \times 10^{-3} \times 2.91}{1.28 \times 53.3 \times 525 \times 1.23 \times 10^{-2}} = \underline{14.8 \times 10^{-6}} \text{ lbft}^{-1}\text{s}^2$$

Using b = 13 lbf s ft^{-1}

$$b' = \frac{2.21 \times 10^{-3} \times 13}{1.28 \times 53.3 \times 525 \times 1.23 \times 10^{-2}} = \underline{6.80 \times 10^{-5}} \text{ lbft}^{-1}\text{s}$$

$$e' = \frac{9300 \times 1.3 \times 10^{-7} \times 2.91}{53.3 \times 525 \times 1.23 \times 10^{-2}} = \underline{1.03 \times 10^{-5}} \text{ lbft}^{-1}\text{s}$$

$$f' = \frac{9300 \times 1.3 \times 10^{-7} \times 13}{53.3 \times 525 \times 1.23 \times 10^{-2}} = \underline{4.76 \times 10^{-5}} \text{ lbft}^{-1}$$

In fig. 3.1 the variable resistor in the pressure feedback path was set at 93KΩ

So $\tau_p = RC = 15 \times 10^{-6} \times (93 + 19.5) \times 10^3 = \underline{1.69s}$

The pressure feedback gain for this setting was 5mA/(lbf/in^2)

So $K_{pr} = \underline{\underline{\frac{5}{144} = 3.47 \times 10^{-2} \frac{mA\ ft^2}{lbf}}}$

Potentiometer settings are shown in table A7.1:-

Table A7.1 Potentiometer Settings for Tests FS1 and FS2

Potentiometer	Function	Setting
1	$\frac{\text{input amplitude (in.)}}{3 \text{ in.}}$	0.330
2	Fixed	0.267
3	$\frac{b' + e'}{a'} \cdot \frac{150}{4000}$	0.199
4	$K_A K_p \frac{0.25}{500.\ 10}$	0.215
5	Fixed	0.300
6	$\frac{b}{A} \cdot \frac{5}{15.\ 10^3}$	0.364
7	$\frac{c' + f'}{a'} \cdot \frac{5}{4000}$	0.353
8	$\frac{m_L}{A} \cdot \frac{150}{15.\ 10^3.\ 10}$	0.237
9	Fixed	0.200
10	$\frac{1}{a'} \cdot \frac{10^{-2}}{4000}$	0.170
11	$\frac{1}{10\tau_p}$	0.055
12	$K_{pr} \cdot \frac{15.\ 10^3}{500.\ 10}$	0.104
14	$K_A K_p \frac{0.25}{500.\ 10}$	0.215
15	Time Base 0.5v/s	0.050
16	Fixed	0.790
17	$\frac{P_{2a}}{15.\ 10^3}$	0.625
21	$\frac{1}{10} \left(\frac{P_e}{15.\ 10^3}\right)^2$	0.021
23	$\frac{1}{10} \left(\frac{P_s}{15.\ 10^3}\right)^2$	0.122

APPENDIX 8 DYNAMIC RESPONSE OF AN ON/OFF DIAPHRAGM ACTUATED VALVE

In the fluidic system described in Chapter 8, a Schmitt trigger acted as the signal source for an on/off valve. The arrangement is shown diagrammatically in fig. A8.1.

A8.1 Symbols for Appendix 8

C	'capacitance' of valve chamber (constant)
D	$\frac{d}{dt}$
m	mass flow rate through connection (pipe)
M_2	instantaneous mass of air in valve actuator
P_1	instantaneous pressure at Schmitt trigger output port
P_2	" " in valve actuator
P_d	'dead ended' pressure from Schmitt trigger
P_s	pressure at ideal (constant pressure) source
R	gas constant
R_c	'resistance' of the connection (constant)
R_s	output 'resistance' of Schmitt trigger (constant)
T_2	instantaneous temperature of air in valve actuator
V_2	instantaneous volume of valve actuator
τ	time constant

A8.2 Analysis

For flow between the source and the valve

$$m = fn_1(P_1, P_2) \qquad 8.1$$

For the air in the valve actuator

$$P_2V_2 = M_2 RT_2 \qquad 8.2$$

For the source, from the characteristic in fig. A8.2

$$P_1 = fn_2(m) \qquad 8.3$$

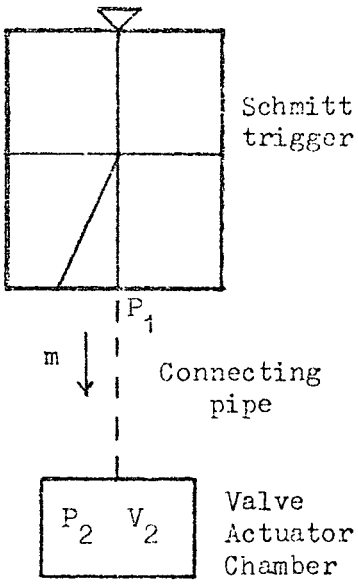

Fig. A8.1 Schmitt trigger plus Valve

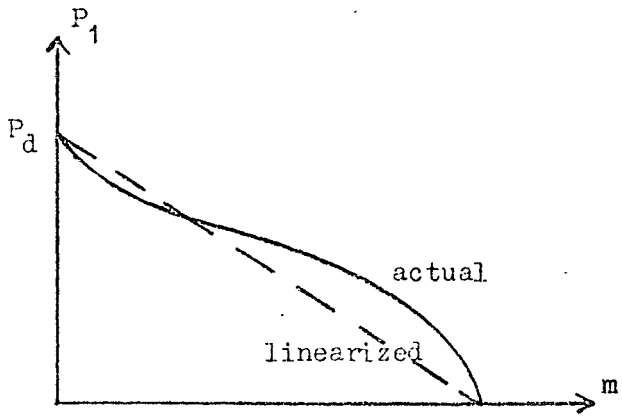

Fig. A8.2 Schmitt Trigger Output Characteristic (see fig. A4.2 for a typical curve)

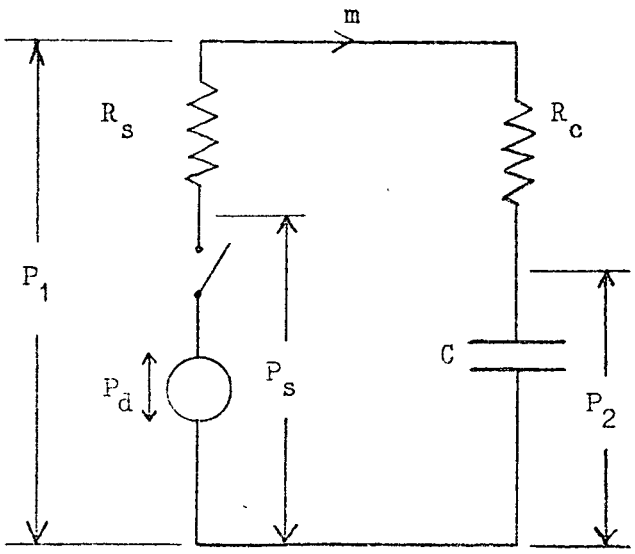

Fig. A8.3 Electrical Analogy

N.B. In this diagram symbols P represent voltages which are analogous to pressures in figs. A8.1 and A8.2

Linearizing these equations and assuming the mass of the moving parts to be negligible:-

Assuming laminar flow between source and valve

$$m = \frac{1}{R_c} (P_1 - P_2) \qquad 8.4$$

Assuming isothermal conditions and constant actuator chamber volume, eqn. 8.2 becomes

$$DP_2 = \frac{m}{C} \qquad 8.5$$

Linearizing the curve in fig. A8.2

$$P_1 = P_d - R_s m \qquad 8.6$$

The electrical analogy for this linearized system, shown in fig. A8.3, represents the Schmitt trigger as a constant voltage (pressure) source with series resistance, so that

$$\frac{P_2}{P_s} = \frac{1}{1 + (R_s + R_c)\, CD} \qquad 8.7$$

Here, when the Schmitt trigger switches on, P_s changes instantaneously from zero to P_d and the valve pressure rises exponentially to P_d, with time constant $\tau = (R_s + R_c)C$. 8.8

A8.3 Discussion

Theoretically, the valve opens instantaneously when the actuator pressure reaches P_d, though in practice, P_2 must slightly exceed the valve switching pressure. (The final equilibrium pressure should not be too high, however, since the air has later to be rapidly exhausted from the chamber.)

A number of gross approximations have been adopted to derive the above transfer operator and its usefulness is therefore limited. It does, however, illustrate that for fast valve response,

(i) valve actuator chamber volume should be minimised,

(ii) the connection should have low resistance,

(iii) the ideal source characteristic (fig. A8.2) is a horizontal line, which represents zero output impedance or $R_s = 0$.

A compromise between (i) and (ii) is clearly necessary since implementing (ii) involves increasing the volume or capacitance of the system.